

Lateral torsional buckling of anisotropic laminated composite beams
subjected to various loading and boundary conditions

by

Habiburrahman Ahmadi

B.S., Kabul University, Afghanistan, 2006
M.S., Kansas State University, 2011

AN ABSTRACT OF A DISSERTATION

submitted in partial fulfillment of the requirements for the degree

DOCTOR OF PHILOSOPHY

Department of Civil Engineering
College of Engineering

KANSAS STATE UNIVERSITY
Manhattan, Kansas

2017

Abstract

Thin-walled structures are major components in many engineering applications. When a thin-walled slender beam is subjected to lateral loads, causing moments, the beam may buckle by a combined lateral bending and twisting of cross-section, which is called lateral-torsional buckling. A generalized analytical approach for lateral-torsional buckling of anisotropic laminated, thin-walled, rectangular cross-section composite beams under various loading conditions (namely, pure bending and concentrated load) and boundary conditions (namely, simply supported and cantilever) was developed using the classical laminated plate theory (CLPT), with all considered assumptions, as a basis for the constitutive equations.

Buckling of such type of members has not been addressed in the literature. Closed form buckling expressions were derived in terms of the lateral, torsional and coupling stiffness coefficients of the overall composite. These coefficients were obtained through dimensional reduction by static condensation of the 6x6 constitutive matrix mapped into an effective 2x2 coupled weak axis bending-twisting relationship. The stability of the beam under different geometric and material parameters, like length/height ratio, ply thickness, and ply orientation, was investigated. The analytical formulas were verified against finite element buckling solutions using ABAQUS for different lamination orientations showing excellent accuracy.

Lateral torsional buckling of anisotropic laminated composite beams
subjected to various loading and boundary conditions

by

Habiburrahman Ahmadi

B.S., Kabul University, Afghanistan, 2006
M.S., Kansas State University, 2011

A DISSERTATION

submitted in partial fulfillment of the requirements for the degree

DOCTOR OF PHILOSOPHY

Department of Civil Engineering
College of Engineering

KANSAS STATE UNIVERSITY
Manhattan, Kansas

2017

Approved by:

Major Professor
Dr. Hayder A. Rasheed

Copyright

© Habiburrahman Ahmadi 2017.

Abstract

Thin-walled structures are major components in many engineering applications. When a thin-walled slender beam is subjected to lateral loads, causing moments, the beam may buckle by a combined lateral bending and twisting of cross-section, which is called lateral-torsional buckling. A generalized analytical approach for lateral-torsional buckling of anisotropic laminated, thin-walled, rectangular cross-section composite beams under various loading conditions (namely, pure bending and concentrated load) and boundary conditions (namely, simply supported and cantilever) was developed using the classical laminated plate theory (CLPT), with all considered assumptions, as a basis for the constitutive equations.

Buckling of such type of members has not been addressed in the literature. Closed form buckling expressions were derived in terms of the lateral, torsional and coupling stiffness coefficients of the overall composite. These coefficients were obtained through dimensional reduction by static condensation of the 6x6 constitutive matrix mapped into an effective 2x2 coupled weak axis bending-twisting relationship. The stability of the beam under different geometric and material parameters, like length/height ratio, ply thickness, and ply orientation, was investigated. The analytical formulas were verified against finite element buckling solutions using ABAQUS for different lamination orientations showing excellent accuracy.

Table of Contents

| | |
|--|-------|
| List of Figures | x |
| List of Tables | xvi |
| Acknowledgements | xvii |
| Dedication | xviii |
| Chapter 1 - Introduction..... | 1 |
| 1.1 Background..... | 1 |
| 1.2 Objectives | 4 |
| 1.3 Scope of Dissertation | 4 |
| 1.4 References..... | 6 |
| Chapter 2 - Literature Review..... | 7 |
| 2.1 Background..... | 7 |
| 2.2 Previous Research on Isotropic Beams..... | 7 |
| 2.3 Previous Research on Composite Beams..... | 8 |
| 2.4 References..... | 15 |
| Chapter 3 - Lateral-Torsional Buckling of Anisotropic Laminated Thin-Walled Rectangular Composite Beams Subjected to Pure Bending in Simply Supported Condition | 17 |
| 3.1 Introduction..... | 17 |
| 3.2 Analytical Formulation..... | 20 |
| 3.2.1 Kinematics | 22 |
| 3.2.2 Constitutive Equations | 22 |
| 3.2.3 Equilibrium Equations | 25 |
| 3.3 Numerical Analysis (FEA) | 26 |
| 3.4 Results..... | 28 |
| 3.4.1 Material Properties and Stacking Sequences | 28 |
| 3.4.2 Buckling Results | 30 |
| 3.5 Parametric Study..... | 31 |
| 3.5.1 Effect of Length/Height Ratio | 31 |
| 3.5.2 Effect of Stacking Sequence | 35 |
| 3.5.3 Effect of Thickness | 36 |

| | |
|--|----|
| 3.6 Conclusions..... | 40 |
| 3.7 References..... | 42 |
| Chapter 4 - Lateral-Torsional Buckling of Simply Supported Anisotropic Steel-FRP Beams | |
| under Pure Bending Condition | 44 |
| 4.1 Introduction..... | 44 |
| 4.2 Analytical Formulation..... | 48 |
| 4.2.1 Kinematics | 50 |
| 4.2.2 Stress-Strain Equations | 50 |
| 4.2.3 Force-Strain Equation | 51 |
| 4.2.4 Equilibrium Equations | 55 |
| 4.3 Numerical Analysis (FEA) | 57 |
| 4.4 Results..... | 59 |
| 4.4.1 Material Properties and Stacking Sequences | 59 |
| 4.4.2 Buckling Results | 62 |
| 4.5 Parametric Study..... | 62 |
| 4.5.1 Effect of Length/Height Ratio | 62 |
| 4.5.2 Effect of Stacking Sequence (ST-I and ST-II)..... | 68 |
| 4.5.3 Effect of Fiber Angle Orientation | 69 |
| 4.5.4 Effect of Layer Thickness | 70 |
| 4.6 Conclusions..... | 74 |
| 4.7 References..... | 76 |
| Chapter 5 - Lateral-Torsional Buckling of Anisotropic Laminated Thin-Walled Rectangular | |
| Composite Cantilever Beams Subjected to Free End Concentrated Load | 77 |
| 5.1 Introduction..... | 77 |
| 5.2 Analytical Formulation..... | 80 |
| 5.2.1 Kinematics | 82 |
| 5.2.2 Constitutive Equations | 84 |
| 5.2.3 Equilibrium Equations | 88 |
| 5.2.3.1 Buckling Counterclockwise | 88 |
| 5.2.3.2 Buckling Clockwise..... | 91 |
| 5.3 Numerical Analysis (FEM)..... | 98 |

| | |
|--|-----|
| 5.4 Results..... | 100 |
| 5.4.1 Material Properties and Stacking Sequences | 100 |
| 5.4.2 Buckling Results | 101 |
| 5.5 Parametric Study..... | 103 |
| 5.5.1 Effect of Length/Height Ratio | 103 |
| 5.5.2 Effect of Stacking Sequence | 108 |
| 5.5.3 Effect of Layer Thickness..... | 109 |
| 5.5.4 Effect of Pre-Buckling Deformation..... | 112 |
| 5.6 Conclusions..... | 114 |
| 5.7 References..... | 116 |
| Chapter 6 - Lateral Torsional Buckling of Anisotropic Laminated Thin-Walled Simply | |
| Supported Beams Subjected to Concentrated Load at Mid-Span..... | 118 |
| 6.1 Introduction..... | 118 |
| 6.2 Analytical Formulation..... | 122 |
| 6.2.1 Kinematics | 123 |
| 6.2.2 Constitutive Equations | 125 |
| 6.2.3 Equilibrium Equations | 129 |
| 6.2.3.1 Buckling Counterclockwise (Left Side of the Beam)..... | 129 |
| 6.2.3.2 Buckling Clockwise (Right Side of the Beam)..... | 132 |
| 6.3 Numerical Analysis (FEA) | 138 |
| 6.4 Results..... | 139 |
| 6.4.1 Material Properties and Stacking Sequences | 139 |
| 6.4.2 Buckling Results | 141 |
| 6.5 Parametric Study..... | 143 |
| 6.5.1 Effect of Length/Height Ratio | 143 |
| 6.5.2 Effect of Stacking Sequence | 147 |
| 6.5.3 Effect of Layer Thickness..... | 150 |
| 6.5.4 Effect of Pre-Buckling Deformation..... | 153 |
| 6.6 Conclusions..... | 155 |
| 6.7 References..... | 157 |
| Chapter 7 - Conclusions and Recommendations | 159 |

| | |
|--------------------------|-----|
| 7.1 Conclusions..... | 159 |
| 7.2 Recommendations..... | 160 |

List of Figures

| | |
|--|----|
| Figure 3.1 A deformed laminated beam subjected to pure bending | 21 |
| Figure 3.2 Force and moment resultants on a beam based on classical laminated plate theory ... | 24 |
| Figure 3.3 Applied load and boundary conditions..... | 27 |
| Figure 3.4 Applied shell element type (S8R) and mesh (element size along beam axis: 2.5 mm) | 27 |
| Figure 3.5 The stacking sequence of the laminates | 29 |
| Figure 3.6 Buckling moments at different stacking sequences: $t_k=0.1$ mm for each layer, $L/h=5$, and element length 2.5mm..... | 30 |
| Figure 3.7 Buckling moments at different stacking sequences: $t_k=0.1$ mm for each layer, $L/h=20$, and element length 2.5mm..... | 31 |
| Figure 3.8 Effect of L/h ratio on the critical moment based on analytical formula for three different layups and layer thickness of 0.1 mm | 32 |
| Figure 3.9 Comparison of buckling result obtained from analytical solution and FEM for the [0/0/0/0] laminate and layer thickness of 0.1 mm by changing L/h ratio | 33 |
| Figure 3.10 Edge deformation of the beam under pure bending for $L/h=5$, (a) [0/0/0/0] (b) [30/- 30/30/-30], and (c) [45/-30/-15/90]..... | 33 |
| Figure 3.11 Comparison of buckling result obtained from analytical solution and FEM for the [45/-30/-15/90] laminate and layer thickness of 0.1 mm by changing L/h ratio | 34 |
| Figure 3.12 Comparison of buckling result obtained from analytical solution and FEM for the [30/-30/30/-30] laminate and layer thickness of 0.1 mm by changing L/h ratio | 35 |
| Figure 3.13 Variation in critical buckling moment with the change in balanced angle-ply layup angle of 0 to 90 with an increment of 5 degrees. (+) Analytical and (●) FEM; layer thickness of 0.1 mm and L/h of 5..... | 36 |
| Figure 3.14 Effect of thickness, t_k , on the critical moment based on analytical method for three different orientations, $L/h=5$ | 37 |
| Figure 3.15 Effect of thickness, t_k , on the critical moment based on FEM method for three different orientations, $L/h=5$ | 38 |
| Figure 3.16 Comparison of buckling result obtained from analytical solution and FEM for the [0/0/0/0] laminate and L/h of 5 by changing layer thickness, t_k | 39 |

| | |
|---|----|
| Figure 3.17 Comparison of buckling result obtained from analytical solution and FEM for the [45/-30/-15/90] laminate and L/h of 5 by changing layer thickness, t_k | 39 |
| Figure 3.18 Comparison of buckling result obtained from analytical solution and FEM for the [30/-30/30/-30] laminate and L/h of 5 by changing layer thickness, t_k | 40 |
| Figure 4.1 A deformed laminated beam subjected to pure bending (structural coordinate system) | 49 |
| Figure 4.2 Force and moment resultants on a beam based on classical laminated plate theory (laminate coordinate system). | 54 |
| Figure 4.3 Applied load and boundary conditions..... | 58 |
| Figure 4.4 Applied shell element type (S8R) and mesh (element size along beam axis: 2.5 mm) | 58 |
| Figure 4.5 The stacking sequence of the laminate and location of steel sheet (ST-I) | 61 |
| Figure 4.6 Buckling moments at different stacking sequences: $t_k=0.1$ mm for each layer, L/h=5, and ST-I configuration | 63 |
| Figure 4.7 Buckling moments at different stacking sequences: $t_k=0.1$ mm for each layer, L/h=5, and ST-II configuration..... | 64 |
| Figure 4.8 Buckling moments at different stacking sequences: $t_k=0.1$ mm for each layer, L/h=20, and ST-I configuration | 64 |
| Figure 4.9 Buckling moments at different stacking sequences: $t_k=0.1$ mm for each layer, L/h=20, and ST-II configuration..... | 65 |
| Figure 4.10 Effect of L/h ratio on the critical moment based on analytical formula for three different layups and layer thickness of 0.1 mm and ST-I arrangement | 65 |
| Figure 4.11 Effect of L/h ratio on the critical moment based on analytical formula for three different layups and layer thickness of 0.1 mm and ST-II arrangement..... | 66 |
| Figure 4.12 Buckling shapes showing distortional buckling mode and lateral-torsional buckling mode for ST-I arrangement..... | 67 |
| Figure 4.13 Comparison of buckling results obtained from analytical solution and FEM for the [0/0/0/ST/0/0/0] (ST-I) laminate and layer thickness of 0.1 mm by changing L/h ratio | 67 |
| Figure 4.14 Comparison of buckling results obtained from analytical solution and FEM for the [0/0/0/0/0/0/ST] (ST-II) laminate and layer thickness of 0.1 mm by changing L/h ratio.. | 68 |
| Figure 4.15 Normalized ST-II/ST-I vs. the stacking sequence with L/h = 5 and L/h = 20 | 69 |

| | |
|---|----|
| Figure 4.16 Variation in critical buckling moment with the change in layup angle of 0 to 90 at an increment of 5 degrees. (+) Analytical and (●) FEM; layer thickness of 0.1 mm and L/h of 5, ST-I | 70 |
| Figure 4.17 Variation in critical buckling moment with the change in layup angle of 0 to 90 at an increment of 5 degrees. (+) Analytical and (●) FEM; layer thickness of 0.1 mm and L/h of 5, ST-II | 70 |
| Figure 4.18 Effect of layer thickness, t_k , on the critical moment based on FEM for three different layups and L/h ratio of 5 and ST-I arrangement | 71 |
| Figure 4.19 Effect of layer thickness, t_k , on the critical moment based on analytical formula for three different layups and L/h ratio of 5 and ST-I arrangement | 72 |
| Figure 4.20 Effect of layer thickness, t_k , on the critical moment based on FEM for three different layups and L/h ratio of 5 and ST-II arrangement..... | 72 |
| Figure 4.21 Effect of layer thickness, t_k , on the critical moment based on analytical formula for three different layups and L/h ratio of 5 and ST-II arrangement | 73 |
| Figure 4.22 Critical buckling moment of three different fiber orientation of ST-I versus different layer thickness and L/h ratios | 73 |
| Figure 4.23 Critical buckling moment of three different fiber orientation of ST-II versus different layer thickness and L/h ratios | 74 |
| Figure 5.1 Buckling shape of the beam; (a) buckling counterclockwise (+ β) and (b) buckling clockwise ($-\beta$) | 82 |
| Figure 5.2 Deformation of a point at beam profile section with respect to mid-surface displacement | 83 |
| Figure 5.3 Representation of curvatures with respect to displacement and angle of twist; (a) beam buckles counterclockwise (+ β) and (b) beam buckles clockwise ($-\beta$)..... | 84 |
| Figure 5.4 Force and moment resultants on a beam based on classical laminated plate theory ... | 87 |
| Figure 5.5 Components of external moments about original and deformed axes of laminated cantilever beam subjected to free end loading, buckled counterclockwise | 91 |
| Figure 5.6 Components of external moments about original and deformed axes of laminated cantilever beam subjected to free end loading, buckled clockwise | 93 |
| Figure 5.7 Flowchart of the semi-analytical solution of the buckling equation using Mathematica | 96 |

| | |
|---|-----|
| Figure 5.8 Screenshot of the script used in Mathematica to solve the buckling differential equation..... | 97 |
| Figure 5.9 C_1 vs C_2 to obtain a representative equation from best fit of the data..... | 98 |
| Figure 5.10 FEM model with $L/h = 20$ and layer thickness $= 0.1$ mm; (a) applied shell element type (S8R)..... | 99 |
| Figure 5.11 The stacking sequence of the laminates | 101 |
| Figure 5.12 Buckling force at different stacking sequences: $t_k = 0.1$ mm for each layer, $L/h = 20$, and finite element length 2.5mm | 102 |
| Figure 5.13 Buckling force at different stacking sequences: $t_k = 0.1$ mm for each layer, $L/h = 10$, and finite element length 2.5mm | 103 |
| Figure 5.14 Effect of L/h ratio on the critical buckling force based on analytical formula for three different layups and layer thickness of 0.1 mm. | 104 |
| Figure 5.15 Buckling (deformed and un-deformed) shape of the cantilever beam for ply thickness of 0.1 mm and lamination orientation of $[30/-30/30/-30]$; (a) $L/h = 50$, (b) $L/h = 20$, and (c) $L/h = 5$ | 105 |
| Figure 5.16 Comparison of buckling result obtained from analytical solution and FEM for the $[15/30/-45/15]$ laminate and layer thickness of 0.1 mm by changing L/h ratio..... | 106 |
| Figure 5.17 Comparison of buckling result obtained from analytical solution and FEM for the $[30/-30/45/-45]$ laminate and ply thickness of 0.1 mm by changing L/h ratio | 107 |
| Figure 5.18 Comparison of buckling result obtained from analytical solution and FEM for the $[30/-30/30/-30]$ laminate and ply thickness of 0.1 mm by changing L/h ratio | 107 |
| Figure 5.19 Variation in critical buckling force with the change in balanced angle-ply layup angle of 0 to 90 with an increment of 5 degrees. (+) Analytical and (●) FEM; ply thickness of 0.1 mm and L/h of 20 | 108 |
| Figure 5.20 Effect of thickness, t_k , on the critical force based on analytical formula for three different orientations, $L/h = 20$ | 110 |
| Figure 5.21 Effect of thickness, t_k , on the critical force based on FEM method for three different orientations, $L/h = 20$ | 110 |
| Figure 5.22 Comparison of buckling result obtained from analytical solution and FEM for the $[15/30/-45/15]$ laminate and L/h of 20 by changing layer thickness, t_k | 111 |

| | |
|---|-----|
| Figure 5.23 Comparison of buckling result obtained from analytical solution and FEM for the [30/-30/45/-45] laminate and L/h of 20 by changing layer thickness, t_k | 112 |
| Figure 5.24 Comparison of buckling result obtained from analytical solution and FEM for the [30/-30/30/-30] laminate and L/h of 20 by changing layer thickness, t_k | 112 |
| Figure 5.25 Analytical vs numerical solutions; deflection at mid-height, L/h=20 and $t_k=0.1$ mm | 113 |
| Figure 6.1 Buckling shape of the beam; (a) left side ($+\beta$), (b) right side ($-\beta$), and (c) top view | 123 |
| Figure 6.2 Deformation of a point at beam profile section with respect to mid-surface displacement | 124 |
| Figure 6.3 Representation of curvatures with respect to displacement and angle of twist; (a) left side of the beam (counterclockwise, $+\beta$) and (b) right side of the beam (clockwise, $-\beta$) | 125 |
| Figure 6.4 Force and moment resultants on a beam based on classical laminated plate theory. | 128 |
| Figure 6.5 Components of external forces about original and deformed axes of laminated simply supported beam subjected to concentrated load; coordinate system from the left end of the beam (counterclockwise, $+\beta$)..... | 132 |
| Figure 6.6 Components of external forces about original and deformed axes of laminated simply supported beam subjected to concentrated load, coordinate system from the right end of the beam (clockwise $-\beta$)..... | 134 |
| Figure 6.7 Flowchart of the semi-analytical solution of the buckling equation using Mathematica | 136 |
| Figure 6.8 Screenshot of the script used in Mathematica to solve the buckling differential equation..... | 137 |
| Figure 6.9 FEM model with L/h =20 and layer thickness = 0.1 mm; (a) applied load and boundary conditions and (b) applied shell element type (S8R) and mesh (element size along beam axis: 1 mm)..... | 138 |
| Figure 6.10 The stacking sequence of the laminates | 141 |
| Figure 6.11 Buckling forces at different stacking sequences: $t_k=0.1$ mm for each layer and L/h=10..... | 142 |
| Figure 6.12 Buckling forces at different stacking sequences: $t_k=0.1$ mm for each layer and L/h=20..... | 143 |

| | |
|--|-----|
| Figure 6.13 Effect of L/h ratio on the critical buckling force based on analytical formula for three different layups and ply thickness of 0.1 mm | 144 |
| Figure 6.14 Buckling (deformed and un-deformed) shape of the simply supported beam for ply thickness of 0.1 mm and lamination orientation of [0/0/0/0]; (a) L/h=50, (b) L/h =20, (c) L/h = 10, and (d) L/h =5..... | 145 |
| Figure 6.15 Comparison of buckling result obtained from analytical solution and FEM for the [15/30/-45/15] laminate and ply thickness of 0.1 mm by changing L/h ratio..... | 146 |
| Figure 6.16 Comparison of buckling result obtained from analytical solution and FEM for the [30/-30/0/90] laminate and ply thickness of 0.1 mm by changing L/h ratio..... | 147 |
| Figure 6.17 Comparison of buckling result obtained from analytical solution and FEM for the [30/-30/30/-30] laminate and ply thickness of 0.1 mm by changing L/h ratio | 147 |
| Figure 6.18 Variation in critical buckling force with the change in balanced angle-ply layup angle of 0 to 90 with an increment of 5 degrees. (+) Analytical and (●) FEM; ply thickness of 0.1 mm and L/h of 20 | 149 |
| Figure 6.19 Variation in critical buckling force with the change in layup angle of 0 to 90 with an increment of 5 degrees from analytical formula for three different layups; ply thickness of 0.1 mm and L/h of 20..... | 149 |
| Figure 6.20 Effect of thickness, t_k , on the critical force based on analytical formula for three different orientations, L/h=20 | 151 |
| Figure 6.21 Effect of thickness, t_k , on the critical force based on FEM method for three different orientations, L/h=20 | 151 |
| Figure 6.22 Comparison of buckling result obtained from analytical solution and FEM for the [15/30/-45/15] laminate and L/h of 20 by changing layer thickness, t_k | 152 |
| Figure 6.23 Comparison of buckling result obtained from analytical solution and FEM for the [30/-30/0/90] laminate and L/h of 20 by changing layer thickness, t_k | 153 |
| Figure 6.24 Comparison of buckling result obtained from analytical solution and FEM for the [30/-30/30/-30] laminate and L/h of 20 by changing layer thickness, t_k | 153 |
| Figure 6.25 Analytical versus numerical solution; deflection at mid-span, L/h=20 and $t_k=0.1$. | 154 |

List of Tables

| | |
|--|-----|
| Table 3.1 Material properties used the in laminates | 29 |
| Table 3.2 Comparison of buckling moment obtained from analytical results and FEM for L/h ratios of 5 and 20 and layer thickness of 0.1 mm in different stacking conditions | 41 |
| Table 4.1 Relation of moment components in structural coordinate and laminate composite coordinate..... | 55 |
| Table 4.2 Material 1 (CFRP) properties used the in laminates..... | 60 |
| Table 4.3 Material 2 (Steel) properties used the in laminates..... | 61 |
| Table 5.1 Relation of moment components in structural coordinate and laminate composite coordinate..... | 88 |
| Table 5.2 CFRP material properties used in the laminates..... | 101 |
| Table 5.3 Comparison of buckling force obtained from analytical results and FEM for L/h ratios of 10 and 20 and layer thickness of 0.1 mm in different stacking conditions | 114 |
| Table 6.1 Relation of moment components in structural coordinate and laminate composite coordinate..... | 129 |
| Table 6.2 CFRP material properties used in the laminates..... | 140 |
| Table 6.3 Comparison of buckling force obtained from analytical results and FEM for L/h ratios of 10 and 20 and layer thickness of 0.1 mm in different stacking conditions | 155 |

Acknowledgements

I wish to express my sincere appreciation and profound gratitude to my major advisor, Dr. Hayder A. Rasheed for his intellectual guidance and support that he provided during my pursuit of the Doctoral Degree.

I would also like to acknowledge and thank Dr. Bacim Alali, Dr. Asad Esmaily, Dr. Hani Melhem, and Dr. Donald Phillippi for their willingness to serve on my supervisory committee and providing invaluable comments and suggestions.

I would also like to thank my group members, Rund Al-Masri, Adrijana Sovic, and AlaaEldin Abouelleill for their inspiration to my research and career.

Most importantly, I would like to thank my wife, Roya Mirzad, and my parents for their support, patience, and encouragement during my studies at Kansas State University to complete this degree.

Dedication

To my parents, my wife, and my children

Chapter 1 - Introduction

1.1 Background

Thin-walled beam structures are major components in many engineering applications. They are widely used as structural components in many types of systems in the field of civil, mechanical, and aerospace engineering. Advanced materials, mainly fiber reinforced polymer (FRP) composites, are partially replacing conventional materials in these types of structural systems. Composites have demonstrated outstanding success in both civilian and military fields. Nearly half of materials, in Boeing 787 Dreamliner, are made by advanced composites. The light-weight of composites also saves 20 percent in fuel compared to other equivalents (Huang, 2013). 2-D laminated and complex 3-D composites are being implemented in transportation systems, offshore structures, chemical facilities, aircraft wings, fuselages, engine blades, door frames, helicopter blades, rib structures, biomedical devices, and ballistic panels.

Characterization of the mechanical behavior of composites is a growing need because of their expanding applications. Composite mechanical properties rely on the structure of the composite reinforcement, which in laminated composites is determined by the orientation of reinforcing fibers. A laminated composite part is made by combining reinforcing fibers and matrix (e.g. resin) through stacking of the fibers in different orientations. This increase in interest for using FRP lies in some critical advantages of this composite over conventional materials. Their high strength to weight ratio, high stiffness to weight ratio, their environmental adaptability represented by corrosion resistance, their ease of transportation and erection, and their fatigue resistance are some of the advantages FRP provides. The most prominent characteristic is the ability of tailoring the material for each particular application. Structural properties depend on the material system and the shape of the cross-section of the member

(Barbero et al., 1993). For isotropic structural shapes, it is possible to optimize the section to increase the bending stiffness without compromising the maximum bending strength. Unlike isotropic shapes, with composite members it is possible to optimize the material itself by choosing among a variety of resins, fiber systems, and fiber orientations. Although FRP structures exhibit high strength, problems of excessive deformation and instability, due to the slenderness of the member, are the major disadvantages in wider acceptance for structural engineering applications (Lin et al., 1996). Because of these limitations, the new generation of composite structures should be designed to work in a safe way and to experience higher performance than the conventional systems. Consideration of stability and deformation limits tend to be the governing design criteria for FRP structures before these structures reach material failure. Thus, the proper establishment of such criteria is an important prerequisite to the practical use of FRP in engineering applications.

When a composite beam is considered sufficiently slender and undergoes bending moments about the strong axis, the beam may fail by sudden combined lateral bending and twisting of cross-section, rather than by rupture or crushing. This phenomenon is known as lateral-torsional buckling. The critical load is primarily dependant on the material and the geometry of the member. It is independent of the ultimate strength. A composite beam which is bent about the major principal axis may buckle laterally at a certain critical value of the load. As long as the load on the beam is less than the critical value, the beam will bend and stay stable. When the load is increased until the critical condition is reached, the beam may bifurcate from the main equilibrium configuration to a different state of equilibrium, which becomes likely or possible. The plane configuration of the beam is now unstable, and the lowest load at which the critical condition occurs represents the critical buckling load of the beam (Tai 2004).

Theory of thin-walled open section beams including axial constraints for isotropic materials was developed by Vlasov (1961). This classical theory neglects the shear deformation in the middle surface of the wall so that for such beams, the shear deformations may significantly increase the displacements and reduce the buckling loads for moderately thick beams. The shear deformation theory for transversely loaded isotropic beams was developed by Timoshenko and Gere (1961).

The lateral-torsional buckling includes two regions, elastic and inelastic lateral-torsional buckling, and they both depend on the slenderness ratio. A beam with higher slenderness will experience elastic lateral-torsional buckling, which is within the scope of this study, whereas a beam with intermediate slenderness ratio will experience inelastic lateral-torsional buckling, which is out of the scope of this study. The lateral-torsional buckling will not occur if the slenderness ratio of the member is low or if the member is bent about the weak principle axis of the cross-section. Lateral-torsional buckling is an important design criterion for higher slenderness ratio structures that the occurrence of it may significantly reduce the maximum load-carrying capacity of the member.

The lateral-torsional buckling for the isotropic materials is well developed in the past century. For instance, the lateral-torsional buckling of isotropic slender beams was developed by Vlasov (1961) as well as Timoshenko and Gere (1961) for various loading and boundary conditions. This limit state is also adopted by the American Institute of Steel Construction (AISC) design criteria for structural steel buildings and bridges and has been applied extensively to design safe steel structures. The use of composite materials gained popularity at the end of 20th century and is playing an important role since then in partial replacement of many structural steel members. However, there hasn't been any standard criterion established for lateral-torsional

buckling of composite thin-walled beams to account for it in design. There has been limited amount of research focusing on lateral-torsional buckling of composite I-section beams, where the beams were either considered to be of symmetric layup, anti-symmetric layup, orthotropic, or specially-orthotropic (pultruded) in nature. There hasn't been any study recorded on the behavior of generally anisotropic laminated composite beams to the best knowledge of the author.

1.2 Objectives

The objective of present study is to develop generalized analytical models applicable to the lateral-torsional buckling of anisotropic laminated rectangular composite beams, subjected to various loading and boundary conditions. The models are based on the classical laminated plate theory (CLPT), and account for the arbitrary laminate stacking sequence configurations. Finite element models are developed in ABAQUS to predict critical buckling loads and compare them with the results obtained from the analytical models. The effects of fiber orientation, beam length/height ratios and wall thickness on the critical buckling loads are studied.

1.3 Scope of Dissertation

The research work in this dissertation includes a literature review of the developments on lateral-torsional buckling of isotropic and special composite beams which is described in chapter two. Lateral torsional buckling of anisotropic laminated thin-walled rectangular composite beams subjected to pure bending in simply supported condition is treated in chapter three. An analytical formula was derived to solve the lateral-torsional buckling of simply supported anisotropic beams under pure bending condition. The analytical solutions are validated with numerical results. Lateral-torsional buckling of simply supported anisotropic hybrid steel-FRP beams under pure bending condition is addressed in chapter four. A generalized analytical approach for lateral-torsional buckling of simply supported anisotropic hybrid (steel-FRP) under

pure bending condition is developed using the classical laminated plate theory (CLPT) as a basis for the constitutive equations. The analytical formula is also verified against finite element buckling solutions using ABAQUS for different lamination orientations as well as the location of the steel sheet in the composite layup. Lateral torsional buckling of anisotropic laminated thin-walled rectangular composite cantilever beams subjected to free end loading is presented in chapter five. A generalized analytical solution for lateral-torsional buckling of anisotropic cantilever beams subjected to free end loading is developed using the classical laminated plate theory as a basis for the constitutive equations. The stability of the beam under different geometric and material parameters is investigated. The analytical formula is verified against finite element buckling solutions using ABAQUS for wide range of lamination orientations in this case as well. Analytical and numerical solutions for the lateral torsional buckling of anisotropic laminated thin walled simply supported beams subjected to concentrated load at mid-span is studied in chapter six. An analytical approach for lateral-torsional buckling of simply supported anisotropic beams under concentrated load at mid-span and mid-height is developed using the classical laminated plate theory as a basis for the constitutive equations. The analytical solution is verified against finite element buckling solutions using ABAQUS for wide range of lamination orientations.

1.4 References

- Barbero, E. J., Lopez-Anido, R., and Davalos, F. (1993). "On the Mechanics of Thin-Walled Laminated Composite Beams." *Journal of Composite Materials*, 27(8), 806-829
- Huang, L. (2013). *Determining micro-and macro-geometry of fabric and fabric reinforced composites* (Doctoral dissertation, Kansas State University).
- Lin, Z. M., Polyzois, D., and Shah, A. (1996). "Stability of Thin-walled Pultruded Structural Members by the Finite Element Method." *Thin-Walled Structures*, 24, 1-18
- Tai, W. T. (2004). *The lateral-torsional buckling analysis of composite laminated beams* (MSc thesis, Feng Chia University, Taiwan ROC).
- Timoshenko, S. P., & Gere, J. M. (1961). *Theory of elastic stability*. 1961. McGrawHill-Kogakusha Ltd, Tokyo.
- Vlassov, V. Z. (1961). *Thin-walled beams* (2nd Ed.) Israel Program for Scientific Translation.

Chapter 2 - Literature Review

2.1 Background

Prandtl and Michell independently investigated the earliest theoretical analysis of lateral stability of beams in 1899. They constructed a beam of narrow rectangular cross-section, simply supported at both ends, and loaded by uniform moment (Narayanan, 1983). Since then many authors continued to develop and research the lateral-torsional problems, such as Timoshenko and Gere (1961) who considered the effect of warping on the torsional aspects of the problem for I-sections. The following sections in this chapter will overview the works done by other researchers on the lateral torsional buckling of isotropic beams and special composite beams.

2.2 Previous Research on Isotropic Beams

One of the first theoretical investigations on the lateral stability of thin-walled beams was conducted by Timoshenko and Gere (1961). Their analytical study aimed at developing critical load expressions for thin-walled beams under three different loading and boundary conditions:

Simply supported beams under pure bending moments

Cantilever beams subjected to free end load

Simply supported beams subjected to concentrated load at mid-span.

Timoshenko and Gere (1961) obtained the critical moment (Eq. 2.1) for pure bending case (1). Eqs. 2.2 and 2.3 were obtained for the loading cases (2) and (3), respectively. All of the three presented equations were for narrow rectangular section beams where warping effects are neglected, which is a major contributing factor for I-section beams.

$$(M_0)_{cr} = \frac{\pi}{L} \sqrt{EI_y' GJ} \quad (2.1)$$

$$P_{cr} = \frac{4.013 \sqrt{EI_y' GJ}}{L^2} \quad (2.2)$$

$$P_{cr} = \frac{16.94\sqrt{EI_y'GJ}}{L^2} \quad (2.3)$$

Equations 2.2 and 2.3 were obtained by applying the loads at the shear center. They also presented Eqs. 2.4 and 2.5 when the load was applied at a vertical distance (a) from the shear center for cases (2) and (3), respectively.

$$P_{cr} = \frac{4.013\sqrt{EI_y'GJ}}{L^2} \left(1 - \frac{a}{L} \sqrt{\frac{EI_y'}{GJ}} \right) \quad (2.4)$$

$$P_{cr} = \frac{16.94\sqrt{EI_y'GJ}}{L^2} \left(1 - \frac{1.74a}{L} \sqrt{\frac{EI_y'}{GJ}} \right) \quad (2.5)$$

Where E is the modulus of elasticity, I_y' is the out of plane moment of inertia, L is the length of the beam, G is shear modulus of elasticity, J is torsional moment of inertia and a is the vertical distance of applied load from the centroid of the section.

2.3 Previous Research on Composite Beams

While research on lateral-torsional buckling of composite beams can be traced back to several decades, most analytical and experimental investigations were carried out in 1990s. A review of available works was presented by Stoddard (1997) and Zhang (2000). This review included the works performed by Mottram (1992), Barbero and Raftoyiannis (1994), Pandey et al (1995), Turvey and Brooks (1996), Razzaq et al (1996), and Davalos and Qiao (1997). Stoddard also reported an experimental investigation of 35 different fiber reinforced polymer I-beams which were simply supported and subject to concentrated loads acting on top flanges at the mid-span.

Previous analytical work performed by Mottram (1992), Pandey et al (1995) and Stoddard (1997) adopted the formulations developed by Bauld and Lih-Shyng (1984) who presented a Vlassov type theory for symmetrical laminated thin-walled composite beams with open cross sections. The constitutive relations between beam forces and displacements were

adopted by Bauld and Lih-Shyng. However, the fundamental assumptions for the derivation of the constitutive relations were originally made from isotropic thin plates. Volovoi et al (1999) pointed out that these assumptions are not suitable for composite thin plates.

Mottram (1992) applied a finite difference approach to solve the governing differential equations obtained by Timoshenko and Gere (1961) to obtain a closed form expression for lateral-torsional buckling loads of fixed end beams subject to concentrated loads at mid-span. Mottram, in this formulation, replaced the isotropic material properties by the corresponding properties of special composite materials. He also conducted experimental test and compared the tests with the analytical formulation. It was found that the analytical formulations were close to the experimental tests. He concluded that the analysis was valid for thin-walled composite doubly symmetric I-beams made from mid-plane symmetric fiber reinforced laminates. His modified formulas might not correctly predict actual composite beam behaviors since the governing differential equations were originally derived for isotropic I-beams and the tested beams were made of orthotropic materials.

Additional analytical investigations of fiber reinforced-polymer I-beams under various loading and boundary conditions were reported by Pandey et al (1995) following the work of Bauld and Lih-Shyng (1984) and that of Mottram (1992). The primary purpose of the study was to find the optimal direction of fibers in the web and flange which maximizes buckling loads. It was concluded that the web fiber angle had an important influence on improving the lateral-torsional buckling load as the beam span becomes longer. A group of closed form expressions for I-beams with different loading and boundary conditions were obtained by using the Galerkin method to solve the equilibrium differential equations. They used energy method, which includes the two coupling terms, H_s and H_c , to obtain the equilibrium differential equations. These two

coupling terms were, however, ignored in the equilibrium differential equations for simplicity. The effects of the two terms on the lateral-torsional buckling were left unknown since no investigation were performed on these two coupling terms. Therefore, the composite material properties were not properly considered in the research. In addition, the constitutive relations between beam forces and beam displacements used in the research was adopted from Bauld and Lih-Shyng's work, which does not consider composite material properties properly in the constitutive relations. Hence, there is no confidence to consider the obtained closed form expressions to be correct for composite I-beams.

Davalos and Qiao (1997) employed the non-linear elastic theory to develop a stability solution for lateral-distortional buckling for composite wide flange beams based on the principle of total potential energy and used a Rayleigh-Ritz method to obtain numerical solutions. An I-beam was divided into top, bottom and web plates in the potential energy calculation. A fifth-order polynomial shape function was adopted for the displacement field construction. A 6x6 matrix for the relations of panel strains and stresses was shown in the research. Since the matrix was quite complicated, closed form expressions were very difficult to obtain. By assuming $B_{ij}=0$, $A_{16}=A_{26}=D_{16}=D_{26}=0$, only one closed form expression for simply supported beams with the load applied at the centroid of mid-span was given.

Lin et al. (1996) studied the stability of thin-walled composite member using the finite element method. Seven degrees of freedom at each node for each two-nodded element were used to model the fiber reinforced plastic. The seven degrees of freedom are the dependent translations in three perpendicular directions and the corresponding rotations in addition to the angle of warping. The stiffness matrices of a beam element were used to develop the element shape functions. A number of examples of thin walled-open sections were solved, different cross

sections like channels, I sections, and Z-sections were tested as well as different boundary conditions. The study concluded the importance of the influence of in-plane shear strain on the critical buckling load for lateral torsional buckling and combined torsional and flexural modes. It also minimized the significance of shear strain effect on critical buckling when the buckling happens in terms of a flexural mode.

Hodges and Peter (1975) developed a general lateral buckling equation for a rectangular cantilever beam subjected to a concentrated load at the centroid of the free end, with the effect of the pre-buckling deflection included in the general equation. Kollar (2001) presented a stability analysis of thin walled composite columns under axial loading conditions. A closed form solution was derived using a modified version of Vlassov's classical theory (1961) for isotropic material to account for the composite action. The effect of shear deformation in the in-plane displacements and in the restrained warping was examined and a shear matrix was formulated in addition to the bending matrix. Lee et al. (2002) studied the lateral buckling of composite laminated beams. An analytical approach based on the classical lamination theory was derived for different boundary conditions and different laminate stacking sequences. The examined beams were tested under various loading configurations and various locations. The beams were then compared against a one dimensional finite element model under different load configurations. The model showed a good agreement against the finite element model of simply supported I beam in cases of pure bending, uniformly distributed loads, and central point load. Yet, the model was not appropriate for pure bending with off-axis fiber orientation due to coupling stiffness.

Sapkas and Kollar (2002) offered closed form solutions for simply supported and cantilever, thin walled, open section, orthotropic composite beams subjected to concentrated end

moments, concentrated forces, or uniformly distributed load. The solution indirectly accounted for shear deformation by adjusting the bending and warping stiffness of the composite beams. Qiao et al. (2003) formulated an analytical solution for flexural-torsional buckling of composite cantilever I beams based on an energy method developed from the non-linear plate theory. A good agreement against finite element method was obtained. Furthermore, four different cantilever beams were tested experimentally under tip loads to examine the flexural-torsional response. Also, good agreements were shown against the experimental results.

Kotelko (2004) presented a theoretical analysis of local buckling which represents material failure. This study covered different cross sections of thin walled beams and columns. These cross sections varied between lipped and plain channels as well as box-section. This theory matched previous theories in a way that it depends on the rigid-plastic model. Yet, it mainly differs by considering a constitutive strain-hardening of the used material. This analytical approach is particularly useful in the initial phase of design process and may be applied as a simplified design tool at the early stage of design process, including crush-oriented design. Karaagac et al. (2007) tested the stability of a cantilever laminated composite beam under static and dynamic conditions. A linear translation spring was attached to the beam to control the lateral deformation. The attached elastic support location varied between the free end and the mid-span of the beam. Length-to-thickness ratio, variation of cross-section in one direction, orientation angle, static and dynamic load parameters, stiffness and position of the elastic support were the main variables to study the stability of the beam. Numerical polynomial approximations for the displacements and the angle of twist were derived and showed a reasonable accuracy against the finite element method.

Machado (2010) derived an analytical solution for lateral stability of cross-ply laminated thin-walled simply supported bisymmetric beams subjected to combined axial and bending loads. The presented theory included shear deformability and took into account large displacements and rotations; moderate bending rotations and large twisting angles. The proposed solution also examined the nonlinear pre-buckling geometrical deformation for more accurate representation of the lateral stability conditions. The buckling loads obtained analytically were, in general, in good agreement with the bifurcation loads observed in the post buckling response. The study concluded that the buckling moments computed from classical theory is overestimated. Also, it presented pre-buckling and post buckling displacement curves to relate the stiffness behavior of the beam to the applied loads and also to study the fiber orientation against the buckling loads.

Bank and Bednarczyk (1988) and Barbero et al. (1993) developed simple expressions for the bending, torsional, and warping stiffness of composite laminated beams. Sherbourne and Kabir (1995) studied an analytical study of the transvers shear strain effect on the lateral buckling of thin-walled, open-section fibrous composite beams. They applied uniformly distributed and transverse central point loads on simply supported and clamped I-beams. They used an analytic-numerical moment method to solve a coupled system of differential equations which they obtained by considering a series function which satisfies boundary condition. They found out that the shear factor drops buckling load in short-span composite beams under concentrated load.

Roberts and Al-Ubaidi (2001) studied influence of shear deformation on restrained torsional warping of pultruded FRP bars of open cross-section by proposing an approximate theory. They concluded that influence of shear deformation on restrained torsional warping is practically negligible for thin walled pultruded FRP I-beams. They performed a series of bending

and torsion tests to confirm their conclusion. They suggest that full section properties should be used for study of the coupled bending and torsional response for such members. Tai (2004) studied lateral- torsional buckling of symmetrically laminated, rectangular cross-section, composite beams under various loading conditions. Discrepancies between his results and the finite element results were detected for various symmetric laminations. A formal engineering approach of mechanics of thin-walled laminated beams based on kinematic assumptions was studied by Barbero, et al. (1993). This approach was consistent with Timoshenko beam theory. They considered thin-walled composited beams with open or closed cross section subjected to bending and axial load. They obtained beam stiffness coefficients accounting for the cross section geometry and for the material anisotropy. They derived an explicit expression for the static shear correction factor of thin-walled composite beams from energy equivalence.

2.4 References

- Bank, L. C., & Bednarczyk, P. J. (1988). A beam theory for thin-walled composite beams. *Composites Science and Technology*, 32(4), 265-277.
- Barbero, E. J., Lopez-Anido, R., and Davalos, J.F. (1993). "On the Mechanics of Thin-Walled Laminated Composite Beams." *Journal of Composite Materials*, 27(8), 806-829
- Barbero, E. J. and Raftoyiannis, I. G. (1994), "Lateral and Distortional Buckling of Pultruded I-Beams", *Composite Structures*, Vol. 27, pp. 261-268.
- Bauld, N. R., & Lih-Shyng, T. (1984). A Vlasov theory for fiber-reinforced beams with thin-walled open cross sections. *International Journal of Solids and Structures*, 20(3), 277-297.
- Davalos, J. F., Qiao, P., & Salim, H. A. (1997). Flexural-torsional buckling of pultruded fiber reinforced plastic composite I-beams: experimental and analytical evaluations. *Composite Structures*, 38(1-4), 241-250.
- Hodges, D. H. and Peters, D. A. (1975), "On the lateral buckling of uniform slender cantilever beams", *International Journal of Solids and Structures*, Vol. 11, pp. 1269-1280.
- Karaagac, C., Öztürk, H., & Sabuncu, M. (2007). Lateral dynamic stability analysis of a cantilever laminated composite beam with an elastic support. *International Journal of Structural Stability and Dynamics*, 7(03), 377-402.
- Kollar, L. P. (2001). "Flexural-torsional buckling of open section composite columns with shear deformation." *International Journal of Solids and Structures*, 38, 7525-7541
- Kotelko, M. (2004). "Load-capacity estimation and collapse analysis of thin-walled beams and columns—recent advances". *Thin-walled Structures*, Vol. 42, No.2, PP.153-175
- Lee, J., Kim, S.-E., Hong, K. (2002). "Lateral buckling of I-section composite beams." *Engineering Structures*, 24, 955-964
- Lin, Z. M., Polyzois, D., and Shah, A. (1996). "Stability of Thin-walled Pultruded Structural Members by the Finite Element Method." *Thin-Walled Structures*, 24, 1-18
- Machado, S. P. (2010). "Interaction of combined loads on the lateral stability of thin-walled composite beams." *Engineering Structures*, 32, 3516-3527
- Michell, A. G. M. (1899). "Elastic stability of long beams under transverse forces." *Philosophical Mag.*, 48, 298.
- Mottram, J. T. (1992a), "Lateral-Torsional buckling of Thin-Walled Composite I-Section Beams by the Finite Difference Method", *Composites Engineering*, Vol. 2, No. 2, pp. 91-104.

- Narayanan, R. (1983). *Beams and beam columns: Stability and strength*. London; New York: New York, NY, USA: Applied Science; Sole distributors in the USA and Canada, Elsevier Science Pub.
- Pandey, M.D., Kabir, M.Z., and Sherbourne, A.N. (1995). "Flexural-Torsional Stability of Thin-Walled Composite I-Section Beams." *Composites Engineering*, 5(3), 321-342
- Prandtl, L. (1899). *Kipperscheinungen*. Dissertation, Munich.
- Qiao, P., Zou, G., and Davalos, J. (2003). "Flexural-torsional buckling of fiber-reinforced plastic composite cantilever I-beams." *Composite Structures*, 60, 205-217
- Razzaq, Z., Prabhakaran, R., & Sirjani, M. M. (1996). Load and resistance factor design (LRFD) approach for reinforced-plastic channel beam buckling. *Composites Part B: Engineering*, 27(3-4), 361-369.
- Roberts, T.M., Al-Ubaidi, H. (2001). "Influence of shear deformation on restrained torsional warping of pultruded FRP bars of open cross-section." *Thin-Walled Structures*, 39, 395-414
- Sapkás, Á., & Kollár, L. P. (2002). Lateral-torsional buckling of composite beams. *International Journal of Solids and Structures*, 39(11), 2939-2963.
- Sherbourne, A. N., Kabir, M. Z. (1995). "Shear Strain Effects in Lateral Stability of Thin-Walled Fibrous Composite Beams." *Journal of Engineering Mechanics*, 640-647
- Stoddard, W. P. (1997). *Lateral-torsional buckling behavior of polymer composite I-shaped members* (Doctoral dissertation, Georgia Institute of Technology).
- Tai, W. T. (2004). *The lateral-torsional buckling analysis of composite laminated beams* (MSc thesis, Feng Chia University, Taiwan ROC).
- Timoshenko, S. P., & Gere, J. M. (1961). *Theory of elastic stability*. 1961.McGrawHill-Kogakusha Ltd, Tokyo.
- Turvey, G. J., & Brooks, R. J. (1996, January). Lateral buckling tests on pultruded GRP I-section beams with simply supported-simply supported and clamped-simply supported end conditions. *In First International Conference on Composites in Infrastructure*.
- Vlassov, V. Z. (1961). *Thin-walled beams* (2nd ed.) Israel Program for Scientific Translation.
- Volovoi, V. V., Hodges, D. H., Berdichevsky, V. L., & Sutyryn, V. G. (1999). Asymptotic theory for static behavior of elastic anisotropic I-beams. *International Journal of Solids and Structures*, 36(7), 1017-1043.
- Zhang, S. (2000). *Lateral-torsional buckling of simply supported and cantilevered fiber reinforced polymeric I-beams* (Doctoral dissertation, Georgia Institute of Technology).

Chapter 3 - Lateral-Torsional Buckling of Anisotropic Laminated Thin-Walled Rectangular Composite Beams Subjected to Pure Bending in Simply Supported Condition

In this chapter, a generalized analytical approach for lateral-torsional buckling of simply supported anisotropic, thin-walled, rectangular cross-section beams under pure bending condition was developed using the classical laminated plate theory (CLPT) as a basis for the constitutive equations. Buckling of such type of members has not been addressed in the literature. A closed form buckling expression is derived in terms of the lateral, torsional and coupling stiffness coefficients of the overall composite. These coefficients are obtained through dimensional reduction by static condensation of the 6x6 constitutive matrix mapped into an effective 2x2 coupled weak axis bending-twisting relationship. The stability of the beam under different geometric and material parameters, like length/height ratio, layer thickness, and ply orientation, was investigated. The analytical formula is verified against finite element buckling solutions using ABAQUS for different lamination orientation showing excellent accuracy.

3.1 Introduction

Thin-walled beam structures are major components in many engineering applications. They are widely used as structural components in many types of systems in the field of civil, mechanical, and aerospace engineering. Advanced materials, mainly fiber reinforced polymer (FRP) composites, are partially replacing conventional materials in these types of structural systems. Composites are being implemented in transportation systems, offshore structures, chemical facilities, aircraft wings and fuselage, helicopter blades, and so on. This increase in interest for using FRP lies in some critical advantages of FRP over conventional materials. Their

high strength to weight ratio, their environmental adaptability, their ease of transportation and erection, and their fatigue resistance are some of the advantages FRP provide. The most prominent characteristic is the ability of tailoring the material for each particular application. Structural properties depend on the material system and the shape of the cross-section of the member (Barbero et al., 1993). For isotropic structural shapes, it is possible to optimize the section to increase the bending stiffness without compromising the maximum bending strength. Unlike isotropic shapes, with composite beams it is possible to optimize the material itself by choosing among a variety of resins, fiber systems, and fiber orientations. Although FRP structures exhibit high strength, problems of excessive deformation and instability, due to their low stiffness and slenderness of the member, are the major disadvantages in wider acceptance for structural engineering applications (Lin et al. 1996). Because of these limitations, the new generation of composite structures should be designed to work in a safe way and to experience higher performance than the conventional systems. Consideration of stability and deformation limits tend to be the governing design criteria for FRP structures before these structures reach material failure. Thus, the proper establishment of such criteria is an important prerequisite to the practical use of FRP in engineering applications.

A thin-walled slender beam subjected to bending moments about the strong axis may buckle by a combined lateral bending and twisting of the cross-section. This phenomenon is known as lateral-torsional buckling. Theory of thin-walled open section beams including axial constraints for isotropic materials was developed by Vlassov (1961). This classical theory neglects the shear deformation in the middle surface of the wall so that for the composite beams, the shear deformations may significantly increase the displacements and reduce the buckling

loads. The shear deformation theory for transversely loaded isotropic beams was developed by Timoshenko and Gere (1961).

For the composite thin-walled beams, Bauld and Lih-Shyng (1984) applied Vlasov's theory for open section composite beams with symmetrical laminated walls neglecting the shear deformation. Bank and Bednarczyk (1988) and Barbero et al. (1993) developed simple expressions for the bending, torsional, and warping stiffness of composite laminated beams. Sherbourne and Kabir (1995) studied analytically the effect of transverse shear strain on the lateral buckling of thin-walled, open-section fibrous composite beams. Pandey et al. (1995) proposed an analytical formulation for finding the optimal direction of fiber for improving the lateral buckling strength of thin-walled I-section composite beams. Lin et al. (1996) studied buckling problems of thin-walled composite structural members by finite element methods. Kollar (2001) suggested a closed form solution for thin-walled open section columns, made of orthotropic composite materials, by considering flexure, shear and the torsional warping induced shear deformations. Roberts and Al-Ubaidi (2001) studied the influence of shear deformation on restrained torsional warping of pultruded FRP bars of open cross-section by proposing an approximate theory. Sapkas and Kollar (2002) studied the stability analysis of thin-walled, open section beams, made of orthotropic composite materials under various loading conditions. Lee et al. (2002) presented a general analytical model applicable to the lateral buckling of composite laminated I-beams subjected to various types of loadings. Qiao et al (2003) presented a combined analytical and experiment evaluation of flexural-torsional buckling of fiber reinforced polymer composite I-beams. Tai (2004) studied lateral- torsional buckling of symmetrically laminated, rectangular cross-section, composite beams under various loading conditions. Karaagac et al. (2007) studied static and dynamic stability of cantilever laminated symmetric and

anti-symmetric composite beams having elastic support. Machado (2010) studied the stability of simply supported thin-walled symmetric laminated composite I-beams subjected to combined axial and lateral loads by approximate analytical solutions and compared them with numerical results.

Most of the work, concerning the lateral- torsional stability of thin-walled composite beams, was focused on I-sections. The beams were either considered to be of symmetric layup, anti-symmetric layup, orthotropic, or pultruded nature. There hasn't been any study recorded on the behavior of general anisotropic laminated composite beams to the best knowledge of the author.

In the present study, a generalized analytical model applicable to the lateral-torsional buckling of a simply supported rectangular cross-section beam, made of anisotropic laminated composite material, subjected to pure bending is developed. This model is based on the classical laminated plate theory (CLPT), and accounts for the arbitrary laminate stacking sequence configurations. A finite element model is developed in ABAQUS to predict critical buckling moments and compare with the results obtained from the analytical model. The effects of fiber orientation, beam length/height ratios and wall thickness on the critical buckling moments are studied.

3.2 Analytical Formulation

A simply supported laminated composite beam with length L and a thin rectangular cross section is subjected to pure bending at the ends, as shown in Figure 3.1. The beam tends to buckle under a lateral-torsional behavior because of its small thickness.

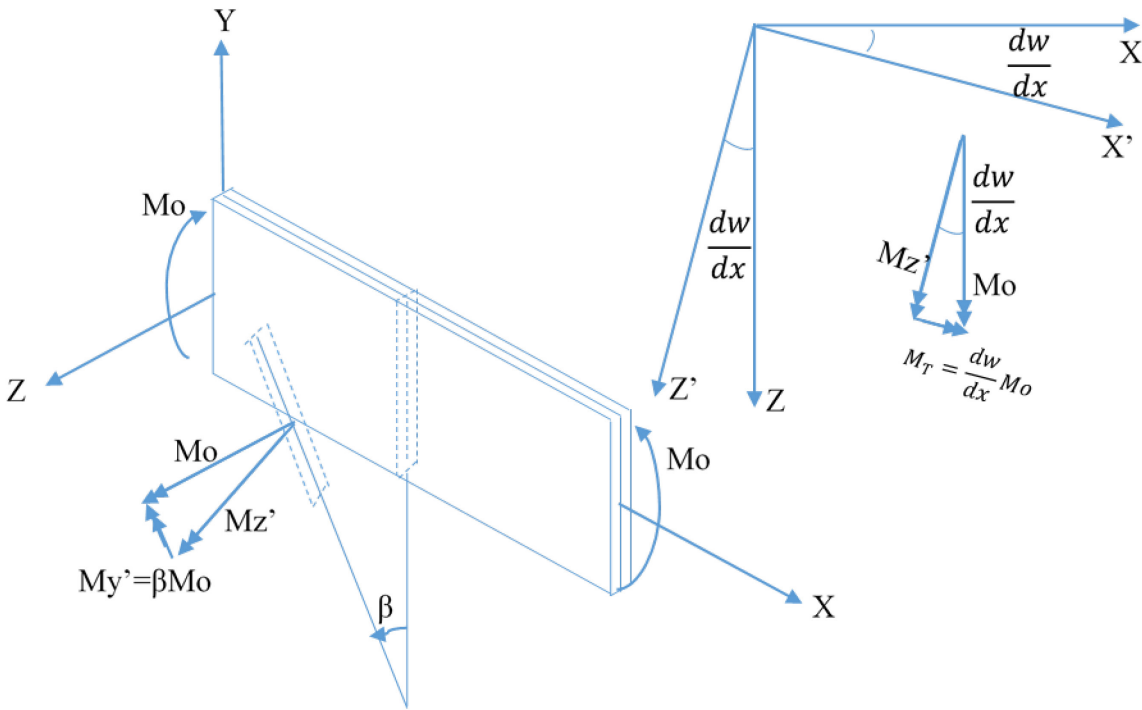


Figure 3.1 A deformed laminated beam subjected to pure bending

The model in this study is based on the classical laminated plate theory, Kollar and Springer (2003) and Barbero (1999). The following assumptions are adopted from the classical laminated plate theory:

1. The normals to mid-plane (reference surface) of the laminate remain normal and straight after deformation.
2. The normal to mid-plane of the laminate do not change length – in other words, the thickness of the laminate stays constant.
3. The shear deformations are neglected.
4. The laminate consists of perfectly bonded layers.
5. The stress-strain relationships are applied under plane-stress conditions.

3.2.1 Kinematics

Based on the assumptions in the classical laminated plate theory, the displacement components u , v , w representing the deformation of a point on the plate profile section are given with respect to mid-surface displacements u_0 , v_0 , and w_0 as follows:

$$u(x, y, z) = u_0(x, y) - z \frac{\partial w_0}{\partial x}(x, y) \quad (3.1)$$

$$v(x, y, z) = v_0(x, y) - z\beta(x, y) \quad (3.2)$$

$$w(x, y, z) = w_0(x, y) \quad (3.3)$$

where $\beta = \frac{\partial w_0}{\partial y}$

The strains associated with small displacements from the theory of elasticity are given by

$$\varepsilon_x = \varepsilon_x^0 + z\kappa_x \quad (3.4)$$

$$\varepsilon_y = \varepsilon_y^0 + z\kappa_y \quad (3.5)$$

$$\gamma_{xy} = \gamma_{xy}^0 + z\kappa_{xy} \quad (3.6)$$

where

$$\varepsilon_x^0 = \frac{\partial u_0}{\partial x}, \varepsilon_y^0 = \frac{\partial v_0}{\partial y}, \text{ and } \gamma_{xy}^0 = \frac{\partial u_0}{\partial y} + \frac{\partial v_0}{\partial x} \quad (3.7)$$

$$\kappa_x = -\frac{\partial^2 w_0}{\partial x^2}, \kappa_y = -\frac{\partial \beta}{\partial y}, \text{ and } \kappa_{xy} = -\left(\frac{\partial^2 w_0}{\partial x \partial y} + \frac{\partial^2 w_0}{\partial y \partial x}\right) = -2\frac{\partial \beta}{\partial x} \quad (3.8)$$

3.2.2 Constitutive Equations

The plate stiffness equations based on classical laminated plate theory, shown in Figure 3.2, are given as follows.

$$\begin{Bmatrix} N_x = 0 \\ N_y = 0 \\ N_{xy} = 0 \\ M_x \\ M_y = 0 \\ M_{xy} \end{Bmatrix} = h \begin{bmatrix} A_{11} & A_{12} & A_{16} & B_{11} & B_{12} & B_{16} \\ A_{12} & A_{22} & A_{26} & B_{11} & B_{12} & B_{16} \\ A_{16} & A_{26} & A_{66} & B_{11} & B_{12} & B_{16} \\ B_{11} & B_{12} & B_{16} & D_{11} & D_{12} & D_{16} \\ B_{12} & B_{22} & B_{26} & D_{12} & D_{22} & D_{26} \\ B_{16} & B_{26} & B_{66} & D_{16} & D_{26} & D_{66} \end{bmatrix} \begin{Bmatrix} \varepsilon_x \\ \varepsilon_y \\ \gamma_{xy} \\ \kappa_x \\ \kappa_y \\ \kappa_{xy} \end{Bmatrix} \quad (3.9)$$

where

$$A_{ij} = \sum_{k=1}^N (\bar{Q}_{ij})_k t_k \quad i, j = 1, 2, 6 \text{ are called extensional stiffness coefficients}$$

$$B_{ij} = \sum_{k=1}^N (\bar{Q}_{ij})_k t_k \bar{z}_k \quad i, j = 1, 2, 6 \text{ are called extension-bending coupling stiffness coefficients and}$$

$$D_{ij} = \sum_{k=1}^N (\bar{Q}_{ij})_k \left(t_k \bar{z}_k^2 + \frac{t_k^3}{12} \right) \quad i, j = 1, 2, 6 \text{ are called bending stiffness coefficients}$$

$(\bar{Q}_{ij})_k$ are the components of the k^{th} layer 2D transformed constitutive matrix in the beam coordinate system

\bar{z}_k is the depth from the middle surface to the centroid of the k^{th} layer, and t_k is the thickness of k^{th} layer.

Knowing the zero components of externally applied forces and moments for the pure bending condition from Figure 3.1, which are expressed in Eq. 3.9, the stiffness matrix can be simplified and dimensionally reduced to an effective 2x2 stiffness matrix by using the static condensation technique:

$$\begin{Bmatrix} M_x \\ M_{xy} \end{Bmatrix} = h \begin{bmatrix} D_Y & D_{YT} \\ D_{YT} & D_T \end{bmatrix} \begin{Bmatrix} \kappa_x \\ \kappa_{xy} \end{Bmatrix} \quad (3.10)$$

where

$$\begin{bmatrix} D_Y & D_{YT} \\ D_{YT} & D_T \end{bmatrix} = \begin{bmatrix} D_{11} & D_{16} \\ D_{16} & D_{66} \end{bmatrix} - \begin{bmatrix} B_{11} & B_{16} \\ B_{12} & B_{26} \\ B_{16} & B_{66} \\ D_{12} & D_{26} \end{bmatrix}^T \begin{bmatrix} A_{11} & A_{12} & A_{16} & B_{12} \\ A_{12} & A_{22} & A_{26} & B_{22} \\ A_{16} & A_{26} & A_{66} & B_{26} \\ B_{12} & B_{22} & B_{26} & D_{22} \end{bmatrix}^{-1} \begin{bmatrix} B_{11} & B_{16} \\ B_{12} & B_{26} \\ B_{16} & B_{66} \\ D_{12} & D_{26} \end{bmatrix}$$

D_Y is the composite lateral stiffness coefficient, D_T is the composite twisting stiffness coefficient, and D_{YT} is the composite lateral-twisting coupling coefficient. In most cases, where the layers are symmetric, anti-symmetric, cross-ply, special angle ply, D_{YT} coefficient will be zero. However, for the generally anisotropic cases, D_{YT} coefficient is not zero and will play a significant role in determining the buckling moments of the beams.

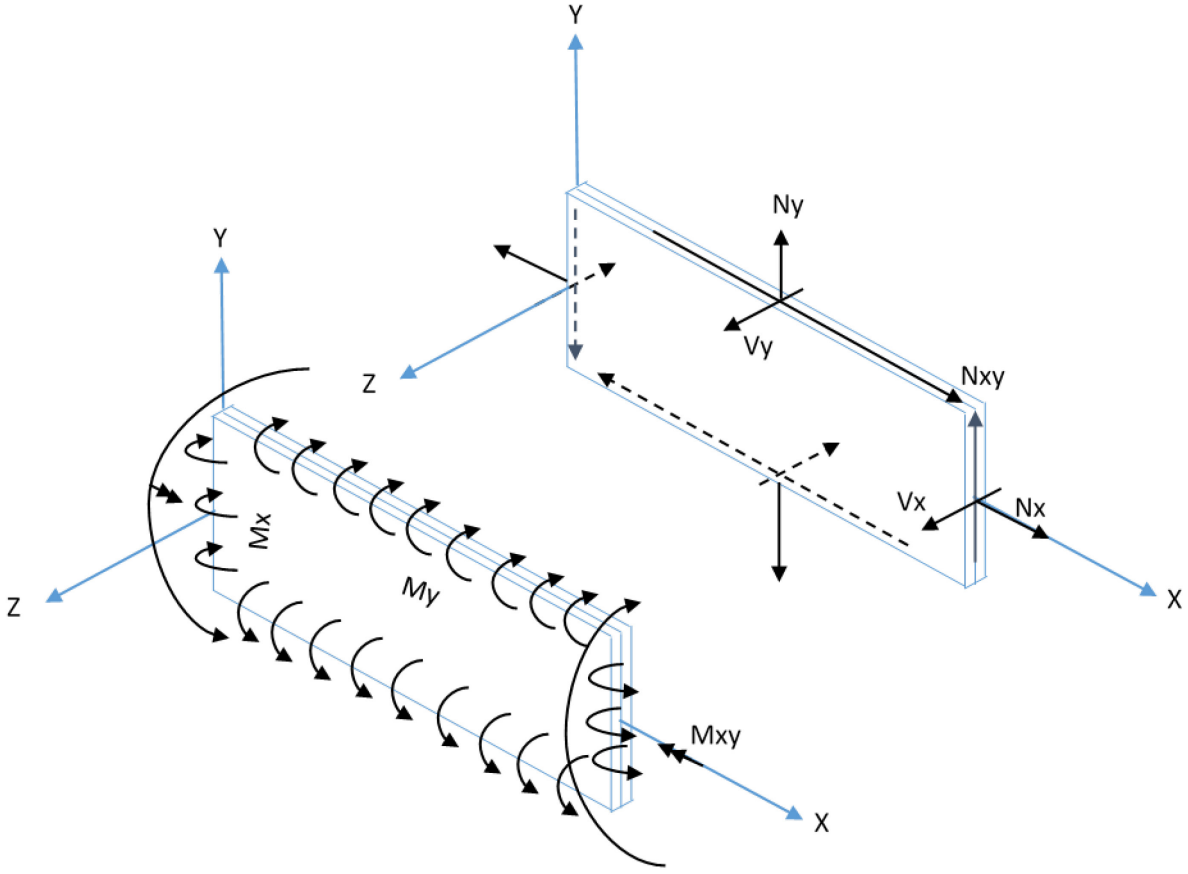


Figure 3.2 Force and moment resultants on a beam based on classical laminated plate theory

Referring to Figure 3.1 (structural) and Figure 3.2 (laminated), the bending moment M_y in structural coordinate is replaced by M_x in laminate coordinate, on the other hand, the shear moment, M_{xy} , in laminate coordinate is in the opposite direction of twisting moment in the structural coordinate system and is found by Kollar and Springer (2003) to be $T = -2 M_{xy}$. Substituting the curvatures in terms of displacement and rotation in Eq. 3.8 into Eq. 3.10, and writing the moments in structural coordinates systems, the following relation will be obtained

$$\begin{Bmatrix} M_{y'} \\ -M_T \end{Bmatrix} = h \begin{bmatrix} D_Y & 2D_{YT} \\ 2D_{YT} & 4D_T \end{bmatrix} \begin{Bmatrix} -\frac{d^2w}{dx^2} \\ -\beta' \end{Bmatrix} \quad (3.11)$$

3.2.3 Equilibrium Equations

Figure 3.1 shows the components of external moments before and after deformation and is obtained as following.

External moments in un-deformed configuration (original axes):

$$M_z = M_o \text{ (Applied Moment)} \quad (3.12)$$

$$M_T = M_y = 0 \quad (3.13)$$

External moments in the deformed configuration (deformed axes):

$$M_z' = M_z = M_o \quad (3.14)$$

$$M_y' = \beta M_o \quad (3.15)$$

$$M_T = M_x' = \frac{dw}{dx} M_o \quad (3.16)$$

The following system of differential equation is obtained after substituting the external moments from Eqs. 3.15 and 3.16 into Eq. 3.11:

$$\begin{Bmatrix} \beta M_o \\ -\frac{dw}{dx} M_o \end{Bmatrix} = h \begin{bmatrix} D_Y & 2D_{YT} \\ 2D_{YT} & 4D_T \end{bmatrix} \begin{Bmatrix} -\frac{d^2w}{dx^2} \\ -\beta' \end{Bmatrix} \quad (3.17)$$

$$-hD_Y \frac{d^2w}{dx^2} - 2hD_{YT}\beta' = \beta M_o \quad (3.18)$$

$$-2hD_{YT} \frac{d^2w}{dx^2} - 4hD_T\beta' = -\frac{dw}{dx} M_o \quad (3.19)$$

Writing Eqs.3.18 and 3.19 in terms of $\frac{d^2w}{dx^2}$ and equating the two expressions, the following relationship can be obtained.

$$\frac{1}{D_Y} [-2hD_{YT}\beta' - \beta M_o] = \frac{1}{2D_{YT}} \left[-4hD_T\beta' + \frac{dw}{dx} M_o \right] \quad (3.20)$$

Differentiating Eq. 3.20 with respect to x and rearranging the resulting expression in terms of $\frac{d^2w}{dx^2}$, Eq.3.21 will be obtained.

$$\frac{d^2w}{dx^2} = -\frac{2D_{YT}}{D_Y}\beta' + \frac{4h}{M_o}\left[D_T - \frac{D_{YT}^2}{D_Y}\right]\beta'' \quad (3.21)$$

Equating the left hand side of Eq.3.20, which is equal to $\frac{d^2w}{dx^2}$ in Eq. 3.18, and the right hand side of Eq.3.21, the resulting expression reduces to a second order ordinary differential equation with constant coefficients, which can be solved analytically.

$$\beta'' + \frac{M_o^2}{4h^2[D_Y D_T - D_{YT}^2]}\beta = 0 \quad (3.22)$$

Setting $\kappa^2 = \frac{M_o^2}{4h^2[D_Y D_T - D_{YT}^2]}$, yields an equation similar to the isotropic condition when the warping effect is neglected.

$$\beta'' + \kappa^2\beta = 0 \quad (3.23)$$

The general solution for this type of differential equation is known to be:

$$\beta = A\sin(kx) + B\cos(kx) \quad (3.24)$$

Applying boundary condition for pure bending as $\beta(0) = \beta(L) = 0$, the critical buckling moment can be obtained according to the following equation.

$$M_{ocr} = \frac{\pi h}{L}\sqrt{4(D_Y D_T - D_{YT}^2)} \quad (3.25)$$

3.3 Numerical Analysis (FEA)

The finite element method in the commercial software, ABAQUS/Standard (implicit) was used to simulate the problem in this study. The model was first created by using 3D planar shells. The shells were assembled based on the stacking arrangement that was used in the analytical solution. The global x-axis was used along beams length, but the local coordinate system was used based on the orientation of the fibers in each ply.

The boundary conditions for this beam were applied as follows. The four corners of the beam, shown in Figure 3.3, were constrained from moving in z-direction. One end of the beam was pinned at mid-height restraining it from all displacements, and a roller was applied at mid-height of other end of the beam to restrain displacement in the y-direction only, as shown in the Figure 3.3.

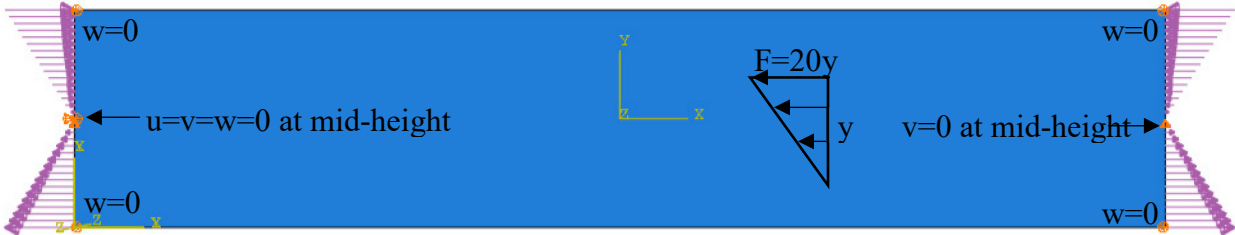


Figure 3.3 Applied load and boundary conditions

A linear shell-edge load was applied at both ends of the beam as tension and compression stresses to create a pure bending moment condition in the beam, as shown in Figure 3.3. Each edge was partitioned into two parts to apply shell-edge load linearly in the desired direction. The following relation was used to determine the magnitude of the linear load.

$$F_x = 20y \tag{3.26}$$

There is no load applied at the mid-height of the edge and the load increases linearly by $20y$, which will act as a pure bending moment when applied as compression above the mid-height and as tension below the mid-height.

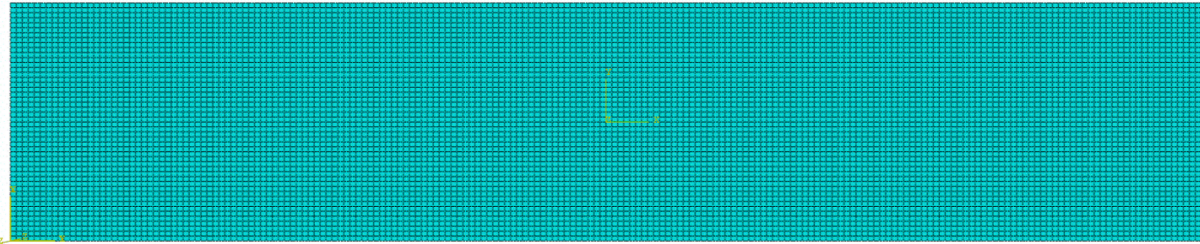


Figure 3.4 Applied shell element type (S8R) and mesh (element size along beam axis: 2.5 mm)

The beam was meshed with a standard quadratic quadrilateral shell element type of S8R (8-node doubly curved thick shell element with reduced integration) using six degrees of freedom per node and an element size of 2.5 mm along beam axis. A beam with $L = 500$ mm and $h = 100$ mm gives total number of 29297 nodes and 9600 elements, as shown in Figure 3.4.

The eigenvalue buckling analysis in ABAQUS solver, which is a linear perturbation procedure, determines the eigenvalue of the buckling mode. ABAQUS extracts the eigenvalues and eigenvectors for symmetric stiffness matrices only. In order to symmetrize the stiffness matrix of the model, Lanczos iteration eigenvalue extraction method was used. To find the critical moment, based on the ABAQUS user guide, the lowest eigenvalue is multiplied by the moment which was applied at the ends of the beam in combined tension and compression line edge loading.

$$M_{0cr} = \lambda M_0 \quad (3.27)$$

3.4 Results

3.4.1 Material Properties and Stacking Sequences

An anisotropic composite material is made by stacking four layers of the lamina properties shown in Table 3.1 at different fiber orientations. The thickness of each layer is the same with the same orthotropic properties, yet it varies in terms of fiber orientation. The orientation of fiber in each layer can be randomly picked, including common laminate types such as symmetric laminates, antisymmetric laminates, balanced laminates, and so on. The stacking sequence starts from the back of the beam to the front of the beam to follow the same order used for typical laminated plates, Figure 3.5. For example, $[30/0/0/-30]$ means that the first ply has an angle of 30 degrees from the x-axis of the beam is placed in the back of the beam counter

clockwise (towards the y-axis) and the other layers follow with the same order through the positive z-axis. Figure 3.5 shows the stacking sequence of the laminates. Different layer thicknesses of (0.05, 0.1, 0.15, and 0.2 mm) and length to height ratios of (2, 5, 10, 20, and 50) were also studied which will be presented later.

Table 3.1 Material properties used the in laminates

| Material | FRP | |
|------------|----------|-----|
| E11 | 142730 | MPa |
| E22 | 13790 | MPa |
| v12 | 0.3 | |
| v21 | 0.028985 | |
| G12 | 4640 | MPa |
| G13 | 4640 | MPa |
| G23 | 3030 | MPa |

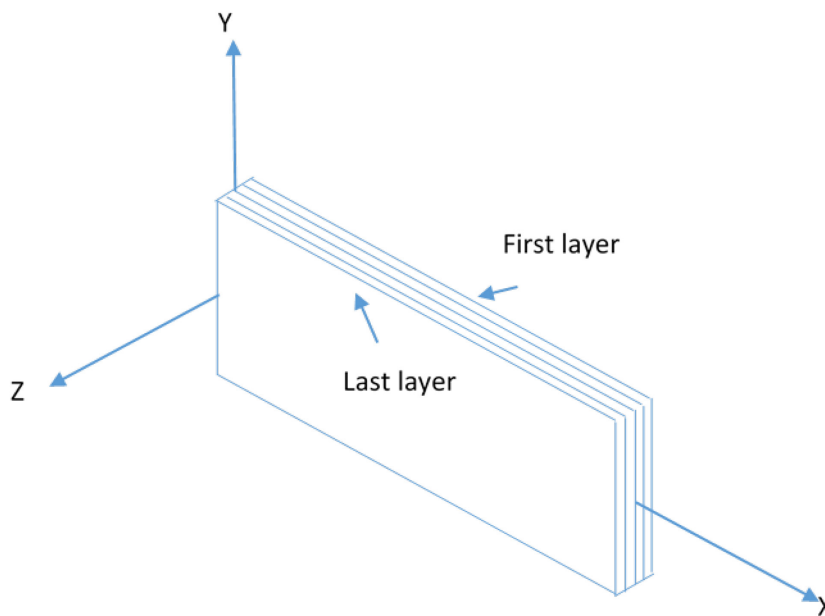


Figure 3.5 The stacking sequence of the laminates

3.4.2 Buckling Results

For the lateral-torsional buckling of thin-walled rectangular laminated composite beams under pure bending conditions, an analytical approach is presented as well as FEM results. Figures 3.6 and 3.7 show the buckling results for different stacking sequences based on the proposed analytical formulation and also results from FEM model for layer thickness of 0.1 mm (total thickness of 0.4 mm), beam length of 500 mm and beam height of 100 mm and 25 mm (i.e. length to height ratio of 5 and 20), respectively. Based on the results obtained, there is an excellent agreement between the proposed analytical formulation and FEM, Figures 3.6 and 3.7. The largest error observed is 3.3% (Figure 3.6) apart from the $[0_4]$ and cross-ply layup cases, which buckled in a distortional mode rather than lateral-torsional mode (as will be discussed below) admitting an error up to 10%, see Table 3.2.

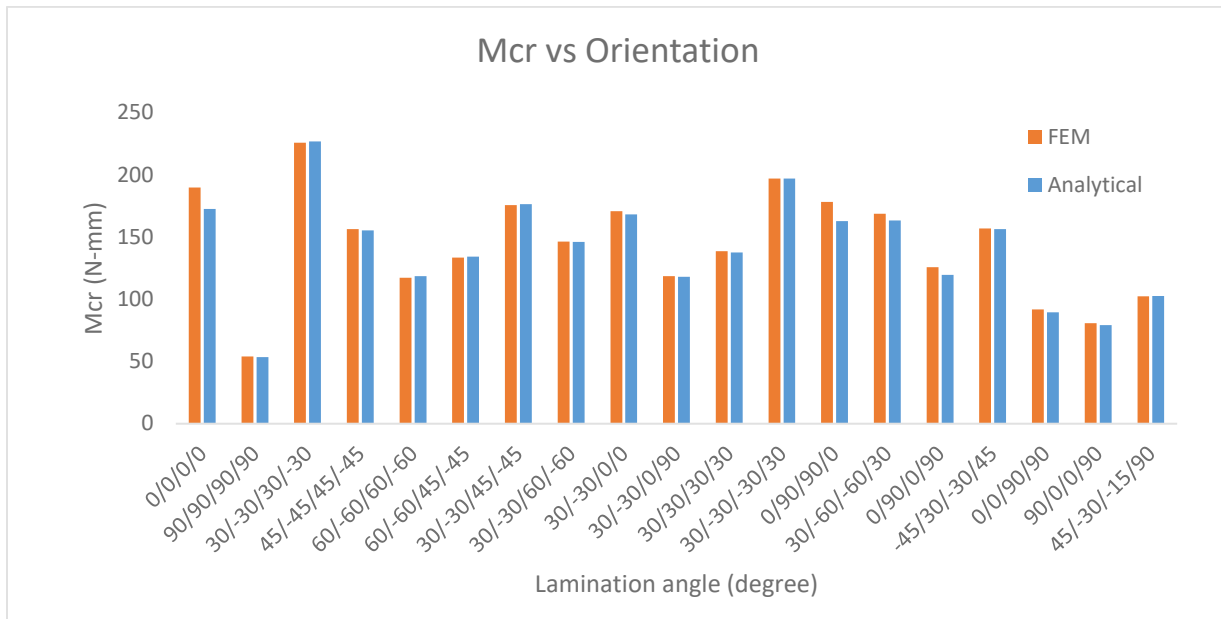


Figure 3.6 Buckling moments at different stacking sequences: tk=0.1 mm for each layer, L/h=5, and element length 2.5mm

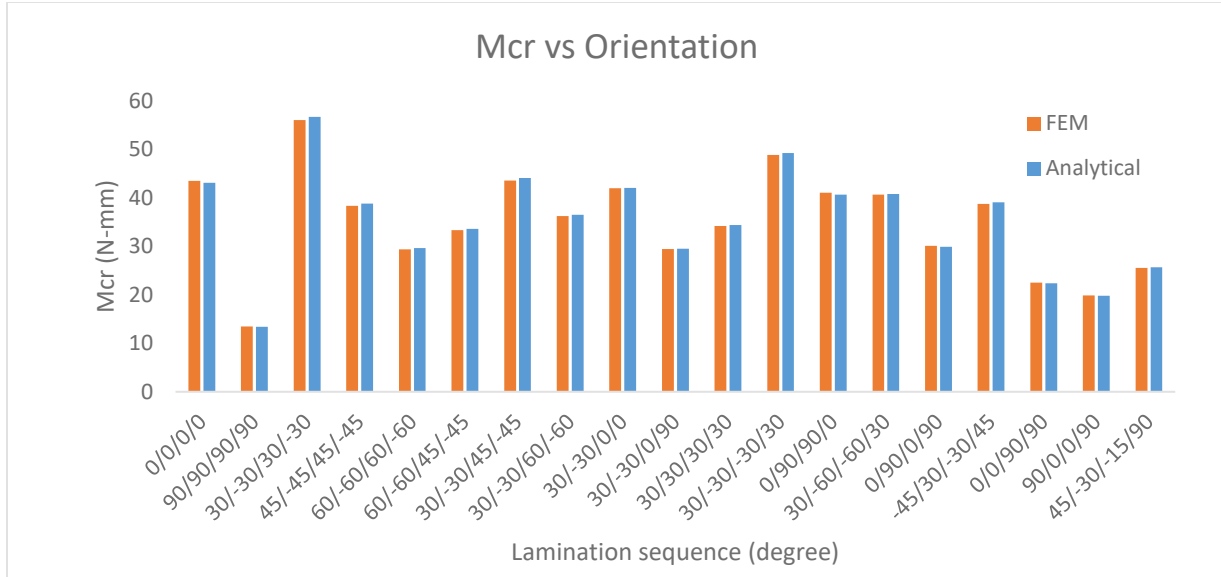


Figure 3.7 Buckling moments at different stacking sequences: tk=0.1 mm for each layer, L/h=20, and element length 2.5mm

3.5 Parametric Study

3.5.1 Effect of Length/Height Ratio

Different Length/height (L/h) ratios of 2, 5, 10, 20, and 50 were used in the analysis to study their effects on the lateral-torsional buckling of simply supported laminated thin-walled rectangular cross-sectional beams. The results show that there is a significant drop in the value of the buckling moments as the L/h ratio increases. The relation between buckling moment and L/h ratio is defined to be a power function which can be written in Eq. 3.28

$$M_{cr} = (M_{cr})_i * \left(\frac{L}{h}\right)_i \left(\frac{L}{h}\right)^{-1} \quad (3.28)$$

where $(M_{cr})_i$ is the initial calculated value of buckling moment from Eq. 3.25 with a given $\left(\frac{L}{h}\right)_i$ ratio for a specific laminate stacking sequence.

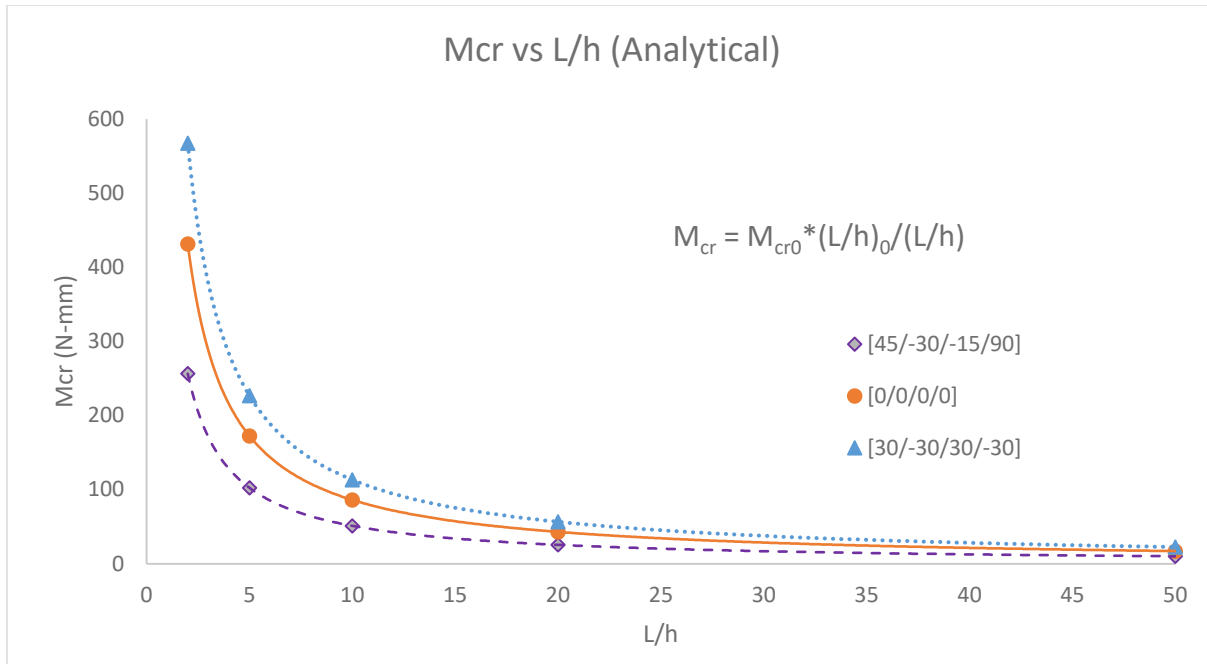


Figure 3.8 Effect of L/h ratio on the critical moment based on analytical formula for three different layups and layer thickness of 0.1 mm

By knowing the value of buckling moment in a selected laminate, Eq. 3.28 helps to calculate the buckling moment for different L/h ratios. Figure 3.8 shows the effect of L/h ratio on the buckling moment for three different stacking sequences of [0/0/0/0], [45/-30/-15/90], and [30/-30/30/-30]. Eq. 3.28 is limited to the analytical formula and is not applicable for the FEM results. There is a noticeable discrepancy between the analytical and numerical results in the case of [0/0/0/0] laminate when the ratio of L/h decreases, as shown in Figure 3.9. This discrepancy is related to the fact that the beam with [0/0/0/0] layup buckles numerically in a distortional mode, in which β at a certain section transverse the beam is not constant, rather than a lateral-torsional mode, in which β is constant for a certain section transverse to the beam. Figure 3.10 shows the deformed mode shape of the beam in three different stacking sequences looking down the beam height. It is evident that the deformed section for the [0/0/0/0] layup buckles numerically in a distortional mode where a constant β cannot be assumed as done analytically. Nevertheless,

Figure 3.9 clearly shows that the analytical and numerical buckling moments match almost exactly as the L/h ratio increases beyond 5.

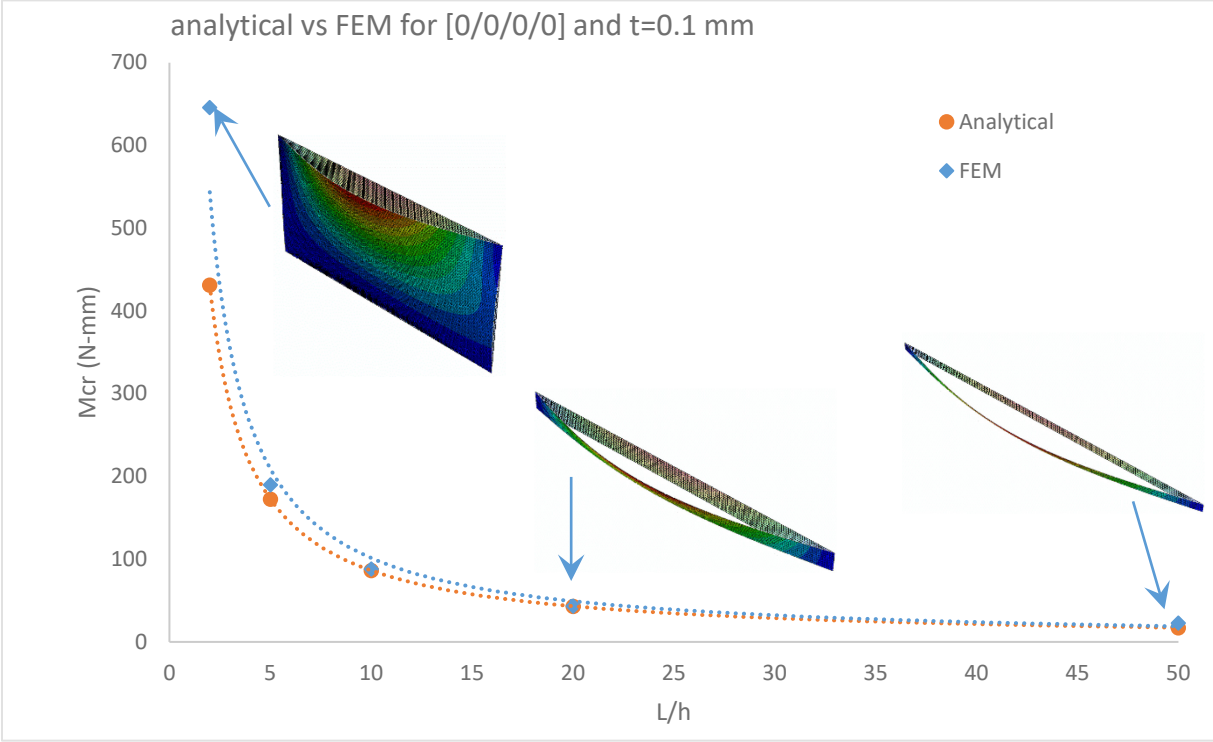


Figure 3.9 Comparison of buckling result obtained from analytical solution and FEM for the [0/0/0/0] laminate and layer thickness of 0.1 mm by changing L/h ratio

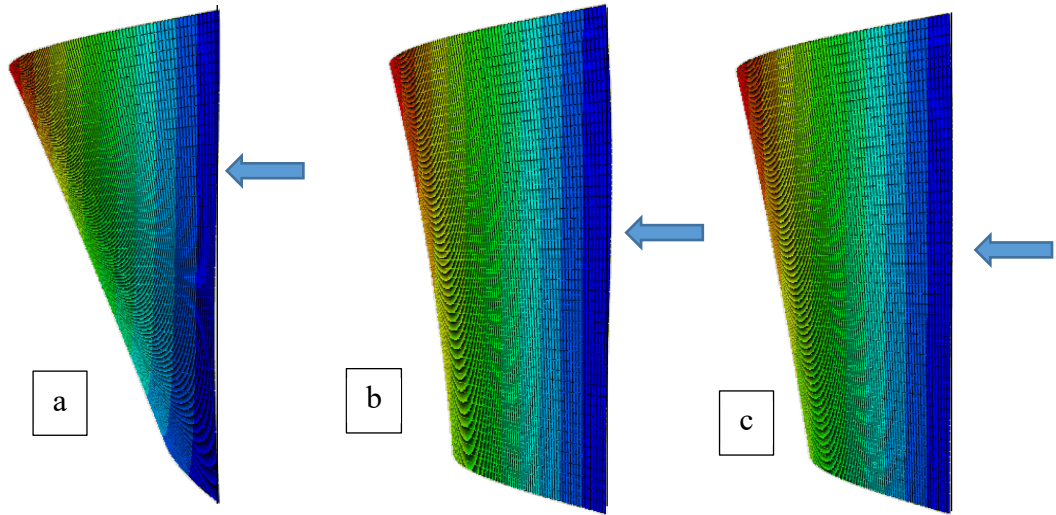


Figure 3.10 Edge deformation of the beam under pure bending for $L/h=5$, (a) [0/0/0/0] (b) [30/-30/30/-30], and (c) [45/-30/-15/90]

Figures 3.9, 3.11, and 3.12 show the comparison of buckling moments between the analytical solution and FEM in three different laminate stacking sequences. It is obvious that in both analytical and FEM the buckling moments increase as the L/h ratio decrease because of the larger height of the beam to resist against lateral-torsional buckling. Again, it is evident from Figure 3.9 that the analytical and numerical results match closely beyond L/h=5 while the two results match up closely in Figures 3.11 and 3.12 throughout the entire range of L/h values.

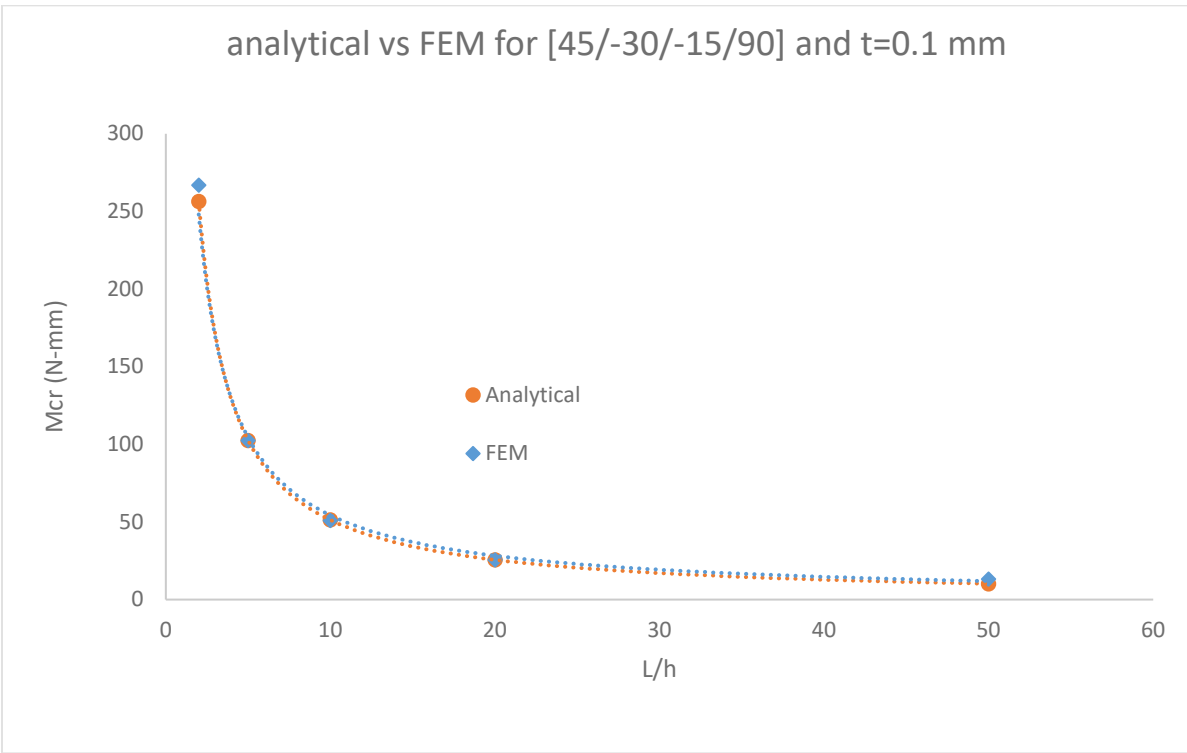


Figure 3.11 Comparison of buckling result obtained from analytical solution and FEM for the [45/-30/-15/90] laminate and layer thickness of 0.1 mm by changing L/h ratio

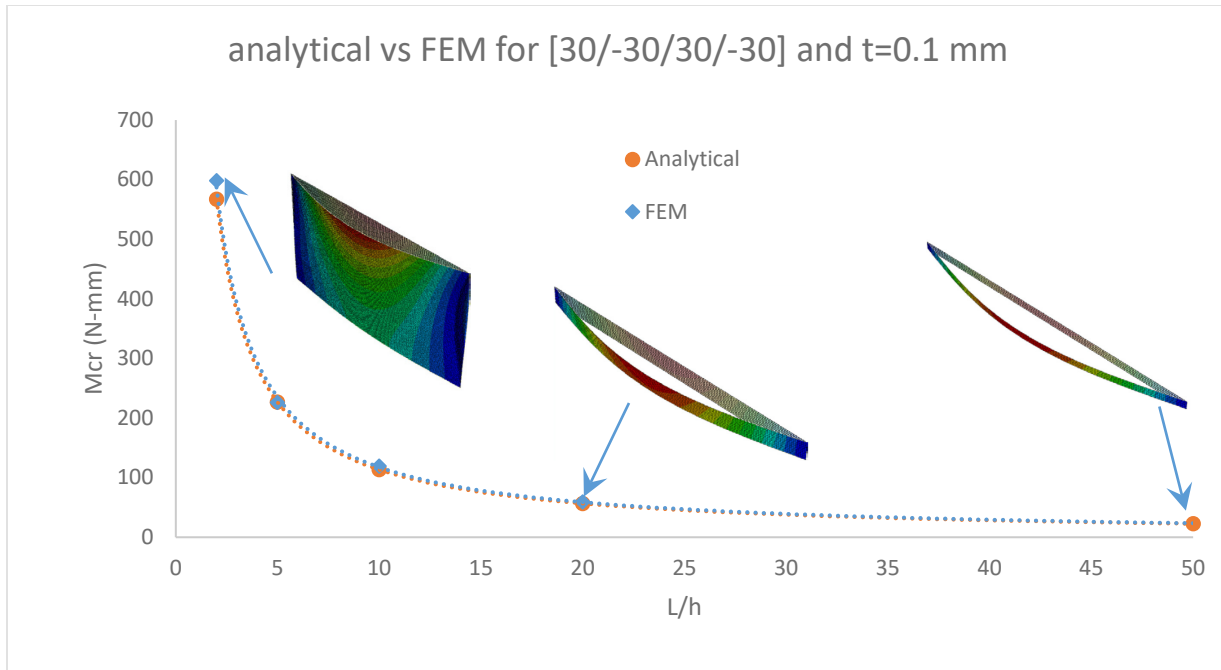


Figure 3.12 Comparison of buckling result obtained from analytical solution and FEM for the [30/-30/30/-30] laminate and layer thickness of 0.1 mm by changing L/h ratio

3.5.2 Effect of Stacking Sequence

As shown in Figures 3.6 and 3.7. The stacking sequences considerably affect the buckling moments if the dimensions of the beam are kept the same. The lowest value for the critical buckling moment is obtained in [90/90/90/90] layup while the highest critical value is obtained for the balanced angle-ply stacking sequence of [30/-30/30/-30] which is the maximum critical moment among the possible stacking sequences selected for Figure 3.6. The optimal maximum critical moment is obtained for the balanced angle-ply layup to be 247N.mm for layup [22/-22/22/-22]. Figure 3.13 shows the variation in critical buckling moment with the change in layup angle of 0 to 90 with an increment of 5 degrees.

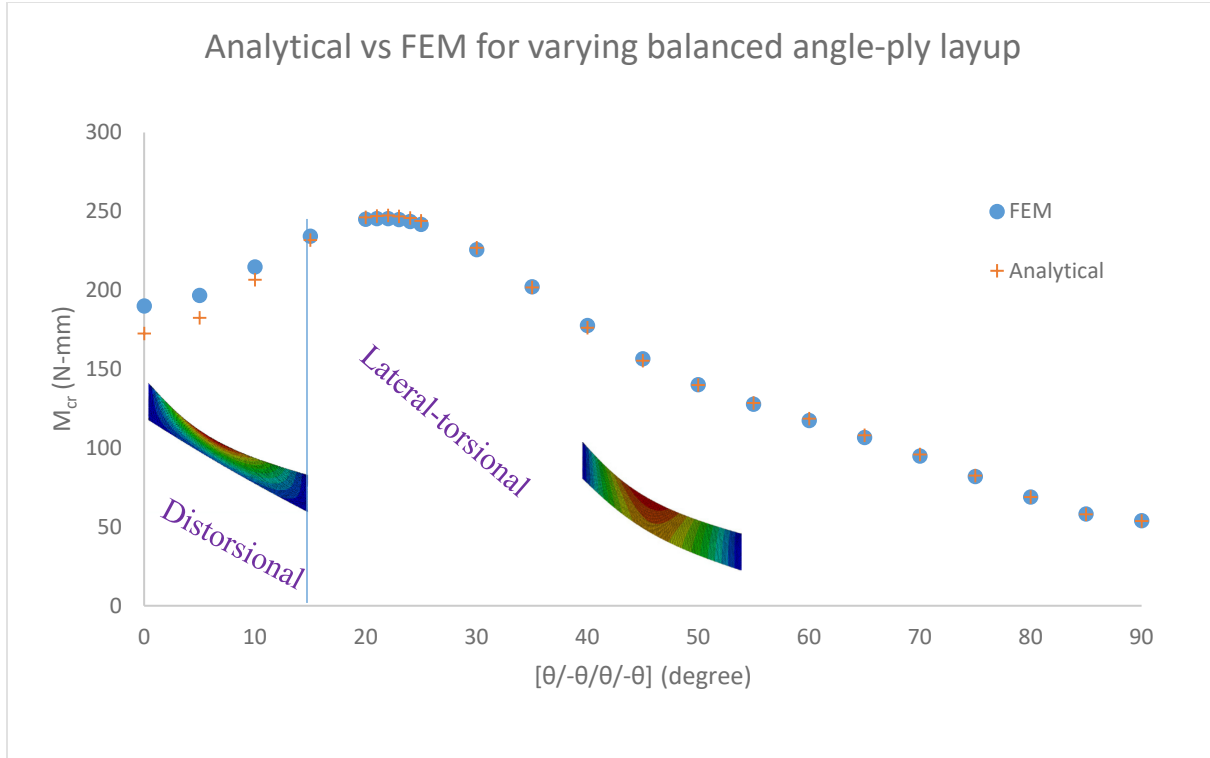


Figure 3.13 Variation in critical buckling moment with the change in balanced angle-ply layup angle of 0 to 90 with an increment of 5 degrees. (+) Analytical and (●) FEM; layer thickness of 0.1 mm and L/h of 5

3.5.3 Effect of Thickness

Different layer thickness of 0.05, 0.1, 0.15, and 0.2 mm were used in the analysis to study their effects on the lateral-torsional buckling of simply supported laminated thin-walled rectangular cross-sectional beams. The L/h ratio of 5 and the stacking sequence was kept the same while changing the layer thickness. The results show that there is a significant increase in the value of buckling moments as the layer thickness increases. The relation between buckling moment and the thickness is defined to be a power function which can be written in Eq. 3.29.

$$M_{cr} = \frac{(M_{cr})_i}{t_i^3} t^3 \quad (3.29)$$

where $(M_{cr})_i$ is the initial calculated value of buckling moment from Eq. 3.24 with a given t_i for a specific laminate stacking sequence. Eq. 3.28 works either considering the thickness to be the

total thickness of the beam or the thickness of each layer as long as all layers have the same constant thicknesses.

By knowing the value of buckling moment in a selected layup, Eq. 3.29 helps to calculate the buckling moment for various layer or total beam thickness. Figure 3.14 shows the effect of layer thickness on the buckling moment based on analytical solution for three different stacking sequence of [0/0/0/0], [45/-30/-15/90], and [30/-30/30/-30]. Figure 3.15 shows the effect of layer thickness on the buckling moment based on the FEM results for the same three stacking sequences of [0/0/0/0], [45/-30/-15/90], and [30/-30/30/-30]. Eq. 3.29 can be obtained from FEM analysis with small error multipliers of (a) and (b), which are tabulated in Figure 3.15. The modification of Eq. 3.29 for FEM is shown in Eq. 3.30.

$$M_{cr} = (at + b) \frac{(M_{cr})_i}{t_i^3} t^3 \quad (3.30)$$

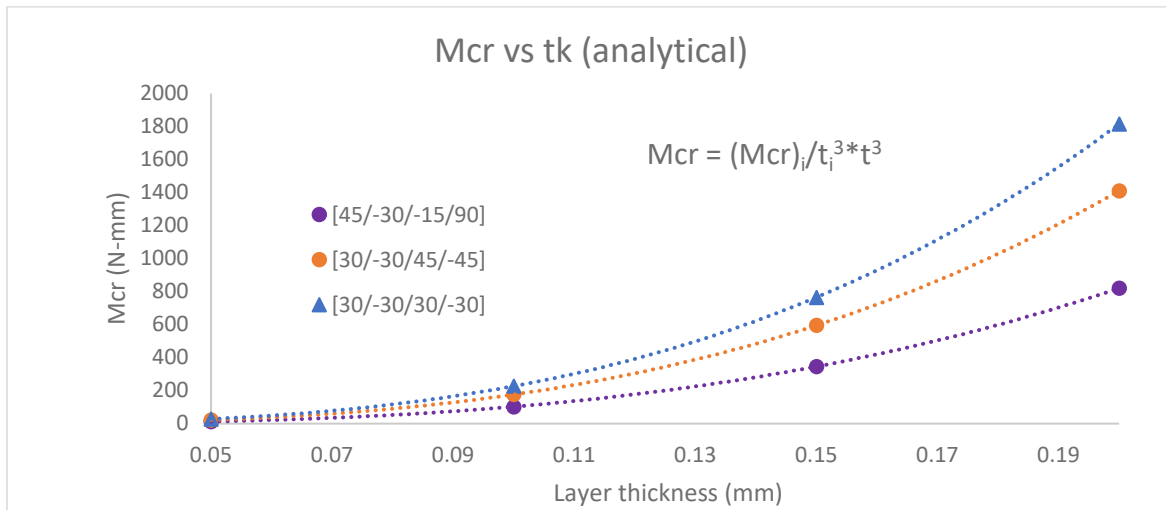


Figure 3.14 Effect of thickness, t_k , on the critical moment based on analytical method for three different orientations, $L/h=5$

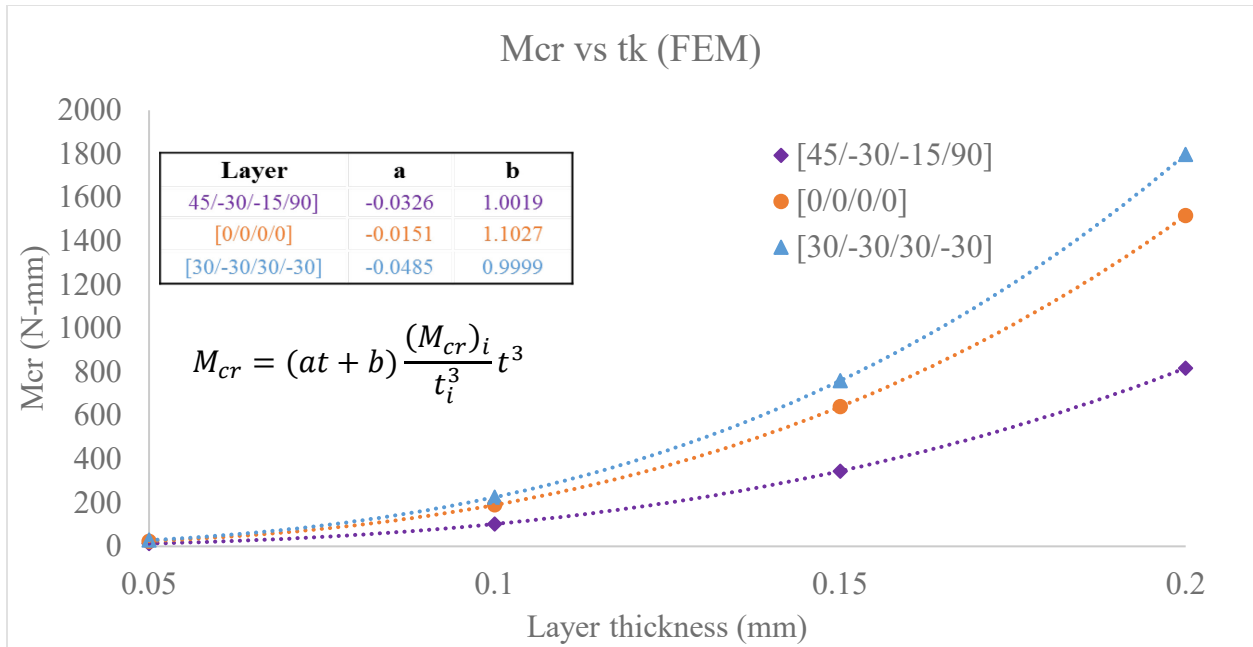


Figure 3.15 Effect of thickness, t_k , on the critical moment based on FEM method for three different orientations, $L/h=5$

Figures 3.16, 3.17, and 3.18 show the comparison of buckling moments between the analytical results and FEM in three different laminate stacking sequences. It is obvious that in both analytical and FEM the buckling moments increase as the layer thickness increases because of larger thickness of the beam to resist against lateral-torsional buckling. Both analytical and FEM have a good agreement on the buckling moment for all three sequences, except for the [0/0/0/0] case when the thickness increases. The anticipated causing factor is discussed earlier in a previous section.

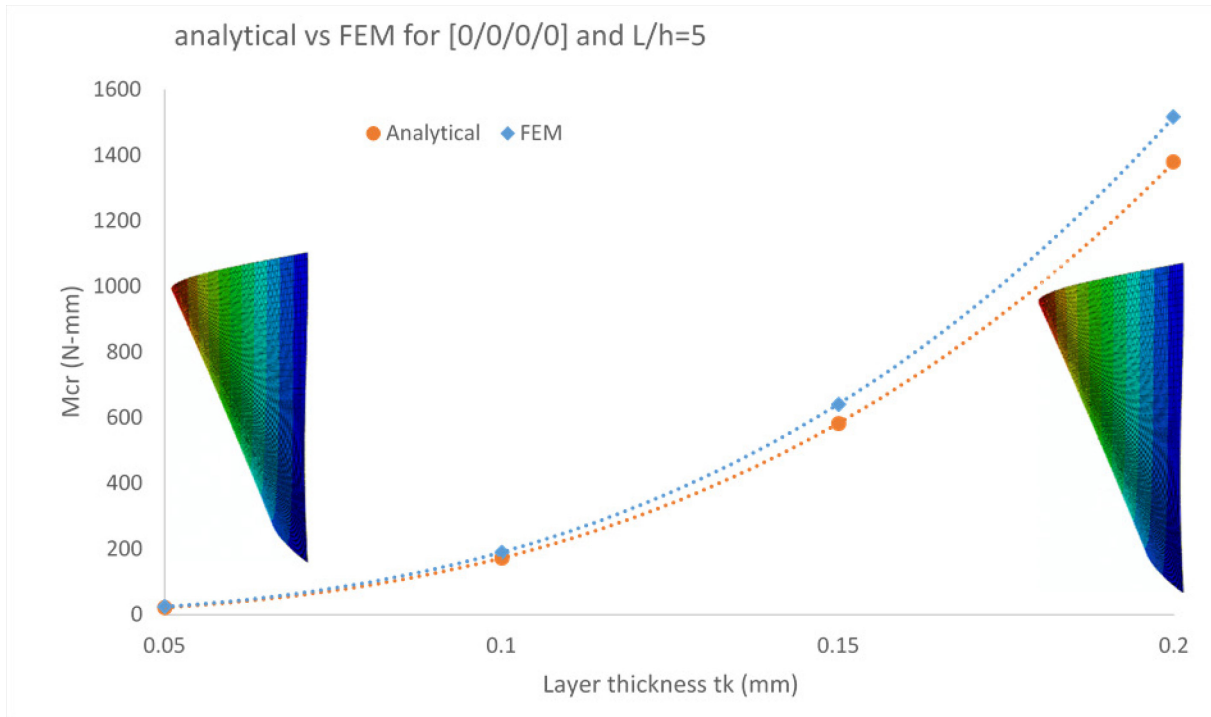


Figure 3.16 Comparison of buckling result obtained from analytical solution and FEM for the [0/0/0/0] laminate and L/h of 5 by changing layer thickness, t_k

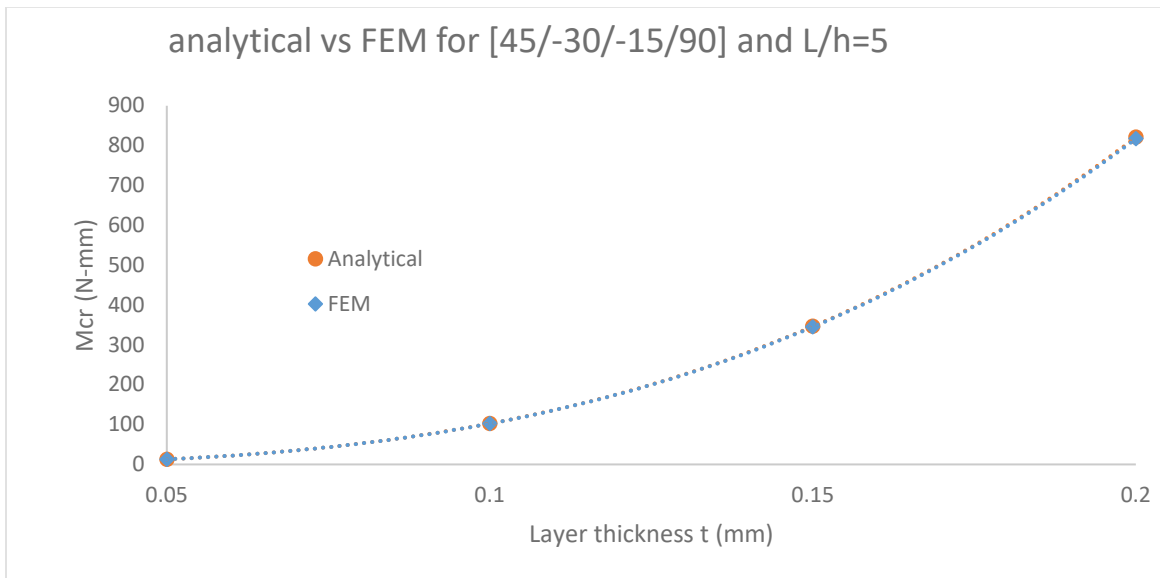


Figure 3.17 Comparison of buckling result obtained from analytical solution and FEM for the [45/-30/-15/90] laminate and L/h of 5 by changing layer thickness, t_k

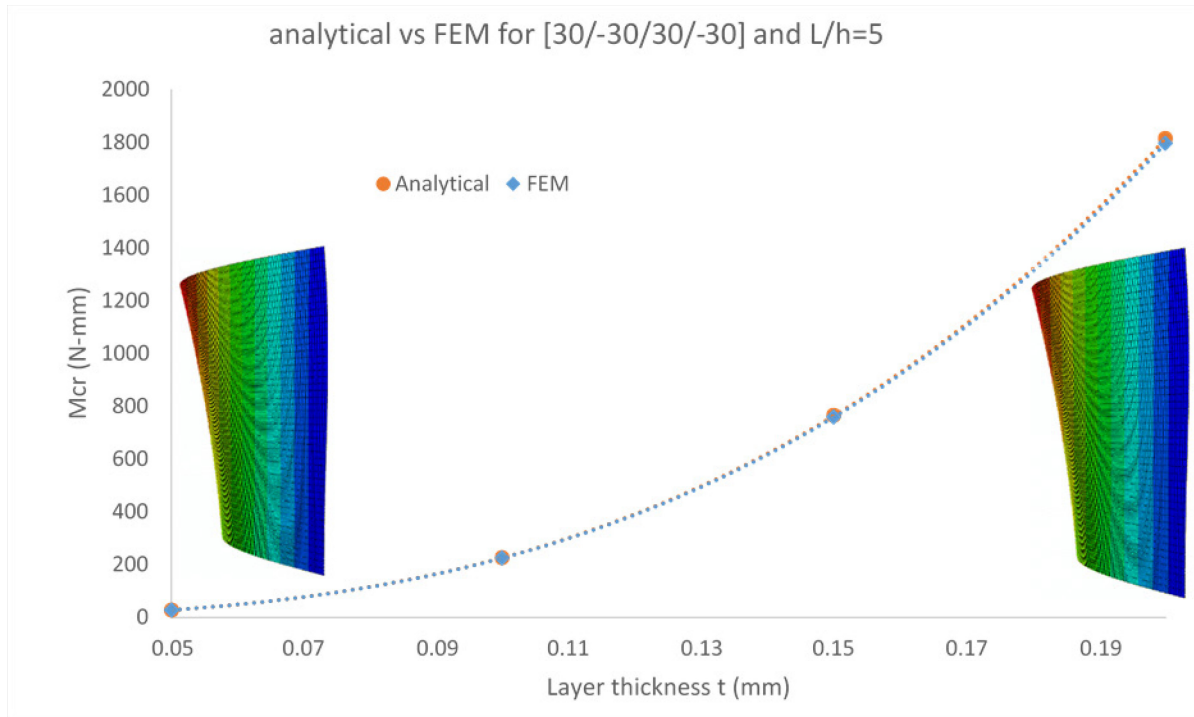


Figure 3.18 Comparison of buckling result obtained from analytical solution and FEM for the [30/-30/30/-30] laminate and L/h of 5 by changing layer thickness, t_k

3.6 Conclusions

In this study, the lateral-torsional buckling of simply supported, thin-walled rectangular cross-section, anisotropic laminated composite beam under pure bending loading was investigated. Based on the assumptions made and the results obtained, an excellent accuracy is observed for a variety of stacking sequences. The applicability of this analytical formulation is proved by comparing the obtained results with FEM results. The study followed the classical laminated plate theory with all considered assumptions and determined an effective lateral-torsional-coupling stiffness matrix.

Based on the study, the stability of the laminated beams under pure bending is greatly affected by the length/height ratio of the beam as well as the thickness of the beam. The critical buckling moment was inversely proportional to the length/height ratios with a power function.

The lowest L/h ratio yields to the highest critical buckling moment. Increase in the thickness of the beam also plays a significant role in increasing the stability resistance of the beam. The importance of the stacking sequence, which does not affect the dimensions of the beam, is seen to greatly influence the stability of the beam.

The critical buckling moment of balanced angle-ply fiber lamination of about [22/-22/22/-22] is found to reach the maximum value, among this class of layups, because of its maximum lateral and torsional effective stiffness. The minimum critical buckling moment obtained from [90/90/90/90] was found to be due to orienting the fibers in the y-direction, thus reducing the lateral and torsional effective stiffness.

Table 3.2 Comparison of buckling moment obtained from analytical results and FEM for L/h ratios of 5 and 20 and layer thickness of 0.1 mm in different stacking conditions

| Laminate | Critical Buckling moments M_{cr} (N.mm) and Error (%) | | | | | |
|---------------|---|-----------------|--------------|------------|-----------------|--------------|
| | L/h =5 | | | L/h = 20 | | |
| | Analytical | FEM (ABAQUS) | Error (%) | Analytical | FEM (ABAQUS) | Error (%) |
| 0/0/0/0 | 172.47 | 189.93 | 10.12 | 43.12 | 43.52 | 0.94 |
| 90/90/90/90 | 53.61 | 53.97 | 0.67 | 13.40 | 13.45 | 0.32 |
| 30/-30/30/-30 | 226.88 | 225.77 | 0.49 | 56.72 | 56.04 | 1.20 |
| 45/-45/45/-45 | 155.26 | 156.48 | 0.79 | 38.82 | 38.33 | 1.24 |
| 60/-60/60/-60 | 118.63 | 117.31 | 1.12 | 29.66 | 29.38 | 0.95 |
| 60/-60/45/-45 | 134.39 | 133.43 | 0.72 | 33.60 | 33.33 | 0.79 |
| 30/-30/45/-45 | 176.38 | 175.70 | 0.39 | 44.10 | 43.59 | 1.14 |
| 30/-30/60/-60 | 146.00 | 146.31 | 0.22 | 36.50 | 36.26 | 0.66 |
| 30/-30/0/0 | 168.14 | 170.76 | 1.55 | 42.04 | 42.01 | 0.06 |
| 30/-30/0/90 | 118.02 | 118.68 | 0.56 | 29.51 | 29.45 | 0.20 |
| 30/30/30/30 | 137.56 | 138.65 | 0.79 | 34.39 | 34.21 | 0.53 |
| 30/-30/-30/30 | 197.10 | 197.05 | 0.02 | 49.28 | 48.86 | 0.84 |
| 0/90/90/0 | 162.79 | 178.32 | 9.54 | 40.70 | 41.06 | 0.89 |
| 30/-60/-60/30 | 163.25 | 168.65 | 3.30 | 40.81 | 40.65 | 0.39 |
| 0/90/0/90 | 119.64 | 125.85 | 5.19 | 29.91 | 30.09 | 0.59 |
| -45/30/-30/45 | 156.45 | 156.92 | 0.30 | 39.11 | 38.76 | 0.91 |
| 0/0/90/90 | 89.63 | 91.80 | 2.43 | 22.41 | 22.51 | 0.44 |
| 90/0/0/90 | 79.12 | 80.76 | 2.08 | 19.78 | 19.86 | 0.43 |
| 45/-30/-15/90 | 102.60 | 102.46 | 0.13 | 25.65 | 25.54 | 0.42 |

3.7 References

- Bank, L. C., & Bednarczyk, P. J. (1988). A beam theory for thin-walled composite beams. *Composites Science and Technology*, 32(4), 265-277.
- Barbero, E. J., Lopez-Anido, R., and Davalos, J.F. (1993). "On the Mechanics of Thin-Walled Laminated Composite Beams." *Journal of Composite Materials*, 27(8), 806-829
- Barbero, E. J. (1999). *Introduction to composite materials design*. CRC press.
- Bauld, N. R., & Lih-Shyng, T. (1984). A Vlasov theory for fiber-reinforced beams with thin-walled open cross sections. *International Journal of Solids and Structures*, 20(3), 277-297.
- Karaagac, C., Öztürk, H., & Sabuncu, M. (2007). Lateral dynamic stability analysis of a cantilever laminated composite beam with an elastic support. *International Journal of Structural Stability and Dynamics*, 7(03), 377-402.
- Kollar, L. P. (2001). "Flexural-torsional buckling of open section composite columns with shear deformation." *International Journal of Solids and Structures*, 38, 7525-7541
- Kollár, L. P., & Springer, G. S. (2003). *Mechanics of composite structures*. Cambridge university press.
- Lee, J., Kim, S.-E., Hong, K. (2002). "Lateral buckling of I-section composite beams." *Engineering Structures*, 24, 955-964
- Lin, Z. M., Polyzois, D., and Shah, A. (1996). "Stability of Thin-walled Pultruded Structural Members by the Finite Element Method." *Thin-Walled Structures*, 24, 1-18
- Machado, S. P. (2010). "Interaction of combined loads on the lateral stability of thin-walled composite beams." *Engineering Structures*, 32, 3516-3527
- Pandey, M.D., Kabir, M.Z., and Sherbourne, A.N. (1995). "Flexural-Torsional Stability of Thin-Walled Composite I-Section Beams." *Composites Engineering*, 5(3), 321-342
- Qiao, P., Zou, G., and Davalos, J. (2003). "Flexural-torsional buckling of fiber-reinforced plastic composite cantilever I-beams." *Composite Structures*, 60, 205-217
- Roberts, T.M., Al-Ubaidi, H. (2001). "Influence of shear deformation on restrained torsional warping of pultruded FRP bars of open cross-section." *Thin-Walled Structures*, 39, 395-414
- Sapkás, Á., & Kollár, L. P. (2002). Lateral-torsional buckling of composite beams. *International Journal of Solids and Structures*, 39(11), 2939-2963.
- Sherbourne, A. N., Kabir, M. Z. (1995). "Shear Strain Effects in Lateral Stability of Thin-Walled Fibrous Composite Beams." *Journal of Engineering Mechanics*, 640-647

Tai, W. T. (2004). *The lateral-torsional buckling analysis of composite laminated beams* (MSc thesis, Feng Chia University, Taiwan ROC).

Timoshenko, S. P., & Gere, J. M. (1961). *Theory of elastic stability*. 1961. McGrawHill-Kogakusha Ltd, Tokyo.

Vlassov, V. Z. (1961). *Thin-walled beams* (2nd ed.) Israel Program for Scientific Translation.

Chapter 4 - Lateral-Torsional Buckling of Simply Supported Anisotropic Steel-FRP Beams under Pure Bending Condition

In this chapter, a generalized analytical approach for lateral-torsional buckling of simply supported anisotropic hybrid (steel-FRP), thin-walled, rectangular cross-section beams under pure bending condition was developed using the classical laminated plate theory as a basis for the constitutive equations. Buckling of such type of hybrid members has not been addressed in the literature. The hybrid beam, in this study, consists of a number of layers of anisotropic fiber reinforced polymer (FRP) and a layer of isotropic steel sheet. The isotropic steel sheet is used in two configurations, (i) in the mid-depth of the beam sandwiched between the different FRP layers and (ii) on the side face of the beam. A closed form buckling expression is derived in terms of the lateral, torsional and coupling stiffness coefficients of the overall composite. These coefficients are obtained through dimensional reduction by static condensation of the 6x6 constitutive matrix mapped into a 2x2 coupled weak axis bending-twisting relationship. The stability of the beam under different geometric and material parameters, like length/height ratio, ply orientation, and layer thickness, was investigated. The analytical formula is verified against finite element buckling solutions using ABAQUS for different lamination orientations showing excellent accuracy.

4.1 Introduction

A thin-walled slender beam subjected to bending moments about the strong axis may buckle by a combined lateral bending and twisting of the cross-section. This phenomenon is known as lateral-torsional buckling. Theory of thin-walled open section beams including axial constraints for isotropic materials was developed by Vlassov (1961). This classical theory

neglects the shear deformation in the middle surface of the wall so that for the composite beams, the shear deformations may significantly increase the displacements and reduce the buckling loads. The shear deformation theory for transversely loaded isotropic beams was developed by Timoshenko and Gere (1961).

Many researchers then started to study the lateral torsional buckling for the laminated composite beams using different theoretical approaches and enhancing their work with experimental programs and finite element models to validate the theory. Lin et al. (1996) studied the stability of thin-walled composite member using the finite element method. Seven degrees of freedom at each node for each two-noded element were used to model the fiber reinforced plastic. The seven degrees of freedom are the dependent translations in three perpendicular directions and the corresponding rotations in addition to the angle of warping. The stiffness matrices of a beam element were used to develop the element shape functions. A number of examples of thin walled-open sections were solved, different cross sections like channels, I sections, and Z-sections were tested as well as different boundary conditions. The study concluded the importance of the influence of in-plane shear strain on the critical buckling load for lateral torsional buckling and combined torsional and flexural modes. It also minimized the significance of shear strain effect on critical buckling when the buckling happens in terms of a flexural mode. Davalos and Qiao (1997) used the non-linear elastic theory to develop a stability solution for lateral-distortional buckling for composite wide flange beams based on the principle of total potential energy. A fifth-order polynomial shape function was adopted for the displacement field construction. Then, the proposed model was validated against two geometrically identical experimental beams loaded at mid-span, with different material characteristics. A good agreement was obtained against the experimental results and a finite

element model. Kollar (2001) presented a stability analysis of thin walled composite columns under axial loading conditions. A closed form solution was derived using a modified version of Vlasov's classical theory (1961) for isotropic material to account for the composite action. The effect of shear deformation in in-plane displacements and in the restrained warping was examined and a shear matrix was formulated in addition to the bending matrix. Lee et al. (2002) studied the lateral buckling of composite laminated beams. An analytical approach based on the classical lamination theory was derived for different boundary conditions and different laminate stacking sequences. The examined beams were tested under various loading configurations and various locations. The beams were then compared against a one dimensional finite element model under different load configurations. The model showed a good agreement against the finite element model of simply supported I beam in cases of pure bending, uniformly distributed loads, and central point load. Yet, the model was not appropriate for pure bending with off-axis fiber orientation due to coupling stiffness. Sapkas and Kollar (2002) offered closed form solutions for simply supported and cantilever, thin walled, open section, orthotropic composite beams subjected to concentrated end moments, concentrated forces, or uniformly distributed load. The solution indirectly accounted for shear deformation by adjusting the bending and warping stiffness of the composite beams. Qiao et al. (2003) formulated an analytical solution for flexural-torsional buckling of composite cantilever I beams based on an energy method developed from the non-linear plate theory. A good agreement against finite element method was obtained. Furthermore, four different cantilever beams were tested experimentally under tip loads to examine the flexural-torsional response. Also, good agreements were shown against the experimental results. Kotelko (2004) presented a theoretical analysis of local buckling which represents material failure. This study covered different cross sections of thin walled beams and

columns. These cross sections varied between lipped and plain channels as well as box-section. This theory matched previous theories in a way that it depends on the rigid-plastic model. Yet, it mainly differs by considering a constitutive strain-hardening of the used material. This analytical approach is particularly useful in the initial phase of design process and may be applied as a simplified design tool at the early stage of design process, including crush-oriented design.

Karaagac et al. (2007) tested the stability of a cantilever laminated composite beam under static and dynamic conditions. A linear translation spring was attached to the beam to control the lateral deformation. The attached elastic support location varied between the free end and the mid-span of the beam. Length-to-thickness ratio, variation of cross-section in one direction, orientation angle, static and dynamic load parameters, stiffness and position of the elastic support were the main variables to study the stability of the beam. Numerical polynomial approximations for the displacements and the angle of twist were derived and showed a reasonable accuracy against the finite element method.

Machado (2010) derived an analytical solution for lateral stability of cross-ply laminated thin-walled simply supported bisymmetric beams subjected to combined axial and bending loads. The presented theory included shear deformability and took into account large displacements and rotations; moderate bending rotations and large twisting angles. The proposed solution also examined the nonlinear pre-buckling geometrical deformation for more accurate representation of the lateral stability conditions. The buckling loads obtained analytically were, in general, in good agreement with the bifurcation loads observed in the post buckling response. The study concluded that the buckling moments computed from classical theory is overestimated. Also, it presented pre-buckling and post buckling displacement curves to relate the stiffness behavior of the beam to the applied loads and also to study the fiber orientation against the buckling loads.

In this study, an analytical model applicable to the lateral-torsional buckling of simply supported anisotropic hybrid (steel-FRP), thin-walled, rectangular cross-section beams, subjected to pure bending is developed. This model is based on the classical laminated plate theory (CLPT), and accounts for the arbitrary laminate stacking sequence configurations. The analyzed beams consist of six layers of fiber reinforced polymer (FRP) sheets and one isotropic steel sheet even though the solution is applicable to any number of layers. The FRP sheets have the same thickness and the same mechanical properties, yet they vary in terms of fiber angle orientation. The location of the steel sheet was examined in order to understand its influence on the lateral torsional buckling critical moment. A sandwich stacking configuration (ST-I) is defined by placing the steel sheet in the mid-thickness of the beam. A sided stacking configuration (ST-II) is defined by placing the steel sheet at the side face of the beam. A series of FRP angle configurations were determined for comparisons against a finite element model and also to compare the different configurations against each other. The finite element model is developed in ABAQUS to predict critical buckling moments and compare with the results obtained from the analytical model. Also, the length of the beam to its height ratio and FRP layer thickness were examined to study the effect of beam size and thickness on the lateral torsional buckling resistance.

4.2 Analytical Formulation

A simply supported hybrid (steel-FRP) laminated composite beam with length L and a thin rectangular cross section is subjected to pure bending at the ends, as shown in Figure 4.1. The beam tends to buckle under a lateral-torsional behavior because of its small thickness.

The model in this study is based on the classical laminated plate theory, Kollar and Springer (2003) and Barbero (1999). The following assumptions are adopted from the classical laminated plate theory:

1. The normals to mid-plane (reference surface) of the laminate remain normal and straight after deformation.
2. The normal to mid-plane of the laminate do not change length – in other words, the thickness of the laminate stays constant.
3. The shear deformations are neglected.
4. The laminate consists of perfectly bonded layers.
5. The stress-strain relationships are applied under plane-stress conditions.

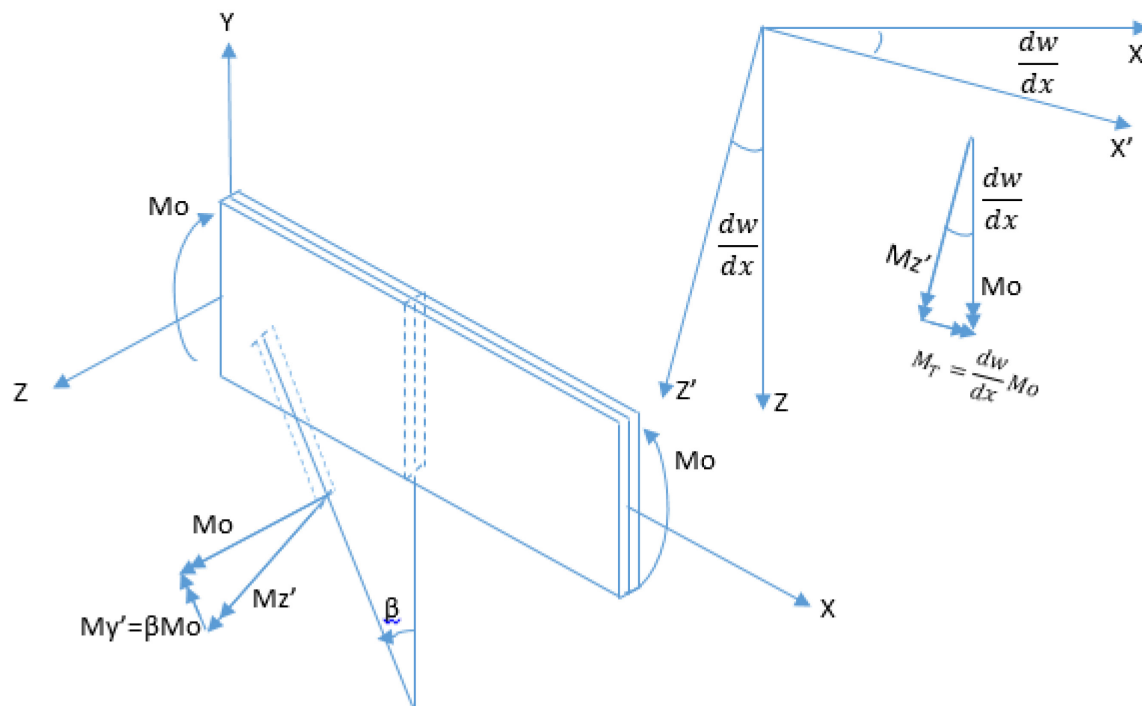


Figure 4.1 A deformed laminated beam subjected to pure bending (structural coordinate system)

4.2.1 Kinematics

Based on the assumptions in the classical laminated plate theory, the displacement components u , v , w representing the deformation of a point on the plate profile section are given with respect to mid-surface displacements u_0 , v_0 , and w_0 as follows:

$$u(x, y, z) = u_0(x, y) - z \frac{dw_0}{dx}(x, y) \quad (4.1)$$

$$v(x, y, z) = v_0(x, y) - z\beta(x, y) \quad (4.2)$$

$$w(x, y, z) = w_0(x, y) \quad (4.3)$$

$$\text{where } \beta = \frac{\partial w_0}{\partial y}$$

The strains associated with small displacements from the theory of elasticity are given by

$$\varepsilon_x = \varepsilon_x^0 + z\kappa_x \quad (4.4)$$

$$\varepsilon_y = \varepsilon_y^0 + z\kappa_y \quad (4.5)$$

$$\gamma_{xy} = \gamma_{xy}^0 + z\kappa_{xy} \quad (4.6)$$

where

$$\varepsilon_x^0 = \frac{\partial u_0}{\partial x}, \varepsilon_y^0 = \frac{\partial v_0}{\partial y}, \gamma_{xy}^0 = \frac{\partial u_0}{\partial y} + \frac{\partial v_0}{\partial x} \quad (4.7)$$

$$\kappa_x = -\frac{\partial^2 w_0}{\partial x^2}, \kappa_y = -\frac{\partial \beta}{\partial y}, \text{ and } \kappa_{xy} = -2\frac{\partial \beta}{\partial x} \quad (4.8)$$

4.2.2 Stress-Strain Equations

The stress-strain relation for a layer is derived in the state of plane stress. For an isotropic material, the stress-strain relation is as follow:

$$\begin{Bmatrix} \sigma_x \\ \sigma_y \\ \tau_{xy} \end{Bmatrix} = \begin{bmatrix} \bar{E} & \bar{E}\nu & 0 \\ \bar{E}\nu & \bar{E} & 0 \\ 0 & 0 & G \end{bmatrix} \begin{Bmatrix} \varepsilon_x \\ \varepsilon_y \\ \gamma_{xy} \end{Bmatrix} \quad (4.9)$$

$$\text{where } \bar{E} = \frac{E}{1-\nu^2} \text{ and } G = \frac{E}{2(1+\nu)}$$

For anisotropic material, the stress-strain relation in the beam coordinate system is defined as follows:

$$\begin{Bmatrix} \sigma_x \\ \sigma_y \\ \tau_{xy} \end{Bmatrix} = \begin{bmatrix} \bar{Q}_{11} & \bar{Q}_{12} & \bar{Q}_{16} \\ \bar{Q}_{12} & \bar{Q}_{22} & \bar{Q}_{26} \\ \bar{Q}_{16} & \bar{Q}_{26} & \bar{Q}_{66} \end{bmatrix} \begin{Bmatrix} \epsilon_x \\ \epsilon_y \\ \gamma_{xy} \end{Bmatrix} \quad (4.10)$$

where $[\bar{Q}_{ij}]$ are the components of the transformed reduced constitutive matrix which are given in standard textbooks like Kollar and Springer (2003) and Barbero (1999).

4.2.3 Force-Strain Equation

The plate stiffness coupling equations based on classical laminated plate theory, shown in Figure 4.2, are given as follows.

$$\begin{Bmatrix} N_x = 0 \\ N_y = 0 \\ N_{xy} = 0 \\ M_x \neq 0 \\ M_y = 0 \\ M_{xy} \neq 0 \end{Bmatrix} = h \begin{bmatrix} A_{11} & A_{12} & A_{16} & B_{11} & B_{12} & B_{16} \\ A_{12} & A_{22} & A_{26} & B_{12} & B_{22} & B_{26} \\ A_{16} & A_{26} & A_{66} & B_{16} & B_{26} & B_{66} \\ B_{11} & B_{12} & B_{16} & D_{11} & D_{12} & D_{16} \\ B_{12} & B_{22} & B_{26} & D_{12} & D_{22} & D_{26} \\ B_{16} & B_{26} & B_{66} & D_{16} & D_{26} & D_{66} \end{bmatrix} \begin{Bmatrix} \epsilon_x \\ \epsilon_y \\ \gamma_{xy} \\ \kappa_x \\ \kappa_y \\ \kappa_{xy} \end{Bmatrix} \quad (4.11)$$

where

$$A_{ij} = \sum_{k=1}^N (\bar{Q}_{ij})_k t_k \quad i, j = 1, 2, 6 \text{ are called extensional stiffness coefficients}$$

$$B_{ij} = \sum_{k=1}^N (\bar{Q}_{ij})_k t_k \bar{z}_k \quad i, j = 1, 2, 6 \text{ are called extension-bending coupling stiffness coefficients and}$$

$$D_{ij} = \sum_{k=1}^N (\bar{Q}_{ij})_k \left(t_k \bar{z}_k^2 + \frac{t_k^3}{12} \right) \quad i, j = 1, 2, 6 \text{ are called bending stiffness coefficients}$$

$(\bar{Q}_{ij})_k$ are the components of the k^{th} layer 2D transformed constitutive matrix in the beam coordinate system

\bar{z}_k is the depth from the middle surface to the centroid of the kth layer, and t_k is the thickness of k^{th} layer of the hybrid beam.

Knowing the zero components of externally applied forces and moments for the pure bending condition from Figure 4.1, which are expressed in Eq. 4.11, the stiffness matrix can be simplified and dimensionally reduced to an effective 2x2 stiffness matrix by using the static condensation technique. In the static condensation technique, the zero and non-zero components of forces and moments from Eq. 4.11 are arranged into separate matrices as follows:

$$h \begin{bmatrix} A_{11} & A_{12} & A_{16} & B_{12} \\ A_{12} & A_{22} & A_{26} & B_{22} \\ A_{16} & A_{26} & A_{66} & B_{26} \\ B_{12} & B_{22} & B_{26} & D_{22} \end{bmatrix} \begin{Bmatrix} \varepsilon_x \\ \varepsilon_y \\ \gamma_{xy} \\ \kappa_y \end{Bmatrix} + h \begin{bmatrix} B_{11} & B_{16} \\ B_{12} & B_{26} \\ B_{16} & B_{66} \\ D_{12} & D_{26} \end{bmatrix} \begin{Bmatrix} \kappa_x \\ \kappa_{xy} \end{Bmatrix} = \begin{Bmatrix} 0 \\ 0 \\ 0 \\ 0 \end{Bmatrix} \quad (4.12)$$

$$\begin{Bmatrix} M_x \\ M_{xy} \end{Bmatrix} = h \begin{bmatrix} D_{11} & D_{16} \\ D_{16} & D_{66} \end{bmatrix} \begin{Bmatrix} \kappa_x \\ \kappa_{xy} \end{Bmatrix} + h \begin{bmatrix} B_{11} & B_{16} \\ B_{12} & B_{26} \\ B_{16} & B_{66} \\ D_{12} & D_{26} \end{bmatrix}^T \begin{Bmatrix} \varepsilon_x \\ \varepsilon_y \\ \gamma_{xy} \\ \kappa_y \end{Bmatrix}$$

(4.13)

The reduced effective 2x2 stiffness matrix (Eq. 4.15) can be obtained by defining $\begin{Bmatrix} \varepsilon_x \\ \varepsilon_y \\ \gamma_{xy} \\ \kappa_y \end{Bmatrix}$ from

Eq. 4.12 in terms of other components, as shown in Eq. 4.14, and substituting it into Eq. 4.13.

$$\begin{Bmatrix} \varepsilon_x \\ \varepsilon_y \\ \gamma_{xy} \\ \kappa_y \end{Bmatrix} = - \begin{bmatrix} A_{11} & A_{12} & A_{16} & B_{12} \\ A_{12} & A_{22} & A_{26} & B_{22} \\ A_{16} & A_{26} & A_{66} & B_{26} \\ B_{12} & B_{22} & B_{26} & D_{22} \end{bmatrix}^{-1} \begin{bmatrix} B_{11} & B_{16} \\ B_{12} & B_{26} \\ B_{16} & B_{66} \\ D_{12} & D_{26} \end{bmatrix} \begin{Bmatrix} \kappa_x \\ \kappa_{xy} \end{Bmatrix} \quad (4.14)$$

$$\begin{Bmatrix} M_x \\ M_{xy} \end{Bmatrix} = h \begin{bmatrix} D_Y & D_{YT} \\ D_{YT} & D_T \end{bmatrix} \begin{Bmatrix} \kappa_x \\ \kappa_{xy} \end{Bmatrix} \quad (4.15)$$

where

$$\begin{bmatrix} D_Y & D_{YT} \\ D_{YT} & D_T \end{bmatrix} = \begin{bmatrix} D_{11} & D_{16} \\ D_{16} & D_{66} \end{bmatrix} - \begin{bmatrix} B_{11} & B_{16} \\ B_{12} & B_{26} \\ B_{16} & B_{66} \\ D_{12} & D_{26} \end{bmatrix}^T \begin{bmatrix} A_{11} & A_{12} & A_{16} & B_{12} \\ A_{12} & A_{22} & A_{26} & B_{22} \\ A_{16} & A_{26} & A_{66} & B_{26} \\ B_{12} & B_{22} & B_{26} & D_{22} \end{bmatrix}^{-1} \begin{bmatrix} B_{11} & B_{16} \\ B_{12} & B_{26} \\ B_{16} & B_{66} \\ D_{12} & D_{26} \end{bmatrix}$$

D_Y is the effective hybrid (steel-FRP) composite lateral stiffness coefficient, D_T is the effective hybrid composite twisting stiffness coefficient, and D_{YT} is the effective hybrid composite lateral-twisting coupling coefficient. In most cases, where the layers are symmetric, anti-symmetric, cross-ply, special angle ply, D_{YT} coefficient will be zero. However, for the generally anisotropic cases, D_{YT} coefficient is not zero and will play a significant role in determining the buckling moments of the beams.

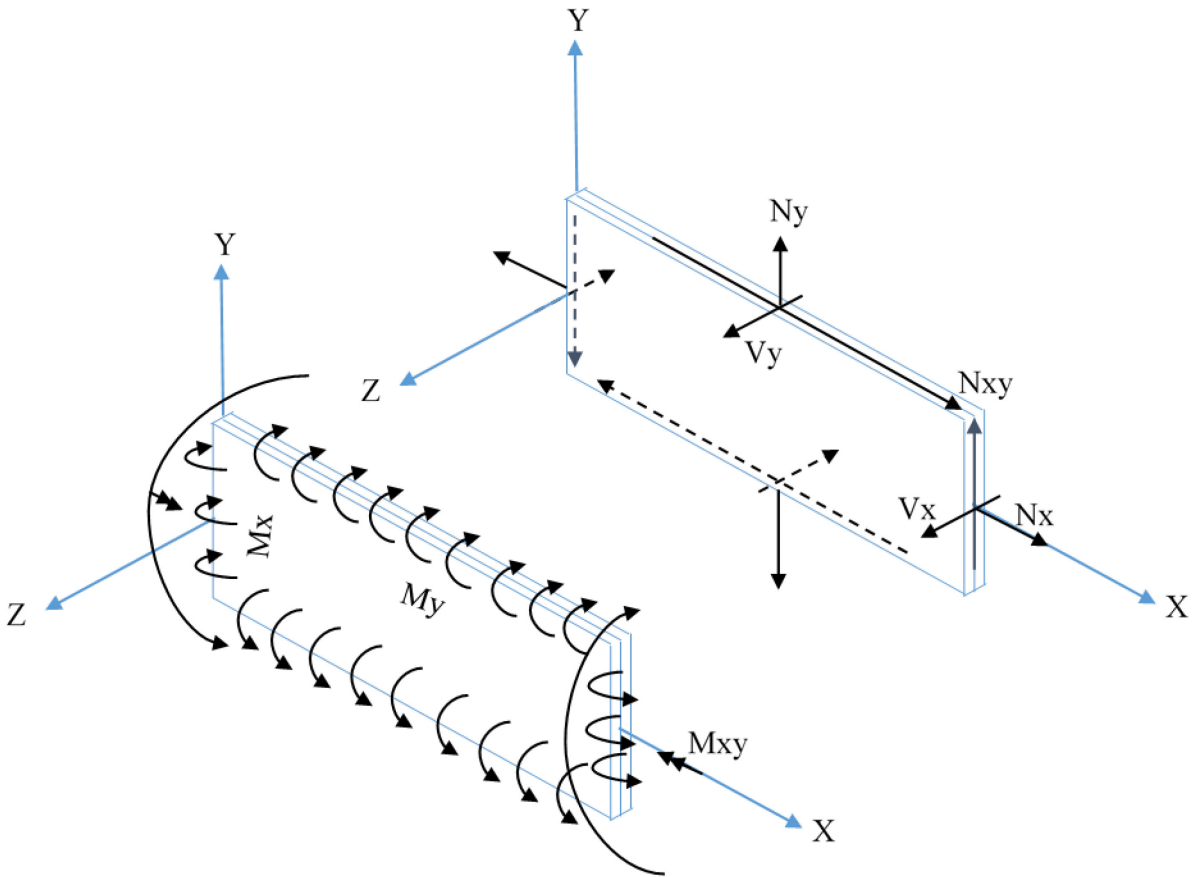
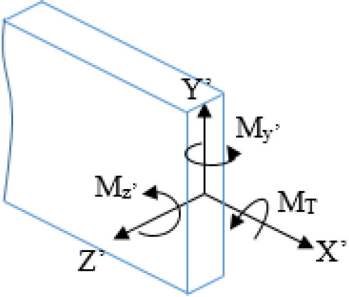
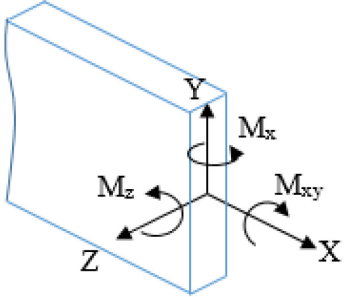


Figure 4.2 Force and moment resultants on a beam based on classical laminated plate theory (laminate coordinate system).

Referring to Figure 4.1 (structural coordinate) and Figure 4.2 (laminate coordinate), the bending moment M_y in structural coordinate is replaced by M_x in laminate coordinate. On the other hand, the shear moment, M_{xy} , in laminate coordinate is in the opposite direction of twisting moment in the structural coordinate system and is found by Kollar and Springer (2003) to be $M_T = -2 M_{xy}$. Table 4.1 shows the relation of moment components in structural coordinate and laminate composite coordinate.

Table 4.1 Relation of moment components in structural coordinate and laminate composite coordinate

| The structural coordinate (deformed axes) | Laminate composite coordinate |
|---|--|
|  | <div style="text-align: center;"> $\begin{aligned} M'_z &= M_z \\ M'_y &= M_x \\ M_T &= -2M_{xy} \end{aligned}$ </div>  |

Substituting the curvatures in terms of displacement and rotation of Eq. 4.8 into Eq. 4.15, and writing the moments in structural coordinates systems, the following relation will be obtained

$$\begin{Bmatrix} M_{y'} \\ -M_T \end{Bmatrix} = h \begin{bmatrix} D_Y & 2D_{YT} \\ 2D_{YT} & 4D_T \end{bmatrix} \begin{Bmatrix} -\frac{d^2w}{dx^2} \\ -\beta' \end{Bmatrix} \quad (4.16)$$

4.2.4 Equilibrium Equations

Figure 4.1 shows the components of external moments about the original and deformed axes and is obtained as follows:

External moments in un-deformed configuration (original axes):

$$M_z = M_o \text{ (Applied Moment)} \quad (4.17)$$

$$M_T = M_y = 0 \quad (4.18)$$

External moments in the deformed configuration (deformed axes):

$$M'_z = M_z = M_o \quad (4.19)$$

$$M'_y = \beta M_o \quad (4.20)$$

$$M_T = M'_x = \frac{dw}{dx} M_o \quad (4.21)$$

The following system of differential equations is obtained after substituting the external moments from Eqs. 4.20 and 4.21 into Eq. 4.16:

$$\begin{Bmatrix} \beta M_o \\ -\frac{dw}{dx} M_o \end{Bmatrix} = h \begin{bmatrix} D_Y & 2D_{YT} \\ 2D_{YT} & 4D_T \end{bmatrix} \begin{Bmatrix} -\frac{d^2w}{dx^2} \\ -\beta' \end{Bmatrix} \quad (4.22)$$

$$-hD_Y \frac{d^2w}{dx^2} - 2hD_{YT} \beta' = \beta M_o \quad (4.23)$$

$$-2hD_{YT} \frac{d^2w}{dx^2} - 4hD_T \beta' = -\frac{dw}{dx} M_o \quad (4.24)$$

Writing Eqs.4.23 and 4.24 in terms of $\frac{d^2w}{dx^2}$ and equating the two expressions, the following relationship can be obtained.

$$\frac{1}{hD_Y} [-2hD_{YT} \beta' - \beta M_o] = \frac{1}{2hD_{YT}} \left[-4hD_T \beta' + \frac{dw}{dx} M_o \right] \quad (4.25)$$

Differentiating Eq. 4.25 with respect to x and rearranging the resulting expression in terms of $\frac{d^2w}{dx^2}$, Eq. 4.26 will be obtained.

$$\frac{d^2w}{dx^2} = -\frac{2D_{YT}}{D_Y} \beta' + \frac{4h}{M_o} \left[D_T - \frac{D_{YT}^2}{D_Y} \right] \beta'' \quad (4.26)$$

Equating the left hand side of Eq.4.25, which is equal to $\frac{d^2w}{dx^2}$ in Eq. 4.23, and the right hand side of Eq. 4.26, the resulting expression reduces to a second order ordinary differential equation with constant coefficients, which can be solved analytically.

$$\beta'' + \frac{M_o^2}{4h^2[D_Y D_T - D_{YT}^2]} \beta = 0 \quad (4.27)$$

Setting $\kappa^2 = \frac{M_o^2}{4h^2[D_Y D_T - D_{YT}^2]}$, yields an equation similar to the isotropic condition when the warping effect is neglected.

$$\beta'' + \kappa^2 \beta = 0 \quad (4.28)$$

The general solution for this type of differential equation is known to be:

$$\beta = A\sin(kx) + B\cos(kx) \quad (4.29)$$

Applying boundary condition for pure bending as $\beta(0) = \beta(L) = 0$, the critical buckling moment is obtained according to the following equation.

$$M_{0cr} = \frac{\pi h}{L} \sqrt{4(D_Y D_T - D_{YT}^2)} \quad (4.30)$$

The critical moment for isotropic beam was obtained by Timoshenko and Gere (1961) as follows:

$$M_{0cr} = \frac{\pi}{L} \sqrt{EI_y GJ} \quad (4.31)$$

where $J = \frac{1}{3} ht^3$

For an isotropic material where $D_{YT} = 0$, the following relation is obtained.

$$EI_y = 2hD_Y \text{ (Lateral stiffness coefficient)} \quad (4.32)$$

$$GJ = 2hD_T \text{ (Torsional stiffness coefficient)} \quad (4.33)$$

4.3 Numerical Analysis (FEA)

The finite element method in the commercial software, ABAQUS/Standard (implicit) was used to simulate the problem in this study. The model was first created by using 3D planar shells. The shells were assembled based on the stacking arrangement that was used in the analytical solution. The global x-axis was used along beams length, but the local coordinate system was used based on the orientation of the fibers in each ply.

The boundary conditions for this beam were applied as follows. The four corners of the beam, shown in Figure 4.3, were constrained from moving in z-direction. One end of the beam was pinned at mid-height restraining it from all displacements, and a roller was applied at mid-

height of other end of the beam to restrain displacement in the y-direction only, as shown in the Figure 4.3.

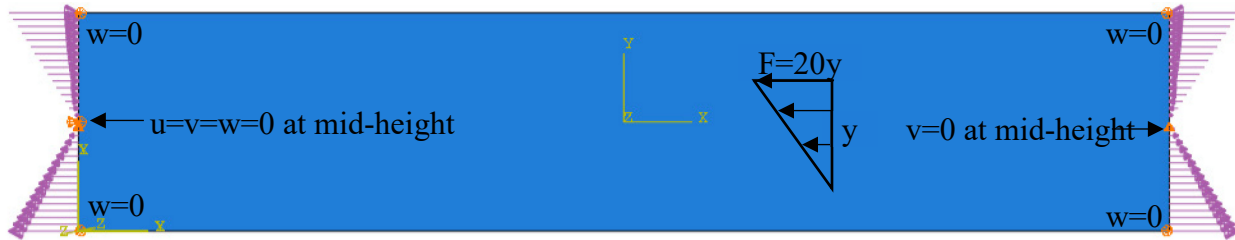


Figure 4.3 Applied load and boundary conditions

A linear shell-edge load was applied at both ends of the beam as tension and compression stresses to create a pure bending moment condition in the beam, as shown in Figure 4.3. Each edge was partitioned into two parts to apply shell-edge load linearly in the desired direction. The following relation was used to determine the magnitude of the linear load.

$$F_x = 20y \quad (4.34)$$

There is no load applied at the mid-height of the edge and the load increases linearly by 20y, which will act as a pure bending moment when applied as compression above the mid-height and as tension below the mid-height.

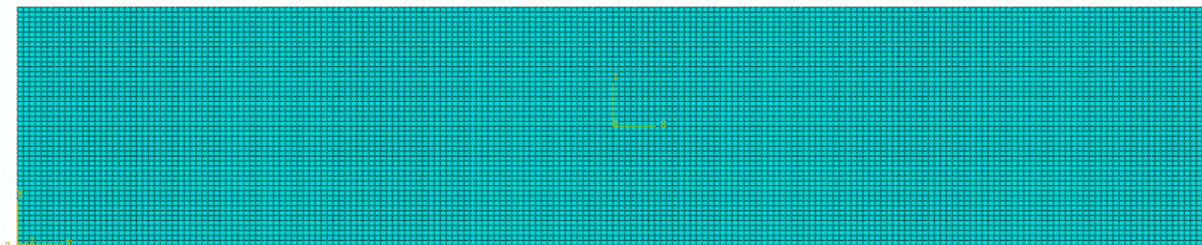


Figure 4.4 Applied shell element type (S8R) and mesh (element size along beam axis: 2.5 mm)

The beam was meshed with a standard quadratic quadrilateral shell element type of S8R (8-node doubly curved thick shell element with reduced integration) using six degrees of freedom per node and an element size of 2.5 mm along beam axis. A beam with $L = 500$ mm and

$h = 100$ mm yields a total number of 29297 nodes and 9600 elements, as shown in Figure 4.4. The eigenvalue buckling analysis in ABAQUS solver, which is a linear perturbation procedure, determines the eigenvalue of the buckling mode. ABAQUS extracts the eigenvalues and eigenvectors for symmetric stiffness matrices only. In order to make the stiffness matrix of the model symmetric, Lanczos iteration eigenvalue extraction method was used. To find the critical moment, based on the ABAQUS user guide, the lowest eigenvalue is multiplied by the moment which was applied at the ends of the beam in combined tension and compression line edge loading.

$$M_{0cr} = \lambda M_0 \quad (4.35)$$

where M_0 is calculated from applied linear edge load.

4.4 Results

4.4.1 Material Properties and Stacking Sequences

An anisotropic hybrid (steel-FRP) composite beam is made by stacking six layers of the FRP of lamina properties shown in Table 4.2 at different fiber orientations and one layer of isotropic steel sheet given in Table 4.3. The thickness of each layer along with steel sheet is the same (typically 0.1 mm), yet it varies in terms of fiber orientation. The orientation of fiber in each layer can be randomly picked, including common laminate types such as symmetric laminates, antisymmetric laminates, balanced laminates, and so on. Two stacking configurations were considered in order to place the steel sheet: (i) sandwich stacking (ST-I) where the steel sheet is placed at mid-depth of the beam and (ii) sided stacking (ST-II) where the steel sheet is placed in the front face of the beam. The stacking sequence starts from the back of the beam to the front of the beam to follow the same order used for typical laminated plates, Figure 4.5. For

example, [30/-30/90/ST/30/-30/90] means that the first ply has an angle of 30 degrees from the x-axis of the beam is placed in the back of the beam counter clockwise (towards the y-axis) and the other layers follow with the same order through the positive z-axis, and ST indicates the location of isotropic steel sheet in the mid-depth. Figure 4.5 shows the stacking sequence of the laminates and location of steel sheet. Different length to height ratios of (5, 10, 20, and 50) were also studied which will be presented later.

Table 4.2 Material 1 (CFRP) properties used the in laminates

| Material | CFRP | |
|-----------------------|----------|-----|
| E₁₁ | 142730 | MPa |
| E₂₂ | 13790 | MPa |
| v₁₂ | 0.3 | |
| v₂₁ | 0.028985 | |
| G₁₂ | 4640 | MPa |
| G₁₃ | 4640 | MPa |
| G₂₃ | 3030 | MPa |

Table 4.3 Material 2 (Steel) properties used the in laminates

| Material | Steel | |
|------------|----------|-----|
| E_{11} | 200000 | MPa |
| E_{22} | 200000 | MPa |
| ν_{12} | 0.3 | |
| ν_{21} | 0.3 | |
| G_{12} | 76923.08 | MPa |
| G_{13} | 76923.08 | MPa |
| G_{23} | 76923.08 | MPa |

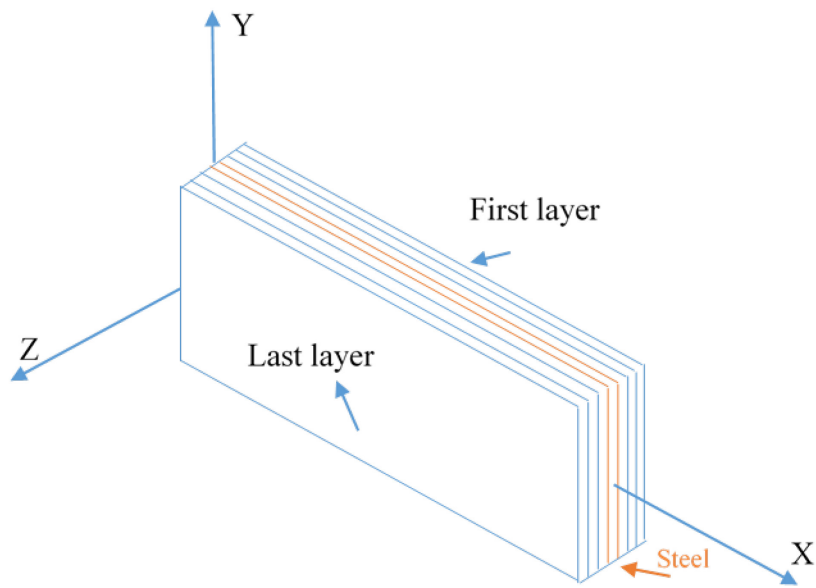


Figure 4.5 The stacking sequence of the laminate and location of steel sheet (ST-I)

4.4.2 Buckling Results

For the lateral-torsional buckling of thin-walled rectangular laminated composite beams under pure bending conditions, an analytical approach is presented as well as FEA results. Figures 4.6 - 4.9 show the buckling results for different stacking sequences based on the proposed analytical formulation as well as results from FEA model. Figures 4.6 and 4.7 show the results of ST-I (sandwich) configuration and ST-II (sided) configuration of 18 different laminate-fiber orientation for beam length/height ratio of 5. Similarly, Figures 4.8 and 4.9 show the results of ST-I configuration and ST-II configuration of 18 different laminate-fiber orientation for beam length/height ratio of 20. The same comparison was held for beam length/height ratios of 10 and 50. Based on the results obtained, there is an excellent agreement between the proposed analytical formulation and FEA for all the orientations with an error that does not exceed 3.5% except for the zero fiber orientation. The largest error observed is 8.7% (Figure 4.6) for the 0/0/0/ST/0/0/0 case, which buckled in a distortional mode rather than lateral-torsional mode, which will be explained in details later in this chapter, Figure 4.12.

4.5 Parametric Study

4.5.1 Effect of Length/Height Ratio

Different Length/height (L/h) ratios of 5, 10, 20, and 50 were used in the analysis to study their effects on the lateral-torsional buckling of simply supported laminated thin-walled rectangular cross-sectional hybrid beams. The results show that there is a significant drop in the value of the buckling moments as the L/h ratio increases. The relation between buckling moment and L/h ratio is defined to be a power function which can be written in Eq. 4.36.

$$M_{cr} = (M_{cr})_i * \left(\frac{L}{h}\right)_i \left(\frac{L}{h}\right)^{-1} \quad (4.36)$$

where $(M_{cr})_i$ is the initial calculated value of buckling moment from Eq. 4.31 with a given $\left(\frac{L}{h}\right)_i$ ratio for a specific laminate stacking sequence.

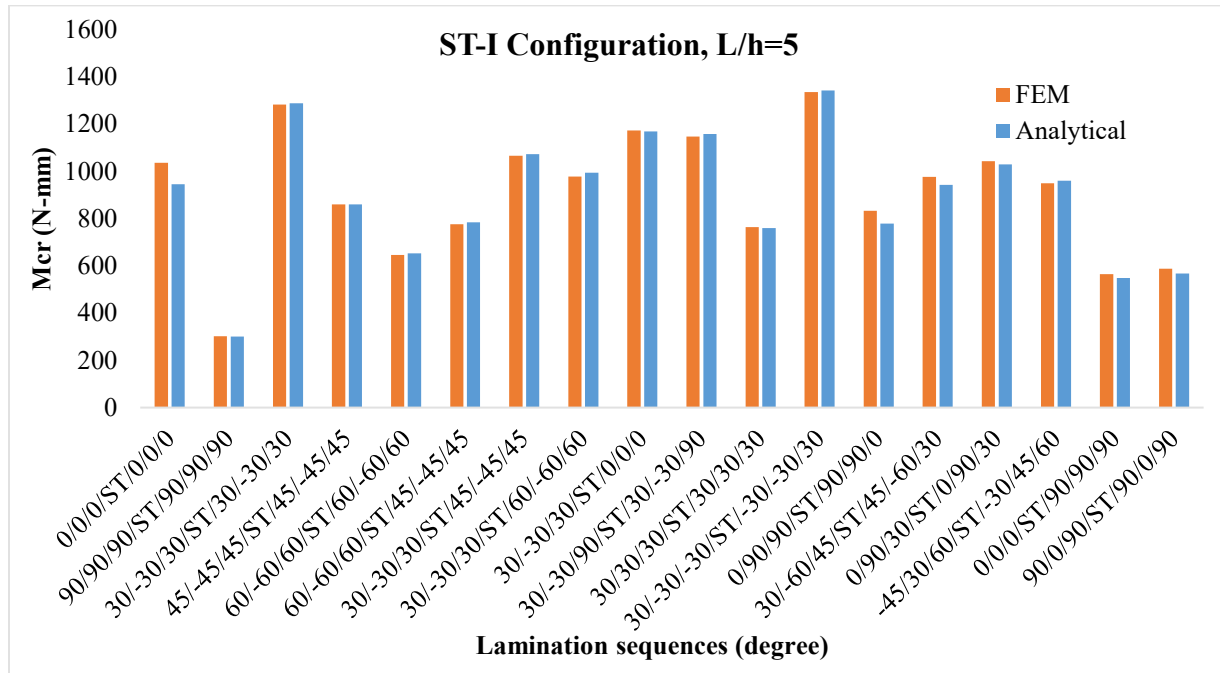


Figure 4.6 Buckling moments at different stacking sequences: $t_k=0.1$ mm for each layer, $L/h=5$, and ST-I configuration

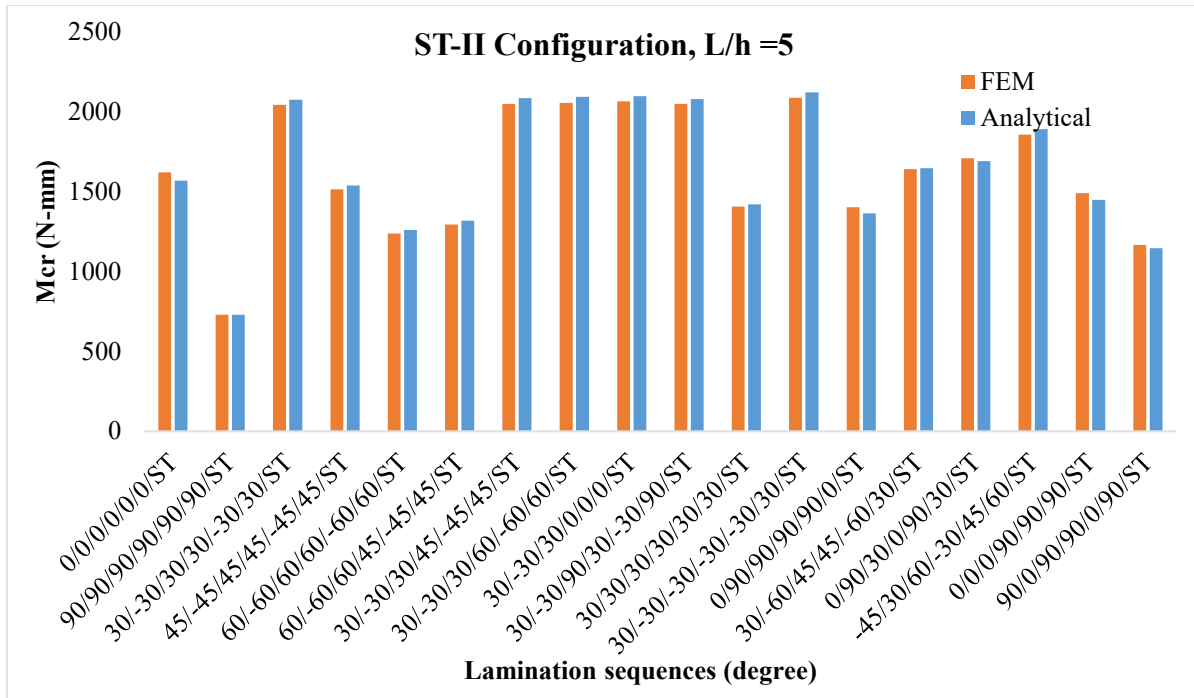


Figure 4.7 Buckling moments at different stacking sequences: $t_k=0.1$ mm for each layer, $L/h=5$, and ST-II configuration

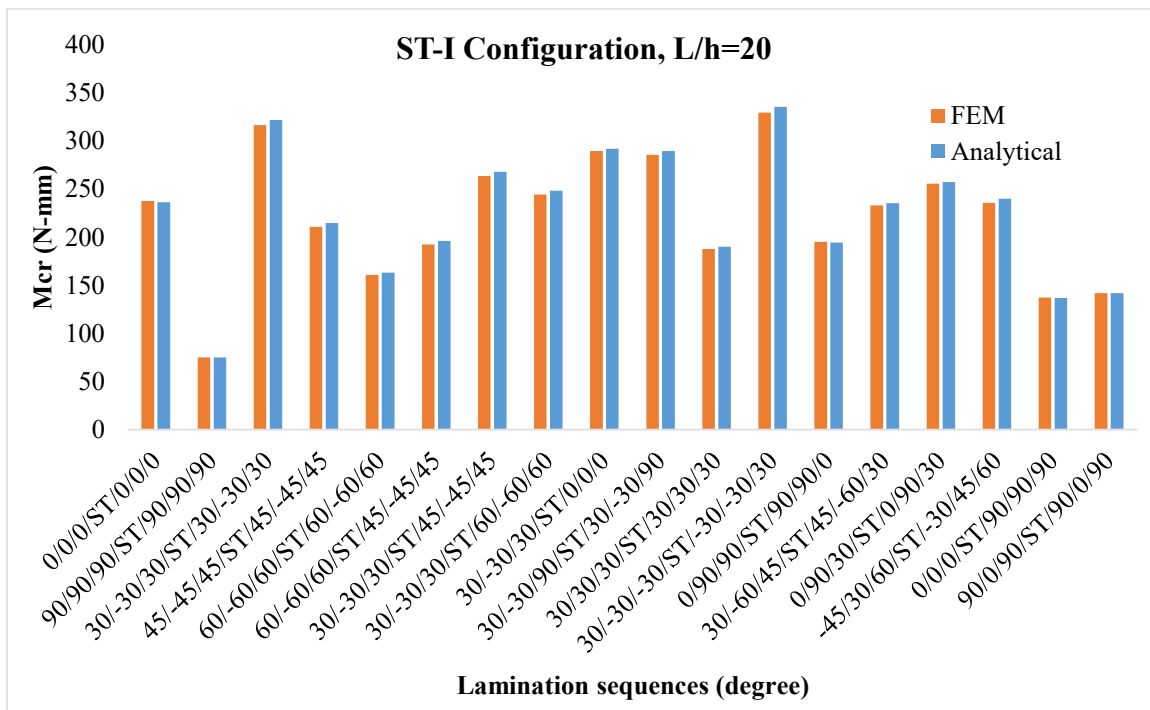


Figure 4.8 Buckling moments at different stacking sequences: $t_k=0.1$ mm for each layer, $L/h=20$, and ST-I configuration

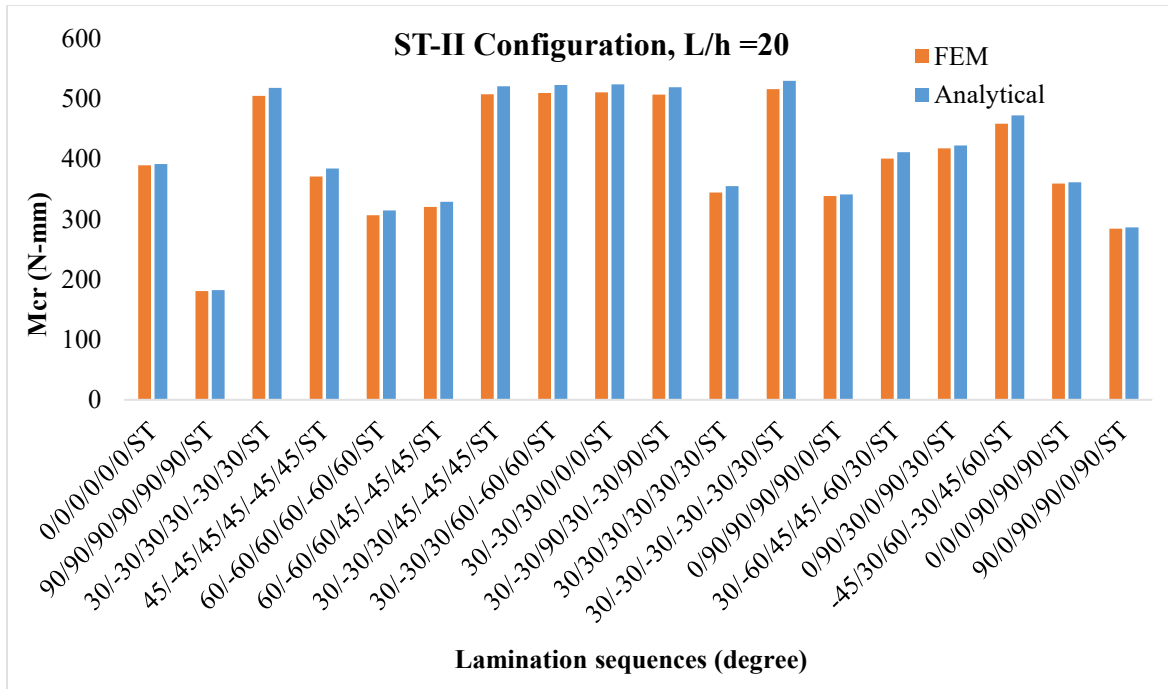


Figure 4.9 Buckling moments at different stacking sequences: $t_k=0.1$ mm for each layer, $L/h=20$, and ST-II configuration

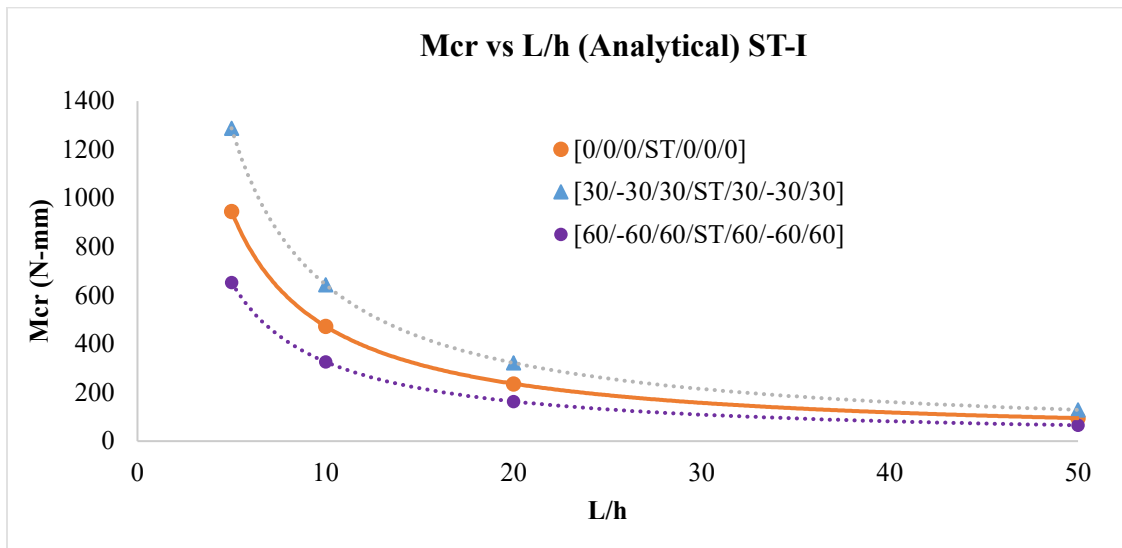


Figure 4.10 Effect of L/h ratio on the critical moment based on analytical formula for three different layups and layer thickness of 0.1 mm and ST-I arrangement

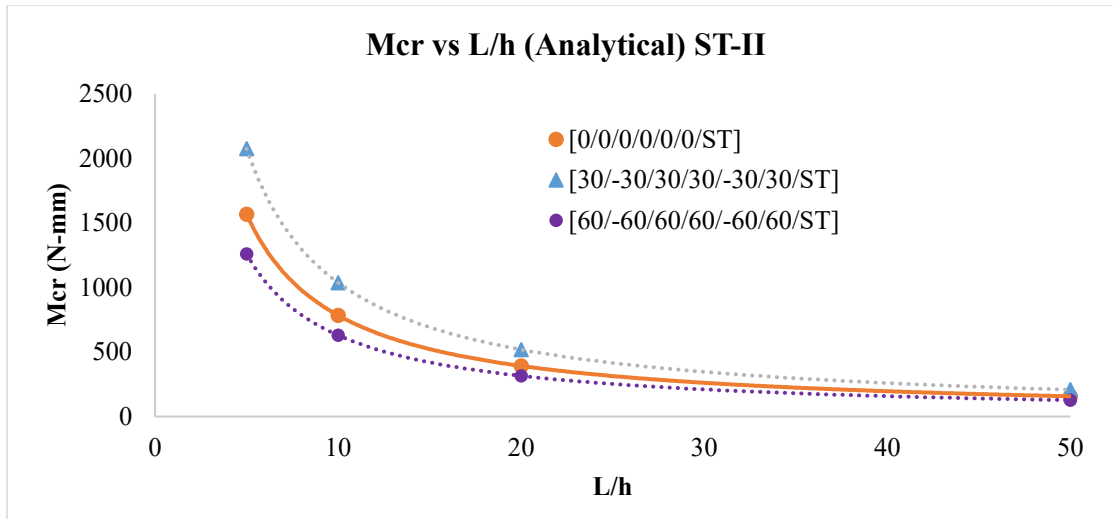


Figure 4.11 Effect of L/h ratio on the critical moment based on analytical formula for three different layups and layer thickness of 0.1 mm and ST-II arrangement

By knowing the value of buckling moment in a selected laminate, Eq. 4.36 helps to calculate the buckling moment for different L/h ratios. Figures 4.10-4.11 show the effect of L/h ratio on the buckling moment for three different orientation sequences of ST-I type for [0/0/0/ST/0/0/0], [30/-30/30/ST/30/-30/30], and [60/-60/60/ST/60/-60/60] and ST-II type for [0/0/0/0/0/ST], [30/-30/30 /30/-30/30/ST], and [60/-60/60 /60/-60/60/ST]. Eq. 4.36 is limited to the analytical formula and is not applicable to the FEM results. There is a noticeable discrepancy between the analytical and numerical results in the cases of [0/0/0/ST/0/0/0] and [0/0/0/0/0/ST] laminates as the ratio of L/h decreases, as shown in Figures 4.13 and 4.14. This discrepancy is related to the fact that the beam with zero fiber orientations buckles numerically in a distortional mode, in which the lateral angle of twist at a certain section transverse to the beam is not constant, rather than a lateral-torsional mode, in which the lateral angle of twist remains constant for a certain section transverse to the beam, Figure 4.12. Nevertheless, Figures 4.13 and 4.14 clearly show that the analytical and numerical buckling moments match almost exactly as the L/h ratio increases beyond 5 for both stacking sequences. It is obvious that in both analytical and

FEM the buckling moments increase as the L/h ratio decrease because of the larger height of the beam to resist against lateral-torsional buckling.

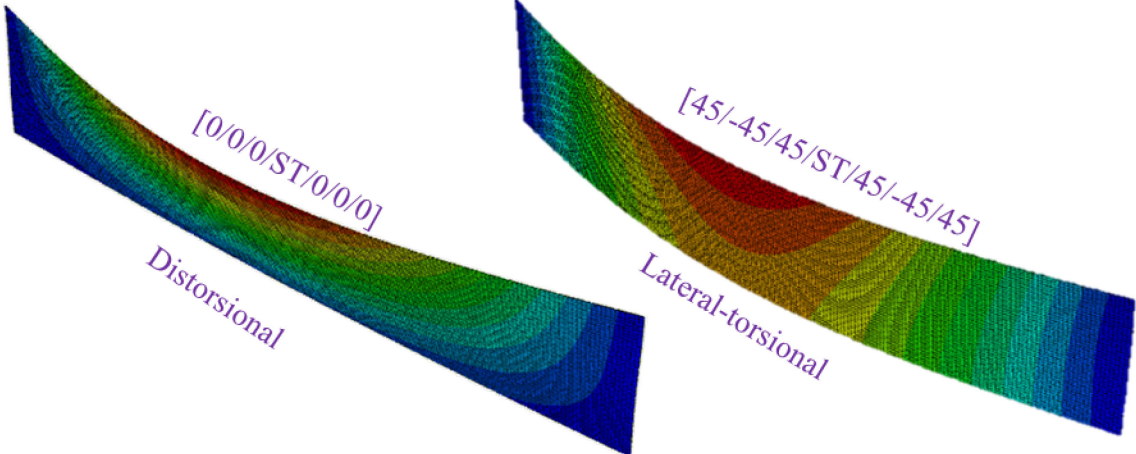


Figure 4.12 Buckling shapes showing distortional buckling mode and lateral-torsional buckling mode for ST-I arrangement

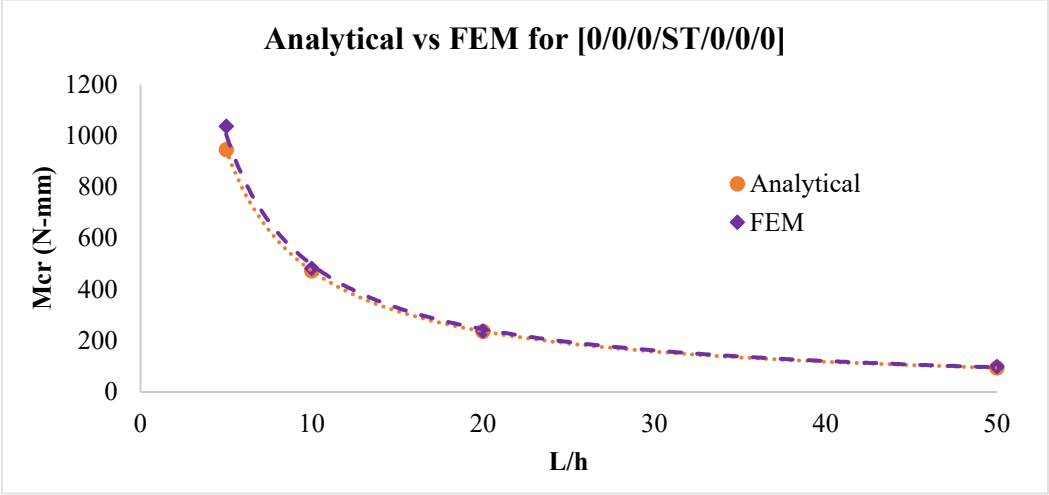


Figure 4.13 Comparison of buckling results obtained from analytical solution and FEM for the [0/0/0/ST/0/0/0] (ST-I) laminate and layer thickness of 0.1 mm by changing L/h ratio

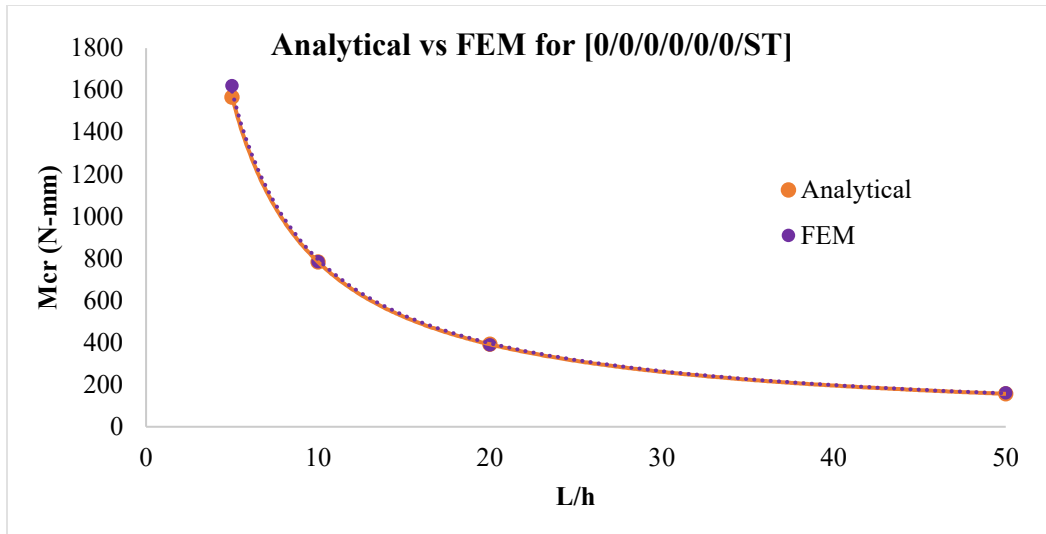


Figure 4.14 Comparison of buckling results obtained from analytical solution and FEM for the [0/0/0/0/0/ST] (ST-II) laminate and layer thickness of 0.1 mm by changing L/h ratio

4.5.2 Effect of Stacking Sequence (ST-I and ST-II)

The previous sections of this chapter discussed the accuracy of the proposed analytical solution for hybrid beams against the finite element method for lateral-torsional buckling. Also, the effect of beam's size was examined against the buckling moment. In this section, and after verifying the accuracy of the solution, the two different stacking orders are studied. Figure 4.15 shows the ratios of the critical lateral torsional buckling moments for ST-II and ST-I for different fiber orientations. The Figure shows ratios bigger than one, which leads to the conclusion that the ST-II, in which the steel sheet is at the side of the beam, has a higher resistance against lateral torsional buckling than the ST-I, in which the steel sheet is in the middle, for all examined fibers orientations.

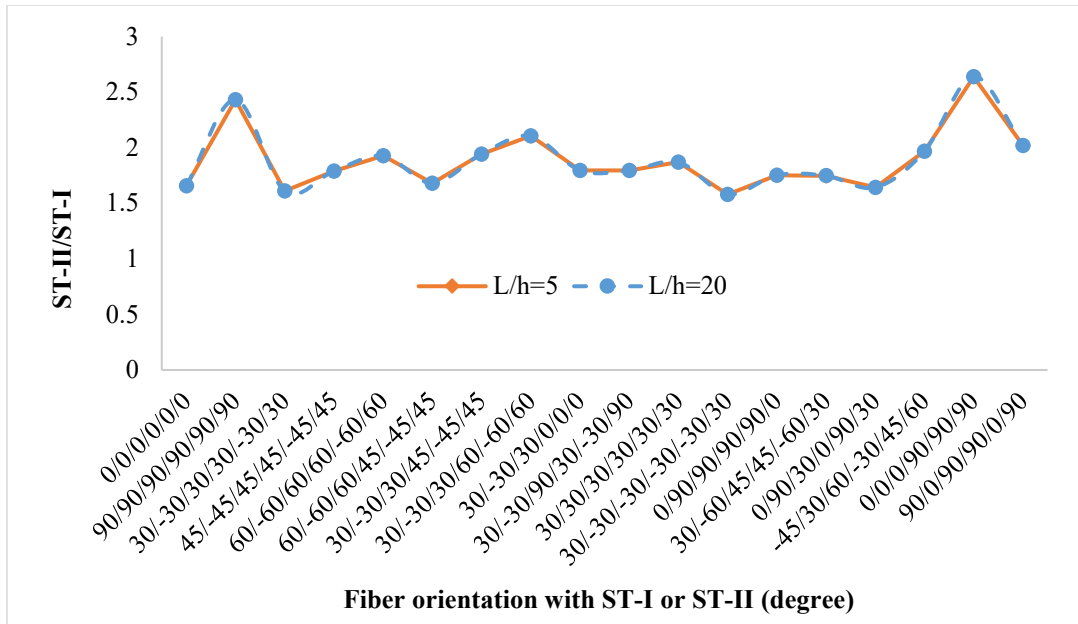


Figure 4.15 Normalized ST-II/ST-I vs. the stacking sequence with L/h = 5 and L/h = 20

4.5.3 Effect of Fiber Angle Orientation

As shown in Figure 4.6. The stacking sequences considerably affect the buckling moments if the dimensions of the beam are kept the same. The lowest value for the critical buckling moment is obtained when the fiber is perpendicular to the beam axis while the highest critical value is obtained for the balanced angle-ply stacking sequence of 30 degrees which is the maximum critical moment among the possible stacking sequences selected for Figure 4.6. Furthermore, a comparison was held to study the effect of fiber angle on critical buckling moment. The orientation $[\theta/-\theta/\theta/ST/\theta/-\theta/\theta]$ (degree) for ST-I and $[\theta/-\theta/\theta/\theta/-\theta/\theta/ST]$ (degree) for ST-II were examined with the change in layup angle of 0 to 90 with an increment of 5 degrees, Figures 4.16 and 4.17. The optimal maximum critical moment is obtained for the balanced angle-ply layup to be around 2100 N.mm for layup $[20/-20/20/20/-20/20/ST]$.

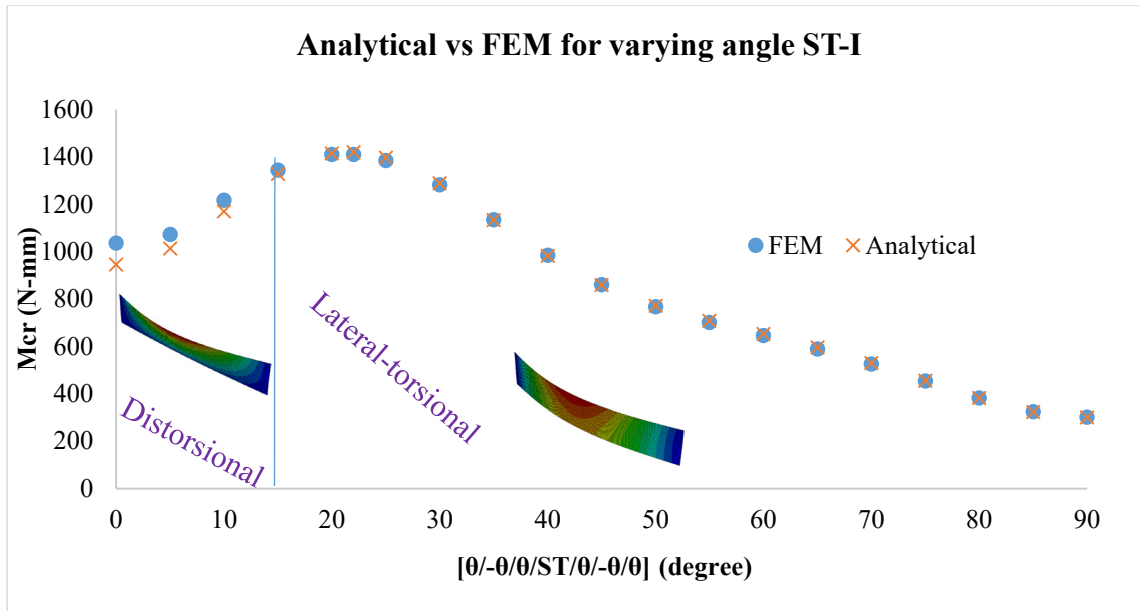


Figure 4.16 Variation in critical buckling moment with the change in layup angle of 0 to 90 at an increment of 5 degrees. (+) Analytical and (●) FEM; layer thickness of 0.1 mm and L/h of 5, ST-I

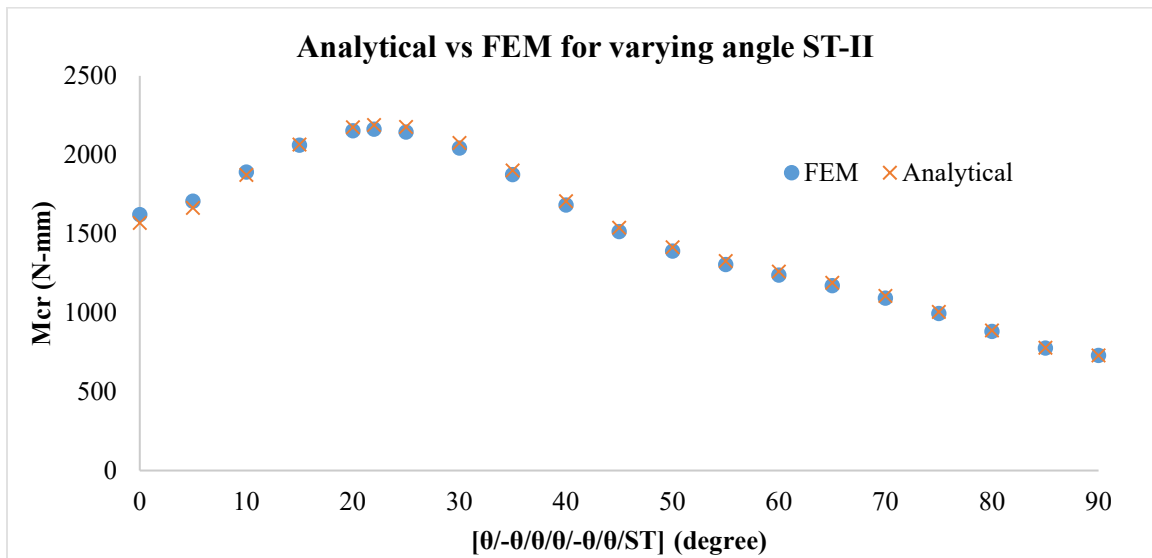


Figure 4.17 Variation in critical buckling moment with the change in layup angle of 0 to 90 at an increment of 5 degrees. (+) Analytical and (●) FEM; layer thickness of 0.1 mm and L/h of 5, ST-II

4.5.4 Effect of Layer Thickness

The previous comparisons in this chapter were held for one layer thickness of 0.1 mm.

Although it is clear that increasing the thickness of the layers will lead to a higher critical

moment for the same L/h ratio, it is essential to mathematically define this relationship. Figures 4.19 and 4.21 present this relation graphically for three different fiber orientations of the two stacking sequences; ST-I and ST-II. A proportional equation (Eq.4.37) is proposed to relate the critical buckling load to the layer thickness for the same stacking sequence and fiber orientation at the same L/h ratio. This equation can predict analytically the critical buckling moment for a known thickness by knowing a different critical buckling moment and its corresponding thickness.

$$\left(\frac{M_{cr}}{t^3}\right)_{unknown} = \left(\frac{M_{cr}}{t^3}\right)_{known} \quad (4.37)$$

A linear correlation (at_k+b) was needed to use this equation to predict the behavior for the finite element model. The parameters (a) and (b) were found numerically for three different fiber orientations for the two stacking sequences, Figures 4.18 and 4.20.

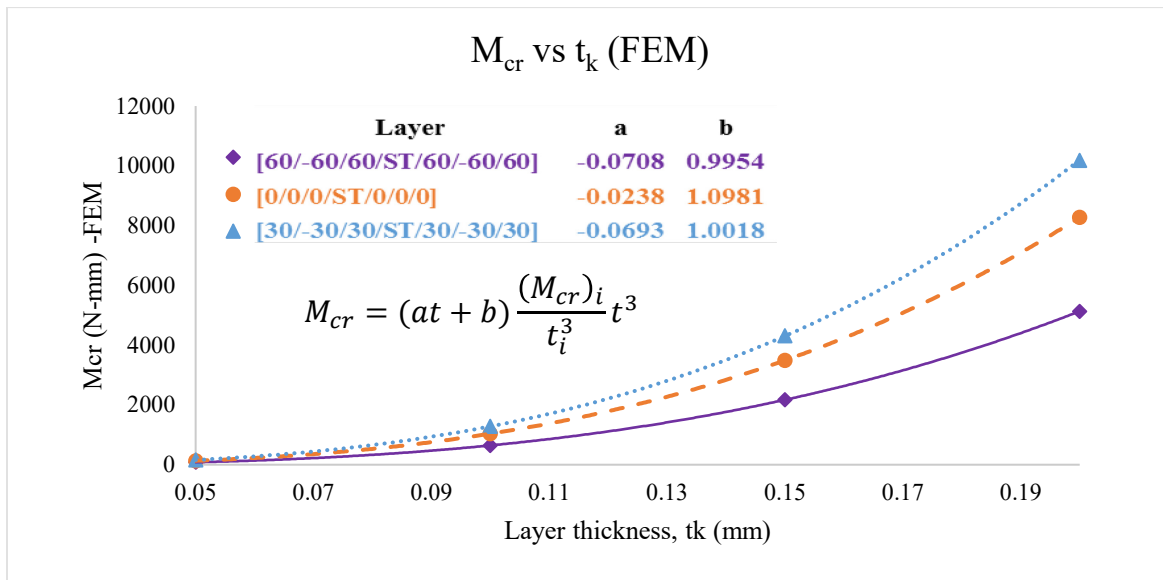


Figure 4.18 Effect of layer thickness, t_k , on the critical moment based on FEM for three different layups and L/h ratio of 5 and ST-I arrangement

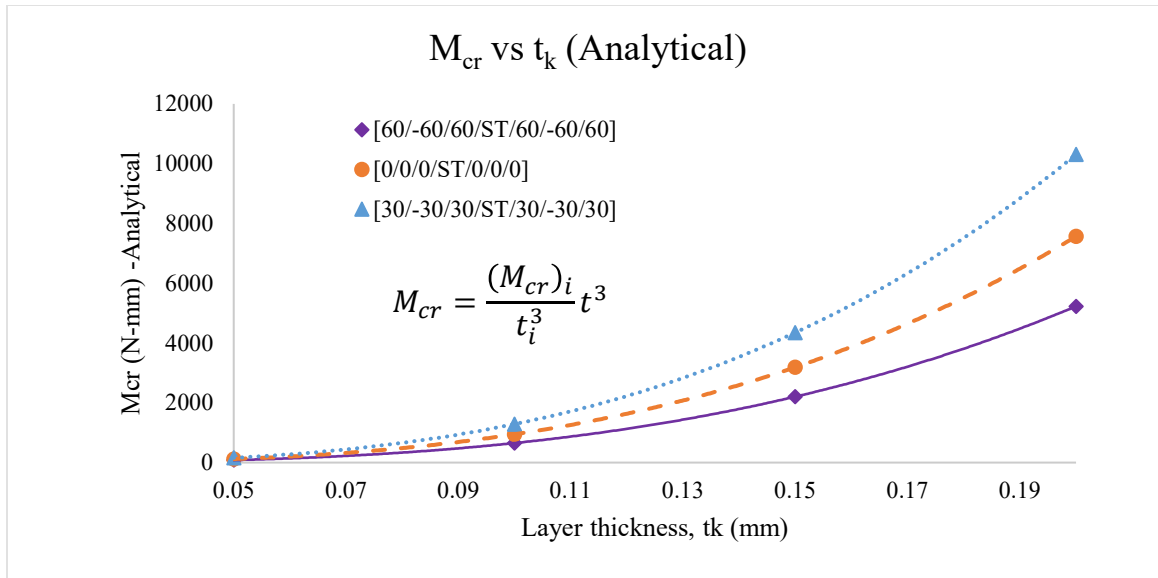


Figure 4.19 Effect of layer thickness, t_k , on the critical moment based on analytical formula for three different layups and L/h ratio of 5 and ST-I arrangement

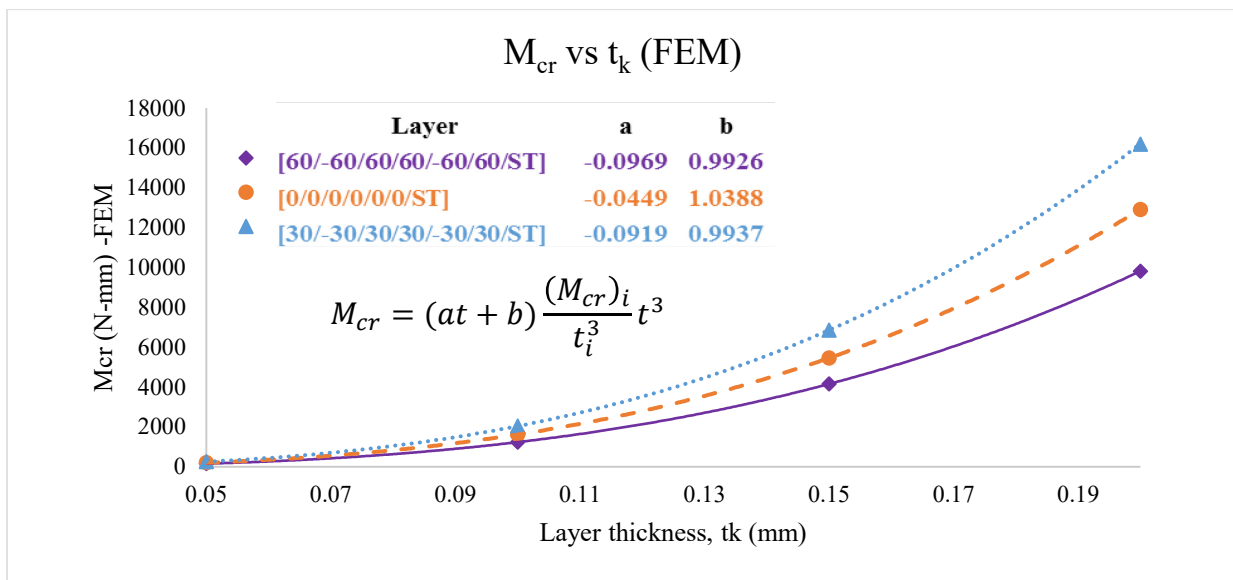


Figure 4.20 Effect of layer thickness, t_k , on the critical moment based on FEM for three different layups and L/h ratio of 5 and ST-II arrangement

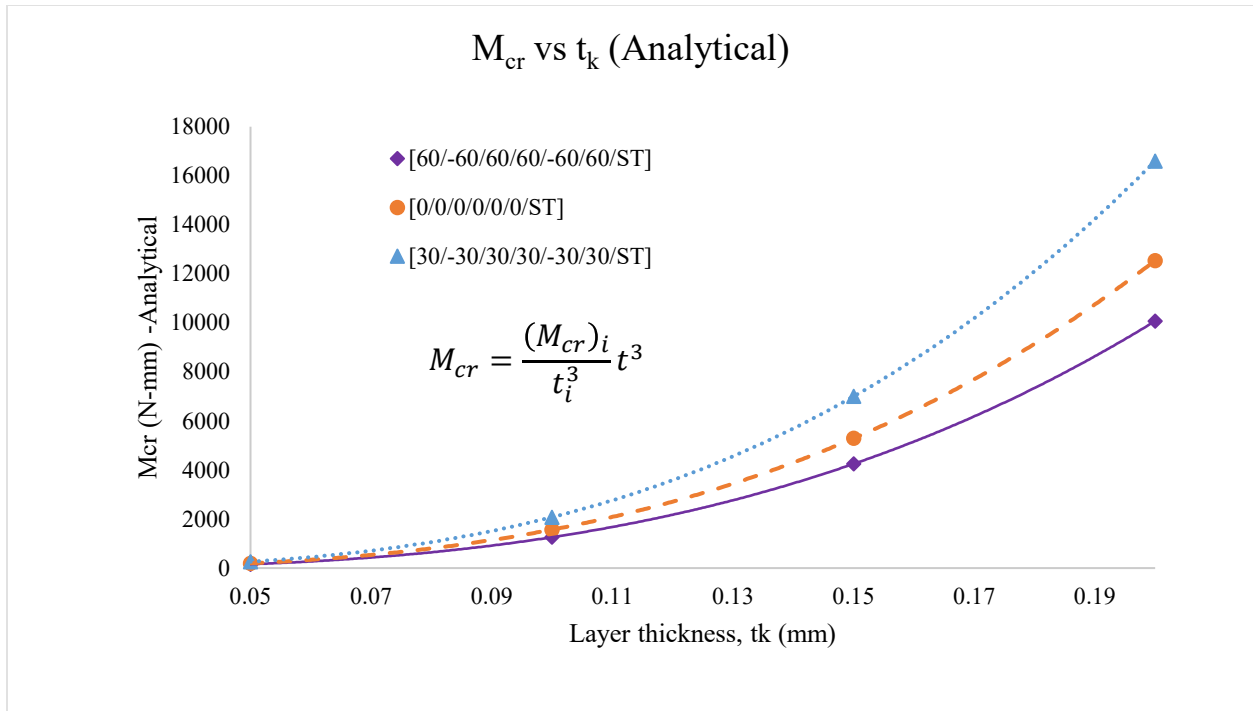


Figure 4.21 Effect of layer thickness, t_k , on the critical moment based on analytical formula for three different layups and L/h ratio of 5 and ST-II arrangement

Figures 4.22 and 4.23 show that, for any thickness and any fiber orientation, as L/h ratio decreases, the critical buckling moment increases for both stacking sequences, confirming the relationship found earlier in Figures 4.10 and 4.11.

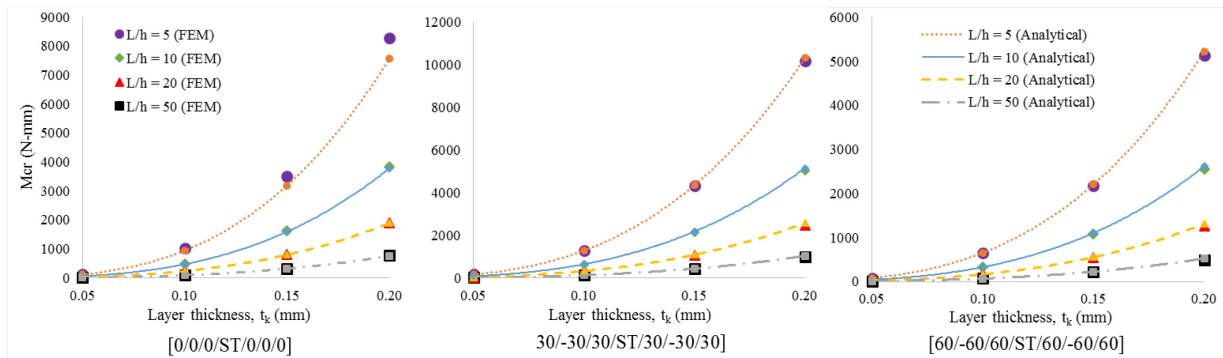


Figure 4.22 Critical buckling moment of three different fiber orientation of ST-I versus different layer thickness and L/h ratios

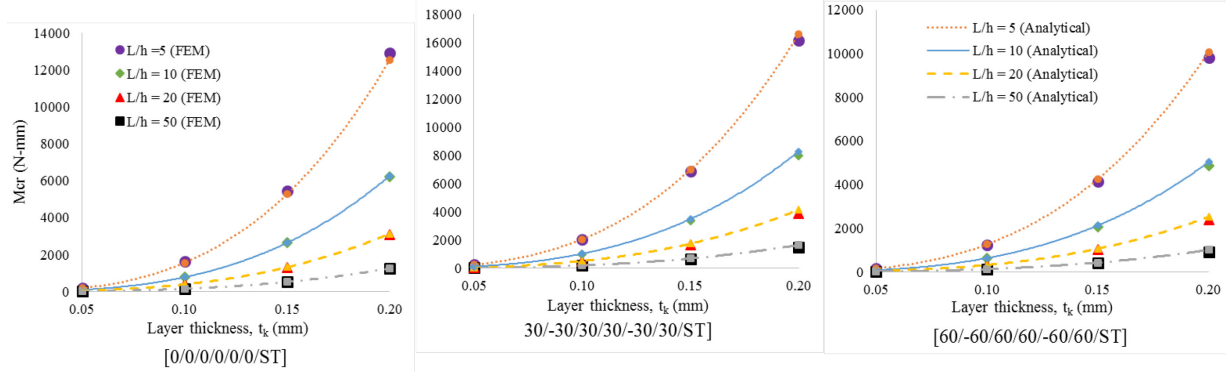


Figure 4.23 Critical buckling moment of three different fiber orientation of ST-II versus different layer thickness and L/h ratios

4.6 Conclusions

In this study, the lateral-torsional buckling of simply supported anisotropic hybrid (steel-FRP), thin-walled, rectangular cross-section beams under pure bending condition was investigated. Based on the assumptions made and the results obtained, an excellent accuracy is observed for a variety of stacking sequences. The applicability of this analytical formulation is proved by comparing the obtained results with FEM results. The study followed the classical laminated plate theory with all considered assumptions and determined an effective lateral-torsional-coupling stiffness matrix.

Based on the study, the stability of the laminated beams under pure bending is greatly affected by the length/height ratio of the beam. The critical buckling moment was inversely proportional to the length/height ratios with a power function. The importance of the stacking sequence, which does not affect the dimensions of the beam, is seen to greatly influence the stability of the beam. The ST-II stacking type, in which the steel laminate is on the side of the beam, shows a higher resistance than the ST-I, in which the steel sheet is located at mid-thickness of the beam. Accordingly, it is more effective to apply the FRP on one side of steel beams to strengthen them against lateral-torsional buckling.

The fiber angle orientation was proven to be a critical variable against the lateral torsional buckling. The critical buckling moment of balanced angle-ply fiber lamination of about [20/-20/20/20/-20/20/ST] is found to reach the maximum value, among this class of layups, because of its maximum lateral and torsional effective stiffness. The minimum critical buckling moment obtained from [90/90/90/ST/90/90] was found to be due to orienting the fibers in the y-direction, thus reducing the torsional effective stiffness. Also, the effect of layer thickness was examined and a proportional equation was developed to relate the layer thickness to the critical buckling load for different fiber orientations and stacking sequences at a certain L/h ratio.

4.7 References

- Barbero, E. J. (1999). *“Introduction to composite materials design”*. CRC press.
- Davalos, J. F., and Qiao, P. (1997), “Analytical and experimental study of lateral and distortional buckling of FRP wide-flange beams”, *Journal of Composites for Construction*, Vol. 1, pp. 150–159
- Karaagac, C., Öztürk, H., & Sabuncu, M. (2007). Lateral dynamic stability analysis of a cantilever laminated composite beam with an elastic support. *International Journal of Structural Stability and Dynamics*, Vol. 7, No.3, PP.377-402.
- Kollár, L. P. (2001). “Flexural-torsional buckling of open section composite columns with shear deformation.” *International Journal of Solids and Structures*, No.38, PP. 7525-7541
- Kollár, L. P., & Springer, G. S. (2003). *Mechanics of composite structures*. Cambridge university press.
- Kotelko, M. (2004). “Load-capacity estimation and collapse analysis of thin-walled beams and columns—recent advances”. *Thin-walled Structures*, Vol. 42, No.2, PP.153-175
- Lee, J., Kim, S.-E., Hong, K. (2002). “Lateral buckling of I-section composite beams.” *Engineering Structures*, No. 24, PP. 955-964
- Lin, Z. M., Polyzois, D., and Shah, A. (1996). “Stability of Thin-walled Pultruded Structural Members by the Finite Element Method.” *Thin-Walled Structures*, No. 24, PP. 1-18
- Machado, S. P. (2010). “Interaction of combined loads on the lateral stability of thin-walled composite beams.” *Engineering Structures*, No. 32, PP. 3516-3527
- Qiao, P., Zou, G., and Davalos, J. (2003). “Flexural-torsional buckling of fiber-reinforced plastic composite cantilever I-beams.” *Composite Structures*, NO. 60, PP. 205-217
- Sapkás, Á. & Kollár, L. P. (2002). Lateral-torsional buckling of composite beams. *International Journal of Solids and Structures*, Vol. 39, No.11, PP. 2939-2963.
- Timoshenko, S. P., & Gere, J. M. (1961). *Theory of elastic stability*. 1961.McGrawHill-Kogakusha Ltd, Tokyo.
- Vlassov, V. Z. (1961). *Thin-walled beams* (2nd ed.) Israel Program for Scientific Translation.

Chapter 5 - Lateral-Torsional Buckling of Anisotropic Laminated Thin-Walled Rectangular Composite Cantilever Beams Subjected to Free End Concentrated Load

In this chapter, a generalized semi-analytical approach for lateral-torsional buckling of anisotropic, thin-walled, rectangular cross-section cantilever beams subjected to free end loading was developed using the classical laminated plate theory as a basis for the constitutive equations. Buckling of such type of members has not been addressed in the literature. A closed form buckling expression is derived in terms of the lateral, torsional and coupling stiffness coefficients of the overall composite. These coefficients are obtained through dimensional reduction by static condensation of the 6x6 constitutive matrix mapped into an effective 2x2 coupled weak axis bending-twisting relationship. The resulting stability differential equation, along with applying boundary conditions, was solved numerically using Mathematica. The resulting solution was found to correlate with the effective lateral-flexure, torsional and coupling stiffness coefficients to yield a general analytical solution. The analytical formula is verified against finite element buckling solutions using ABAQUS for a wide range of lamination orientations showing excellent accuracy. The stability of the beam under different geometric and material parameters, like length/height ratio, layer thickness, and ply orientation, was investigated.

5.1 Introduction

Thin-walled beam structures are major components in many engineering applications. They are widely used as structural components in many types of systems in the field of civil, mechanical, and aerospace engineering. Advanced materials, mainly fiber reinforced polymer (FRP) composites, are partially replacing conventional materials in these types of structural

systems. Composites are being implemented in transportation systems, offshore structures, chemical facilities, aircraft wings and fuselage, helicopter blades, and so on. This increase in interest for using FRP lies in some critical advantages of FRP over conventional materials. Their high strength to weight ratio, high stiffness to weight ratio, their environmental adaptability, their ease of transportation and erection, and their fatigue resistance are some of the advantages FRP provide. The most prominent characteristic is the ability of tailoring the material for each particular application. Structural properties depend on the material system and the shape of the cross-section of the member (Barbero et al.1993). For isotropic structural shapes, it is possible to optimize the section to increase the bending stiffness without compromising the maximum bending strength. Unlike isotropic shapes, with composite members it is possible to optimize the material itself by choosing among a variety of resins, fiber systems, and fiber orientations. Although thin-walled FRP structures exhibit high strength, problems of excessive deformation and instability, due to their low stiffness and slenderness of the member, are the major disadvantages in wider acceptance for structural engineering applications (Lin et al. 1996). Because of these limitations, the new generation of composite structures should be designed to work in a safe way and to experience higher performance than the conventional systems. Consideration of stability and deformation limits tends to be the governing design criteria for FRP structures before these structures reach material failure. Thus, the proper establishment of such criteria is an important prerequisite to the practical use of FRP in engineering applications.

A thin-walled slender beam subjected to in-plane bending moments (about the strong axis) may buckle by a combined lateral bending and twisting of the cross-section. This phenomenon is known as lateral- torsional buckling. Theory of thin-walled open section beams including axial constraints for isotropic materials was developed by Vlassov (1961). This

classical theory neglects the shear deformation in the middle surface of the wall so for thicker-walled beams, the shear deformations may significantly increase the displacements and reduce the buckling loads. The shear deformation theory for transversely loaded isotropic beams was developed by Timoshenko and Gere (1961).

For thin-walled beams, Bauld and Lih-Shyng (1984) applied Vlasov's theory for open section composites with symmetrical laminated walls neglecting the shear deformation. Bank and Bednarczyk (1988) and Barbero et al. (1993) developed simple expressions for the bending, torsional, and warping stiffness of composite laminated beams. Sherbourne and Kabir (1995) studied analytically the effect of transvers shear strain on the lateral buckling of thin-walled, open-section fibrous composite beams. Pandey et al. (1995) proposed an analytical formulation for finding the optimal direction of fiber for improving the lateral buckling strength of thin-walled I-section composite beams. Lin et al. (1996) studied buckling problems of thin-walled composite structural members by finite element methods. Kollar (2001) suggested a closed form solution for thin-walled open section columns, made of orthotropic composite materials, by considering flexure, shear and the torsional warping induced shear deformations. Roberts and Al-Ubaidi (2001) studied the influence of shear deformation on restrained torsional warping of pultruded FRP bars of open cross-section by proposing an approximate theory. Sapkas and Kollar (2002) studied the stability analysis of thin-walled, open section beams, made of orthotropic composite materials under various loading conditions. Lee et al. (2002) presented a general analytical model applicable to the lateral buckling of composite laminated I-beams subjected to various types of loadings. Qiao et al (2003) presented a combined analytical and experimental evaluation of flexural-torsional buckling of fiber reinforced polymer composite I-beams. Tai (2004) studied lateral- torsional buckling of symmetrically laminated, rectangular

cross-section, composite beams under various loading conditions. Karaagac et al. (2007) studied static and dynamic stability of cantilever laminated symmetric and anti-symmetric composite beams having elastic support. Machado (2010) studied the stability of simply supported thin-walled symmetric laminated composite I-beams subjected to combined axial and lateral loads by approximate analytical solutions and compared them with numerical results.

Most of the work, concerning the lateral- torsional stability of thin-walled composite beams, was focused on I-sections. The beams were either considered to be of symmetric layup, anti-symmetric layup, orthotropic, or pultruded in nature. There hasn't been any study recorded on the behavior of general anisotropic laminated composite beams to the best knowledge of the authors.

In the present chapter, a generalized analytical model applicable to the lateral-torsional buckling of a cantilever rectangular cross-section beam, made of anisotropic laminated composite material, subjected to end loading is developed. This model is based on the classical laminated plate theory (CLPT), and accounts for the arbitrary laminate stacking sequence configurations. A finite element model is developed in ABAQUS to predict critical buckling loads and compare with the results obtained from the analytical model. The effects of fiber orientation, beam length/height ratios and wall thickness on the critical buckling forces are studied.

5.2 Analytical Formulation

A cantilever laminated composite beam with length L and a thin rectangular cross section is subjected to free end loading, as shown in Figure 5.1. The model in this study is based on the classical laminated plate theory, Kollar and Springer (2003) and Barbero (1999). The following assumptions are adopted from the classical laminated plate theory:

1. The normals to mid-plane (reference surface) of the laminate remain normal and straight after deformation.
2. The normal to mid-plane of the laminate do not change length – in other words, the thickness of the laminate stays constant.
3. The shear deformations are neglected.
4. The laminate consists of perfectly bonded layers.
5. The stress-strain relationships are applied under plane-stress conditions.

The beam tends to buckle under a lateral-torsional behavior because of its small thickness. The buckling can occur in either clockwise or counterclockwise twisting angle based upon the orientation of controlling fibers in the stacking sequence, as is observed from FEM. If the beam buckles counterclockwise, the angle of twist, β , is considered to be positive, Figure 1a. On the other hand, β , is considered to be negative if the beam buckles clockwise, Figure 5.1b. Separate buckling equation is derived in each case based on the buckling mode shape.

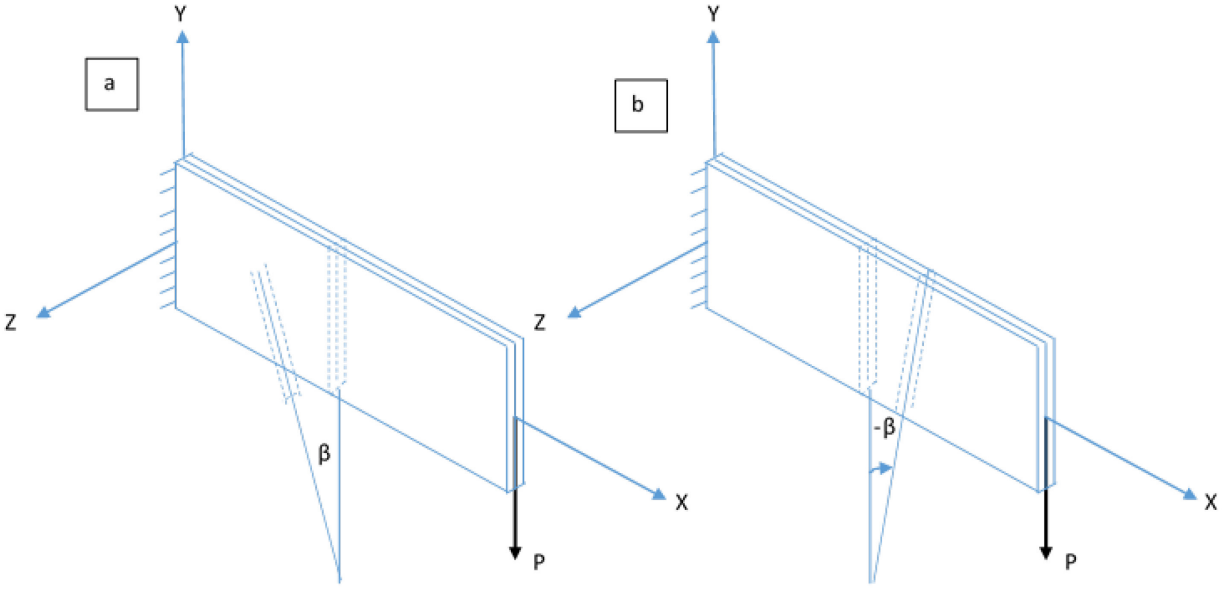


Figure 5.1 Buckling shape of the beam; (a) buckling counterclockwise (+β) and (b) buckling clockwise (-β)

5.2.1 Kinematics

Based on the assumptions in the classical laminated plate theory, the displacement components u, v, w representing the deformation of a point in the beam profile section, as shown in Figure 5.2, are given with respect to mid-surface displacements $u_0, v_0,$ and w_0 as follows:

$$u(x, y, z) = u_0(x, y) - z \frac{\partial w_0}{\partial x}(x, y) \tag{5.1}$$

$$v(x, y, z) = v_0(x, y) - z\beta(x, y) \tag{5.2}$$

$$w(x, y, z) = w_0(x, y) \tag{5.3}$$

where $\beta = \frac{\partial w_0}{\partial y}$ (angle of twist)

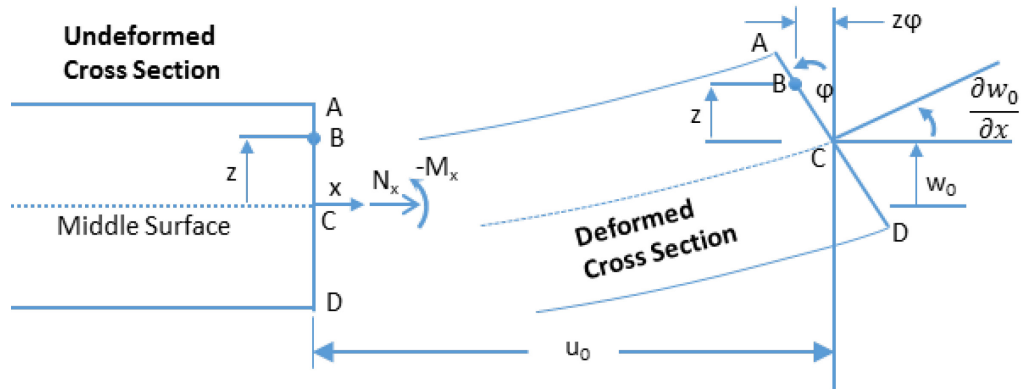


Figure 5.2 Deformation of a point at beam profile section with respect to mid-surface displacement

The strains associated with small displacements from the theory of elasticity are given by

$$\varepsilon_x = \varepsilon_x^0 + z\kappa_x \quad (5.4)$$

$$\varepsilon_y = \varepsilon_y^0 + z\kappa_y \quad (5.5)$$

$$\gamma_{xy} = \gamma_{xy}^0 + z\kappa_{xy} \quad (5.6)$$

where

$$\varepsilon_x^0 = \frac{\partial u_0}{\partial x}, \varepsilon_y^0 = \frac{\partial v_0}{\partial y}, \text{ and } \gamma_{xy}^0 = \frac{\partial u_0}{\partial y} + \frac{\partial v_0}{\partial x} \quad (5.7)$$

$$\kappa_x = -\frac{\partial^2 w_0}{\partial x^2}, \kappa_y = -\frac{\partial \beta}{\partial y}, \text{ and } \kappa_{xy} = -\left(\frac{\partial^2 w_0}{\partial x \partial y} + \frac{\partial^2 w_0}{\partial y \partial x}\right) = -2\frac{\partial \beta}{\partial x} \quad (5.8)$$

The relationship of curvature and displacement are shown in Figure 5.3a and b in the case of β being positive or negative, verifying Eq. 5.8.

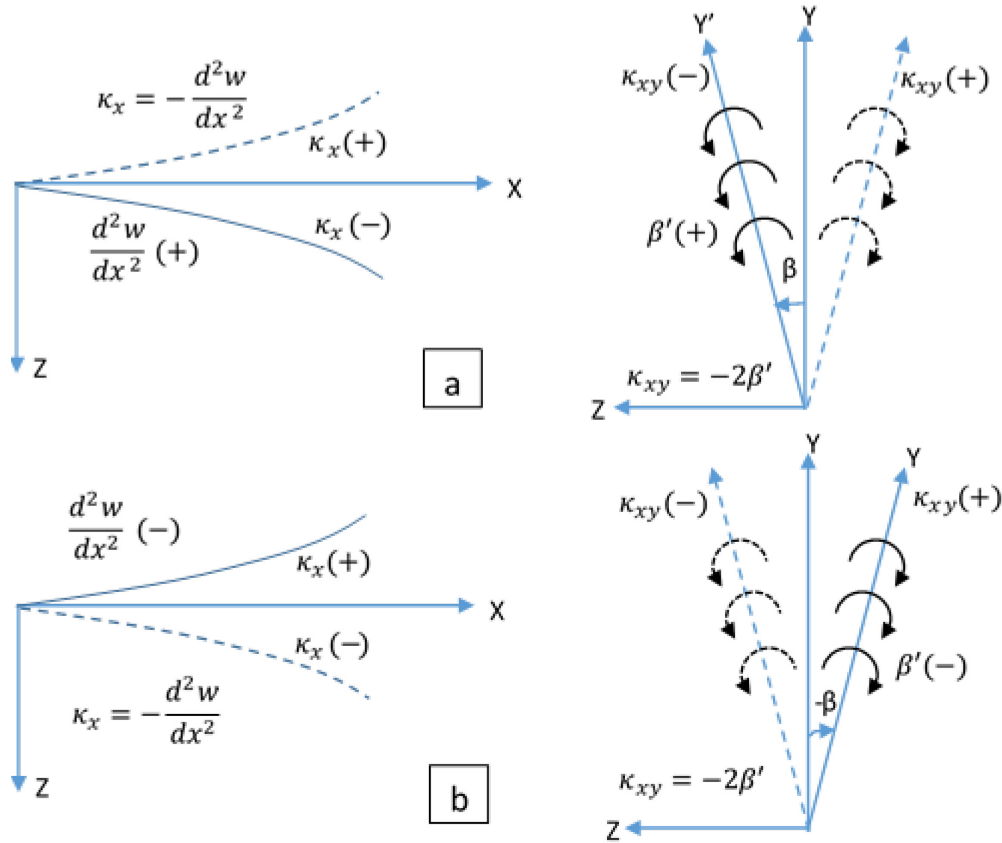


Figure 5.3 Representation of curvatures with respect to displacement and angle of twist; (a) beam buckles counterclockwise ($+\beta$) and (b) beam buckles clockwise ($-\beta$)

5.2.2 Constitutive Equations

The plate stiffness coupling equations based on classical laminated plate theory, shown in Figure 5.4, are given as follows.

$$\begin{Bmatrix} N_x = 0 \\ N_y = 0 \\ N_{xy} = 0 \\ M_x \neq 0 \\ M_y = 0 \\ M_{xy} \neq 0 \end{Bmatrix} = h \begin{bmatrix} A_{11} & A_{12} & A_{16} & B_{11} & B_{12} & B_{16} \\ A_{12} & A_{22} & A_{26} & B_{11} & B_{12} & B_{16} \\ A_{16} & A_{26} & A_{66} & B_{11} & B_{12} & B_{16} \\ B_{11} & B_{12} & B_{16} & D_{11} & D_{12} & D_{16} \\ B_{12} & B_{22} & B_{26} & D_{12} & D_{22} & D_{26} \\ B_{16} & B_{26} & B_{66} & D_{16} & D_{26} & D_{66} \end{bmatrix} \begin{Bmatrix} \varepsilon_x \\ \varepsilon_y \\ \gamma_{xy} \\ \kappa_x \\ \kappa_y \\ \kappa_{xy} \end{Bmatrix} \quad (5.9)$$

where

$$A_{ij} = \sum_{k=1}^N (\bar{Q}_{ij})_k t_k \quad i, j = 1, 2, 6 \text{ are called extensional stiffness coefficients}$$

$B_{ij} = \sum_{k=1}^N (\bar{Q}_{ij})_k t_k \bar{z}_k$ $i, j = 1, 2, 6$ are called extension-bending coupling stiffness coefficients

$D_{ij} = \sum_{k=1}^N (\bar{Q}_{ij})_k \left(t_k \bar{z}_k^2 + \frac{t_k^3}{12} \right)$ $i, j = 1, 2, 6$ are called bending stiffness coefficients

$(\bar{Q}_{ij})_k$ are the components of the k^{th} layer 2D transformed constitutive matrix in the beam coordinate system

\bar{z}_k is the depth from the middle surface to the centroid of the k^{th} layer, and t_k is the thickness of k^{th} layer.

Knowing the zero components of externally applied forces and moments for the loading condition shown in Figures 5.5 and 5.6, which are expressed in Eq. 5.9, the stiffness matrix can be simplified and dimensionally reduced to an effective 2x2 stiffness matrix by using the static condensation technique. In the static condensation technique, the zero and non-zero components of forces and moments from Eq. 5.9 are arranged into separate matrices as follows:

$$h \begin{bmatrix} A_{11} & A_{12} & A_{16} & B_{12} \\ A_{12} & A_{22} & A_{26} & B_{22} \\ A_{16} & A_{26} & A_{66} & B_{26} \\ B_{12} & B_{22} & B_{26} & D_{22} \end{bmatrix} \begin{Bmatrix} \varepsilon_x \\ \varepsilon_y \\ \gamma_{xy} \\ \kappa_y \end{Bmatrix} + h \begin{bmatrix} B_{11} & B_{16} \\ B_{12} & B_{26} \\ B_{16} & B_{66} \\ D_{12} & D_{26} \end{bmatrix} \begin{Bmatrix} \kappa_x \\ \kappa_{xy} \end{Bmatrix} = \begin{Bmatrix} 0 \\ 0 \\ 0 \\ 0 \end{Bmatrix} \quad (5.10)$$

$$\begin{Bmatrix} M_x \\ M_{xy} \end{Bmatrix} = h \begin{bmatrix} D_{11} & D_{16} \\ D_{16} & D_{66} \end{bmatrix} \begin{Bmatrix} \kappa_x \\ \kappa_{xy} \end{Bmatrix} + h \begin{bmatrix} B_{11} & B_{16} \\ B_{12} & B_{26} \\ B_{16} & B_{66} \\ D_{12} & D_{26} \end{bmatrix}^T \begin{Bmatrix} \varepsilon_x \\ \varepsilon_y \\ \gamma_{xy} \\ \kappa_y \end{Bmatrix} \quad (5.11)$$

The reduced effective 2x2 stiffness matrix (Eq. 5.13) can be obtained by defining $\begin{Bmatrix} \varepsilon_x \\ \varepsilon_y \\ \gamma_{xy} \\ \kappa_y \end{Bmatrix}$ from

Eq. 5.10 in terms of two other curvature components, as shown in Eq. 5.12, and substituting it into Eq. 5.11.

$$\begin{Bmatrix} \varepsilon_x \\ \varepsilon_y \\ \gamma_{xy} \\ \kappa_y \end{Bmatrix} = - \begin{bmatrix} A_{11} & A_{12} & A_{16} & B_{12} \\ A_{12} & A_{22} & A_{26} & B_{22} \\ A_{16} & A_{26} & A_{66} & B_{26} \\ B_{12} & B_{22} & B_{26} & D_{22} \end{bmatrix}^{-1} \begin{bmatrix} B_{11} & B_{16} \\ B_{12} & B_{26} \\ B_{16} & B_{66} \\ D_{12} & D_{26} \end{bmatrix} \begin{Bmatrix} \kappa_x \\ \kappa_{xy} \end{Bmatrix} \quad (5.12)$$

$$\begin{Bmatrix} M_x \\ M_{xy} \end{Bmatrix} = h \begin{bmatrix} D_Y & D_{YT} \\ D_{YT} & D_T \end{bmatrix} \begin{Bmatrix} \kappa_x \\ \kappa_{xy} \end{Bmatrix} \quad (5.13)$$

where

$$\begin{bmatrix} D_Y & D_{YT} \\ D_{YT} & D_T \end{bmatrix} = \begin{bmatrix} D_{11} & D_{16} \\ D_{16} & D_{66} \end{bmatrix} - \begin{bmatrix} B_{11} & B_{16} \\ B_{12} & B_{26} \\ B_{16} & B_{66} \\ D_{12} & D_{26} \end{bmatrix}^T \begin{bmatrix} A_{11} & A_{12} & A_{16} & B_{12} \\ A_{12} & A_{22} & A_{26} & B_{22} \\ A_{16} & A_{26} & A_{66} & B_{26} \\ B_{12} & B_{22} & B_{26} & D_{22} \end{bmatrix}^{-1} \begin{bmatrix} B_{11} & B_{16} \\ B_{12} & B_{26} \\ B_{16} & B_{66} \\ D_{12} & D_{26} \end{bmatrix}$$

D_Y is the effective composite lateral stiffness coefficient, D_T is the effective composite twisting stiffness coefficient, and D_{YT} is the effective composite lateral-twisting coupling coefficient. In most cases, where the layers are symmetric, anti-symmetric, cross-ply, special angle ply, D_{YT} coefficient will be zero. However, for the generally anisotropic cases, D_{YT} coefficient is not zero and will play a significant role in determining the buckling forces of the beams.

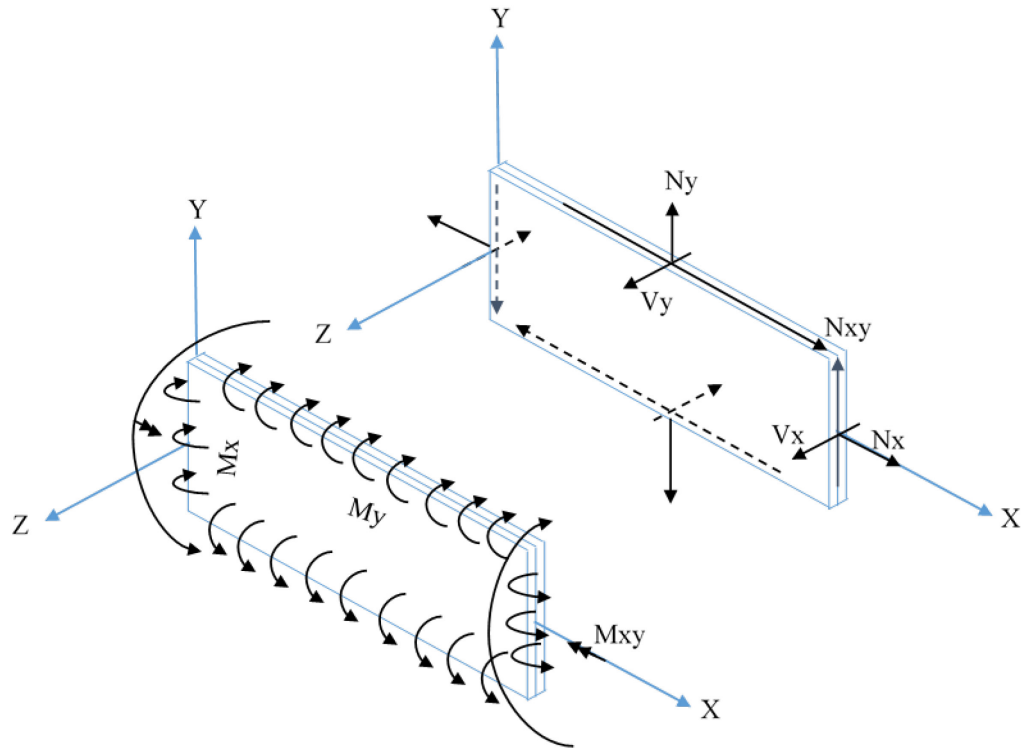
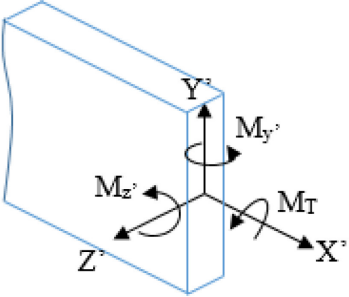
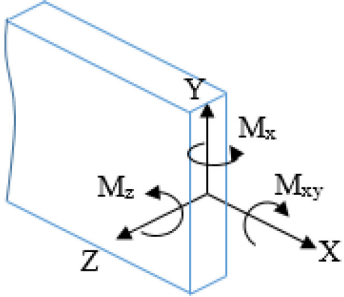


Figure 5.4 Force and moment resultants on a beam based on classical laminated plate theory

Referring to Figure 5.1 (structural coordinate) and Figure 5.4 (laminate coordinate), the bending moment M_y in structural coordinate is replaced by M_x in laminate coordinate, on the other hand, the shear moment, M_{xy} , in laminate coordinate is in the opposite direction of twisting moment in the structural coordinate system and is found by Kollar and Springer (2003) to be $M_T = -2 M_{xy}$. Table 5.1 shows the relation of moment components in structural coordinate and laminate composite coordinate systems.

Table 5.1 Relation of moment components in structural coordinate and laminate composite coordinate

| The structural coordinate (deformed axes) | Laminate composite coordinate |
|---|---|
|  | <div style="text-align: center;"> $M'_z = M_z$ $M'_y = M_x$ $M_T = -2M_{xy}$ </div>  |

Substituting the curvatures in terms of displacement and rotation from Eq. 5.8 into Eq. 5.13, and writing the moments in structural coordinate system, the following relation will be obtained.

$$\begin{Bmatrix} M_{y'} \\ -M_T \end{Bmatrix} = h \begin{bmatrix} D_Y & 2D_{YT} \\ 2D_{YT} & 4D_T \end{bmatrix} \begin{Bmatrix} -\frac{d^2w}{dx^2} \\ -\beta' \end{Bmatrix} \quad (5.14)$$

5.2.3 Equilibrium Equations

As discussed earlier, two configurations of buckling mode, counterclockwise and clockwise, were considered for the analytical formulation. The derivation of equilibrium equations will be discussed in the following sub-sections.

5.2.3.1 Buckling Counterclockwise

Figure 5.5 shows the components of external moments about original and deformed axes when the beam buckles counterclockwise, where β is considered to be positive. The moment components are shown in the following equations:

External moments in un-deformed configuration (original axes):

$$M_z = -P(L - x) \quad (5.15)$$

$$M_y = 0 \quad (5.16)$$

$$M_T = P(w_1 - w) \quad (5.17)$$

External moments in the deformed configuration (deformed axes):

$$M_z' = -P(L - x) - P(w_1 - w) \frac{dw}{dx} \quad (5.18)$$

$$M_y' = -P(L - x)\beta + P(w_1 - w) \frac{dv}{dx} \quad (5.19)$$

$$M_T = -\frac{dw}{dx}P(L - x) + P(w_1 - w) \quad (5.20)$$

where $P(w_1 - w) \frac{dw}{dx}$ and $P(w_1 - w) \frac{dv}{dx}$ are higher order terms which will be neglected.

The following system of differential equations is obtained after substituting the external moments from Eqs. 5.19 and 5.20 into Eq. 5.14:

$$\begin{Bmatrix} -P(L - x)\beta \\ \frac{dw}{dx}P(L - x) - P(w_1 - w) \end{Bmatrix} = h \begin{bmatrix} D_Y & 2D_{YT} \\ 2D_{YT} & 4D_T \end{bmatrix} \begin{Bmatrix} -\frac{d^2w}{dx^2} \\ -\beta' \end{Bmatrix} \quad (5.21)$$

$$-hD_Y \frac{d^2w}{dx^2} - 2hD_{YT}\beta' = -P(L - x)\beta \quad (5.22)$$

$$-2hD_{YT} \frac{d^2w}{dx^2} - 4hD_T\beta' = \frac{dw}{dx}P(L - x) - P(w_1 - w) \quad (5.23)$$

Writing Eqs.5.22 and 5.23 in terms of $\frac{d^2w}{dx^2}$ and equating the two expressions, the following relationship can be obtained.

$$\frac{1}{hD_Y} [-2hD_{YT}\beta' + P(L - x)\beta] = \frac{1}{2hD_{YT}} \left[-4hD_T\beta' - \frac{dw}{dx}P(L - x) + P(w_1 - w) \right] \quad (5.24)$$

Differentiating Eq.5.24 with respect to x and rearranging the resulting expression in terms of

$\frac{d^2w}{dx^2}$, Eq.5.25 will be obtained.

$$\frac{d^2w}{dx^2} = -\frac{2D_{YT}}{D_Y}\beta' - \frac{4h}{P(L-x)} \left[D_T - \frac{D_{YT}^2}{D_Y} \right] \beta'' + \frac{2PD_{YT}\beta}{PD_Y(L-x)} \quad (5.25)$$

Equating the left hand side of Eq.5.24, which is equal to $\frac{d^2w}{dx^2}$ in Eq. 5.22, and the right hand side of Eq.5.25, the resulting expression reduces to a second order ordinary differential equation with non-constant coefficients.

$$\beta'' - \frac{2hPD_{YT}}{4h^2[D_Y D_T - D_{YT}^2]} \beta + \frac{P^2(L-x)^2}{4h^2[D_Y D_T - D_{YT}^2]} \beta = 0 \quad (5.26)$$

Setting $\psi_1^2 = \frac{P^2}{4h^2[D_Y D_T - D_{YT}^2]}$ and $\psi_2 = \frac{2hPD_{YT}}{4h^2[D_Y D_T - D_{YT}^2]}$, a simplified form of differential equation is obtained.

$$\beta'' + (\psi_1^2(L-x)^2 - \psi_2)\beta = 0 \quad (5.27)$$

This form of differential equation is a Weber function which can be solved by a numerical iterative procedure in commercial software which can solve these types of equations.

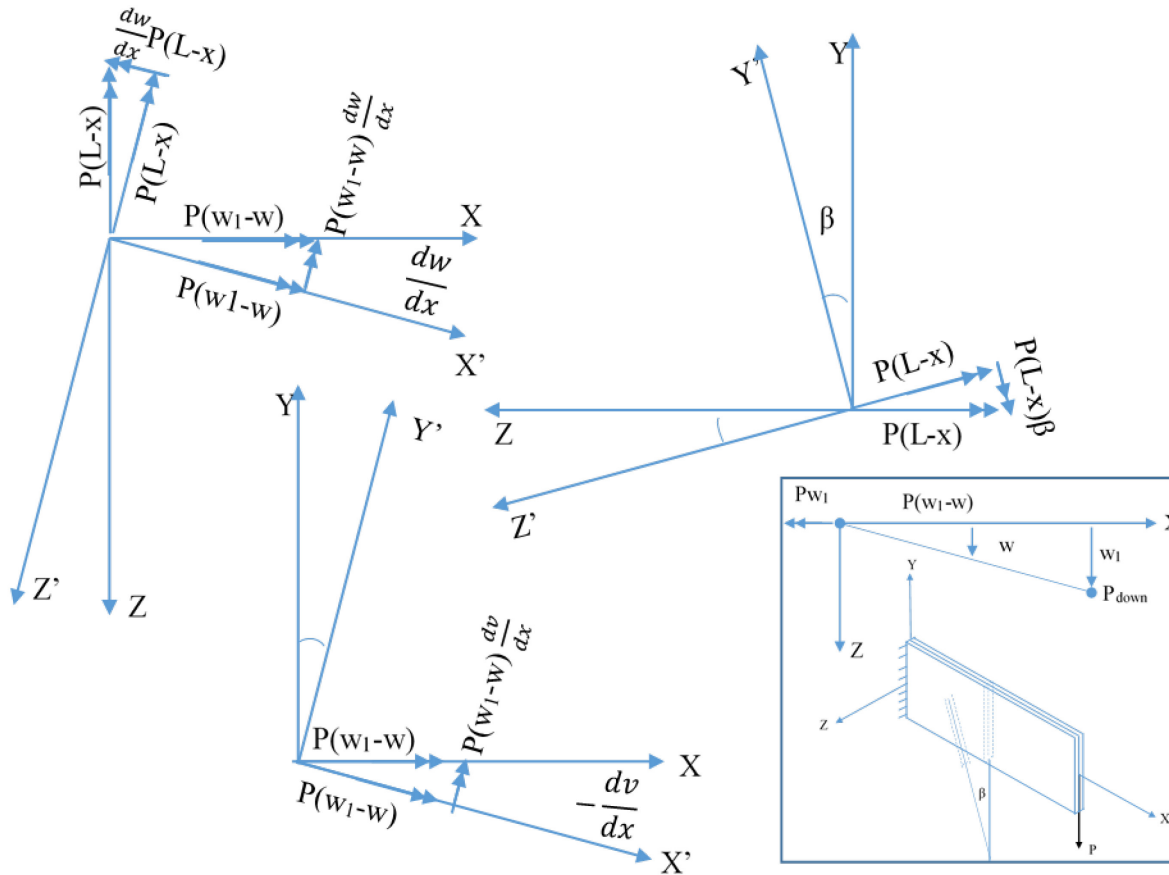


Figure 5.5 Components of external moments about original and deformed axes of laminated cantilever beam subjected to free end loading, buckled counterclockwise

5.2.3.2 Buckling Clockwise

Figure 5.6 shows the components of external moments about the original and deformed axes when the beam buckles clockwise, where β is considered to be negative. The moment components are shown in the following equations:

External moments in un-deformed configuration (original axes):

$$M_z = -P(L - x) \tag{5.28}$$

$$M_y = 0 \tag{5.29}$$

$$M_T = -P(w_1 - w) \tag{5.30}$$

External moments in the deformed configuration (deformed axes):

$$M_z' = -P(L - x) - P(w_1 - w) \frac{dw}{dx} \quad (5.31)$$

$$M_y' = P(L - x)\beta - P(w_1 - w) \frac{dv}{dx} \quad (5.32)$$

$$M_T = \frac{dw}{dx} P(L - x) - P(w_1 - w) \quad (5.33)$$

where $P(w_1 - w) \frac{dw}{dx}$ and $P(w_1 - w) \frac{dv}{dx}$ are higher order terms which can be neglected.

The following system of differential equations is obtained after substituting the external moments from Eqs. 5.32 and 5.33 into Eq. 5.14:

$$\left\{ \begin{array}{l} P(L - x)\beta \\ -\frac{dw}{dx} P(L - x) + P(w_1 - w) \end{array} \right\} = h \begin{bmatrix} D_Y & 2D_{YT} \\ 2D_{YT} & 4D_T \end{bmatrix} \left\{ \begin{array}{l} -\frac{d^2w}{dx^2} \\ -\beta' \end{array} \right\} \quad (5.34)$$

$$-hD_Y \frac{d^2w}{dx^2} - 2hD_{YT}\beta' = P(L - x)\beta \quad (5.35)$$

$$-2hD_{YT} \frac{d^2w}{dx^2} - 4hD_T\beta' = -\frac{dw}{dx} P(L - x) + P(w_1 - w) \quad (5.36)$$

Writing Eqs. 5.35 and 5.36 in terms of $\frac{d^2w}{dx^2}$ and equating the two expressions, the following relationship can be obtained.

$$\frac{1}{hD_Y} [-2hD_{YT}\beta' - P(L - x)\beta] = \frac{1}{2hD_{YT}} \left[-4hD_T\beta' + \frac{dw}{dx} P(L - x) - P(w_1 - w) \right] \quad (5.37)$$

Differentiating Eq. 5.37 with respect to x and rearranging the resulting expression in terms of $\frac{d^2w}{dx^2}$, Eq. 5.38 will be obtained.

$$\frac{d^2w}{dx^2} = -\frac{2D_{YT}}{D_Y} \beta' + \frac{4h}{P(L-x)} \left[D_T - \frac{D_{YT}^2}{D_Y} \right] \beta'' + \frac{2PD_{YT}\beta}{PD_Y(L-x)} \quad (5.38)$$

Equating the left hand side of Eq. 5.37, which is equal to $\frac{d^2w}{dx^2}$ in Eq. 5.35, and the right hand side of Eq. 5.38, the resulting expression reduces to a second order ordinary differential equation with non-constant coefficients.

$$\beta''' + \frac{2hPD_{YT}}{4h^2[D_Y D_T - D_{YT}^2]} \beta + \frac{P^2(L-x)^2}{4h^2[D_Y D_T - D_{YT}^2]} \beta = 0 \quad (5.39)$$

Setting $\psi_1^2 = \frac{P^2}{4h^2[D_Y D_T - D_{YT}^2]}$ and $\psi_2 = \frac{2hPD_{YT}}{4h^2[D_Y D_T - D_{YT}^2]}$, a simplified form of differential equation is obtained.

$$\beta''' + (\psi_1^2(L-x)^2 + \psi_2)\beta = 0 \quad (5.40)$$

This form of differential equation is a Weber function which can be solved by a numerical iterative procedure in commercial software which can solve these types of equations.

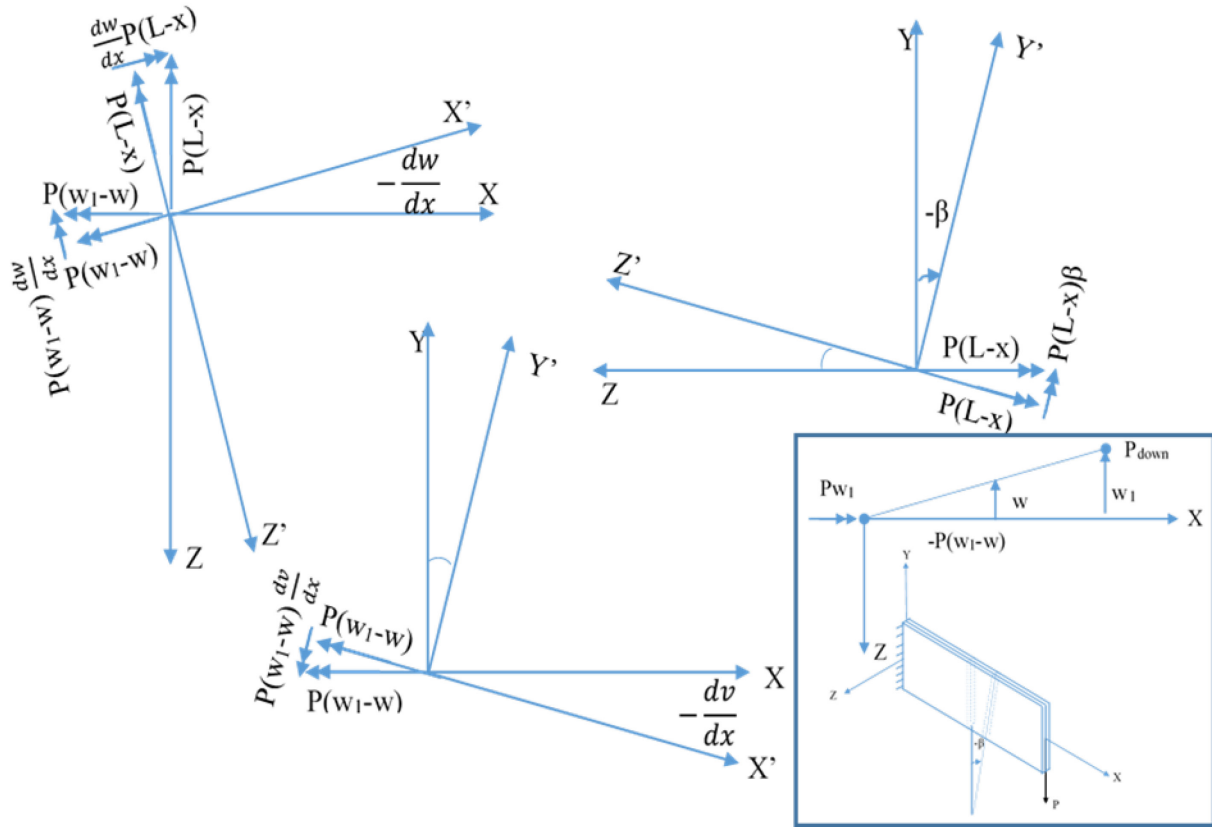


Figure 5.6 Components of external moments about original and deformed axes of laminated cantilever beam subjected to free end loading, buckled clockwise

Comparing Eqs. 5.27 and 5.40, derived from the above two cases, one can see that the only difference is the sign of coefficient ψ_2 , where it is negative for counterclockwise bucking

and positive for the case of clockwise buckling. By introducing a new coefficient, C_1 , which defines ψ_2 in terms of ψ_1 .

$$\psi_2 = C_1 \psi_1 \quad (5.41)$$

$$\text{where } C_1 = \frac{D_{YT}}{\sqrt{[D_Y D_T - D_{YT}^2]}}$$

The differential equation for two cases is as follows:

$$\beta'' + (\psi_1^2 (L - x)^2 \pm C_1 \psi_1) \beta = 0 \quad (5.42)$$

The value of C_1 is positive if the coefficient D_{YT} is positive. This case was observed through finite element analysis to buckle in the clockwise direction making the net sign of the C_1 term positive. On the other hand, C_1 is negative if D_{YT} is negative. This case was observed through finite element analysis to buckle in the counterclockwise direction making the net sign of the C_1 term positive as well. Therefore, the second term of the equation, which includes C_1 , is always positive. As a result, the final form of differential equation can be presented as follows:

$$\beta'' + (\psi_1^2 (L - x)^2 + C_1 \psi_1) \beta = 0 \quad (5.43)$$

$$\text{where } C_1 = \frac{|D_{YT}|}{\sqrt{[D_Y D_T - D_{YT}^2]}}$$

The critical buckling force is

$$P_{cr} = \psi_1 h \sqrt{4[D_Y D_T - D_{YT}^2]} \quad (5.44)$$

A generalized buckling equation can be written by introducing a normalized coefficient to Eq. 5.44.

$$P_{cr} = \frac{C_2 h}{L^2} \sqrt{4[D_Y D_T - D_{YT}^2]} \quad (5.45)$$

$$\text{where } C_2 = \psi_1 L^2$$

The value of ψ_1 in Eq. 5.43 is solved for arbitrary stacking sequences using a numerical iterative procedure in Mathematica by applying the following boundary conditions: $\beta(0) = 0$ and $\beta'(L) = 0$. The general solution of Eq. 5.43 contains a nonlinear polynomial function which is called ParabolicCylinderD (or D) in Mathematica. In this process, the program first solves for the general solution of the differential equation. The boundary conditions are applied to the general solution. After applying the boundary conditions, a polynomial function of $f_n(\psi_1)$ is obtained, which must be set equal to zero. This function contains real and imaginary parts. To obtain a numerical solution for ψ_1 , the numerical values for a certain stacking sequence and beam geometric parameters should be iterated until the equation converges. The process is repeated for each stacking sequence. Figure 5.7 shows the flowchart of the procedure used in Mathematica to obtain values of ψ_1 . A screenshot of the script, used in Mathematica, is shown in Figure 5.8.

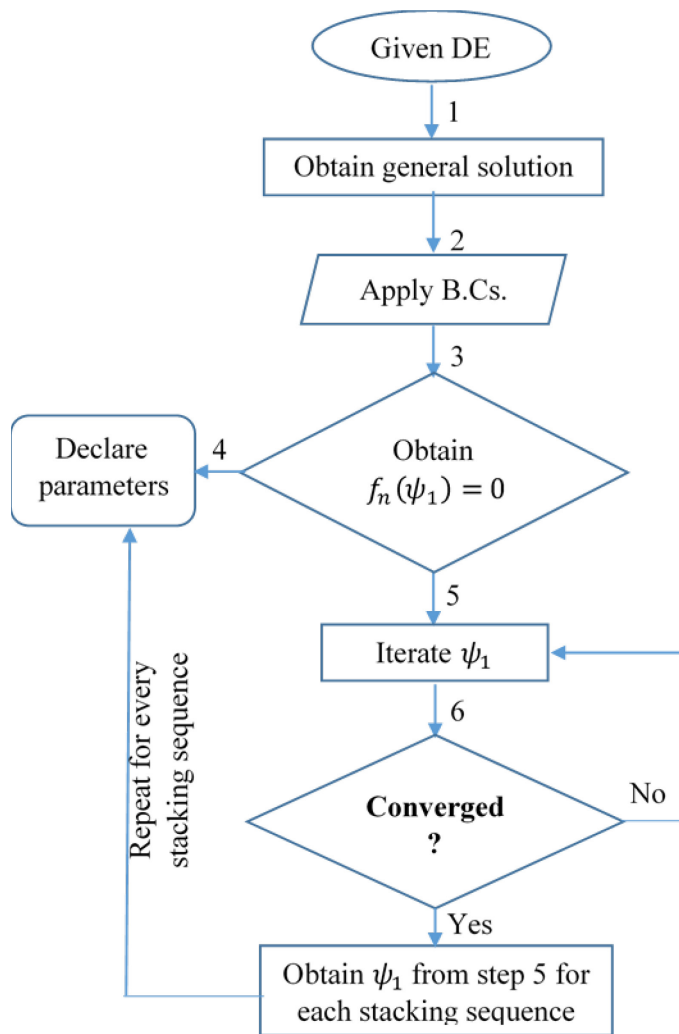


Figure 5.7 Flowchart of the semi-analytical solution of the buckling equation using Mathematica

```

sol = DSolve[ $\beta[x] (\alpha \psi + \psi^2 (L - x)^2) + \beta''[x] = 0, \beta, x]$  (* the differential equation to be solved*)

{{ $\beta \rightarrow \left\{ (x) \mapsto c_1 D_{-\frac{1}{2}i(-i+\alpha)} \left( \sqrt[4]{-1} \sqrt{2} x \sqrt{\psi} - \sqrt[4]{-1} \sqrt{2} L \sqrt{\psi} \right) + c_2 D_{\frac{1}{2}i(i+\alpha)} \left( i \left( \sqrt[4]{-1} \sqrt{2} x \sqrt{\psi} - \sqrt[4]{-1} \sqrt{2} L \sqrt{\psi} \right) \right) \right\}}$ }}

m = sol[[1]]

 $\beta \rightarrow \left\{ (x) \mapsto c_1 D_{-\frac{1}{2}i(-i+\alpha)} \left( \sqrt[4]{-1} \sqrt{2} x \sqrt{\psi} - \sqrt[4]{-1} \sqrt{2} L \sqrt{\psi} \right) + c_2 D_{\frac{1}{2}i(i+\alpha)} \left( i \left( \sqrt[4]{-1} \sqrt{2} x \sqrt{\psi} - \sqrt[4]{-1} \sqrt{2} L \sqrt{\psi} \right) \right) \right\}$ 

BC1 =  $\beta'[L] /. m$  (* =0; first boundary condition*)


$$\frac{\sqrt[4]{-1} \sqrt{\pi} 2^{\frac{1}{2} + \frac{1}{2}i} (1 - \frac{1}{2}i(\alpha - i)) c_1 \sqrt{\psi} - (-1)^{3/4} \sqrt{\pi} 2^{\frac{1}{2} + \frac{1}{2}i} (1 - \frac{1}{2}i(\alpha + i)) c_2 \sqrt{\psi}}{\Gamma(\frac{1}{4}i(-i + \alpha))} - \frac{(-1)^{3/4} \sqrt{\pi} 2^{\frac{1}{2} + \frac{1}{2}i} (1 - \frac{1}{2}i(\alpha + i)) c_2 \sqrt{\psi}}{\Gamma(-\frac{1}{4}i(i + \alpha))}$$


solveC2 = Solve[{BC1 == 0}, {C[2]}] (* solves C[2] in terms of C[1] from first B.C.*)

{{ $c_2 \rightarrow \frac{i 2^{-\frac{1}{2}(i\alpha)} c_1 \Gamma(-\frac{1}{4}i(i + \alpha))}{\Gamma(\frac{1}{4}i(-i + \alpha))}$ }}

BC2 =  $\beta[0] /. m$  (* =0 ; second boundary condition *)

 $c_1 D_{-\frac{1}{2}i(-i+\alpha)} \left( -\sqrt[4]{-1} \sqrt{2} L \sqrt{\psi} \right) + c_2 D_{\frac{1}{2}i(i+\alpha)} \left( -(-1)^{3/4} \sqrt{2} L \sqrt{\psi} \right)$ 

(* Substitute C[2] in terms of C[1] into the above eq. and equate to zero*)

 $D_{\frac{1}{2}i(i+\alpha)} \left( -(-1)^{3/4} \sqrt{2} L \sqrt{\psi} \right) \left\{ \frac{i 2^{-\frac{1}{2}(i\alpha)} c_1 \Gamma(-\frac{1}{4}i(i + \alpha))}{\Gamma(\frac{1}{4}i(-i + \alpha))} \right\} + c_1 D_{-\frac{1}{2}i(-i+\alpha)} \left( -\sqrt[4]{-1} \sqrt{2} L \sqrt{\psi} \right) = 0$ 

(* The above equation is defined only in terms of C[1] and  $\psi$ . Pull C[1] out of the equation and equation inside of the equation to zero*)

 $c_1 \left\{ \frac{i 2^{-\frac{1}{2}(i\alpha)} \Gamma(-\frac{1}{4}i(i + \alpha))}{\Gamma(\frac{1}{4}i(-i + \alpha))} D_{\frac{1}{2}i(i+\alpha)} \left( -(-1)^{3/4} \sqrt{2} L \sqrt{\psi} \right) + D_{-\frac{1}{2}i(-i+\alpha)} \left( -\sqrt[4]{-1} \sqrt{2} L \sqrt{\psi} \right) \right\} = 0$ 

 $\left\{ \frac{i 2^{-\frac{1}{2}(i\alpha)} \Gamma(-\frac{1}{4}i(i + \alpha))}{\Gamma(\frac{1}{4}i(-i + \alpha))} D_{\frac{1}{2}i(i+\alpha)} \left( -(-1)^{3/4} \sqrt{2} L \sqrt{\psi} \right) + D_{-\frac{1}{2}i(-i+\alpha)} \left( -\sqrt[4]{-1} \sqrt{2} L \sqrt{\psi} \right) \right\} = 0$ 

(***** DEFINE THE VALUES OF PARIMETERS*****)

L = 500 (* LENGTH OF THE BEAM *)

500

 $\psi = 0.978344399885 * 10^{-5}$  (* keep changing until the equation converges. *)

 $9.78344 \times 10^{-6}$ 

 $\alpha = 0.670712669$  (* this is C1 in the differential equation and is different for each stacking sequence*)

0.670713

 $\left\{ \frac{i 2^{-\frac{1}{2}(i\alpha)} \Gamma(-\frac{1}{4}i(i + \alpha))}{\Gamma(\frac{1}{4}i(-i + \alpha))} D_{\frac{1}{2}i(i+\alpha)} \left( -(-1)^{3/4} \sqrt{2} L \sqrt{\psi} \right) + D_{-\frac{1}{2}i(-i+\alpha)} \left( -\sqrt[4]{-1} \sqrt{2} L \sqrt{\psi} \right) \right\} = 0$ 

 $\{3.54355 \times 10^{-13} + 1.26343 \times 10^{-12} i\} = 0$ 

```

Figure 5.8 Screenshot of the script used in Mathematica to solve the buckling differential equation

The normalized coefficient, C_2 , is shown in the following equation by best fit of curve in Figure 5.9, where normalized value of C_1 is obtained from a broad range of stacking sequences.

$$C_2 = 4.0038e^{-0.719C_1} \quad (5.46)$$

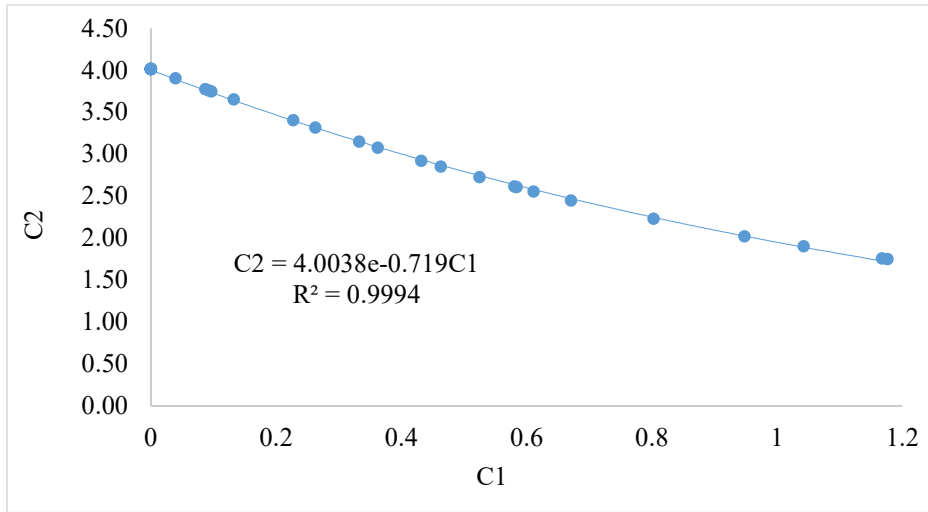


Figure 5.9 C_1 vs C_2 to obtain a representative equation from best fit of the data

5.3 Numerical Analysis (FEM)

The derived semi analytical formula was verified by applying finite element buckling analysis using the commercial software package ABAQUS/Standard (implicit) for laminated anisotropic cantilever beams. The model was first created by using 3D planar shells. The shells were assembled based on the stacking arrangement that was used in the analytical solution. The global x-axis was assigned along beams length, but the local coordinate system was used based on the orientation of the fibers in each ply.

The beam was rotationally and translationally fixed at one end. A concentrated load of 100 pounds was applied at mid-height of the free end of the beam. The boundary conditions and applied load are shown in Figure 5.10b.

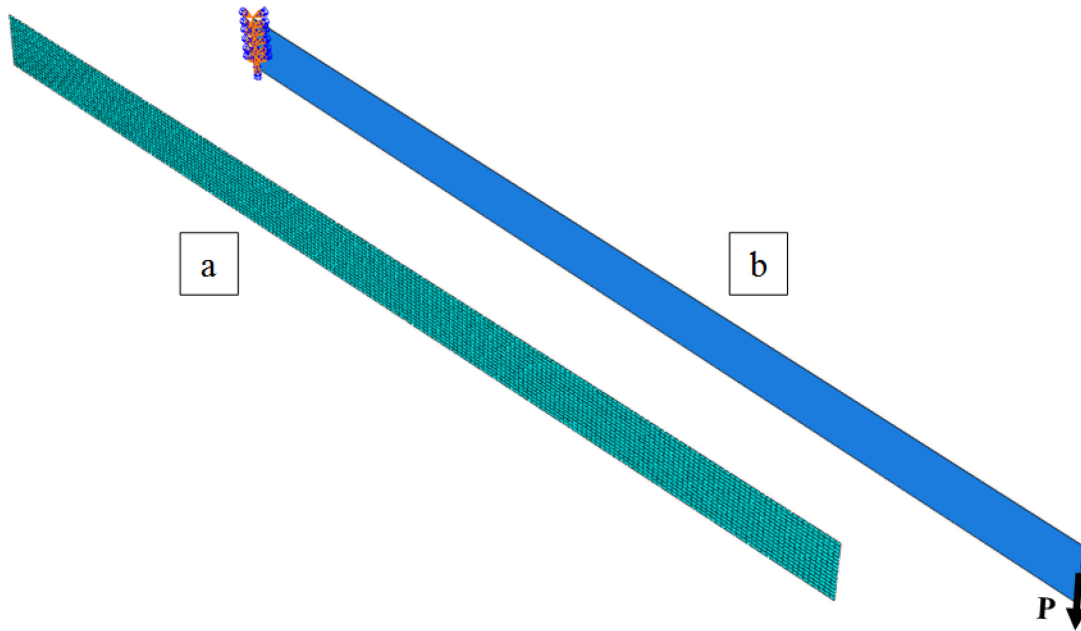


Figure 5.10 FEM model with $L/h = 20$ and layer thickness = 0.1 mm; (a) applied shell element type (S8R)

The beam was meshed with a standard quadratic quadrilateral shell element type of S8R (8-node doubly curved thick shell element with reduced integration) using six degrees of freedom per node and an element size of 2.5 mm along beam axis. A beam with $L = 500$ mm and $h = 25$ mm gives total number of 10033 nodes and 3200 elements, as shown in Figure 5.10a.

The eigenvalue buckling analysis in ABAQUS solver, which is a linearized perturbation procedure, determines the eigenvalue of the buckling mode. ABAQUS extracts the eigenvalues and eigenvectors for symmetric stiffness matrices only. In order to turn the stiffness matrix of the model symmetric, Lanczos iteration eigenvalue extraction method was used. To find the critical force, based on the ABAQUS user guide, the lowest eigenvalue is multiplied by the applied force at the mid-height free end of the beam.

$$P_{ocr} = \lambda P \quad (5.47)$$

In addition, a nonlinear stability analysis (pre-buckling and buckling) of the laminated anisotropic cantilever beam was performed by adopting the nonlinear geometry analysis using the modified Riks approach, Al-Masri and Rasheed (2017) and Memon and Sun (2004). The modified Riks analysis uses the Arc-length method to follow the equilibrium path, representing either bifurcation points or limit points. Suitable limits of load increments are applied during the analysis in which the iteration converges to equilibrium along the Arc-length.

5.4 Results

5.4.1 Material Properties and Stacking Sequences

An anisotropic composite cantilever beam is made by stacking four layers of the FRP lamina properties shown in Table 5.2 at different fiber orientations. The thickness of each layer is the same (typically 0.1 mm) with the same orthotropic properties, yet it varies in terms of fiber orientation. The orientation of fiber in each layer can be randomly picked, including common laminate types such as symmetric laminates, antisymmetric laminates, balanced laminates, and so on. The stacking sequence starts from the back of the beam to the front of the beam to follow the same order used for typical laminated plates, see Figure 5.11. For example, $[30/-30/30/-30]$ means that the first ply has an angle of 30 degrees from the x-axis of the beam is placed in the back of the beam counterclockwise (towards the y-axis) and the other layers follow with the same order through the positive z-axis direction. Figure 5.9 shows the stacking sequence of the laminates. Different layer thicknesses of (0.05, 0.1, 0.15, and 0.2 mm) and length to height ratios of (5, 10, 20, and 50) were also studied which will be presented later. Furthermore, the effect of fiber orientation for antisymmetric balanced angle ply layup was studied.

Table 5.2 CFRP material properties used in the laminates

| Material | CFRP | |
|------------|----------|-----|
| E_{11} | 142730 | MPa |
| E_{22} | 13790 | MPa |
| ν_{12} | 0.3 | |
| ν_{21} | 0.028985 | |
| G_{12} | 4640 | MPa |
| G_{13} | 4640 | MPa |
| G_{23} | 3030 | MPa |

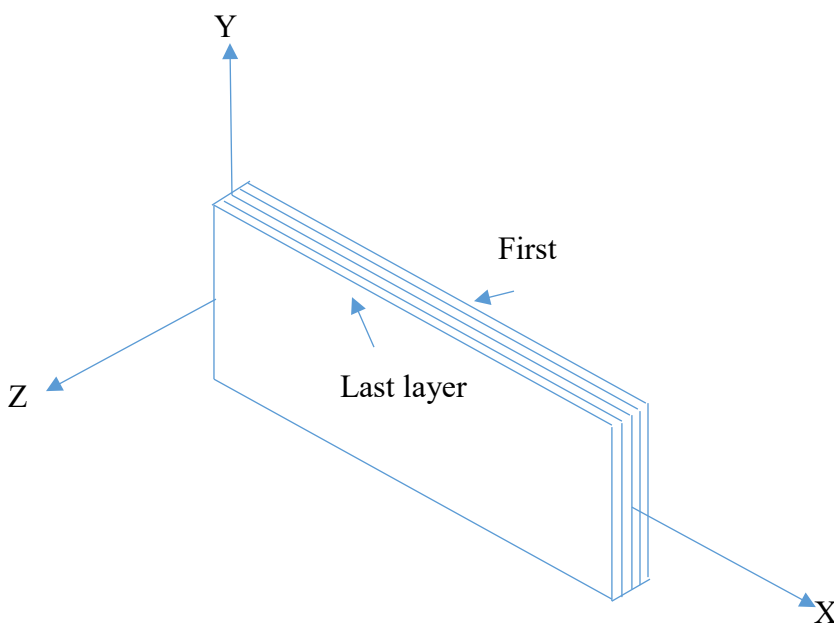


Figure 5.11 The stacking sequence of the laminates

5.4.2 Buckling Results

For the lateral-torsional buckling of thin-walled rectangular laminated composite cantilever beams subjected to central free end loading, a semi-analytical approach is presented as

well as FEM results. Figures 5.12 and 5.13 show the buckling results for different stacking sequences (20 different laminate-fiber orientations) based on the proposed analytical formulation and also results from FEM model for layer thickness of 0.1 mm (total thickness of 0.4 mm), beam length of 500 mm and beam height of 25 mm and 50 mm (i.e. length to height ratio of 20 and 10), respectively. Based on the results obtained, there is an excellent agreement between the proposed analytical formulation and FEM with higher L/h ratio (Figure 5.12). For the lower value of L/h ratio (Figure 5.13), the error observed is noticeable in the cases of [0₄] and cross-ply layup, which buckled in a distortional mode rather than lateral-torsional mode admitting up to 19% deviation, due to the beam being too deep behaving like a plate, see Table 5.3.

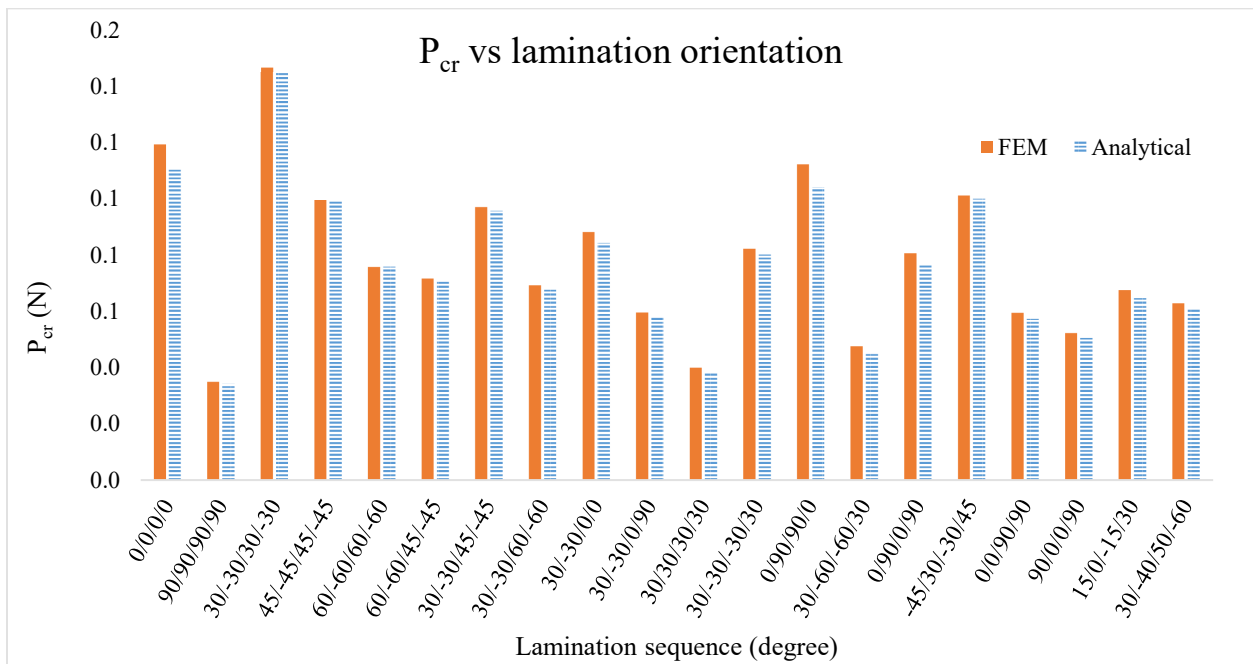


Figure 5.12 Buckling force at different stacking sequences: $t_k=0.1$ mm for each layer, $L/h=20$, and finite element length 2.5mm

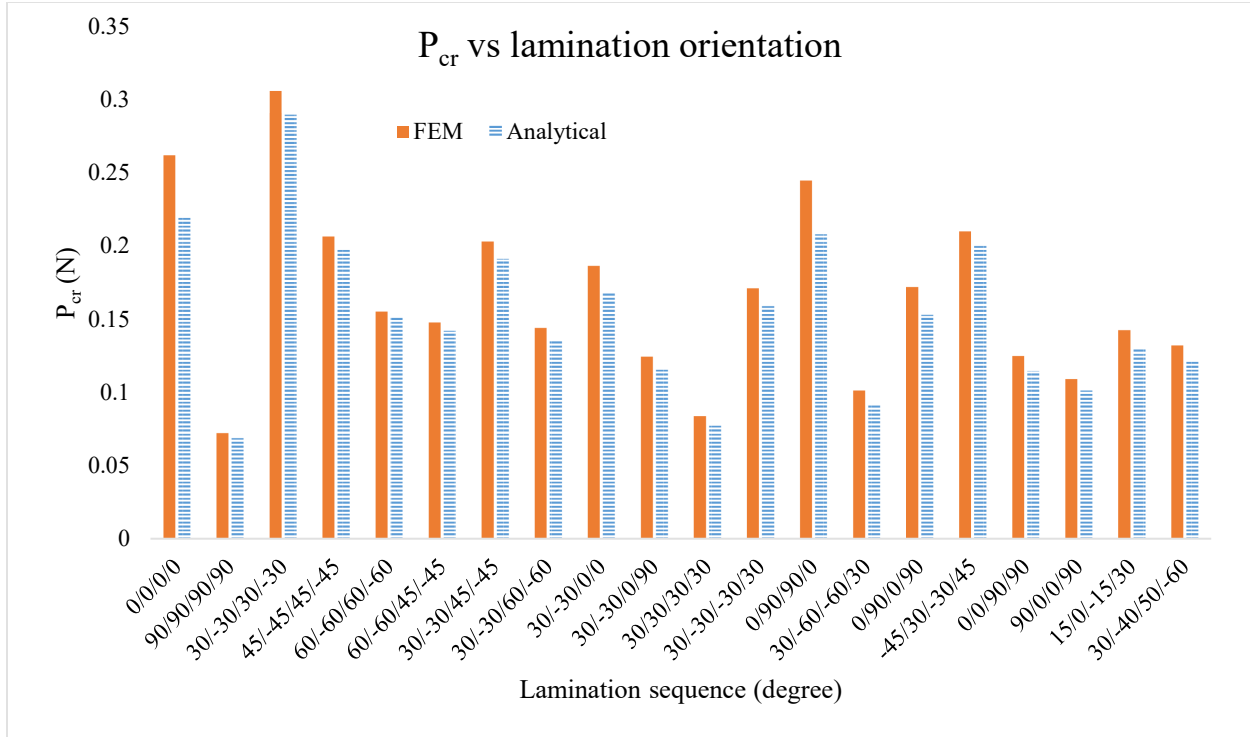


Figure 5.13 Buckling force at different stacking sequences: $t_k=0.1$ mm for each layer, $L/h=10$, and finite element length 2.5mm

5.5 Parametric Study

5.5.1 Effect of Length/Height Ratio

Different Length/height (L/h) ratios of 5, 10, 20, and 50 were used in the analysis to study their effects on the lateral-torsional buckling of cantilever laminated thin-walled rectangular cross-sectional beams. The results show that there is a significant drop in the value of the buckling force as the L/h ratio increases. The relation between buckling force and L/h ratio is defined to be a power function which can be written in Eq. 5.48

$$P_{cr} = (P_{cr})_i * \left(\frac{L}{h}\right)_i \left(\frac{L}{h}\right)_i^{-1} \quad (5.48)$$

where $(P_{cr})_i$ is the initial calculated value of buckling force from Eq. 5.45 with a given $\left(\frac{L}{h}\right)_i$ ratio for a specific laminate stacking sequence.

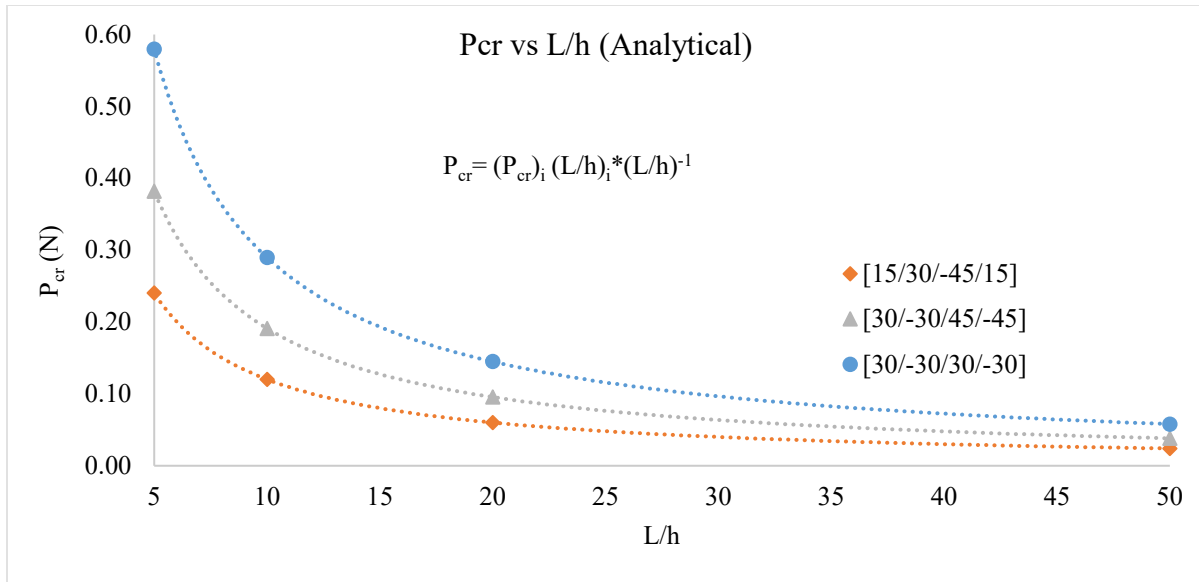


Figure 5.14 Effect of L/h ratio on the critical buckling force based on analytical formula for three different layups and layer thickness of 0.1 mm.

By knowing the value of buckling force in a selected laminate, Eq. 5.48 helps to calculate the buckling force for different L/h ratios while the stacking sequence is retained the same. Figure 5.14 shows the effect of L/h ratio on the buckling force for three different stacking sequences of [15/30/-45/15], [30/-30/45/-45], and [30/-30/30/-30]. Eq. 5.48 is limited to the analytical formula and is not applicable to the FEM results. There is a noticeable discrepancy between the analytical and numerical results in the cases where L/h ratio decreases, especially for the case of [0/0/0/0] laminate when the ratio of L/h is 5. As shown in Figure 5.15, due to the fact that the beam with lower L/h ratio behaves like a plate and buckles numerically in a distortional mode, in which β at a certain section transverse to the beam is not constant, rather than a lateral-torsional mode, in which the lateral angle of twist, β , remains constant for a certain section transverse to the beam. Figure 5.15 shows the deformed mode shape of the beam in three different L/h ratios of 5, 20 and 50 comparing to the original shapes for layup of [30/-30/30/-30]. It is evident that the deformed shape for L/h ratio of 5 buckles numerically in a distortional mode

where a constant β cannot be assumed as done analytically. Nevertheless, Figures 5.16-5.18 clearly show that the analytical and numerical buckling forces match almost exactly as the L/h ratio increases beyond 20. On the other hand, the discrepancy between the analytical and numerical results for L/h ratios lower than 20 are seen to reflect conservative predictions of the analytical solution.

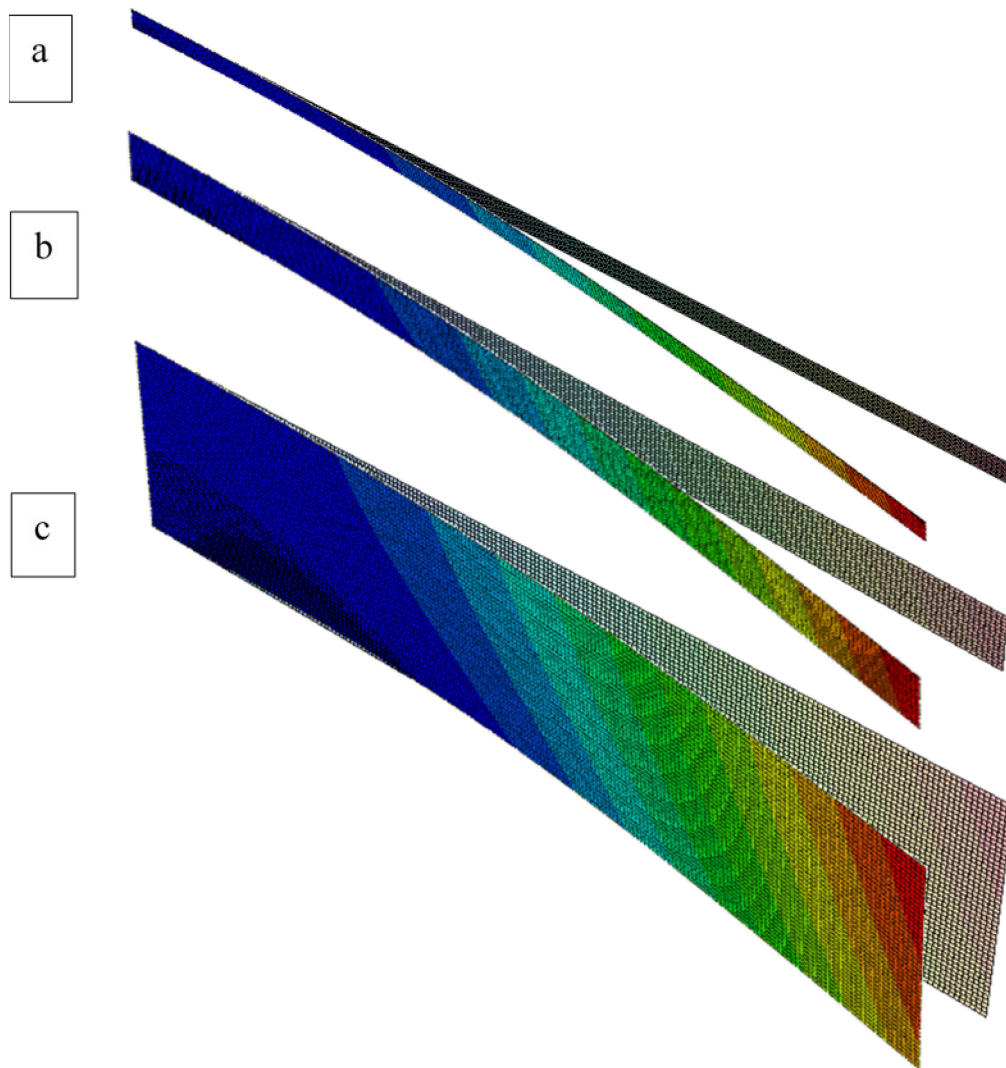


Figure 5.15 Buckling (deformed and un-deformed) shape of the cantilever beam for ply thickness of 0.1 mm and lamination orientation of [30/-30/30/-30]; (a) $L/h=50$, (b) $L/h=20$, and (c) $L/h=5$

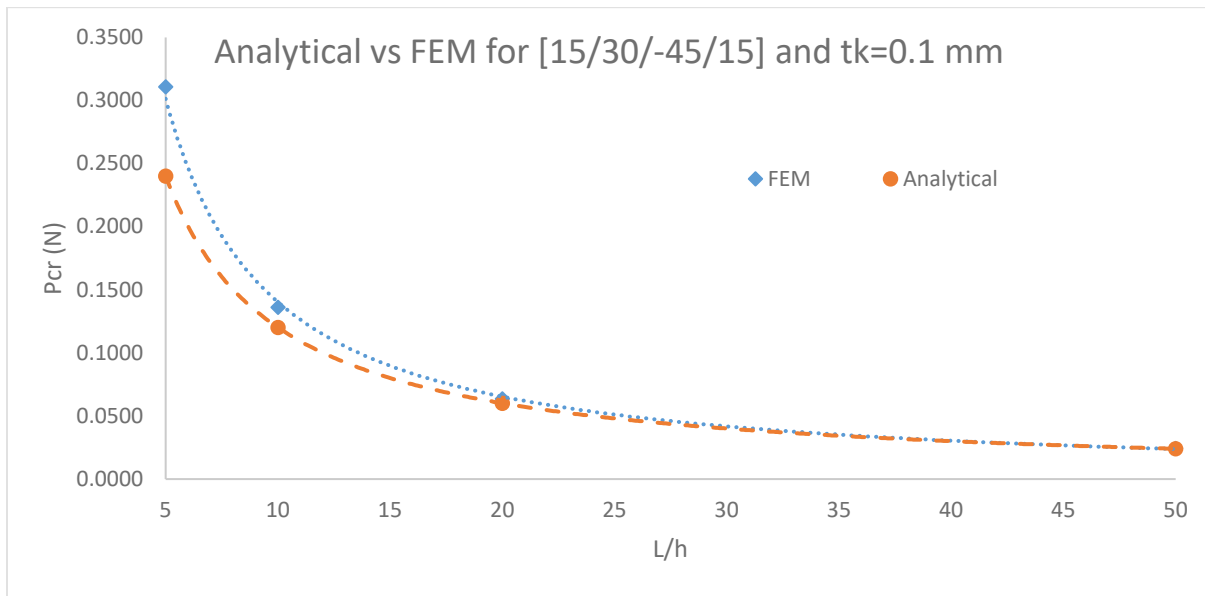


Figure 5.16 Comparison of buckling result obtained from analytical solution and FEM for the [15/30/-45/15] laminate and layer thickness of 0.1 mm by changing L/h ratio

Figures 5.16 - 5.18 show the comparison of buckling forces between the semi-analytical solution and FEM in three different laminate stacking sequences. It is obvious that in both analytical and FEM solutions the buckling forces increase as the L/h ratio decrease because of the larger height of the beam to resist against lateral-torsional buckling. Again, it is evident that the analytical and numerical results match closely at $L/h=20$ while for most cases the results match up closely beyond $L/h =10$, as shown in Figures 5.17 and 5.18.

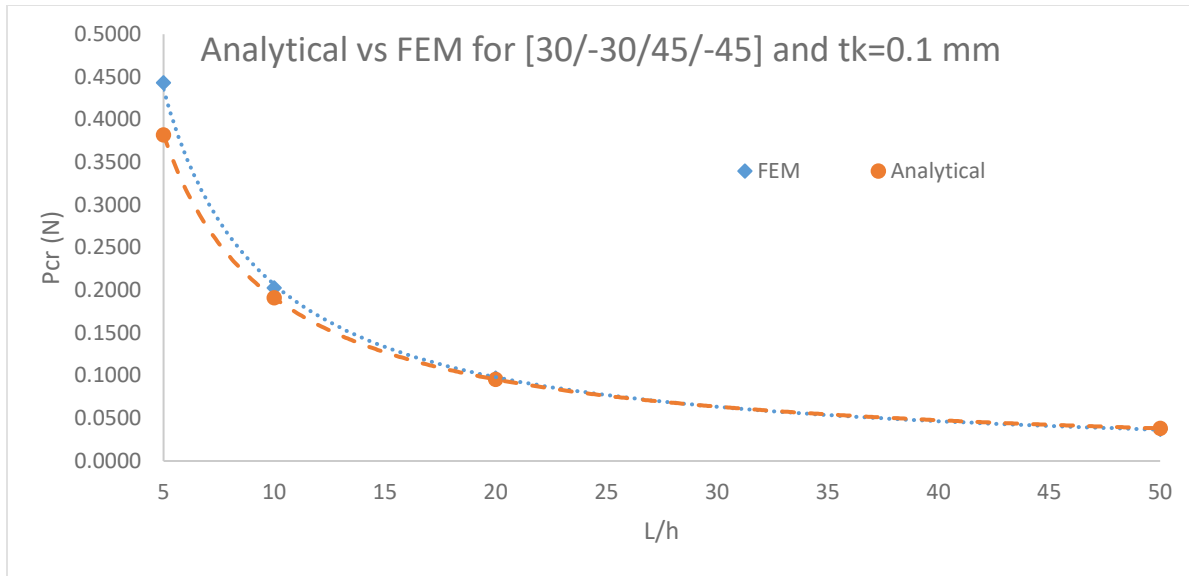


Figure 5.17 Comparison of buckling result obtained from analytical solution and FEM for the [30/-30/45/-45] laminate and ply thickness of 0.1 mm by changing L/h ratio

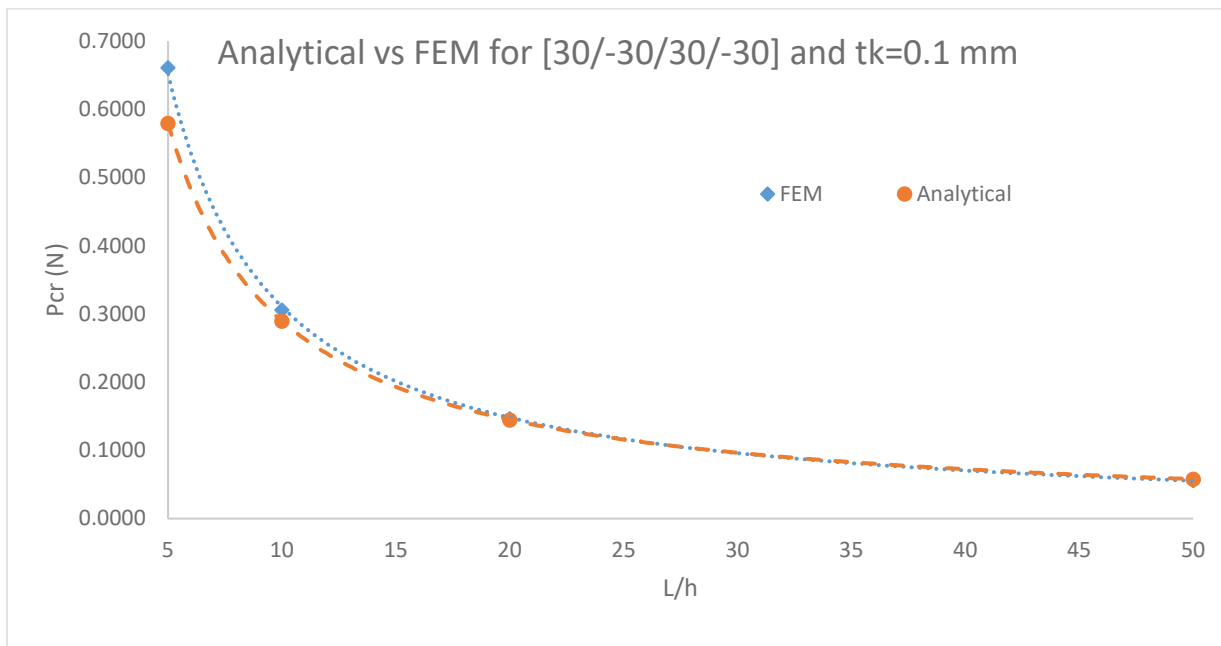


Figure 5.18 Comparison of buckling result obtained from analytical solution and FEM for the [30/-30/30/-30] laminate and ply thickness of 0.1 mm by changing L/h ratio

5.5.2 Effect of Stacking Sequence

As shown in Figures 5.12 and 5.13. The stacking sequences considerably affect the buckling forces if the dimensions of the beam are kept the same. The lowest value for the critical buckling force is obtained in $[90/90/90/90]$ layup while the highest critical value is obtained for the balanced angle-ply stacking sequence of $[30/-30/30/-30]$ which is the maximum critical force among the possible stacking sequences selected for Figures 5.12 and 5.13. The optimal maximum critical force is obtained for the balanced angle-ply layup to be 0.157 N for layup $[20/-20/20/-20]$ and $L/h = 20$. Figure 5.19 shows the variation in critical buckling force with the change in layup angle of 0 to 90 with an increment of 5 degrees. The analytical part of the curve is calculated using Eq. 5.46 which shows the usefulness of best fit equation obtained from Figure 5.9.

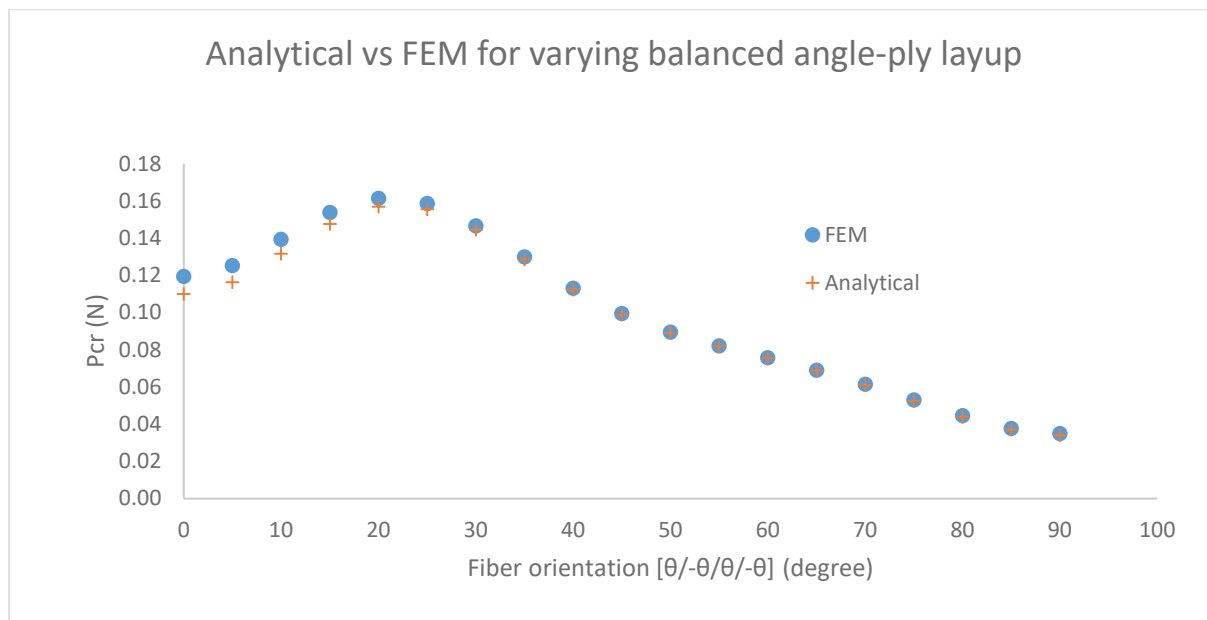


Figure 5.19 Variation in critical buckling force with the change in balanced angle-ply layup angle of 0 to 90 with an increment of 5 degrees. (+) Analytical and (●) FEM; ply thickness of 0.1 mm and L/h of 20

5.5.3 Effect of Layer Thickness

Different layer thickness of 0.05, 0.1, 0.15, and 0.2 mm were used in the analysis to study their effects on the lateral-torsional buckling of cantilever laminated thin-walled rectangular cross-sectional beams. The L/h ratio of 20 and the stacking sequence were kept the same while changing the layer thickness. The results show that there is a significant increase in the value of buckling force as the layer thickness increases. The relationship between buckling force and the thickness is defined mathematically to be a power function which can be written in Eq. 5.49.

$$P_{cr} = \frac{(P_{cr})_i}{t_i^3} t^3 \quad (5.49)$$

where $(P_{cr})_i$ is the initially calculated value of buckling force from Eq. 5.45 with a given t_i for a specific laminate stacking sequence. Eq. 5.49 works either considering the thickness to be the total thickness of the beam or the thickness of each layer as long as all layers have the same constant thickness.

By knowing the value of buckling force in a selected layup, Eq. 5.49 helps to calculate the buckling force for various layer or total beam thickness. Figure 5.20 shows the effect of layer thickness on the buckling force based on analytical solution for three different stacking sequence of [15/30/-45/15], [30/-30/45/-45], and [30/-30/30/-30]. Figure 5.21 shows the effect of layer thickness on the buckling force based on the FEM results for the same three stacking sequences of [15/30/-45/15], [30/-30/45/-45], and [30/-30/30/-30]. Eq. 5.49 can be obtained from FEM analysis with small deviation multipliers of (a) and (b) , which are tabulated in Figure 5.21 for each layup. The modification of Eq. 5.49 for FEM is shown in Eq. 5.50.

$$P_{cr} = (at + b) \frac{(P_{cr})_i}{t_i^3} t^3 \quad (5.50)$$

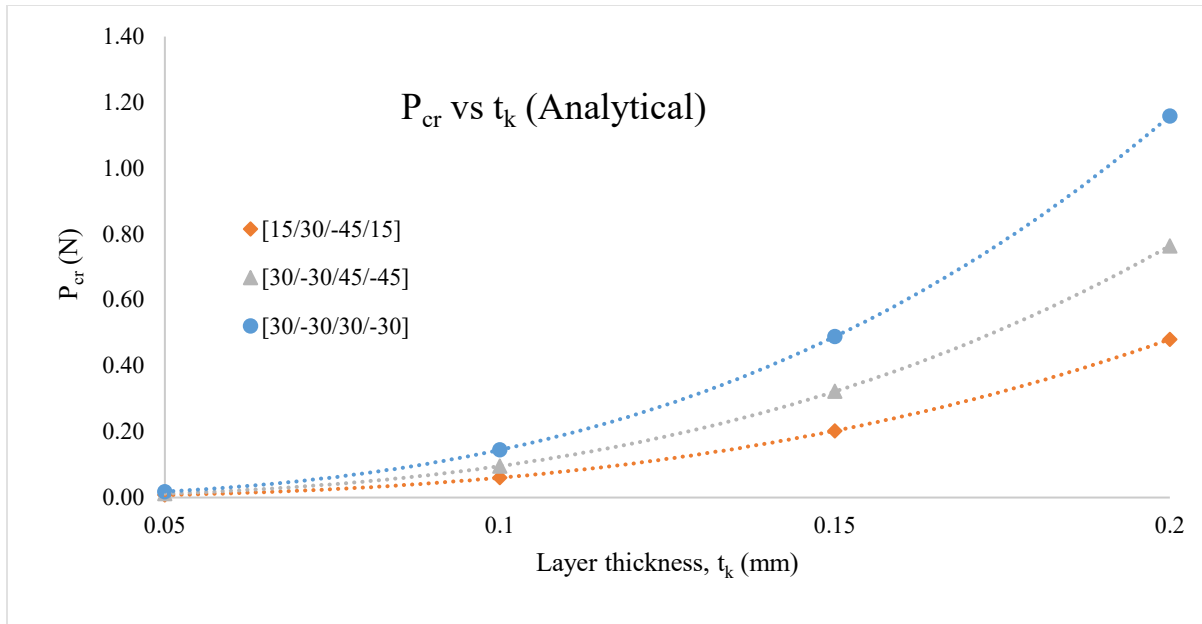


Figure 5.20 Effect of thickness, t_k , on the critical force based on analytical formula for three different orientations, $L/h=20$

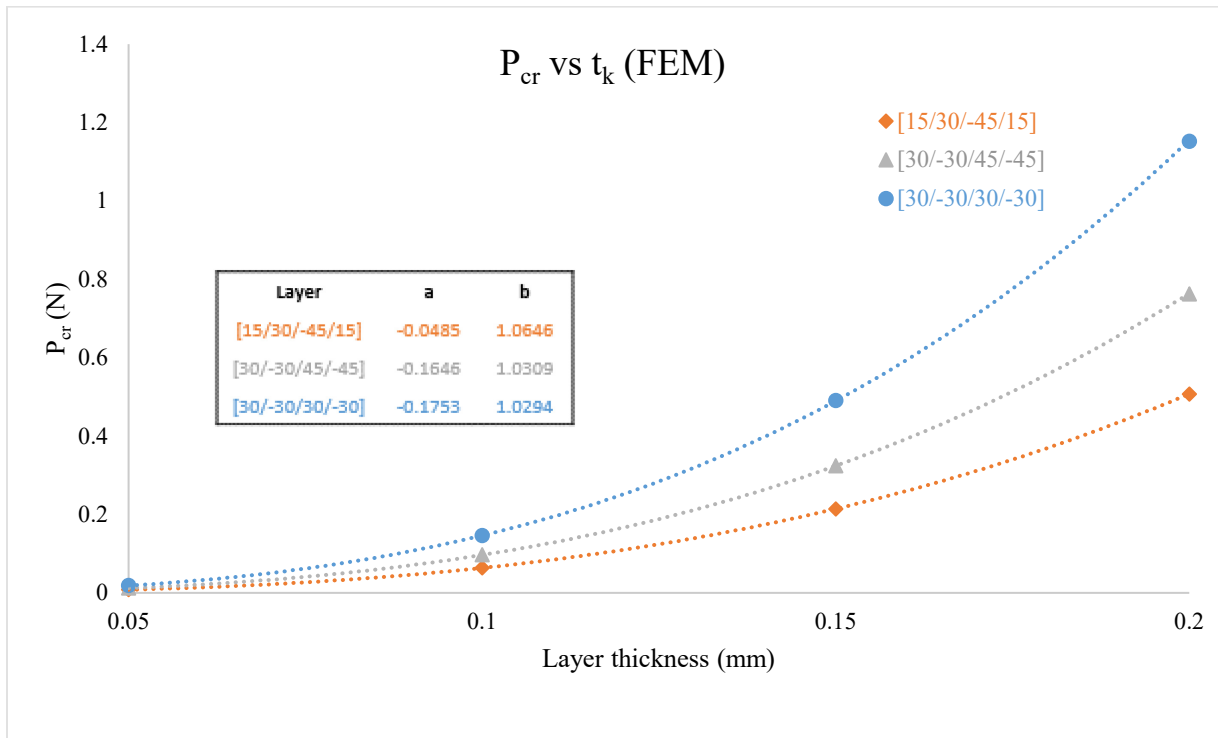


Figure 5.21 Effect of thickness, t_k , on the critical force based on FEM method for three different orientations, $L/h=20$

Figures 5.22 - 5.24 show the comparison of buckling forces between the semi-analytical results and FEM in three different laminate stacking sequences. It is obvious that in both analytical and FEM solutions the buckling forces increase as the layer thickness increases because of the fact larger thickness of the beam can resist more against lateral-torsional buckling. Both analytical and FEM results have an excellent agreement on the buckling force for all three sequences, except for the [15/30/-45/15] case when the thickness increases. The anticipated reason might be tendency of distortional buckling of beam or the admission of shear deformation at certain orientation of fibers as the layer thickness increases while keeping L/h ratio the same.

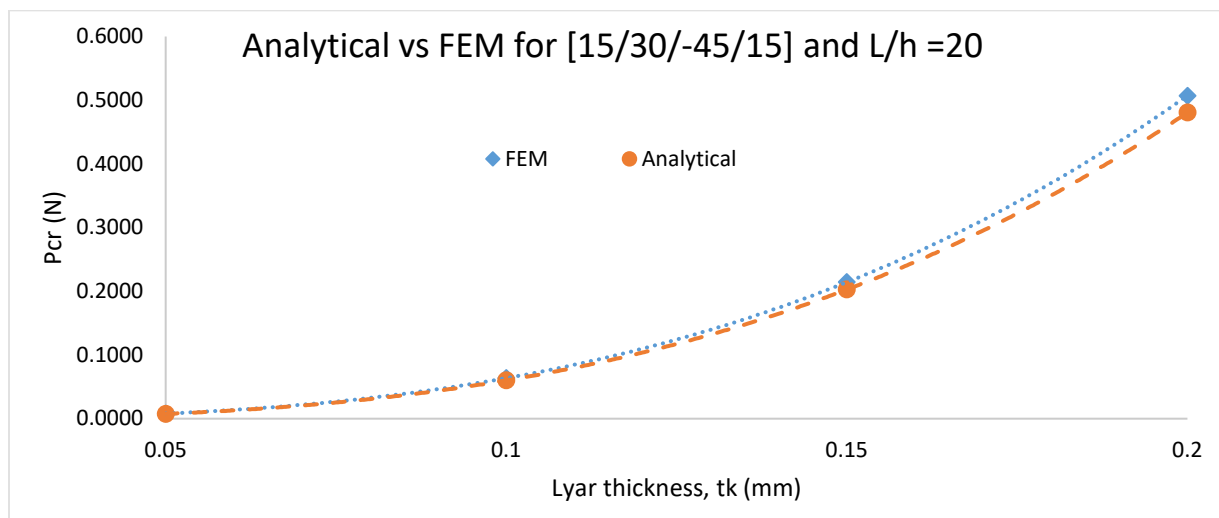


Figure 5.22 Comparison of buckling result obtained from analytical solution and FEM for the [15/30/-45/15] laminate and L/h of 20 by changing layer thickness, t_k

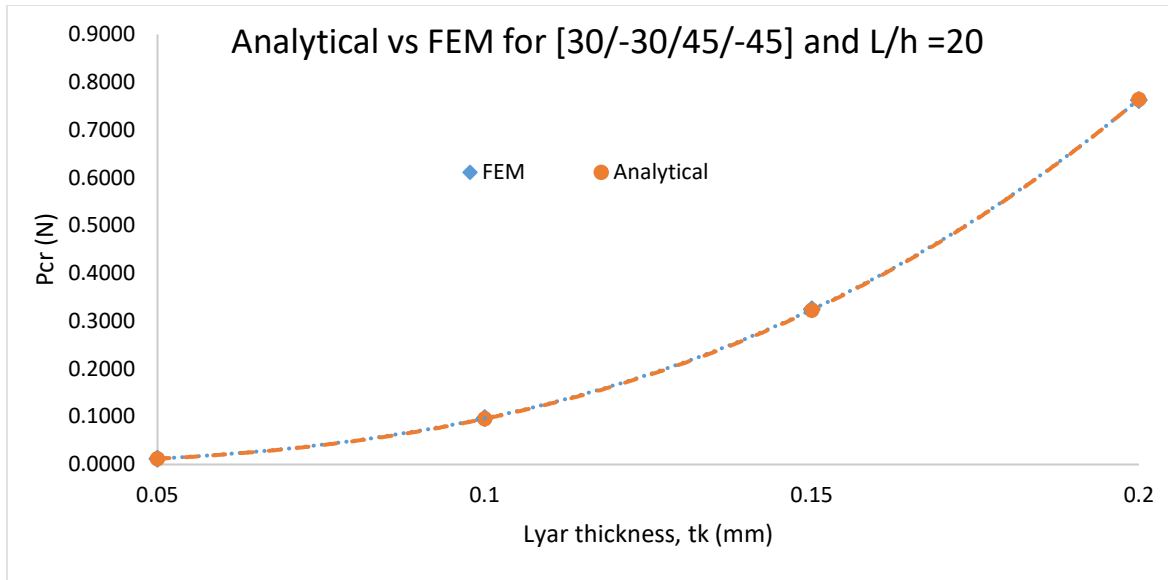


Figure 5.23 Comparison of buckling result obtained from analytical solution and FEM for the [30/-30/45/-45] laminate and L/h of 20 by changing layer thickness, t_k

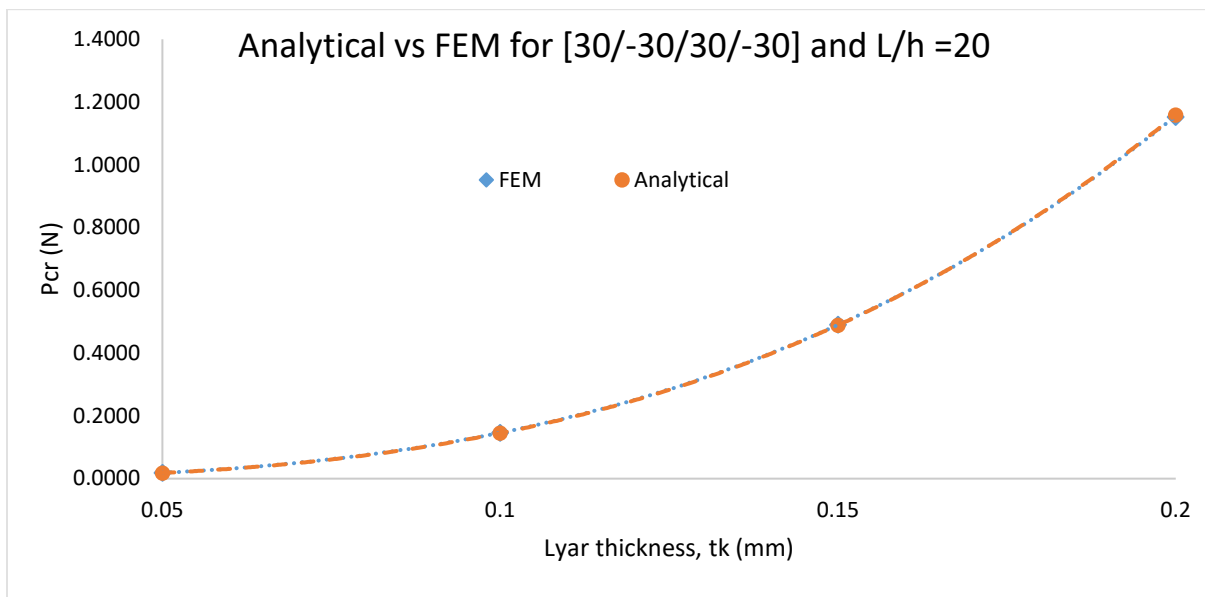


Figure 5.24 Comparison of buckling result obtained from analytical solution and FEM for the [30/-30/30/-30] laminate and L/h of 20 by changing layer thickness, t_k

5.5.4 Effect of Pre-Buckling Deformation

Furthermore, to indicate the existence of pre-buckling deformation in the transvers direction, the load versus free end mid-height deflection curves are plotted for the different

stacking sequences of [30/-30/30/-30], [30/-30/45/-45], and [15/30/-45/15] obtained from finite element nonlinear Riks analysis along with the analytical solution for comparison. The results in Figure 5.25 for three different stacking sequences and L/h ratio of 20 show excellent agreement.

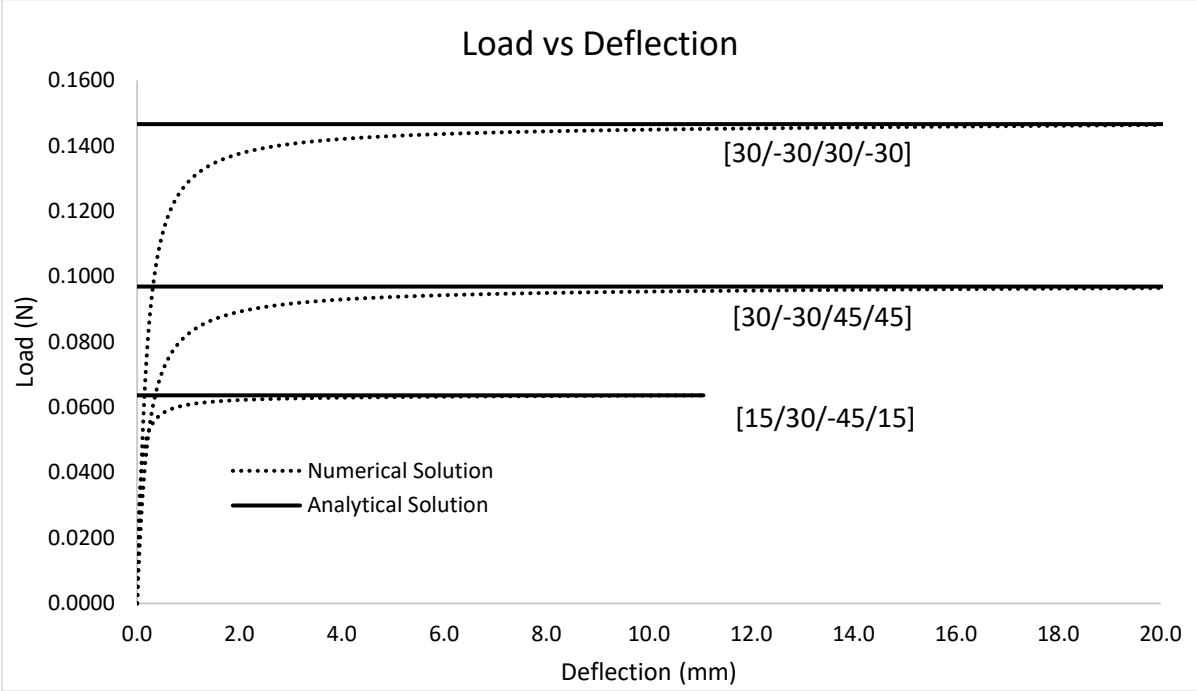


Figure 5.25 Analytical vs numerical solutions; deflection at mid-height, L/h=20 and $t_k=0.1$ mm

Table 5.3 Comparison of buckling force obtained from analytical results and FEM for L/h ratios of 10 and 20 and layer thickness of 0.1 mm in different stacking conditions

| Laminate | Critical Buckling Force P_{cr} (N) and Error (%) | | | | | |
|---------------|--|-----------------|--------------|------------|-----------------|--------------|
| | L/h =10 | | | L/h = 20 | | |
| | Analytical | FEM (ABAQUS) | Error (%) | Analytical | FEM (ABAQUS) | Error (%) |
| 0/0/0/0 | 0.220 | 0.262 | 18.93 | 0.110 | 0.119 | 8.39 |
| 90/90/90/90 | 0.068 | 0.072 | 5.03 | 0.034 | 0.035 | 1.95 |
| 30/-30/30/-30 | 0.290 | 0.306 | 5.57 | 0.145 | 0.147 | 1.20 |
| 45/-45/45/-45 | 0.198 | 0.206 | 4.12 | 0.099 | 0.099 | 0.26 |
| 60/-60/60/-60 | 0.152 | 0.155 | 2.26 | 0.076 | 0.076 | 0.06 |
| 60/-60/45/-45 | 0.142 | 0.148 | 4.15 | 0.071 | 0.072 | 0.97 |
| 30/-30/45/-45 | 0.191 | 0.203 | 6.19 | 0.096 | 0.097 | 1.46 |
| 30/-30/60/-60 | 0.136 | 0.144 | 6.02 | 0.068 | 0.069 | 1.94 |
| 30/-30/0/0 | 0.168 | 0.186 | 10.70 | 0.084 | 0.088 | 4.57 |
| 30/-30/0/90 | 0.116 | 0.124 | 7.43 | 0.058 | 0.059 | 2.95 |
| 30/30/30/30 | 0.077 | 0.084 | 8.71 | 0.038 | 0.040 | 3.75 |
| 30/-30/-30/30 | 0.160 | 0.171 | 6.80 | 0.080 | 0.082 | 2.48 |
| 0/90/90/0 | 0.208 | 0.245 | 17.67 | 0.104 | 0.112 | 7.75 |
| 30/-60/-60/30 | 0.091 | 0.101 | 11.24 | 0.045 | 0.048 | 4.72 |
| 0/90/0/90 | 0.153 | 0.172 | 12.42 | 0.076 | 0.080 | 5.36 |
| -45/30/-30/45 | 0.200 | 0.210 | 5.06 | 0.100 | 0.101 | 1.17 |
| 0/0/90/90 | 0.114 | 0.125 | 8.98 | 0.057 | 0.059 | 3.85 |
| 90/0/0/90 | 0.101 | 0.109 | 7.80 | 0.051 | 0.052 | 3.26 |
| 15/0/-15/30 | 0.129 | 0.142 | 10.20 | 0.065 | 0.067 | 4.38 |
| 30/-40/50/-60 | 0.122 | 0.132 | 8.22 | 0.061 | 0.063 | 3.19 |
| 15/30/-45/15 | 0.120 | 0.136 | 13.45 | 0.060 | 0.064 | 5.97 |

5.6 Conclusions

In this study, the lateral-torsional buckling of cantilever, thin-walled rectangular cross-section, anisotropic laminated composite beams subjected to central free end loading was investigated. Based on the assumptions made and the results obtained, an excellent accuracy is observed for a wide range stacking sequences when L/h exceeds 10. The applicability of this analytical formulation is proved by comparing the obtained results with FEM results. The study

followed the classical laminated plate theory with all considered assumptions and determined an effective lateral-torsional-coupling stiffness matrix.

Based on the study, the stability of the laminated cantilever beams under free end loading is greatly affected by the length/height ratio of the beam as well as the thickness of the beam. The critical buckling force was inversely proportional to the length/height ratios with a power function. The lowest L/h ratio corresponds to the highest critical buckling force. Increase in the thickness of the beam also plays a significant role in increasing the stability resistance of the beam. The importance of the stacking sequence, which does not affect the dimensions of the beam, is seen to greatly influence the stability of the beam.

The critical buckling force of balanced angle-ply fiber lamination of about [20/-20/20/-20] is found to reach the maximum value, among this class of layups, because of its maximum lateral and torsional effective stiffness. The minimum critical buckling force obtained from [90/90/90/90] was found to be due to orienting the fibers in the y-direction, thus reducing the lateral effective stiffness. Also, a nonlinear Riks analysis was performed to indicate the existence of pre-buckling deformation in transverse direction while comparing favorably with analytical buckling limit load.

5.7 References

- Al-Masri, R. and Rasheed, H.A. (2017). "Analytical and Finite Element Buckling Solutions of Fixed-Fixed Anisotropic Laminated Composite Columns under Axial Compression." *International Journal of Structural Stability and Dynamics*, 17(9), 1750103.
- Bank, L. C., & Bednarczyk, P. J. (1988). "A beam theory for thin-walled composite beams." *Composites Science and Technology*, 32(4), 265-277.
- Barbero, E. J., Lopez-Anido, R., and Davalos, F. (1993). "On the Mechanics of Thin-Walled Laminated Composite Beams." *Journal of Composite Materials*, 27(8), 806-829
- Barbero, E. J. (1999). *Introduction to composite materials design*. CRC press.
- Bauld, N. R., & Lih-Shyng, T. (1984). "A Vlasov theory for fiber-reinforced beams with thin-walled open cross sections." *International Journal of Solids and Structures*, 20(3), 277-297.
- Karaagac, C., Öztürk, H., & Sabuncu, M. (2007). "Lateral dynamic stability analysis of a cantilever laminated composite beam with an elastic support." *International Journal of Structural Stability and Dynamics*, 7(03), 377-402.
- Kollar, L. P. (2001). "Flexural-torsional buckling of open section composite columns with shear deformation." *International Journal of Solids and Structures*, 38, 7525-7541.
- Kollár, L. P., & Springer, G. S. (2003). *Mechanics of composite structures*. Cambridge university press.
- Lee, J., Kim, S.-E., Hong, K. (2002). "Lateral buckling of I-section composite beams." *Engineering Structures*, 24, 955-964.
- Lin, Z. M., Polyzois, D., and Shah, A. (1996). "Stability of Thin-walled Pultruded Structural Members by the Finite Element Method." *Thin-Walled Structures*, 24, 1-18.
- Machado, S. P. (2010). "Interaction of combined loads on the lateral stability of thin-walled composite beams." *Engineering Structures*, 32, 3516-3527.
- Memon, B.A. and Su, X.S. (2004). "Arc-length technique for nonlinear finite element analysis." *Journal of Zhejiang University SCI*, 5(5), 618-628.
- Pandey, M.D., Kabir, M.Z., and Sherbourne, A.N. (1995). "Flexural-Torsional Stability of Thin-Walled Composite I-Section Beams." *Composites Engineering*, 5(3), 321-342.
- Qiao, P., Zou, G., and Davalos, J. (2003). "Flexural-torsional buckling of fiber-reinforced plastic composite cantilever I-beams." *Composite Structures*, 60, 205-217.

- Roberts, T.M., Al-Ubaidi, H. (2001). "Influence of shear deformation on restrained torsional warping of pultruded FRP bars of open cross-section." *Thin-Walled Structures*, 39, 395-414.
- Sapkás, Á., & Kollár, L. P. (2002). Lateral-torsional buckling of composite beams. *International Journal of Solids and Structures*, 39(11), 2939-2963.
- Sherbourne, A. N., Kabir, M. Z. (1995). "Shear Strain Effects in Lateral Stability of Thin-Walled Fibrous Composite Beams." *Journal of Engineering Mechanics*, 640-647.
- Tai, W. T. (2004). *The lateral-torsional buckling analysis of composite laminated beams* (MSc thesis, Feng Chia University, Taiwan ROC).
- Timoshenko, S. P., & Gere, J. M. (1961). *Theory of elastic stability*. 1961. McGrawHill-Kogakusha Ltd, Tokyo.
- Vlassov, V. Z. (1961). *Thin-walled beams* (2nd ed.) Israel Program for Scientific Translation.

Chapter 6 - Lateral Torsional Buckling of Anisotropic Laminated Thin-Walled Simply Supported Beams Subjected to Concentrated Load at Mid-Span

In this chapter, a generalized semi-analytical approach for lateral-torsional buckling of simply supported anisotropic, thin-walled, rectangular cross-section beams under concentrated load at mid-span/mid-height was developed using the classical laminated plate theory as a basis for the constitutive equations. A closed form buckling expression was derived in terms of the lateral, torsional and coupling stiffness coefficients of the overall composite. These coefficients were obtained through dimensional reduction by static condensation of the general 6x6 constitutive matrix mapped into an effective 2x2 coupled weak axis bending-twisting relationship. The resulting two coupled stability differential equations are manipulated to yield a single governing differential equation in terms of the twisting angle. This differential equation with variable coefficients, along with applying boundary conditions, was solved numerically using Mathematica. The resulting solution was found to correlate with the effective lateral-flexure, torsional and coupling stiffness coefficients to yield a general analytical solution. An analytical formula was possible to extract, which was verified against finite element buckling solutions using ABAQUS for a wide range of lamination orientations showing excellent accuracy. The stability of the beam under different geometric and material parameters, like length/height ratio, layer thickness, and ply orientation, was investigated.

6.1 Introduction

Thin-walled beam structures are major components in many engineering applications. They are widely used as structural components in many types of systems in the field of

aerospace, mechanical, marine, and civil engineering. Fiber reinforced polymer (FRP) composites, are replacing conventional materials in some of these types of structural systems. This increase in interest for using FRP lies in some critical advantages of these materials over conventional counterparts. Their high strength to weight ratio, high stiffness to weight ratio, their corrosion resistance, their ease of transportation and erection, and their fatigue resistance are some of the advantages FRP offer. The most distinguished characteristic is the ability of tailoring the material for each particular application. Structural properties depend on the material system and the shape of the cross-section of the member (Barbero et al.1993). Unlike isotropic shapes, composite members are possible to optimize by altering the material itself through choosing among a variety of resins, fiber systems, and fiber orientations. Although thin-walled FRP structures exhibit high strength, problems of excessive deformation and instability, due to their low stiffness and slenderness of the member, are the major disadvantages in wider acceptance for structural engineering applications (Lin et al. 1996). Because of these limitations, the new generation of composite structures should be designed to work in a safe way and to experience higher performance than the conventional systems. Consideration of stability and deformation limits tend to be the governing design criteria for FRP structures before these structures reach material failure. Thus, the proper establishment of such criteria is an important prerequisite to the practical use of FRP in engineering applications.

A thin-walled slender beam subjected to in-plane bending moments (about the strong axis) may buckle in a combined lateral bending and twisting of the cross-section. This phenomenon is known as lateral- torsional buckling. Theory of thin-walled open section beams including axial constraints for isotropic materials was developed by Vlassov (1961). This classical theory neglects shear deformation in the middle surface of the wall so for thicker-walled

beams, the shear deformations may significantly increase the displacements and reduce the buckling loads. The shear deformation theory for transversely loaded isotropic beams was developed by Timoshenko and Gere (1961).

Many researchers have focused on studying the lateral torsional buckling of composite beams using different theoretical approaches while validating their work with experimental programs or finite element analysis. Among those, Bauld and Lih-Shyng (1984) applied Vlasov's theory for open section composites with symmetrical laminated walls neglecting the shear deformation. Bank and Bednarczyk (1988) and Barbero et al. (1993) developed simple expressions for the bending, torsional, and warping stiffness of composite laminated beams. Sherbourne and Kabir (1995) studied analytically the effect of transverse shear strain on the lateral buckling of thin-walled, open-section fibrous composite beams. Pandey et al. (1995) proposed an analytical formulation for finding the optimal direction of fiber for improving the lateral buckling strength of thin-walled I-section composite beams. Lin et al. (1996) studied stability of thin-walled composite structural members using finite element method. Davalos and Qiao (1997) used the non-linear elastic theory to develop a stability solution for lateral-distortional buckling for wide flange composite beams based on the principle of total potential energy. Kollar (2001) suggested a closed form solution for thin-walled open section columns, made of orthotropic composite materials, by considering flexure, shear and the torsional warping induced shear deformations. Roberts and Al-Ubaidi (2001) studied the influence of shear deformation on restrained torsional warping of pultruded FRP bars of open cross-section by proposing an approximate theory. Sapkas and Kollar (2002) studied the stability analysis of thin-walled, open section beams, made of orthotropic composite materials under various loading conditions. The solution indirectly accounted for shear deformation by adjusting the bending and

warping stiffness of the composite beams. Lee et al. (2002) presented a general analytical model, based on the classical lamination theory, applicable to the lateral buckling of composite laminated I-beams subjected to various types of loadings. Qiao et al (2003) studied a combined analytical and experimental evaluation of flexural-torsional buckling of fiber reinforced polymer composite I-beams based on energy method developed from the non-linear plate theory. Tai (2004) studied lateral- torsional buckling of symmetrically laminated, rectangular cross-section, composite beams under various loading conditions. Kotelko (2004) studied theoretical analysis for local buckling of different cross section thin-walled beams and columns. Karaagac et al. (2007) studied stability of cantilever laminated symmetric and anti-symmetric composite beams under static and dynamic conditions by applying elastic support. Machado (2010) studied the stability of simply supported thin-walled symmetric laminated composite I-beams subjected to combined axial and lateral loads by approximate analytical solutions and compared them with numerical results. The proposed solution also examined the nonlinear pre-buckling geometrical deformation for more accurate representation of the lateral stability conditions.

Most of the work, related to lateral- torsional stability of thin-walled composite beams, was focused on I-sections. The beams were either considered to be of symmetric layup, anti-symmetric layup, orthotropic, or pultruded in nature. There hasn't been any study recorded on the behavior of general anisotropic laminated composite beams to the best knowledge of the authors.

In the present chapter, a generalized semi-analytical model applicable to the lateral-torsional buckling of a simply supported rectangular cross-section beams, made of anisotropic laminated composite materials, subjected to concentrated load at mid-span/mid-height is developed. This model is based on the classical laminated plate theory (CLPT), and accounts for

the arbitrary laminate stacking sequence configurations. A finite element model is developed in ABAQUS to predict critical buckling loads and compare them with the results obtained from the analytical model. The effects of fiber orientation, beam length/height ratios and wall thickness on the critical buckling forces are studied. A finite element nonlinear pre-buckling geometrical deformation analysis was also examined and compared against semi-analytical solution to examine the pre-buckling deformation.

6.2 Analytical Formulation

A simply supported laminated composite beam with length L and a thin rectangular cross section is subjected to concentrated load at mid-span/mid-height, as shown in Figure 1. The model in this study is based on the classical laminated plate theory, Kollar and Springer (2003) and Barbero (1999). The following assumptions are adopted from the classical laminated plate theory:

1. The normals to mid-plane (reference surface) of the laminate remain normal and straight after deformation.
2. The normal to mid-plane of the laminate do not change length – in other words, the thickness of the laminate stays constant.
3. The shear deformations are neglected.
4. The laminate consists of perfectly bonded layers.
5. The stress-strain relationships are applied under plane-stress conditions.

The beam tends to buckle under a lateral-torsional behavior because of its small thickness. The beam is divided into two halves from the point of applied load (mid-span) in order to derive buckling equation. The coordinate system is assigned from the support end of each part as x -axis to be positive moving towards the center of the beam. The angle of twist, β , is positive

(counterclockwise buckling) in the left side of the beam (Figure 1a), while it is negative (clockwise buckling) to the right side of the beam (Figure 1b). The buckling equation is derived for each side of the beam, separately, then reconciled together. Figure 1c shows the boundary conditions for the beam shown from top view.

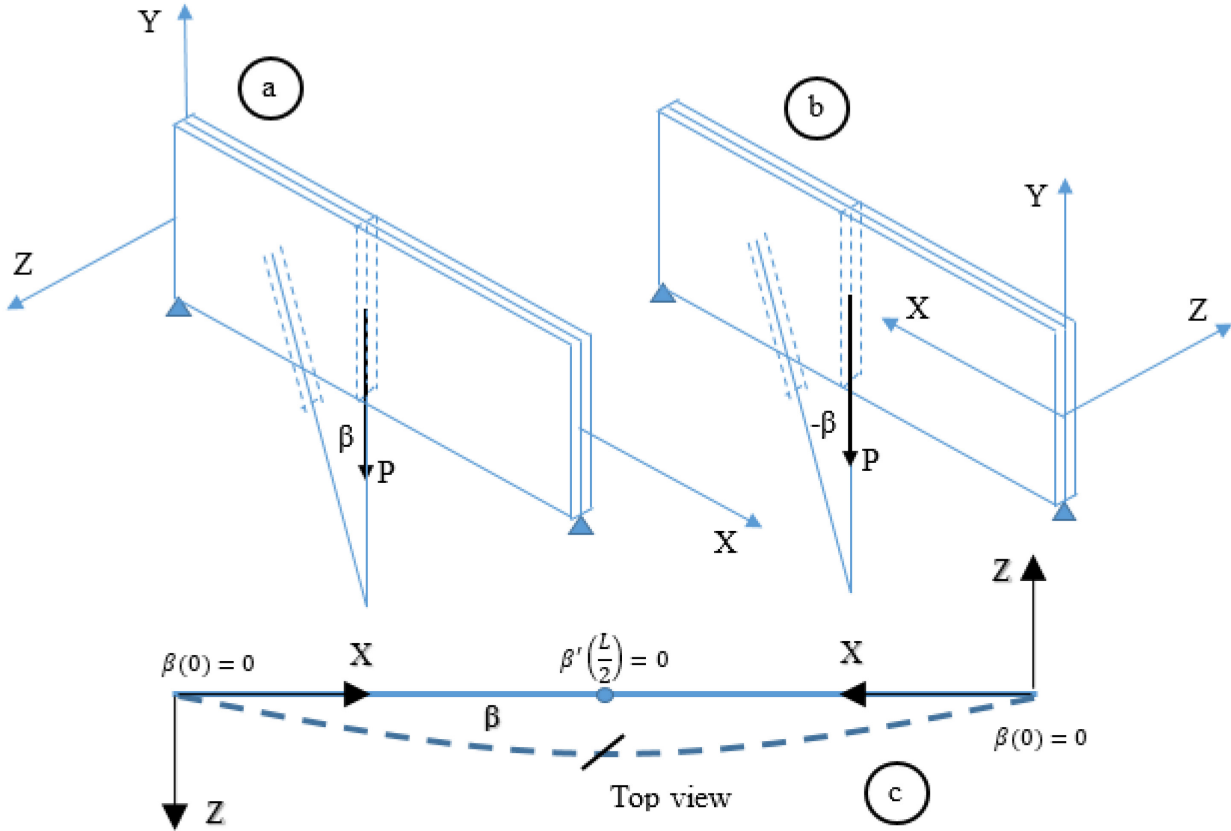


Figure 6.1 Buckling shape of the beam; (a) left side (+β), (b) right side (-β), and (c) top view

6.2.1 Kinematics

Based on the assumptions in the classical laminated plate theory, the displacement components u, v, w representing the deformation of a point in the plate profile section, as shown in Figure 2, are given with respect to mid-surface displacements $u_0, v_0,$ and w_0 as follows:

$$u(x, y, z) = u_0(x, y) - z \frac{\partial w}{\partial x}(x, y) \quad (6.1)$$

$$v(x, y, z) = v_0(x, y) - z\beta(x, y) \quad (6.2)$$

$$w(x, y, z) = w_0(x, y) \quad (6.3)$$

where $\beta = \frac{\partial w_0}{\partial y}$ (angle of twist)

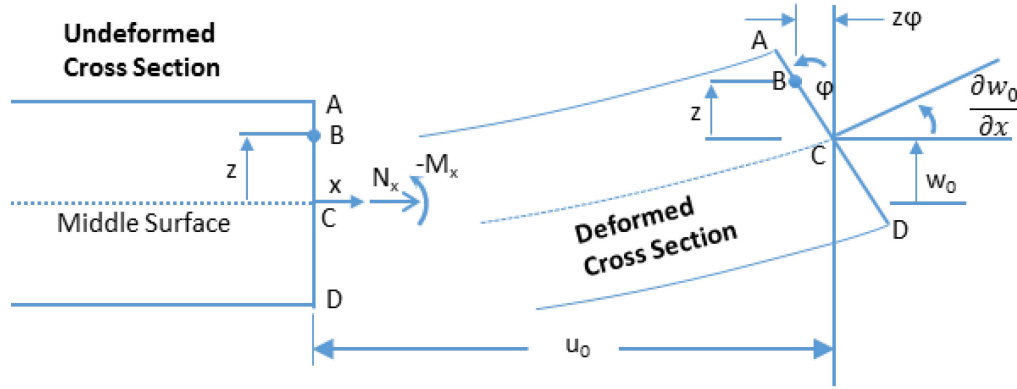


Figure 6.2 Deformation of a point at beam profile section with respect to mid-surface displacement

The strains associated with small displacements from the theory of elasticity are given by

$$\varepsilon_x = \varepsilon_x^0 + z\kappa_x \quad (6.4)$$

$$\varepsilon_y = \varepsilon_y^0 + z\kappa_y \quad (6.5)$$

$$\gamma_{xy} = \gamma_{xy}^0 + z\kappa_{xy} \quad (6.6)$$

where

$$\varepsilon_x^0 = \frac{\partial u_0}{\partial x}, \varepsilon_y^0 = \frac{\partial v_0}{\partial y}, \text{ and } \gamma_{xy}^0 = \frac{\partial u_0}{\partial y} + \frac{\partial v_0}{\partial x} \quad (6.7)$$

$$\kappa_x = -\frac{\partial^2 w_0}{\partial x^2}, \kappa_y = -\frac{\partial \beta}{\partial y}, \text{ and } \kappa_{xy} = -\left(\frac{\partial^2 w_0}{\partial x \partial y} + \frac{\partial^2 w_0}{\partial y \partial x}\right) = -2 \frac{\partial \beta}{\partial x} \quad (6.8)$$

The relationship of curvature and displacement is shown in Figure 3a and b in the case of β

being positive or negative which confirms Eq. 6.8.

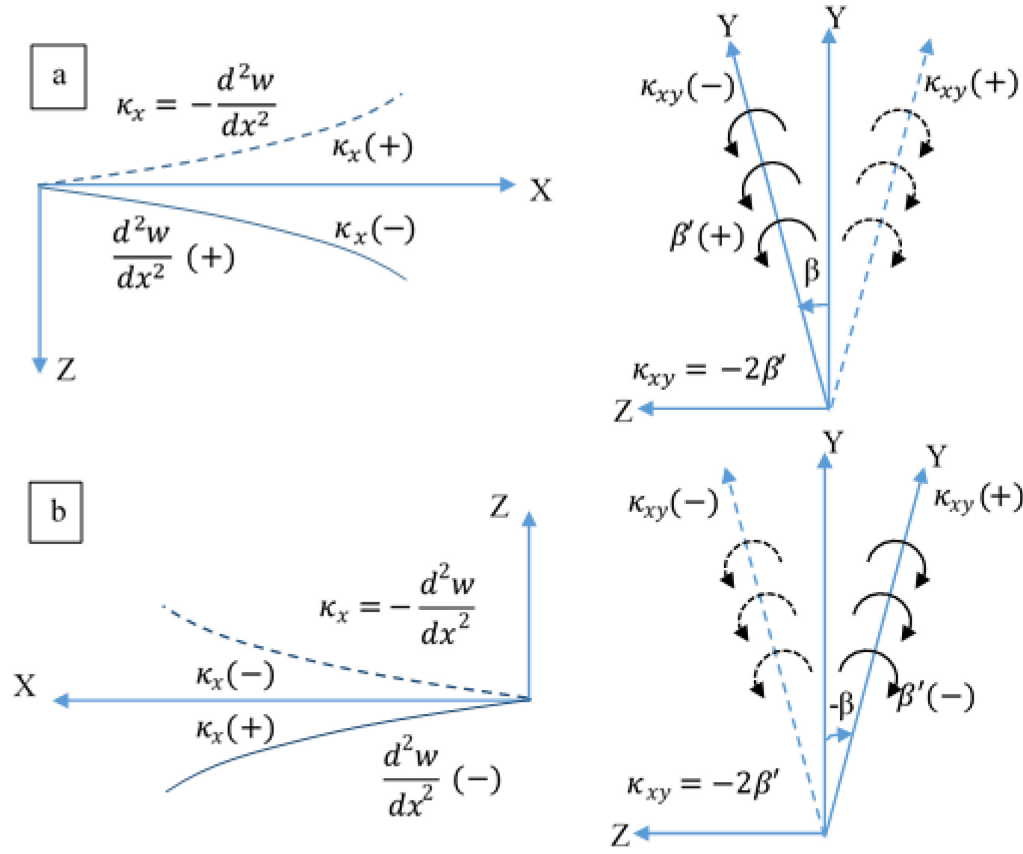


Figure 6.3 Representation of curvatures with respect to displacement and angle of twist; (a) left side of the beam (counterclockwise, $+\beta$) and (b) right side of the beam (clockwise, $-\beta$)

6.2.2 Constitutive Equations

The plate stiffness equations based on classical laminated plate theory, shown in Figure 6.4, are given as follows.

$$\begin{Bmatrix} N_x = 0 \\ N_y = 0 \\ N_{xy} = 0 \\ M_x \neq 0 \\ M_y = 0 \\ M_{xy} \neq 0 \end{Bmatrix} = h \begin{bmatrix} A_{11} & A_{12} & A_{16} & B_{11} & B_{12} & B_{16} \\ A_{12} & A_{22} & A_{26} & B_{11} & B_{12} & B_{16} \\ A_{16} & A_{26} & A_{66} & B_{11} & B_{12} & B_{16} \\ B_{11} & B_{12} & B_{16} & D_{11} & D_{12} & D_{16} \\ B_{12} & B_{22} & B_{26} & D_{12} & D_{22} & D_{26} \\ B_{16} & B_{26} & B_{66} & D_{16} & D_{26} & D_{66} \end{bmatrix} \begin{Bmatrix} \varepsilon_x \\ \varepsilon_y \\ \gamma_{xy} \\ \kappa_x \\ \kappa_y \\ \kappa_{xy} \end{Bmatrix} \quad (6.9)$$

where

$$A_{ij} = \sum_{k=1}^N (\bar{Q}_{ij})_k t_k \quad i, j = 1, 2, 6 \text{ are called extensional stiffness coefficients}$$

$B_{ij} = \sum_{k=1}^N (\bar{Q}_{ij})_k t_k \bar{z}_k$ $i, j = 1, 2, 6$ are called extension-bending coupling stiffness

coefficients and

$D_{ij} = \sum_{k=1}^N (\bar{Q}_{ij})_k \left(t_k \bar{z}_k^2 + \frac{t_k^3}{12} \right)$ $i, j = 1, 2, 6$ are called bending stiffness coefficients

$(\bar{Q}_{ij})_k$ are the components of the k^{th} layer 2D transformed constitutive matrix in the beam coordinate system

\bar{z}_k is the depth from the middle surface to the centroid of the k^{th} layer, and t_k is the thickness of k^{th} layer.

Knowing the zero components of externally applied forces and moments for the loading condition shown in Figures 6.5 and 6.6, which are expressed in Eq. 6.9, the stiffness matrix can be simplified and dimensionally reduced to an effective 2x2 stiffness matrix by using the static condensation technique. In the static condensation technique, the zero and non-zero components of forces and moments from Eq. 6.9 are arranged into separate matrices as follows:

$$h \begin{bmatrix} A_{11} & A_{12} & A_{16} & B_{12} \\ A_{12} & A_{22} & A_{26} & B_{22} \\ A_{16} & A_{26} & A_{66} & B_{26} \\ B_{12} & B_{22} & B_{26} & D_{22} \end{bmatrix} \begin{Bmatrix} \varepsilon_x \\ \varepsilon_y \\ \gamma_{xy} \\ \kappa_y \end{Bmatrix} + h \begin{bmatrix} B_{11} & B_{16} \\ B_{12} & B_{26} \\ B_{16} & B_{66} \\ D_{12} & D_{26} \end{bmatrix} \begin{Bmatrix} \kappa_x \\ \kappa_{xy} \end{Bmatrix} = \begin{Bmatrix} 0 \\ 0 \\ 0 \\ 0 \end{Bmatrix} \quad (6.10)$$

$$\begin{Bmatrix} M_x \\ M_{xy} \end{Bmatrix} = h \begin{bmatrix} D_{11} & D_{16} \\ D_{16} & D_{66} \end{bmatrix} \begin{Bmatrix} \kappa_x \\ \kappa_{xy} \end{Bmatrix} + h \begin{bmatrix} B_{11} & B_{16} \\ B_{12} & B_{26} \\ B_{16} & B_{66} \\ D_{12} & D_{26} \end{bmatrix}^T \begin{Bmatrix} \varepsilon_x \\ \varepsilon_y \\ \gamma_{xy} \\ \kappa_y \end{Bmatrix} \quad (6.11)$$

The reduced effective 2x2 stiffness matrix (Eq. 6.13) can be obtained by defining $\begin{Bmatrix} \varepsilon_x \\ \varepsilon_y \\ \gamma_{xy} \\ \kappa_y \end{Bmatrix}$ from

Eq. 6.10 in terms of the two other curvature components, as shown in Eq. 6.12, and substituting it into Eq. 6.11.

$$\begin{Bmatrix} \varepsilon_x \\ \varepsilon_y \\ \gamma_{xy} \\ \kappa_y \end{Bmatrix} = - \begin{bmatrix} A_{11} & A_{12} & A_{16} & B_{12} \\ A_{12} & A_{22} & A_{26} & B_{22} \\ A_{16} & A_{26} & A_{66} & B_{26} \\ B_{12} & B_{22} & B_{26} & D_{22} \end{bmatrix}^{-1} \begin{bmatrix} B_{11} & B_{16} \\ B_{12} & B_{26} \\ B_{16} & B_{66} \\ D_{12} & D_{26} \end{bmatrix} \begin{Bmatrix} \kappa_x \\ \kappa_{xy} \end{Bmatrix} \quad (6.12)$$

$$\begin{Bmatrix} M_x \\ M_{xy} \end{Bmatrix} = h \begin{bmatrix} D_Y & D_{YT} \\ D_{YT} & D_T \end{bmatrix} \begin{Bmatrix} \kappa_x \\ \kappa_{xy} \end{Bmatrix} \quad (6.13)$$

where

$$\begin{bmatrix} D_Y & D_{YT} \\ D_{YT} & D_T \end{bmatrix} = \begin{bmatrix} D_{11} & D_{16} \\ D_{16} & D_{66} \end{bmatrix} - \begin{bmatrix} B_{11} & B_{16} \\ B_{12} & B_{26} \\ B_{16} & B_{66} \\ D_{12} & D_{26} \end{bmatrix}^T \begin{bmatrix} A_{11} & A_{12} & A_{16} & B_{12} \\ A_{12} & A_{22} & A_{26} & B_{22} \\ A_{16} & A_{26} & A_{66} & B_{26} \\ B_{12} & B_{22} & B_{26} & D_{22} \end{bmatrix}^{-1} \begin{bmatrix} B_{11} & B_{16} \\ B_{12} & B_{26} \\ B_{16} & B_{66} \\ D_{12} & D_{26} \end{bmatrix}$$

D_Y is the composite effective lateral stiffness coefficient, D_T is the composite effective twisting stiffness coefficient, and D_{YT} is the composite effective lateral-twisting coupling coefficient. In most cases, where the layers are symmetric, anti-symmetric, cross-ply, special angle ply, D_{YT} coefficient will be zero. However, for the generally anisotropic cases, D_{YT} coefficient is not zero and will play a significant role in determining the buckling load of the beams.

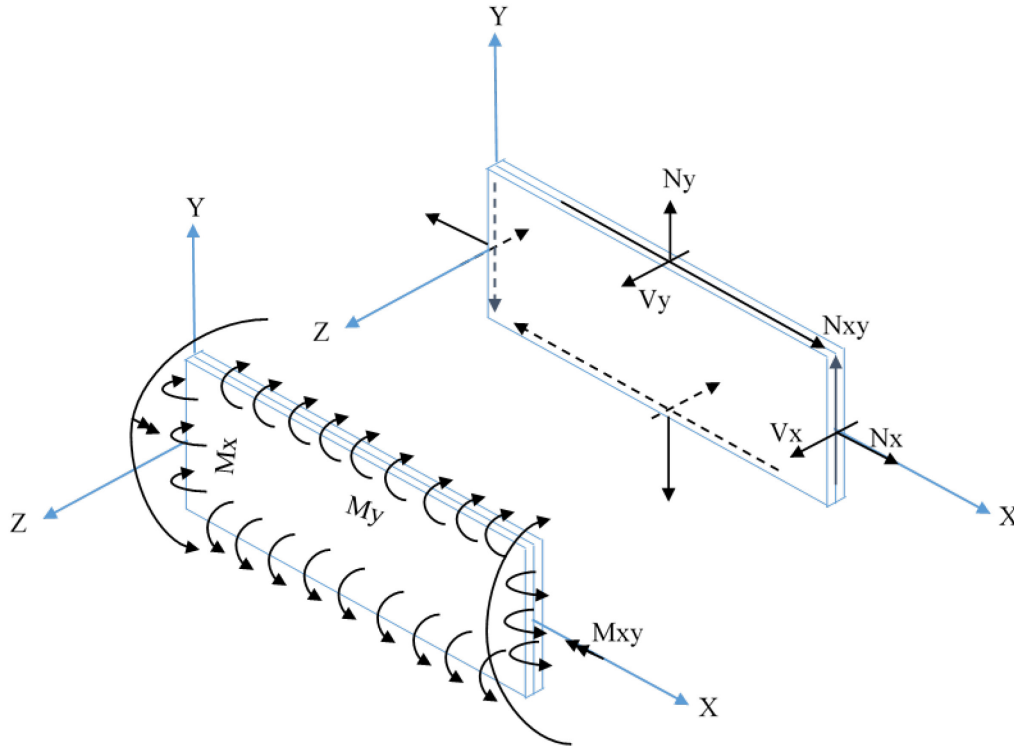
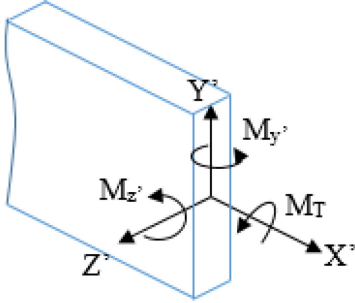
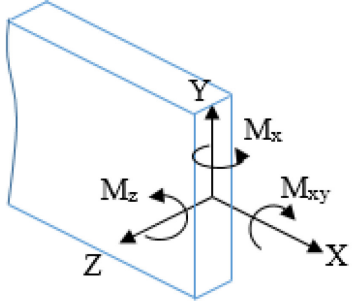


Figure 6.4 Force and moment resultants on a beam based on classical laminated plate theory

Referring to Figure 6.1 (structural coordinate) and Figure 6.4 (laminated coordinate), the bending moment M_y in structural coordinate is replaced by M_x in laminate coordinate, on the other hand, the shear moment, M_{xy} , in laminate coordinate is in the opposite direction of twisting moment in the structural coordinate system and is found by Kollar and Springer (2003) to be $M_T = -2 M_{xy}$, Table 6.1 shows the relation of moment components in structural coordinate and laminate composite coordinate systems.

Table 6.1 Relation of moment components in structural coordinate and laminate composite coordinate

| The structural coordinate (deformed axes) | Laminate composite coordinate |
|---|---|
|  | <div style="text-align: center;"> $M'_z = M_z$ $M'_y = M_x$ $M_T = -2M_{xy}$ </div>  |

Substituting the curvatures in terms of displacement and rotation from Eq. 6.8 into Eq. 6.13, and writing the moments in structural coordinates system, the following relation will be obtained

$$\begin{Bmatrix} M_{y'} \\ -M_T \end{Bmatrix} = h \begin{bmatrix} D_Y & 2D_{YT} \\ 2D_{YT} & 4D_T \end{bmatrix} \begin{Bmatrix} -\frac{d^2w}{dx^2} \\ -\beta' \end{Bmatrix} \quad (6.14)$$

6.2.3 Equilibrium Equations

As discussed earlier, two coordinate systems were considered (one for each half from the point of support) for simply supported beam under concentrated load at mid-span. The coordinate system is arranged from the ends of the beam as x-axis to be positive moving towards the center of the beam. The derivation of equilibrium equations is discussed in the following subsections.

6.2.3.1 Buckling Counterclockwise (Left Side of the Beam)

Figure 6.5 shows the components of external moments about original and deformed axes in the left side of the beam when it is considered to buckle counterclockwise, where β is considered to be positive. The moment components are shown in the following equations:

External moments about original axes:

$$M_z = \frac{P}{2}(x) \quad (6.15)$$

$$M_y = 0 \quad (6.16)$$

$$M_x = \frac{P}{2}(w_1 - w) \quad (6.17)$$

External moments about deformed axes:

$$M_z' = \frac{P}{2}(x) - \frac{P}{2}(w_1 - w) \frac{dw}{dx} \quad (6.18)$$

$$M_y' = \frac{P}{2}(x)\beta + \frac{P}{2}(w_1 - w) \frac{dv}{dx} \quad (6.19)$$

$$M_x' = \frac{P}{2}(x) \frac{dw}{dx} + \frac{P}{2}(w_1 - w) \quad (6.20)$$

where $\frac{P}{2}(w_1 - w) \frac{dw}{dx}$ and $\frac{P}{2}(w_1 - w) \frac{dv}{dx}$ are higher order terms which can be neglected.

The following system of differential equations is obtained after substituting the external moments from Eqs. 6.19 and 6.20 into Eq. 6.14:

$$\left\{ \begin{array}{l} \frac{P}{2}(x)\beta \\ -\frac{P}{2}(x) \frac{dw}{dx} - \frac{P}{2}(w_1 - w) \end{array} \right\} = h \begin{bmatrix} D_Y & 2D_{YT} \\ 2D_{YT} & 4D_T \end{bmatrix} \left\{ \begin{array}{l} -\frac{d^2w}{dx^2} \\ -\beta' \end{array} \right\} \quad (6.21)$$

$$-hD_Y \frac{d^2w}{dx^2} - 2hD_{YT}\beta' = \frac{P}{2}(x)\beta \quad (6.22)$$

$$-2hD_{YT} \frac{d^2w}{dx^2} - 4hD_T\beta' = -\frac{P}{2}(x) \frac{dw}{dx} - \frac{P}{2}(w_1 - w) \quad (6.23)$$

Writing Eqs.6.22 and 6.23 in terms of $\frac{d^2w}{dx^2}$ and equating the two expressions, the following relationship can be obtained.

$$\frac{1}{hD_Y} \left[-2hD_{YT}\beta' - \frac{P}{2}(x)\beta \right] = \frac{1}{2hD_{YT}} \left[-4hD_T\beta' + \frac{P}{2}(x) \frac{dw}{dx} + \frac{P}{2}(w_1 - w) \right] \quad (6.24)$$

Differentiating Eq.6.24 with respect to x and rearranging the resulting expression in terms of

$\frac{d^2w}{dx^2}$, Eq.6.25 will be obtained.

$$\frac{d^2w}{dx^2} = -\frac{2D_{YT}}{D_Y} \beta' + \frac{4h}{\frac{P}{2}(x)} \left[D_T - \frac{D_{YT}^2}{D_Y} \right] \beta'' - \frac{PD_{YT}\beta}{D_Y \frac{P}{2}(x)} \quad (6.25)$$

Equating the left hand side of Eq.6.24, which is equal to $\frac{d^2w}{dx^2}$ in Eq. 6.22, and the right hand side of Eq.6.25, the resulting expression reduces to a second order ordinary differential equation with non-constant coefficients.

$$\beta'' - \frac{hPD_{YT}}{4h^2[D_Y D_T - D_{YT}^2]} \beta + \frac{\frac{P^2}{4}(x)^2}{4h^2[D_Y D_T - D_{YT}^2]} \beta = 0 \quad (6.26)$$

Setting $\psi_1^2 = \frac{\frac{P^2}{4}}{4h^2[D_Y D_T - D_{YT}^2]}$ and $\psi_2 = \frac{hPD_{YT}}{4h^2[D_Y D_T - D_{YT}^2]}$, a simplified form of differential equation is obtained.

$$\beta'' + (\psi_1^2(x)^2 - \psi_2)\beta = 0 \quad (6.27)$$

This form of differential equation is a Weber function which can be solved by a numerical iterative procedure in commercial software which can solve these types of equations.

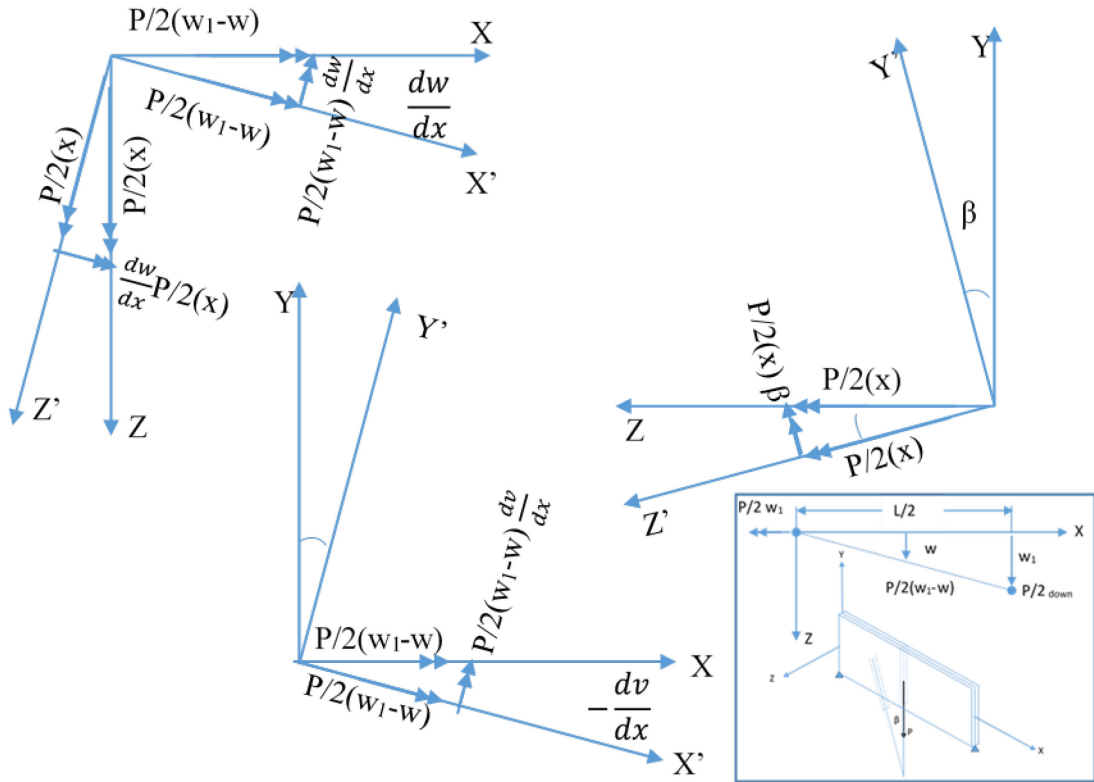


Figure 6.5 Components of external forces about original and deformed axes of laminated simply supported beam subjected to concentrated load; coordinate system from the left end of the beam (counterclockwise, $+\beta$)

6.2.3.2 Buckling Clockwise (Right Side of the Beam)

Figure 6.6 shows the components of external moments about the original and deformed axes when the right side of the beam is considered, where β is considered to be negative. The moment components are shown in the following equations:

External moments about original axes:

$$M_z = \frac{P}{2}(x) \tag{6.28}$$

$$M_y = 0 \tag{6.29}$$

$$M_x = -\frac{P}{2}(w_1 - w) \tag{6.30}$$

External moments about deformed axes:

$$M_z' = \frac{P}{2}(x) - (w_1 - w) \frac{dw}{dx} \quad (6.31)$$

$$M_y' = -\frac{P}{2}(x)\beta - \frac{P}{2}(w_1 - w) \frac{dv}{dx} \quad (6.32)$$

$$M_x' = -\frac{P}{2}(x) \frac{dw}{dx} - \frac{P}{2}(w_1 - w) \quad (6.33)$$

where $\frac{P}{2}(w_1 - w) \frac{dw}{dx}$ and $\frac{P}{2}(w_1 - w) \frac{dv}{dx}$ are higher order terms which can be neglected.

The following system of differential equations is obtained after substituting the external moments from Eqs. 6.32 and 6.33 into Eq. 6.14:

$$\left\{ \begin{array}{c} -\frac{P}{2}(x)\beta \\ \frac{P}{2}(x) \frac{dw}{dx} + \frac{P}{2}(w_1 - w) \end{array} \right\} = h \begin{bmatrix} D_Y & 2D_{YT} \\ 2D_{YT} & 4D_T \end{bmatrix} \left\{ \begin{array}{c} -\frac{d^2w}{dx^2} \\ -\beta' \end{array} \right\} \quad (6.34)$$

$$-hD_Y \frac{d^2w}{dx^2} - 2hD_{YT}\beta' = -\frac{P}{2}(x)\beta \quad (6.35)$$

$$-2hD_{YT} \frac{d^2w}{dx^2} - 4hD_T\beta' = \frac{P}{2}(x) \frac{dw}{dx} + \frac{P}{2}(w_1 - w) \quad (6.36)$$

Writing Eqs. 6.35 and 6.36 in terms of $\frac{d^2w}{dx^2}$ and equating the two expressions, the following relationship can be obtained.

$$\frac{1}{hD_Y} \left[-2hD_{YT}\beta' + \frac{P}{2}(x)\beta \right] = \frac{1}{2hD_{YT}} \left[-4hD_T\beta' - \frac{P}{2}(x) \frac{dw}{dx} - \frac{P}{2}(w_1 - w) \right] \quad (6.37)$$

Differentiating Eq. 6.37 with respect to x and rearranging the resulting expression in terms of $\frac{d^2w}{dx^2}$, Eq. 6.38 will be obtained.

$$\frac{d^2w}{dx^2} = -\frac{2D_{YT}}{D_Y} \beta' - \frac{4h}{\frac{P}{2}(x)} \left[D_T - \frac{D_{YT}^2}{D_Y} \right] \beta'' - \frac{PD_{YT}\beta}{D_Y \frac{P}{2}(x)} \quad (6.38)$$

Equating the left hand side of Eq. 6.37, which is equal to $\frac{d^2w}{dx^2}$ in Eq. 6.35, and the right hand side of Eq. 6.38, the resulting expression reduces to a second order ordinary differential equation with non-constant coefficients.

$$\beta'' + \frac{hPD_{YT}}{4h^2[D_Y D_T - D_{YT}^2]} \beta + \frac{\frac{P^2}{4}(x)^2}{4h^2[D_Y D_T - D_{YT}^2]} \beta = 0 \quad (6.39)$$

Setting $\psi_1^2 = \frac{\frac{P^2}{4}}{4h^2[D_Y D_T - D_{YT}^2]}$ and $\psi_2 = \frac{hPD_{YT}}{4h^2[D_Y D_T - D_{YT}^2]}$, a simplified form of differential equation is obtained.

$$\beta'' + (\psi_1^2(x)^2 + \psi_2)\beta = 0 \quad (6.40)$$

This form of differential equation is a Weber function which can be solved by a numerical iterative procedure in a commercial software which can solve these types of equations.

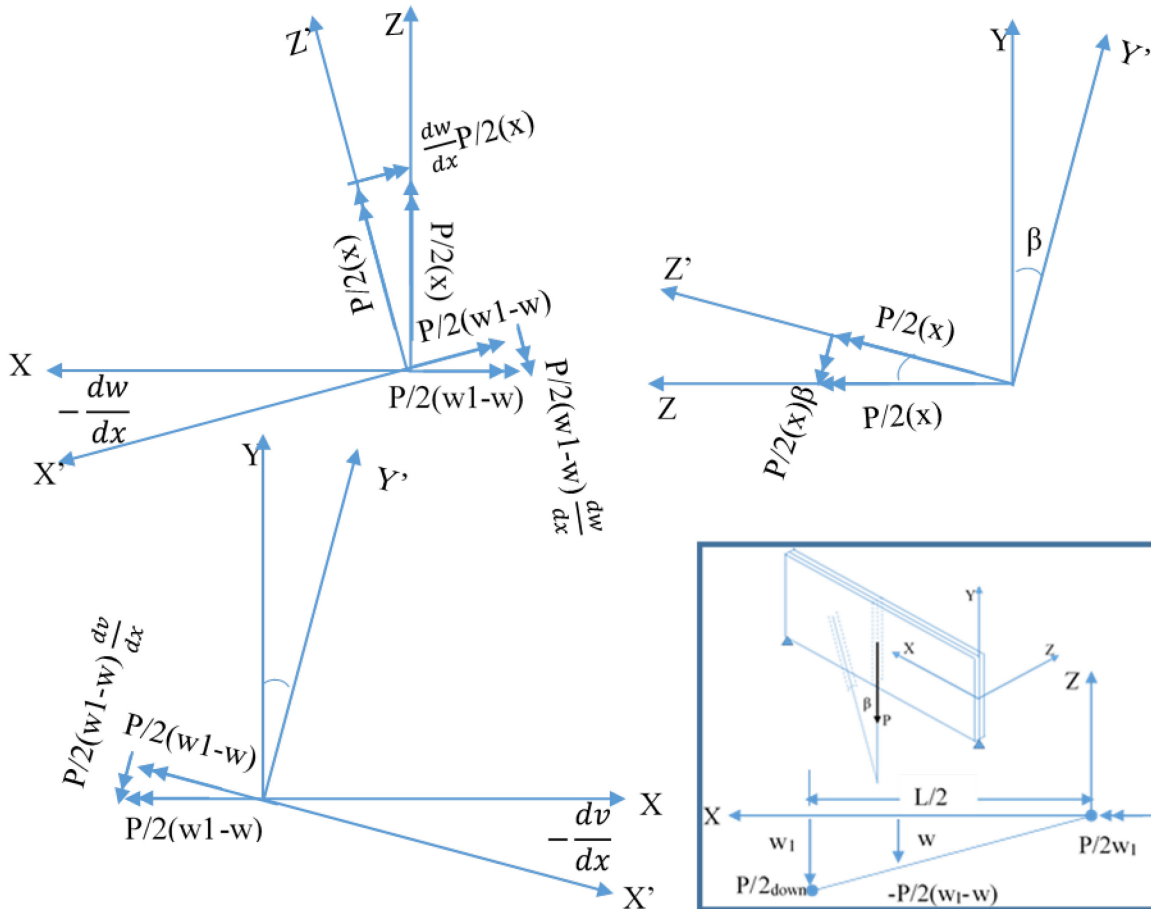


Figure 6.6 Components of external forces about original and deformed axes of laminated simply supported beam subjected to concentrated load, coordinate system from the right end of the beam (clockwise— β)

Comparing Eqs. 6.27 and 6.40, derived from the above two halves of the beam, one can see that the only difference is the sign of coefficient ψ_2 , where it is negative for counterclockwise buckling (left side of the beam) and positive for the case of clockwise buckling (right side of the beam).

The differential equation for two cases is as follows:

$$\beta'' + (\psi_1^2(x)^2 \mp \psi_2)\beta = 0 \quad (6.41)$$

Since Eqs. 6.27 and 6.40 come from the same configuration, a term cannot have two different signs. Therefore, the second term of Eq. 6.41 which is $\mp\psi_2$ has to vanish, and the final equation simplifies to

$$\beta'' + \psi_1^2 x^2 \beta = 0 \quad (6.42)$$

Thus the critical buckling force is

$$P = 2\psi_1 h \sqrt{4[D_Y D_T - D_{YT}^2]} \quad (6.43)$$

The value of ψ_1 in Eq. 6.42 is determined by numerical iterative solution using Mathematica by applying the following boundary conditions: $\beta(0) = 0$ and $\beta'(\frac{L}{2}) = 0$. The general solution of Eq. 6.42 contains a nonlinear polynomial function which is called `ParabolicCylinderD` (or `D`) in Mathematica. In this process, the program first solves for the general solution of the differential equation. The boundary conditions are applied to the general solution. After applying the boundary conditions, a polynomial function of $f_n(\psi_1)$ is obtained, which must be set equal to zero. This function contains real and imaginary parts. To obtain a numerical solution for ψ_1 , the numerical values for a certain beam geometric parameters should be iterated until the equation converges. Following this procedure, Eq. 6.42 converged at a value of $\psi_1 = 3.38723E - 5$ regardless of the lamination stacking sequence for a length of 500 mm.

To obtain a general solution, ψ_1 is normalized with respect to length yielding a constant of 16.94. It is interesting to observe that this constant matches that of isotropic beams shown by Timoshenko and Gere (1961). The general buckling solution is presented in Eq. 6.44. Figure 6.7 shows the flowchart of the procedure used in Mathematica to obtain the value of ψ_1 . A screenshot of the script, used in Mathematica, is shown in Figure 6.8.

$$P = \frac{16.94h}{L^2} \sqrt{4[D_Y D_T - D_{YT}^2]} \quad (6.44)$$

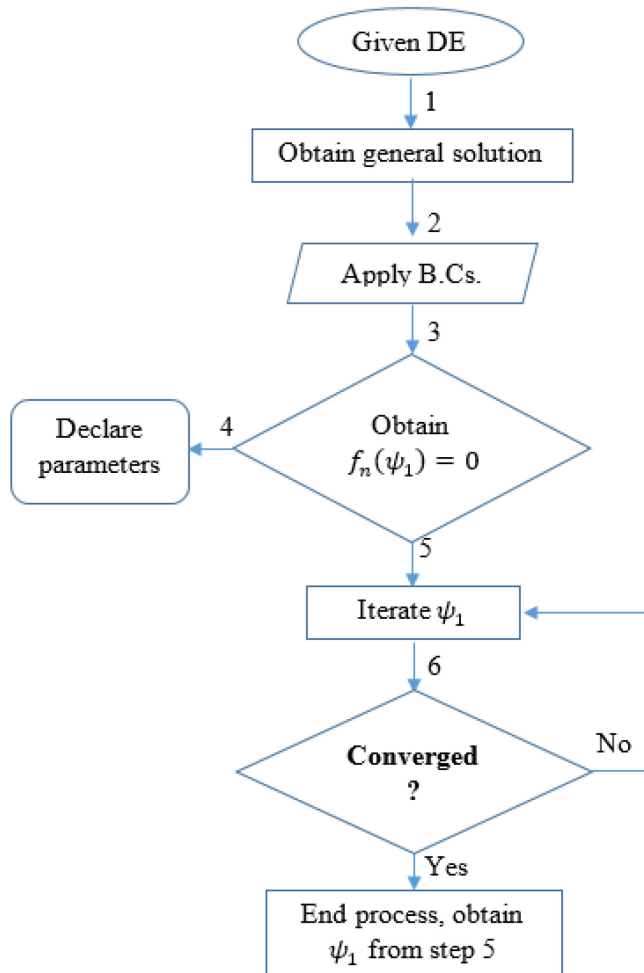


Figure 6.7 Flowchart of the semi-analytical solution of the buckling equation using Mathematica

```

sol = DSolve[ $\beta[x] (\psi^2 x^2) + \beta''[x] = 0, \beta, x]$ 
{{ $\beta \rightarrow \left( \{x\} \mapsto c_1 D_{-\frac{1}{2}} \left( \sqrt[4]{-1} \sqrt{2} x \sqrt{\psi} \right) + c_2 D_{-\frac{1}{2}} \left( (-1)^{3/4} \sqrt{2} x \sqrt{\psi} \right) \right)}$ }}
m = sol[[1]]
 $\beta \rightarrow \left( \{x\} \mapsto c_1 D_{-\frac{1}{2}} \left( \sqrt[4]{-1} \sqrt{2} x \sqrt{\psi} \right) + c_2 D_{-\frac{1}{2}} \left( (-1)^{3/4} \sqrt{2} x \sqrt{\psi} \right) \right)$ 
BC1 =  $\beta[0] /. m$  (* = 0 ; FIRST BOUNDARY CONDITION APPLIED*)
 $\frac{\sqrt{\pi} c_1}{\sqrt[4]{2} \Gamma\left(\frac{3}{4}\right)} + \frac{\sqrt{\pi} c_2}{\sqrt[4]{2} \Gamma\left(\frac{3}{4}\right)}$ 
solveC2 = Solve[{BC1 == 0}, {C[2]}] (* solves C[2] in terms of C[1] from the first boundary condition*)
{{c2 -> -c1}}
BC2 =  $\beta\left[\frac{L}{2}\right] /. m$  (* = 0 : SECOND BOUNDARY CONDITION APPLIED*)
 $\sqrt[4]{-1} \sqrt{2} c_1 \sqrt{\psi} \left( \frac{\sqrt[4]{-1} L \sqrt{\psi} D_{-\frac{1}{2}} \left( \frac{\sqrt[4]{-1} L \sqrt{\psi}}{\sqrt{2}} \right)}{2 \sqrt{2}} - D_{\frac{1}{2}} \left( \frac{\sqrt[4]{-1} L \sqrt{\psi}}{\sqrt{2}} \right) \right) + (-1)^{3/4} \sqrt{2} c_2 \sqrt{\psi} \left( \frac{(-1)^{3/4} L \sqrt{\psi} D_{-\frac{1}{2}} \left( \frac{(-1)^{3/4} L \sqrt{\psi}}{\sqrt{2}} \right)}{2 \sqrt{2}} - D_{\frac{1}{2}} \left( \frac{(-1)^{3/4} L \sqrt{\psi}}{\sqrt{2}} \right) \right)$ 
(*****COMMENTS: substitute the value of C[2] in terms of C[1] *****)
 $\left( \sqrt[4]{-1} \sqrt{2} c_1 \sqrt{\psi} \left( \frac{\sqrt[4]{-1} L \sqrt{\psi} D_{-\frac{1}{2}} \left( \frac{\sqrt[4]{-1} L \sqrt{\psi}}{\sqrt{2}} \right)}{2 \sqrt{2}} - D_{\frac{1}{2}} \left( \frac{\sqrt[4]{-1} L \sqrt{\psi}}{\sqrt{2}} \right) \right) - (-1)^{3/4} \sqrt{2} c_1 \sqrt{\psi} \left( \frac{(-1)^{3/4} L \sqrt{\psi} D_{-\frac{1}{2}} \left( \frac{(-1)^{3/4} L \sqrt{\psi}}{\sqrt{2}} \right)}{2 \sqrt{2}} - D_{\frac{1}{2}} \left( \frac{(-1)^{3/4} L \sqrt{\psi}}{\sqrt{2}} \right) \right) \right) = 0$ 
(* COMMENT: the above equation is defined only in terms of C[1] and a (psi). Pull C[1] out of the equation and make inside of the equation equal to zero.*)
 $\left( \sqrt[4]{-1} \sqrt{2} \sqrt{\psi} \left( \frac{\sqrt[4]{-1} L \sqrt{\psi} D_{-\frac{1}{2}} \left( \frac{\sqrt[4]{-1} L \sqrt{\psi}}{\sqrt{2}} \right)}{2 \sqrt{2}} - D_{\frac{1}{2}} \left( \frac{\sqrt[4]{-1} L \sqrt{\psi}}{\sqrt{2}} \right) \right) - (-1)^{3/4} \sqrt{2} \sqrt{\psi} \left( \frac{(-1)^{3/4} L \sqrt{\psi} D_{-\frac{1}{2}} \left( \frac{(-1)^{3/4} L \sqrt{\psi}}{\sqrt{2}} \right)}{2 \sqrt{2}} - D_{\frac{1}{2}} \left( \frac{(-1)^{3/4} L \sqrt{\psi}}{\sqrt{2}} \right) \right) \right) = 0$ 
(*****DEFINE THE VALUES OF PAREMITERS *****)
L = 500 (* Length of the beam*)
500
 $\psi = 3.387226430095 \times 10^{-5}$  (* keep changing this value until the real and imaginary parts of the equation converges*)
0.0000338723
 $\left( \sqrt[4]{-1} \sqrt{2} \sqrt{\psi} \left( \frac{\sqrt[4]{-1} L \sqrt{\psi} D_{-\frac{1}{2}} \left( \frac{\sqrt[4]{-1} L \sqrt{\psi}}{\sqrt{2}} \right)}{2 \sqrt{2}} - D_{\frac{1}{2}} \left( \frac{\sqrt[4]{-1} L \sqrt{\psi}}{\sqrt{2}} \right) \right) - (-1)^{3/4} \sqrt{2} \sqrt{\psi} \left( \frac{(-1)^{3/4} L \sqrt{\psi} D_{-\frac{1}{2}} \left( \frac{(-1)^{3/4} L \sqrt{\psi}}{\sqrt{2}} \right)}{2 \sqrt{2}} - D_{\frac{1}{2}} \left( \frac{(-1)^{3/4} L \sqrt{\psi}}{\sqrt{2}} \right) \right) \right) = 0$ 
{6.43496  $\times 10^{-15}$  + 3.6799  $\times 10^{-18} i$ } = 0

```

Figure 6.8 Screenshot of the script used in Mathematica to solve the buckling differential equation

6.3 Numerical Analysis (FEA)

The finite element method through the commercial software package, ABAQUS/Standard (implicit) was used to simulate the problem in this study in order to verify the derived semi-analytical formula for simply supported beams under concentrated loads at mid-span. The model was first created by using 3D planar shells. The shells were assembled based on the stacking arrangement that was used in the analytical solution. The global x-axis was assigned along beam's length, but the local coordinate system was used based on the orientation of the fibers in each ply.

The beam was rotationally and translationally restrained at one end. A concentrated load was applied at the centroid of the beam's mid-span. The boundary condition and applied load are shown in Figure 6.9a.

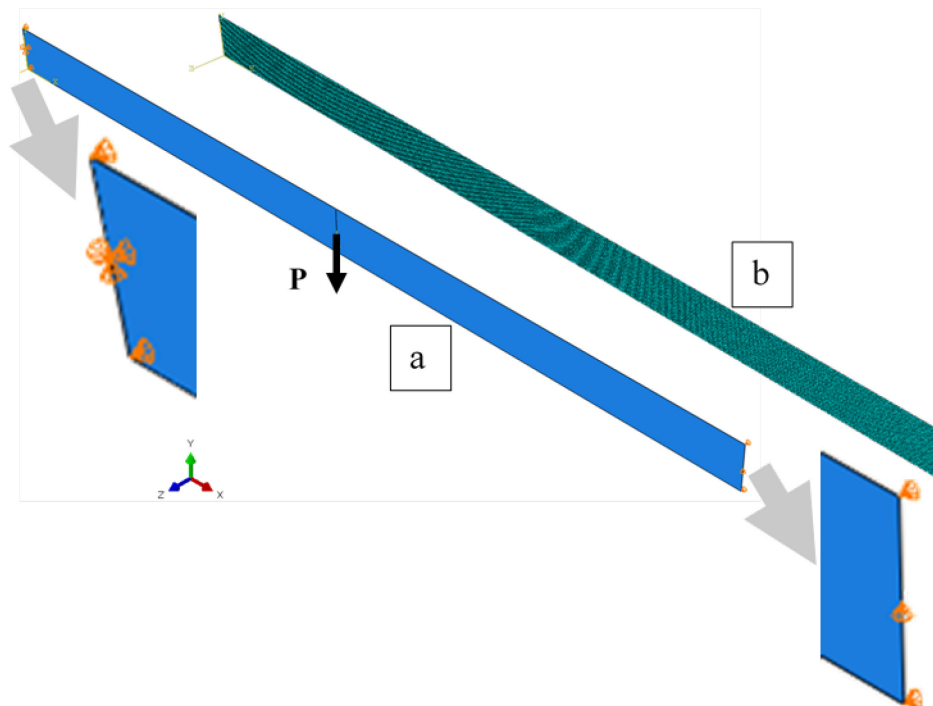


Figure 6.9 FEM model with $L/h = 20$ and layer thickness = 0.1 mm; (a) applied load and boundary conditions and (b) applied shell element type (S8R) and mesh (element size along beam axis: 1 mm)

The beam was meshed with a standard quadratic quadrilateral shell element type of S8R (8-node doubly curved thick shell element with reduced integration) using six degrees of freedom per node and an element size of 1 mm along beam axis. A beam with $L = 500$ mm and $h = 25$ mm gives total number of 40053 nodes and 13000 elements, as shown in Figure 6.9b.

The eigenvalue buckling analysis in ABAQUS solver, which is a linearized perturbation procedure, determines the eigenvalue of the buckling mode. ABAQUS extracts the eigenvalues and eigenvectors for symmetric stiffness matrices only. In order to turn the stiffness matrix of the model symmetric, Lanczos iteration eigenvalue extraction method was used. To find the critical force, based on the ABAQUS user guide, the lowest eigenvalue is multiplied by the applied force at the centroid of mid-span of the beam.

$$P_{0cr} = \lambda P \quad (6.45)$$

In addition, a nonlinear stability analysis (pre-buckling and buckling) of the laminated anisotropic simply supported beam was performed by adopting the nonlinear geometry analysis using the modified Riks approach, Al-Masri and Rasheed (2017) and Memon and Sun (2004). The modified Riks analysis uses the Arc-length method to follow the equilibrium path, representing either bifurcation points or limit points. Reasonable load increments are applied during the analysis in which the iteration converges to equilibrium along the Arc-length.

6.4 Results

6.4.1 Material Properties and Stacking Sequences

An anisotropic composite material is made by stacking four layers of the lamina properties shown in Table 6.2 at different fiber orientations. The thickness of each layer is the same with the same orthotropic properties, yet it varies in terms of fiber orientation. The

orientation of fiber in each layer can be randomly picked, including common laminate types such as symmetric laminates, antisymmetric laminates, balanced laminates, and so on. The stacking sequence starts from the back of the beam to the front of the beam to follow the same order used for typical laminated plates, shown in Figure 6.10. For example, [30/-30/30/-30] means that the first ply has an angle of 30 degrees from the x-axis of the beam is placed in the back of the beam counter clockwise (towards the y-axis) and the other layers follow with the same order through the positive z-axis direction. Figure 6.10 shows the stacking sequence of the laminates. Different layer thicknesses of (0.05, 0.1, 0.15, and 0.2 mm) and length to height ratios of (5, 10, 20, and 50) were also studied which will be presented later. Furthermore, the effect of fiber orientation for antisymmetric balanced angle ply, symmetric balanced angle ply, and single angle anisotropic layups were studied by varying angle of orientation.

Table 6.2 CFRP material properties used in the laminates

| Material | CFRP | |
|------------|----------|-----|
| E11 | 142730 | MPa |
| E22 | 13790 | MPa |
| v12 | 0.3 | |
| v21 | 0.028985 | |
| G12 | 4640 | MPa |
| G13 | 4640 | MPa |
| G23 | 3030 | MPa |

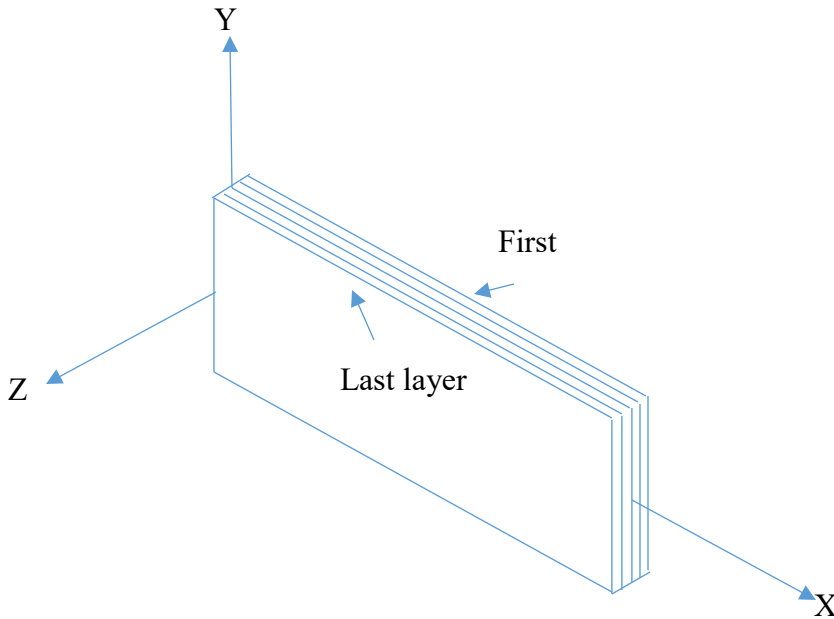


Figure 6.10 The stacking sequence of the laminates

6.4.2 Buckling Results

For the lateral-torsional buckling of thin-walled rectangular simply supported laminated composite beams under concentrated load, a semi-analytical approach is presented as well as FEM results. Figures 6.11 and 6.12 show the buckling solutions for different stacking sequences (19 different laminate-fiber orientations) based on the proposed analytical formulation as well as results from FEM model for layer thickness of 0.1 mm (total thickness of 0.4 mm), beam length of 500 mm and beam height of 50 mm and 25 mm (i.e. length to height ratio of 10 and 20), respectively. Based on the results obtained, there is an excellent agreement between the proposed analytical formulation and FEM, Figures 6.11 and 6.12. The largest error observed is 6.34% for L/h ratio of 10 (Figure 6.11) and 8.90% for L/h ratio of 20 from anisotropic layup of [30/30/30/30], see Table 6.3. From the observation of Figures 6.11 and 6.12, the analytical formula slightly overestimates the buckling load for higher L/h ratio (Figure 6.12). It might be

due to the fact the height to thickness (h/t) ratio of the beam decreases causing it to behave as a less-slender beam.

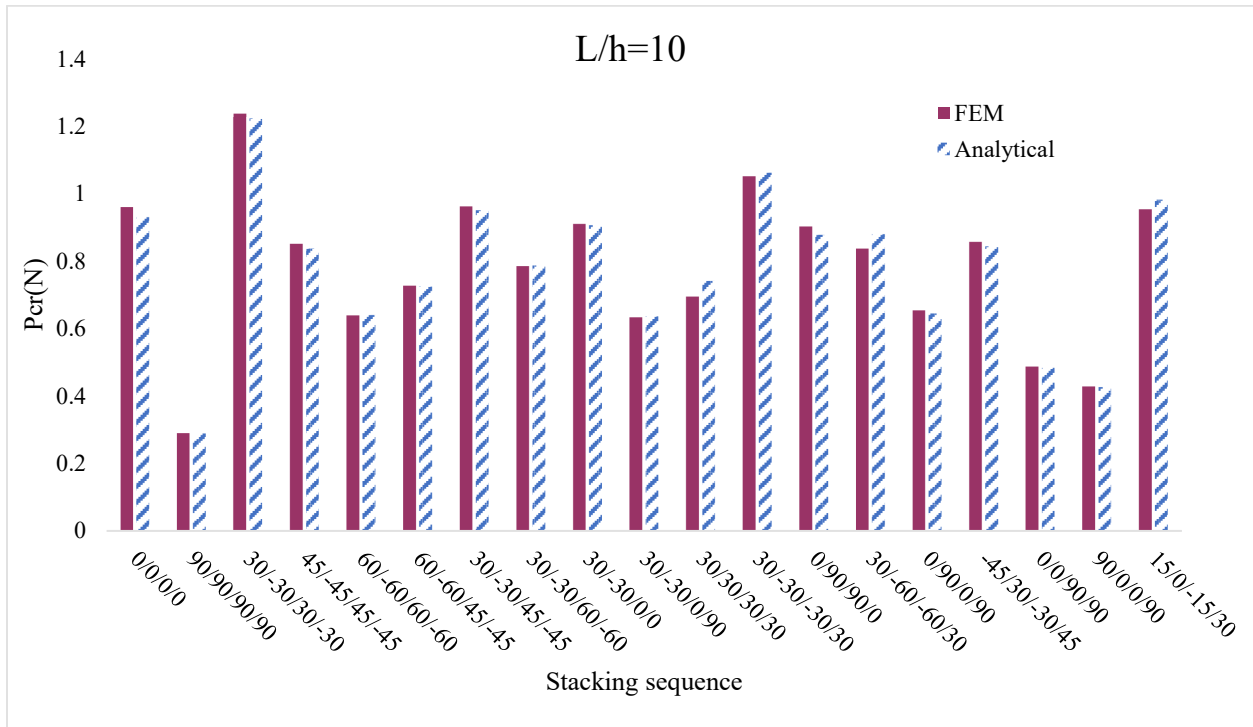


Figure 6.11 Buckling forces at different stacking sequences: $t_k=0.1$ mm for each layer and $L/h=10$

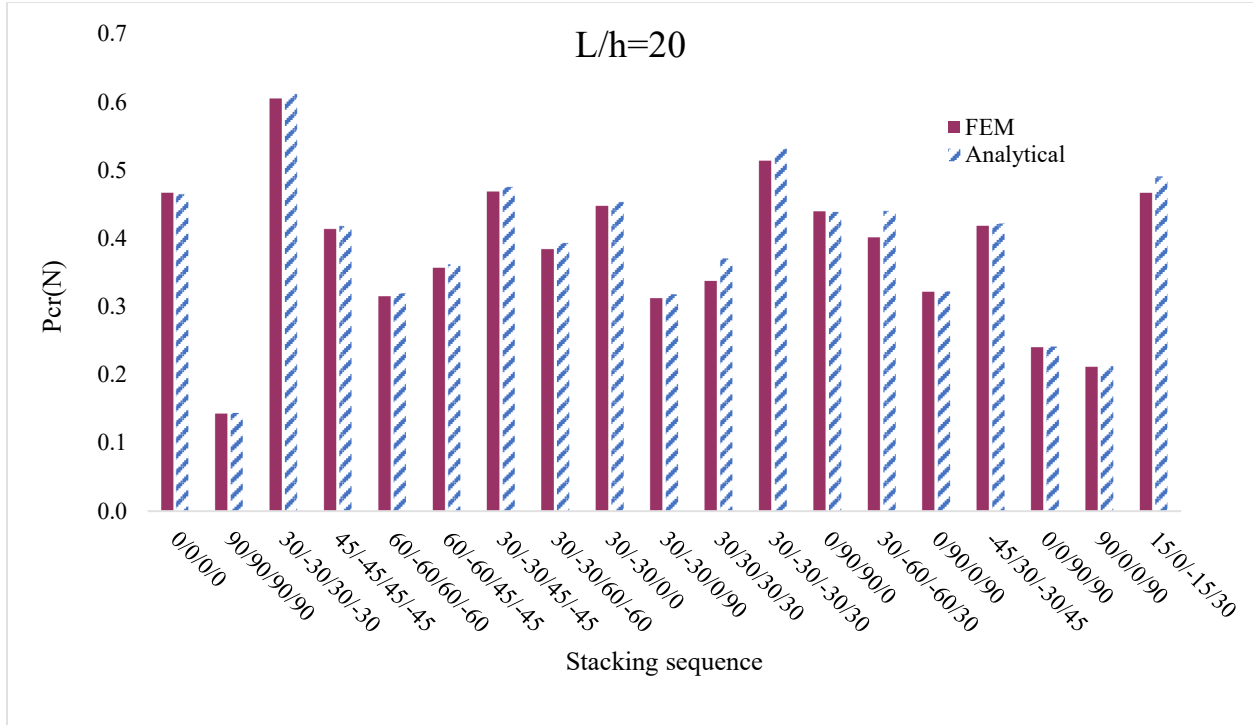


Figure 6.12 Buckling forces at different stacking sequences: $t_k=0.1$ mm for each layer and $L/h=20$

6.5 Parametric Study

6.5.1 Effect of Length/Height Ratio

Different Length/height (L/h) ratios of 5, 10, 20, and 50 were used in the analysis to study their effects on the lateral-torsional buckling of simply supported anisotropic laminated thin-walled rectangular cross-section beams. The results show that there is a significant drop in the value of the buckling forces as the L/h ratio increases. The relation between buckling force and L/h ratio is defined to be a power function which can be written in Eq. 6.46.

$$P_{cr} = (P_{cr})_i * \left(\frac{L}{h}\right)_i \left(\frac{L}{h}\right)^{-1} \quad (6.46)$$

where $(P_{cr})_i$ is the initial calculated value of buckling force from Eq. 6.44 with a given $\left(\frac{L}{h}\right)_i$ ratio for a specific laminate stacking sequence.

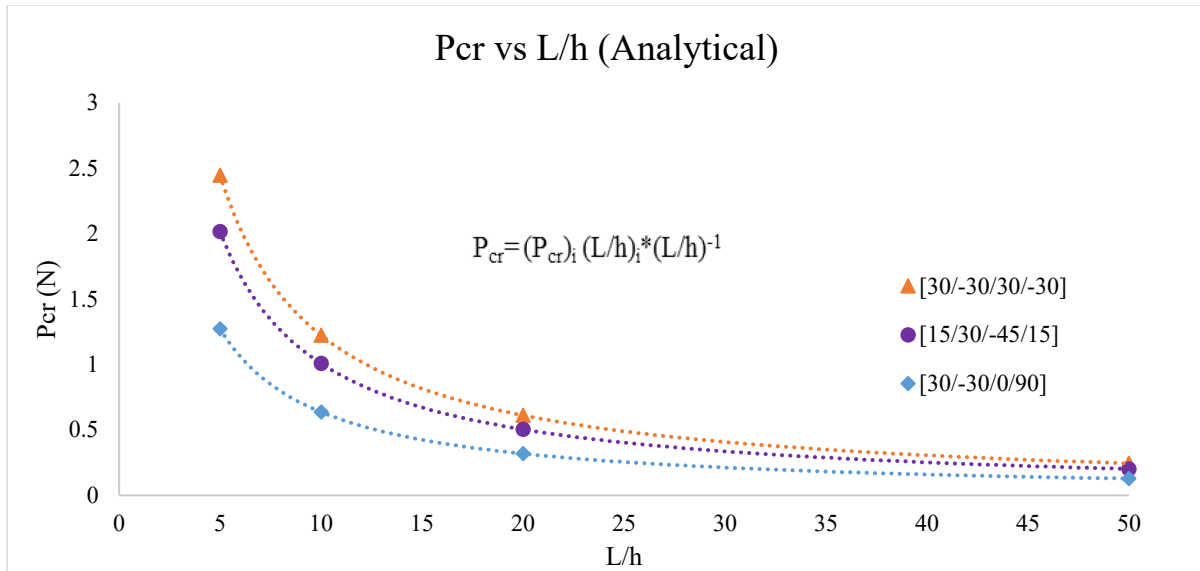


Figure 6.13 Effect of L/h ratio on the critical buckling force based on analytical formula for three different layups and ply thickness of 0.1 mm

By knowing the value of buckling force in a selected laminate, Eq. 6.46 helps to calculate the buckling force for different L/h ratios while the stacking sequence is retained the same. Figure 6.13 shows the effect of L/h ratio on the buckling force for three different stacking sequences of [30/-30/0/90], [15/30/-45/15], and [30/-30/30/-30]. Eq. 6.46 is limited to the analytical formula and is not applicable to the FEM results. There is a noticeable discrepancy between the analytical and numerical results in the cases where L/h ratio decreases, especially when the ratio of L/h is 5 or lower, as shown in Figures 6.15-6.17 for three different cases. The beam with lower L/h ratio behaves like a plate and buckles numerically in a distortional mode, in which β at a certain section transverse to the beam is not constant, rather than a lateral-torsional mode, in which the lateral angle of twist, β , remains constant for a certain section transverse to the beam. Figure 6.14 shows the deformed mode shape of the beam in four different L/h ratios of 5, 10, 20 and 50 comparing to the original shapes for layup of [0/0/0/0] in isometric view. It is evident that the deformed shape for the cases (a), (b) and (c) buckles numerically in a lateral

torsional mode where a constant β can be assumed as done analytically while β cannot be assumed constant for L/h ratio of 5, Figure 6.14d, as it buckles numerically in a distortional mode. Figures 6.15 – 6.17 clearly shows that the analytical and numerical buckling loads match almost exactly as the L/h ratio increases beyond 5.

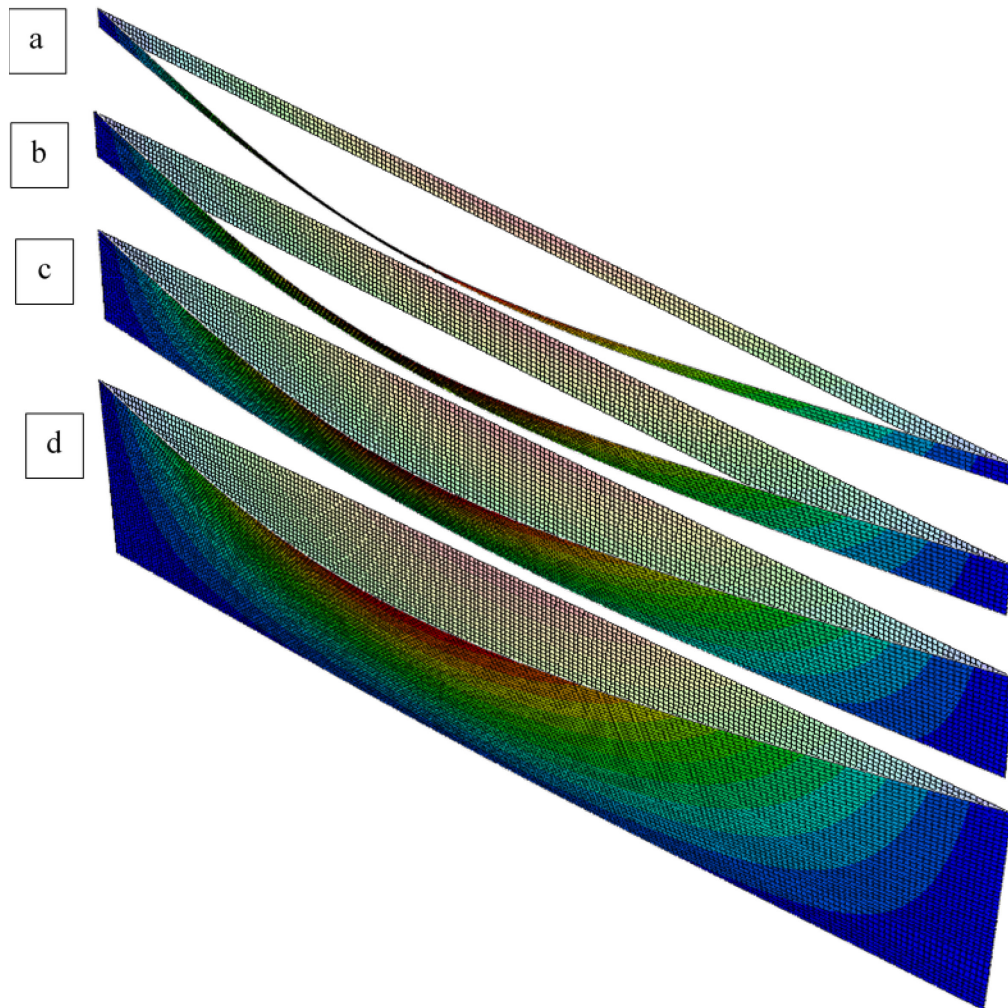


Figure 6.14 Buckling (deformed and un-deformed) shape of the simply supported beam for ply thickness of 0.1 mm and lamination orientation of [0/0/0/0]; (a) $L/h=50$, (b) $L/h =20$, (c) $L/h = 10$, and (d) $L/h =5$

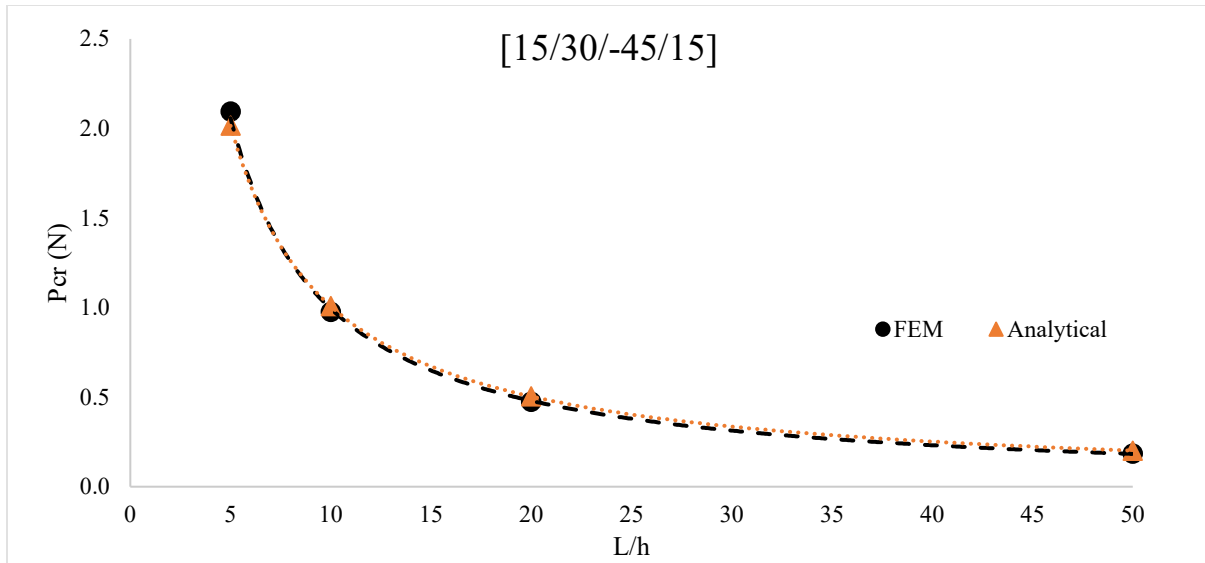


Figure 6.15 Comparison of buckling result obtained from analytical solution and FEM for the [15/30/-45/15] laminate and ply thickness of 0.1 mm by changing L/h ratio

Figures 6.15 – 6.17 show the comparison of buckling forces between the analytical solution and FEM in three different laminate stacking sequences. It is obvious that in both analytical and FEM the buckling forces increase as the L/h ratio decrease because of the larger height of the beam to resist against lateral-torsional buckling. Again, it is evident from Figures 6.15 – 6.17 that the analytical and numerical results match closely beyond L/h=5.

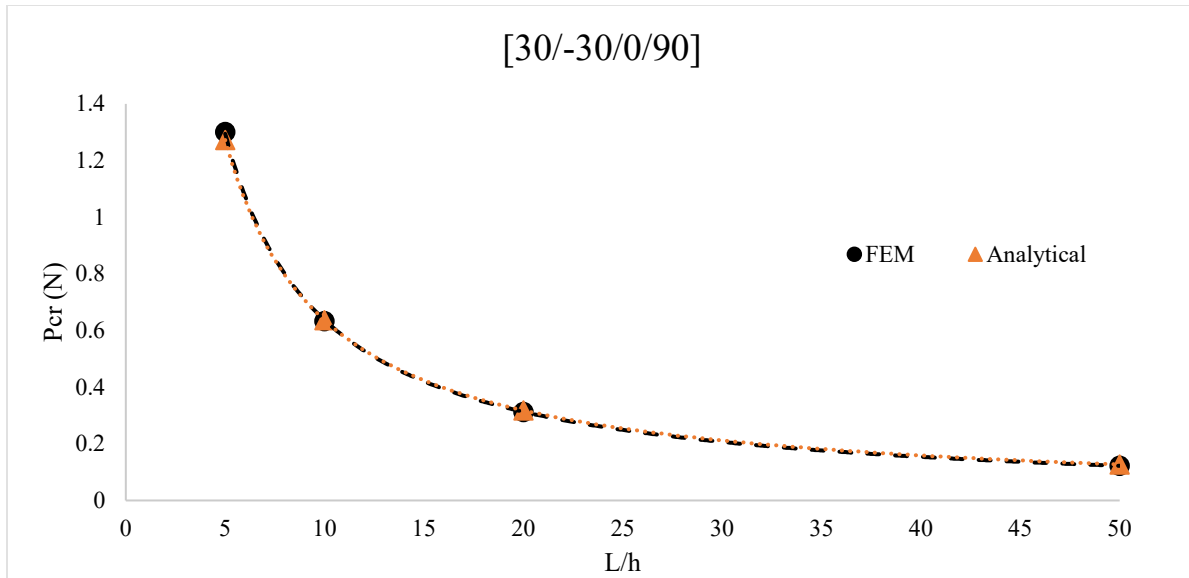


Figure 6.16 Comparison of buckling result obtained from analytical solution and FEM for the [30/-30/0/90] laminate and ply thickness of 0.1 mm by changing L/h ratio

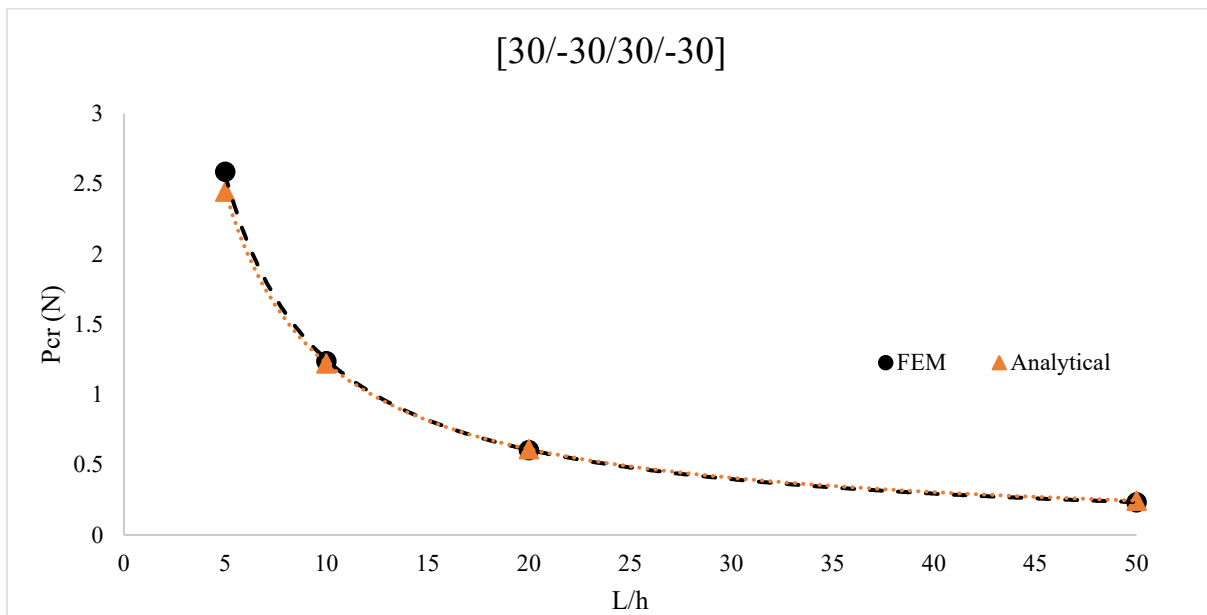


Figure 6.17 Comparison of buckling result obtained from analytical solution and FEM for the [30/-30/30/-30] laminate and ply thickness of 0.1 mm by changing L/h ratio

6.5.2 Effect of Stacking Sequence

As shown in Figures 6.11 and 6.12. The stacking sequences considerably affect the buckling forces if the dimensions of the beam are kept the same. The lowest value for the critical

buckling forces is obtained in [90/90/90/90] layup while the highest critical value is obtained for the balanced angle-ply stacking sequence of [30/-30/30/-30] which is the maximum critical force among the possible stacking sequences selected for Figures 6.11 and 6.12. The optimal maximum critical force is obtained for the balanced angle-ply layup to be 0.663 N for layup [20/-20/20/-20] using L/h ratio of 20. Figure 6.18 shows the variation in critical buckling force with the change in layup angle of 0 to 90 with an increment of 5 degrees. The analytical and FEM results match closely for the entire range of layup angle reaching a maximum value at about [20/-20/20/-20]. Figure 6.19 shows the variation in critical buckling force obtained from analytical formula with the change in layup angle of 0 to 90 with an increment of 5 degrees for three different cases of antisymmetric balanced angle ply [θ /- θ / θ /- θ], symmetric balanced angle ply [θ /- θ /- θ / θ], and anisotropic single angle [θ / θ / θ / θ]. Again it is obvious that the optimal maximum critical force is obtained for the symmetric and antisymmetric balanced angle ply layups at around 20 degrees while for anisotropic single angle layup the maximum critical forces is obtained at 0 degree layup. For single angle anisotropic layup, the lateral-twisting coupling coefficient, D_{YT} , is higher comparing to lateral and twisting coefficient which causes the beam to be critical in other angle layup rather than 0 degrees.

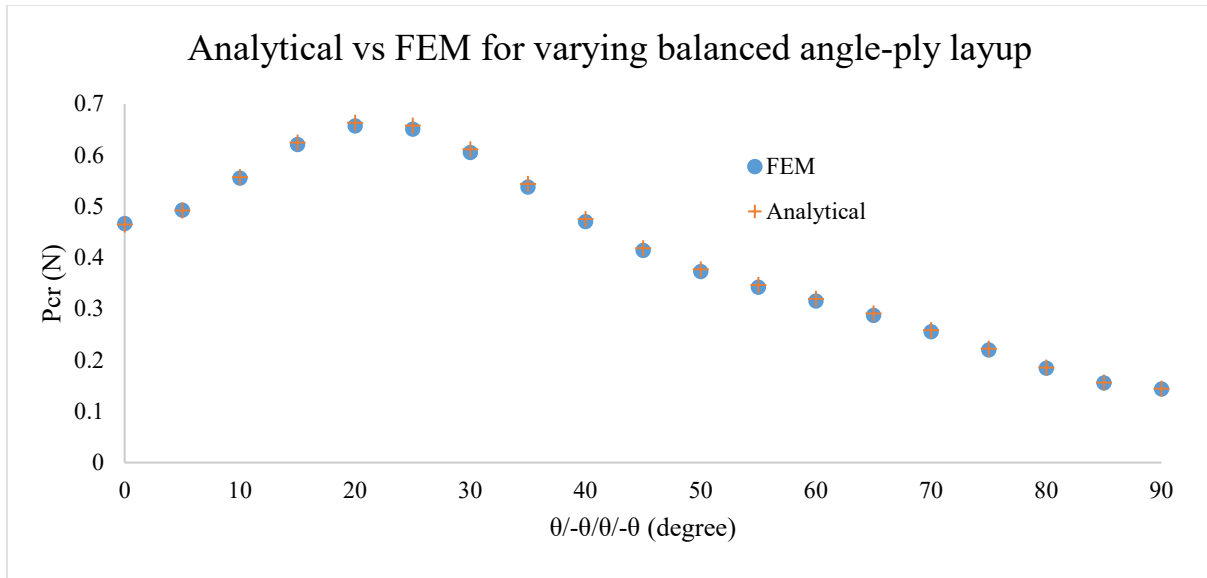


Figure 6.18 Variation in critical buckling force with the change in balanced angle-ply layup angle of 0 to 90 with an increment of 5 degrees. (+) Analytical and (●) FEM; ply thickness of 0.1 mm and L/h of 20

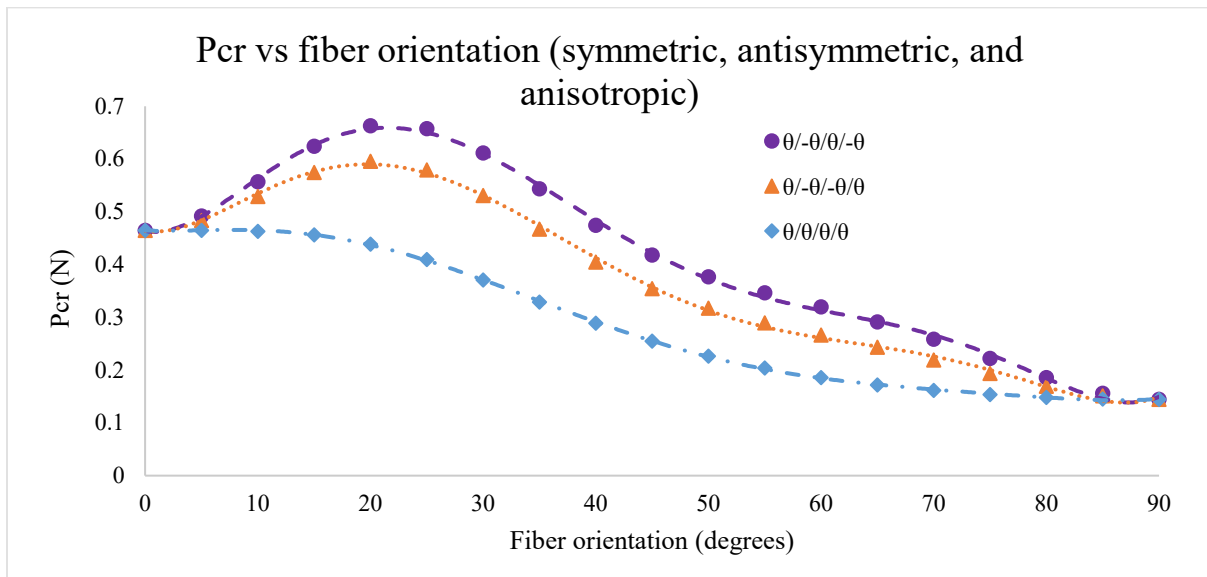


Figure 6.19 Variation in critical buckling force with the change in layup angle of 0 to 90 with an increment of 5 degrees from analytical formula for three different layups; ply thickness of 0.1 mm and L/h of 20

6.5.3 Effect of Layer Thickness

Different layer thickness of 0.05, 0.1, 0.15, and 0.2 mm were used in the analysis to study their effects on the lateral-torsional buckling of simply supported laminated thin-walled rectangular cross-section beams. The L/h ratio of 20 and the stacking sequence were kept the same while changing the layer thickness. The results show that there is a significant increase in the value of buckling forces as the layer thickness increases. The relationship between buckling force and the thickness is defined to be a power function which can be written in Eq. 6.47.

$$P_{cr} = \frac{(P_{cr})_i}{t_i^3} t^3 \quad (6.47)$$

where $(P_{cr})_i$ is the initially calculated value of buckling force from Eq. 6.44 with a given t_i for a specific laminate stacking sequence. Eq. 6.47 works either considering the thickness to be the total thickness of the beam or the thickness of each layer as long as all layers have the same constant thickness.

By knowing the value of buckling force in a selected layup, Eq. 6.47 helps to calculate the buckling force for various layer or beam thickness. Figure 6.20 shows the effect of layer thickness on the buckling force based on analytical solution for three different stacking sequence of [30/-30/0/90], [15/30/-45/15], and [30/-30/30/-30]. Figure 6.21 shows the effect of layer thickness on the buckling force based on the FEM results for the same three stacking sequences of [30/-30/0/90], [15/30/-45/15], and [30/-30/30/-30]. Eq. 6.47 can be obtained from FEM analysis with small deviation multipliers of (a) and (b), which are tabulated in Figure 6.21 for the three mentioned layups. The modification of Eq. 6.47 for FEM results is shown in Eq. 6.48.

$$P_{cr} = (at + b) \frac{(P_{cr})_i}{t_i^3} t^3 \quad (6.48)$$

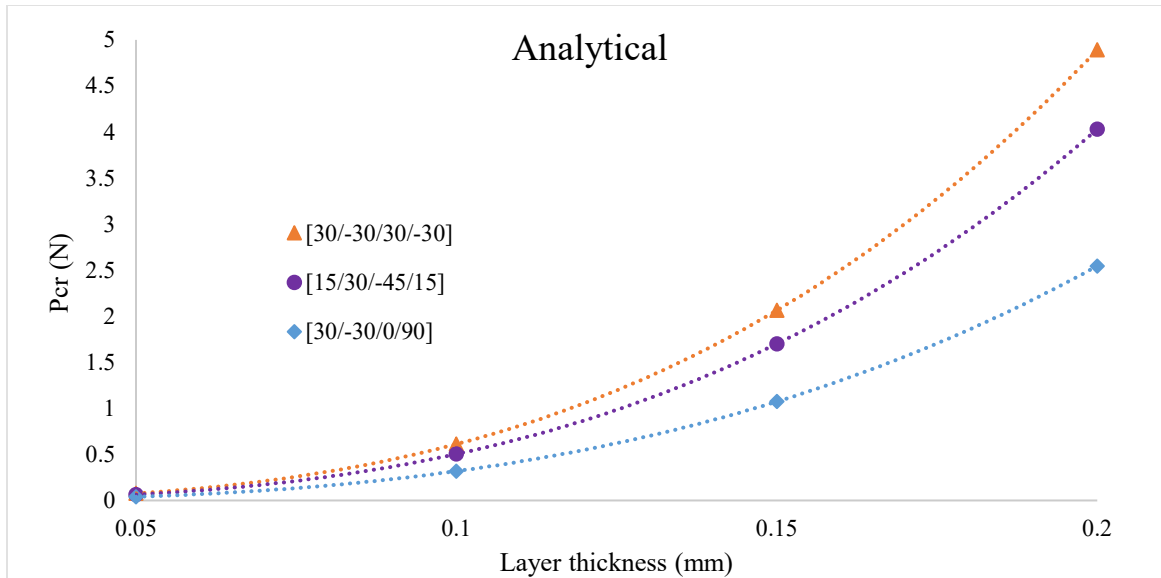


Figure 6.20 Effect of thickness, t_k , on the critical force based on analytical formula for three different orientations, $L/h=20$

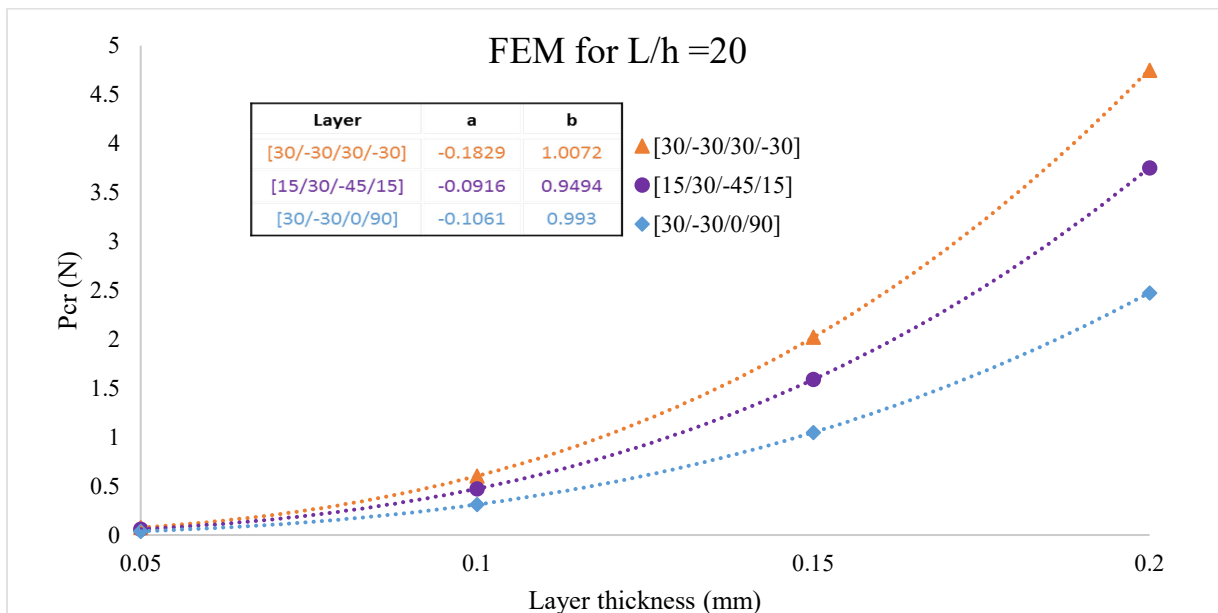


Figure 6.21 Effect of thickness, t_k , on the critical force based on FEM method for three different orientations, $L/h=20$

Figures 6.22 – 6.24 show the comparison of buckling forces between the semi-analytical results and FEM in three different laminate stacking sequences. It is obvious that in both analytical and FEM solutions the buckling forces increase as the layer thickness increases

because of the fact larger thickness of the beam can resist more against lateral-torsional buckling. Both analytical and FEM results have a good agreement on the buckling force for all three sequences, except for the [15/30/-45/15] case when the thickness increases. The anticipated reason might be tendency of distortional buckling of beam or the admission of shear deformation at certain orientation of fibers as the layer thickness increases while keeping L/h ratio the same. Timoshenko and Gere (1961) states that lateral buckling occurs theoretically for any value of t/h but it is necessary to consider lateral buckling only for in the case of a very narrow cross section where t/h is very small quantity.

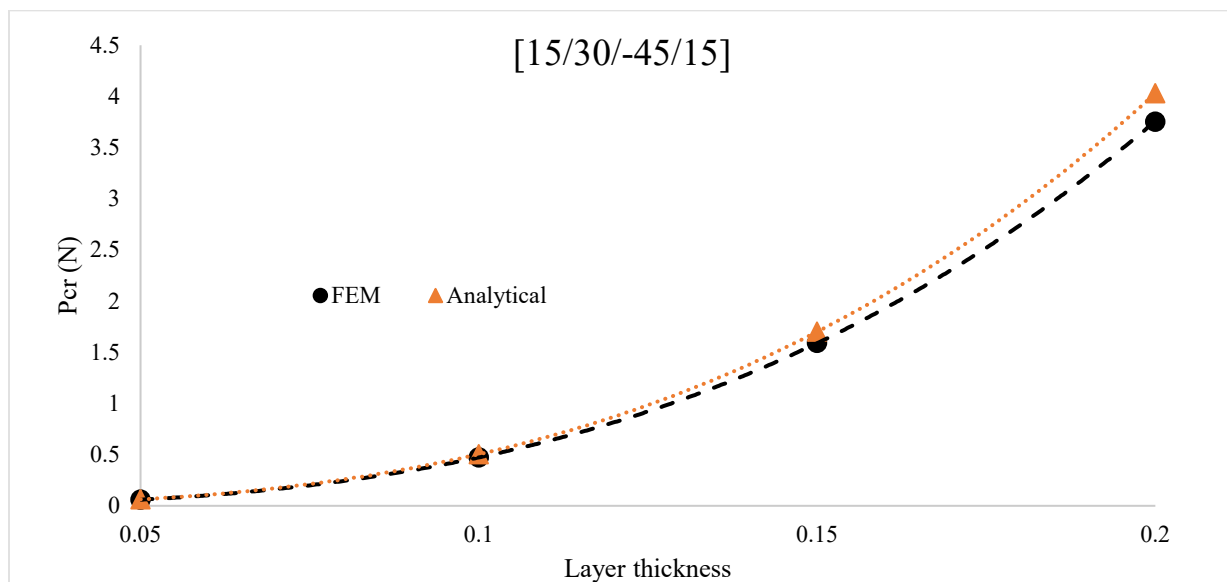


Figure 6.22 Comparison of buckling result obtained from analytical solution and FEM for the [15/30/-45/15] laminate and L/h of 20 by changing layer thickness, t_k

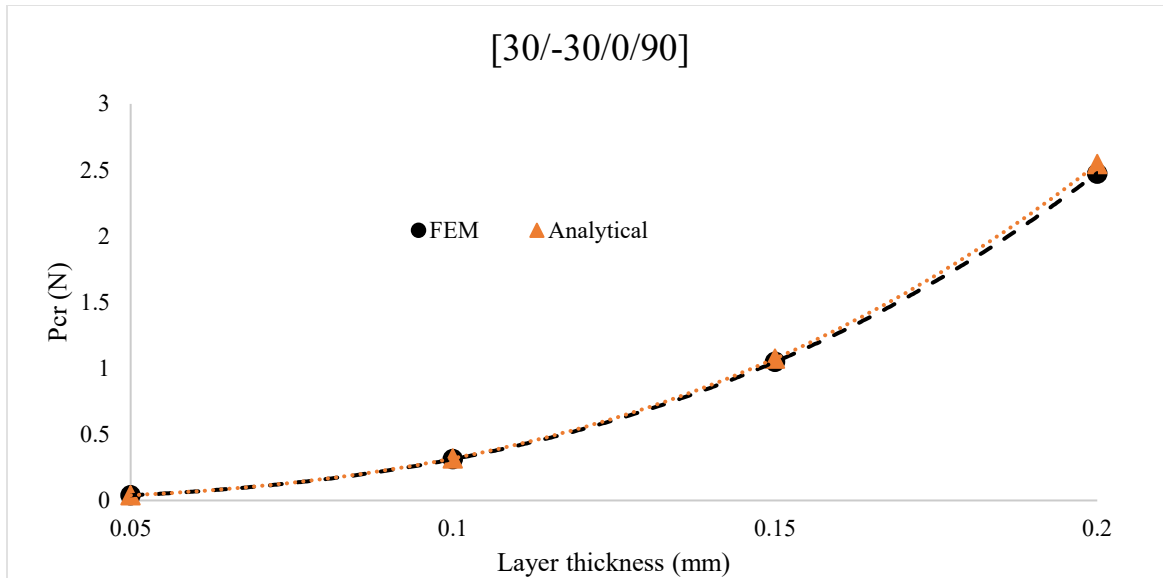


Figure 6.23 Comparison of buckling result obtained from analytical solution and FEM for the [30/-30/0/90] laminate and L/h of 20 by changing layer thickness, t_k

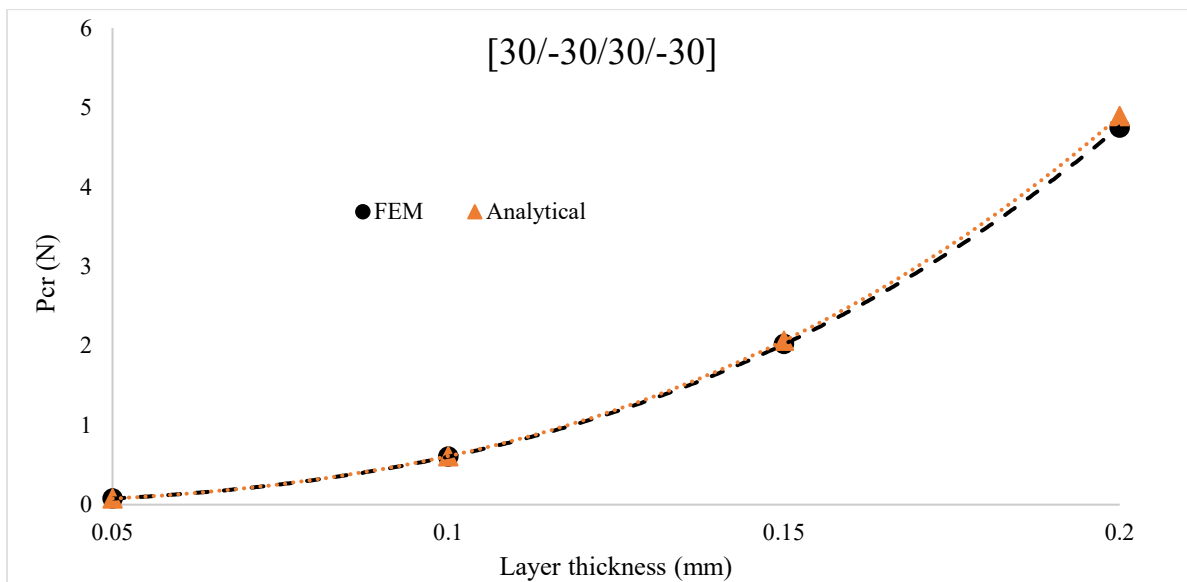


Figure 6.24 Comparison of buckling result obtained from analytical solution and FEM for the [30/-30/30/-30] laminate and L/h of 20 by changing layer thickness, t_k

6.5.4 Effect of Pre-Buckling Deformation

Furthermore, to indicate the existence of pre-buckling deformation in the transverse direction, the load versus mid-span deflection curves are plotted for the different stacking

sequences of [30/-30/0/90], [15/30/-45/15], and [30/-30/30/-30] obtained from finite element nonlinear Riks analysis along with the analytical solution for comparison. The buckling loads in Figure 6.25 for anisotropic layups of [30/-30/0/90] and [15/30/-45/15] show excellent agreement and a pre-buckling deformation. On the other hand, the antisymmetric angle ply [30/-30/30/-30] exhibits higher buckling load with a clear bifurcation buckling.

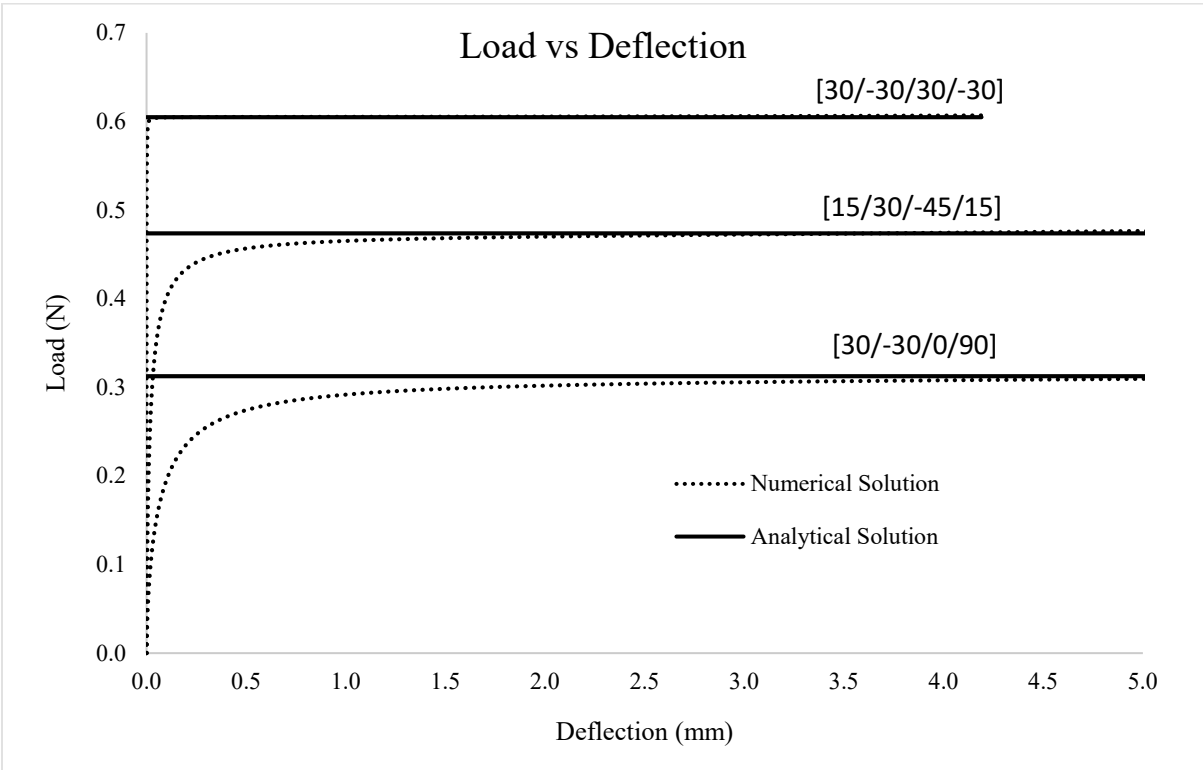


Figure 6.25 Analytical versus numerical solution; deflection at mid-span, $L/h=20$ and $t_k=0.1$

Table 6.3 Comparison of buckling force obtained from analytical results and FEM for L/h ratios of 10 and 20 and layer thickness of 0.1 mm in different stacking conditions

| Laminate | Critical Buckling Forces Pcr (N.mm) and Error (%) | | | | | |
|---------------|---|--------|-----------|------------|--------|-----------|
| | L/h =10 | | | L/h = 20 | | |
| | Analytical | FEM | Error (%) | Analytical | FEM | Error (%) |
| 0/0/0/0 | 0.9298 | 0.9602 | 3.27 | 0.4649 | 0.4668 | 0.40 |
| 90/90/90/90 | 0.2890 | 0.2891 | 0.03 | 0.1445 | 0.1437 | 0.57 |
| 30/-30/30/-30 | 1.2231 | 1.2376 | 1.19 | 0.6115 | 0.6049 | 1.09 |
| 45/-45/45/-45 | 0.8370 | 0.8517 | 1.76 | 0.4185 | 0.4139 | 1.09 |
| 60/-60/60/-60 | 0.6395 | 0.6387 | 0.13 | 0.3198 | 0.3154 | 1.37 |
| 60/-60/45/-45 | 0.7245 | 0.7274 | 0.40 | 0.3623 | 0.3572 | 1.40 |
| 30/-30/45/-45 | 0.9509 | 0.9622 | 1.20 | 0.4754 | 0.4690 | 1.35 |
| 30/-30/60/-60 | 0.7871 | 0.7853 | 0.22 | 0.3935 | 0.3846 | 2.27 |
| 30/-30/0/0 | 0.9064 | 0.9098 | 0.37 | 0.4532 | 0.4477 | 1.21 |
| 30/-30/0/90 | 0.6363 | 0.6327 | 0.56 | 0.3181 | 0.3125 | 1.76 |
| 30/30/30/30 | 0.7416 | 0.6946 | 6.34 | 0.3708 | 0.3378 | 8.90 |
| 30/-30/-30/30 | 1.0626 | 1.0521 | 0.98 | 0.5313 | 0.5138 | 3.29 |
| 0/90/90/0 | 0.8776 | 0.9027 | 2.87 | 0.4388 | 0.4398 | 0.22 |
| 30/-60/-60/30 | 0.8801 | 0.8376 | 4.83 | 0.4400 | 0.4016 | 8.74 |
| 0/90/0/90 | 0.6450 | 0.6542 | 1.43 | 0.3225 | 0.3218 | 0.21 |
| -45/30/-30/45 | 0.8434 | 0.8569 | 1.60 | 0.4217 | 0.4186 | 0.74 |
| 0/0/90/90 | 0.4832 | 0.4866 | 0.70 | 0.2416 | 0.2408 | 0.34 |
| 90/0/0/90 | 0.4265 | 0.4285 | 0.46 | 0.2133 | 0.2123 | 0.44 |
| 15/30/-45/15 | 1.0077 | 0.9759 | 3.15 | 0.5038 | 0.4737 | 5.97 |

6.6 Conclusions

In this study, the lateral-torsional buckling of simply supported, thin-walled rectangular cross-section, anisotropic laminated composite beam under concentrated load at mid-span was investigated. Based on the assumptions made and the results obtained, an excellent accuracy is observed for a variety of stacking sequences. The applicability of this analytical formulation is proved by comparing the obtained results with FEM results. The study followed the classical

laminated plate theory with all considered assumptions and determined an effective lateral-torsional-coupling stiffness matrix.

Based on the study, the stability of the laminated beams under concentrated load is greatly affected by the length/height ratio of the beam as well as the thickness of the beam. The importance of the stacking sequence, which does not affect the dimensions of the beam, is seen to greatly influence the stability of the beam.

The critical buckling force of symmetric and antisymmetric balanced angle-ply fiber lamination of about $[20/-20/-20/20]$ and $[20/-20/20/-20]$ are found to reach the maximum value, among these two classes of layups, because of their maximum lateral and torsional effective stiffness. On the other hand, single angle anisotropic fiber lamination of $[0/0/0/0]$ is found to reach the maximum value because of its zero value of lateral-twisting coupling coefficient. The minimum critical buckling load obtained from $[90/90/90/90]$ was found to be due to orienting the fibers in the y-direction, thus reducing the lateral effective stiffness. A finite element nonlinear Riks analysis was performed to indicate the existence of pre-buckling deformation in transverse direction for anisotropic layups while comparing favorably with analytical buckling limit loads in two stacking sequences. It further showed perfect bifurcation buckling for antisymmetric angle ply layup.

6.7 References

- Al-Masri, R. and Rasheed, H.A. (2017). “Analytical and Finite Element Buckling Solutions of Fixed-Fixed Anisotropic Laminated Composite Columns under Axial Compression.” *International Journal of Structural Stability and Dynamics*, 17(9), 1750103.
- Bank, L. C., & Bednarczyk, P. J. (1988). A beam theory for thin-walled composite beams. *Composites Science and Technology*, 32(4), 265-277.
- Barbero, E. J., Lopez-Anido, R., and Davalos, F. (1993). “On the Mechanics of Thin-Walled Laminated Composite Beams.” *Journal of Composite Materials*, 27(8), 806-829
- Barbero, E. J. (1999). *Introduction to composite materials design*. CRC press.
- Bauld, N. R., & Lih-Shyng, T. (1984). A Vlasov theory for fiber-reinforced beams with thin-walled open cross sections. *International Journal of Solids and Structures*, 20(3), 277-297.
- Davalos, J. F., and Qiao, P. (1997), “Analytical and experimental study of lateral and distortional buckling of FRP wide-flange beams”, *Journal of Composites for Construction*, Vol. 1, pp. 150–159
- Karaagac, C., Öztürk, H., & Sabuncu, M. (2007). Lateral dynamic stability analysis of a cantilever laminated composite beam with an elastic support. *International Journal of Structural Stability and Dynamics*, 7(03), 377-402.
- Kollar, L. P. (2001). “Flexural-torsional buckling of open section composite columns with shear deformation.” *International Journal of Solids and Structures*, 38, 7525-7541
- Kollár, L. P., & Springer, G. S. (2003). *Mechanics of composite structures*. Cambridge university press.
- Kotelko, M. (2004). “Load-capacity estimation and collapse analysis of thin-walled beams and columns—recent advances”. *Thin-walled Structures*, Vol. 42, No.2, PP.153-175
- Lee, J., Kim, S.-E., Hong, K. (2002). “Lateral buckling of I-section composite beams.” *Engineering Structures*, 24, 955-964
- Lin, Z. M., Polyzois, D., and Shah, A. (1996). “Stability of Thin-walled Pultruded Structural Members by the Finite Element Method.” *Thin-Walled Structures*, 24, 1-18
- Machado, S. P. (2010). “Interaction of combined loads on the lateral stability of thin-walled composite beams.” *Engineering Structures*, 32, 3516-3527
- Pandey, M.D., Kabir, M.Z., and Sherbourne, A.N. (1995). “Flexural-Torsional Stability of Thin-Walled Composite I-Section Beams.” *Composites Engineering*, 5(3), 321-342

- Qiao, P., Zou, G., and Davalos, J. (2003). "Flexural-torsional buckling of fiber-reinforced plastic composite cantilever I-beams." *Composite Structures*, 60, 205-217
- Roberts, T.M., Al-Ubaidi, H. (2001). "Influence of shear deformation on restrained torsional warping of pultruded FRP bars of open cross-section." *Thin-Walled Structures*, 39, 395-414
- Sapkás, Á., & Kollár, L. P. (2002). Lateral-torsional buckling of composite beams. *International Journal of Solids and Structures*, 39(11), 2939-2963.
- Sherbourne, A. N., Kabir, M. Z. (1995). "Shear Strain Effects in Lateral Stability of Thin-Walled Fibrous Composite Beams." *Journal of Engineering Mechanics*, 640-647
- Tai, W. T. (2004). *The lateral-torsional buckling analysis of composite laminated beams* (MSc thesis, Feng Chia University, Taiwan ROC).
- Timoshenko, S. P., & Gere, J. M. (1961). *Theory of elastic stability*. 1961. McGrawHill-Kogakusha Ltd, Tokyo.
- Vlassov, V. Z. (1961). *Thin-walled beams* (2nd ed.) Israel Program for Scientific Translation.

Chapter 7 - Conclusions and Recommendations

7.1 Conclusions

In this research, the lateral-torsional buckling of thin-walled rectangular cross-section, anisotropic laminated composite beams under various loading and boundary conditions, as well as hybrid steel-FRP beams under pure bending condition, are analytically and semi-analytically investigated. Based on the assumptions made and the results obtained, an excellent accuracy is observed for a variety of stacking sequences. The applicability of this analytical formulation is proved by comparing the obtained solutions with FEM results. The study followed the classical laminated plate theory with all considered assumptions and determined an effective lateral-torsional-coupling stiffness matrix.

Based on the study, the stability of the laminated beams under various loading and boundary conditions is greatly affected by the length/height ratio of the beam as well as the thickness of the beam. The critical buckling moment or force are inversely proportional to the length/height ratios with a power function. Increase in the thickness of the beam also plays a significant role in increasing the stability resistance of the beams. The importance of the stacking sequence, which does not affect the dimensions of the beam, is seen to greatly influence the stability of the beams.

For the hybrid steel-FRP beams, the ST-II stacking type, in which the steel laminate is on the side of the beam, shows a higher resistance than the ST-I, in which the steel sheet is located at mid-thickness of the beam. Accordingly, it is more effective to apply the FRP on one side of steel beams to strengthen them against lateral-torsional buckling.

The fiber angle orientation was proven to be a critical variable against the lateral torsional buckling. The critical buckling moment or force of symmetric and anti-symmetric balanced

angle-ply fiber lamination of about $[22/-22/-22/22]$ and $[22/-22/22/-22]$ are found to reach the maximum value, among these two classes of layups, because of their maximum lateral and torsional effective stiffness. For single angle anisotropic fiber lamination of $[\theta/\theta/\theta/\theta]$ is found to reach the maximum value with $[0/0/0/0]$, among this class of layups, because of its zero value of lateral-twisting coupling coefficient and highest value of lateral coefficient at zero degrees. The minimum critical buckling moment or force obtained from $[90/90/90/90]$ was found to be due to orienting the fibers in the y-direction, thus reducing the lateral effective stiffness coefficient.

A finite element nonlinear geometrical deformation analysis, using modified Riks simulation by ABAQUS, is used for the cases of cantilever beams under free end loading and simply supported beams under concentrated load at mid-span. This analysis was examined and compared against analytical solution for determining the existence of pre-buckling deformation vs. bifurcation behavior. As a result the buckling loads showed excellent agreement with those predicted analytically.

7.2 Recommendations

From the major conclusions presented in the preceding section, additional works could be made in the future, as follows:

1. Extend this approach to investigate stability of different types of rectangular laminated composite beams by changing the vertical location of applied load with respect to the centroid of cross-section
2. Develop analytical approach for anisotropic and hybrid laminated composite I-section beams.

3. Develop an Excel based program to solve the lateral-torsional buckling of laminated composite rectangular beams for any loading and boundary conditions.